UNIVERSITÉ DU QUÉBEC À TROIS-RIVIÈRES

MODÉLISATION, OPTIMISATION ET ÉTUDE DE PROTOCOLE POUR UN SYSTÈME DE RAVITAILLEMENT EN HYDROGÈNE EFFICACE ET SÛR

THÈSE PRÉSENTÉE
COMME EXIGENCE PARTIELLE DU

DOCTORAT EN SCIENCES DE L'ÉNERGIE ET DES MATÉRIAUX

PAR
HAO LUO

MAI 2024

Modelling, Optimization and Protocol Study for Efficient and Safe Hydrogen Refuelling System

Ph.D. Candidate: Hao Luo

Under the guidance of

Prof. Pierre Bénard & Prof. Jinsheng Xiao

(*Supervisor*) (*Co-supervisor*)

7 May, 2024

Members of Jury:

Pierre Bénard, Ph. D., directeur de recherché	Université du Québec à Trois-Rivières
Jinsheng Xiao, Ph. D., codirecteur de recherche	Wuhan University of Technology, China
Zaoxiao Zhang, Ph. D., président du jury	Xi'an Jiaotong University, China
Xianjun Hou, Ph. D., évaluateur	Wuhan University of Technology, China
Richard Chahine, Ph. D., évaluateur	Université du Québec à Trois-Rivières
Qifeng Tian, Ph. D., évaluateur	Wuhan Institute of Technology, China
Pang-Chieh Sui, Ph. D., évaluateur	Wuhan University of Technology, China
Shichun Mu, Ph. D., évaluateur	Wuhan University of Technology, China

摘 要

氢能作为能源转型的替代燃料提供了吸引人的机会，因为它在使用时对环境影响较小且应用范围广泛。氢燃料电池汽车（HFCV）是氢能的重要应用场景。在加注过程中，氢气的焦耳-汤姆逊效应和压缩效应会导致储罐内温度显著升高。目前，加氢站普遍采用预冷加注方法来降低温升。制冷装置的使用直接增加了的投资成本。同时，冷却能耗也会增加加氢站的运营成本。目前，加氢站采用美国汽车工程师协会（SAE）发布的 SAE J2601 协议中的查表法和 MC 法来加注 HFCV。MC 方法在加注控制过程中的精度还有较大的提升潜力。因此，有必要对氢气加注系统开展数值建模、能耗功率优化和协议改进研究，提升其高效性与安全性。

建立和验证氢气加注系统储氢罐的集总参数热力学模型、解析模型和数值模型，确定各模型的应用范畴。基于质量守恒、能量守恒及气体状态方程，建立储氢罐的单区、双区、三区和零维气体一维罐壁（0D1D）集总参数热力学模型；求解单区和双区热力学模型的数学物理方程，得到对应的单区氢气温度、双区氢气温度和罐壁温度的解析模型，结合 Redlich-Kwong 气体状态方程得到对应氢气压力的解析模型；基于储氢罐的单区、双区、三区和 0D1D 热力学模型的数学物理方程，在 Matlab/Simulink 中建立相应的数值模型；采用参考文献中的实验数据和 CFD 模拟结果，验证模型的准确性。

确定最佳的气体状态方程类型和换热系数模型，即储氢罐数值模型采用基于美国国家标准与技术研究院（NIST）数据库计算氢气温度和压力，储氢罐解析模型采用 Redlich-Kwong 修正的气体状态方程，第 6 章的新加注方法采用多项式气体状态方程，换热系数采用基于雷诺数的经验公式模型。对比不同类型气体状态方程的计算结果，以基于NIST数据库计算的氢气压力为标准，则多项式气体状态方程计算的相对误差为 0.30%，Redlich-Kwong 气体状态方程为 1.83%，范德瓦尔斯气体状态方程为 17.90%，即多项式的精度最高，Redlich-

Kwong 次之，范德瓦尔斯最低；对比不同换热系数模型的计算结果，相对于基于实时压力以及指数函数的经验公式换热系数，基于雷诺数的经验公式换热系数与标准的能量守恒换热系数之间误差更小。

为了提高氢气加注系统的高效性，优化氢气加注系统的梯级储罐配置和加注策略，降低最大冷却功率需求和冷却能耗，降低制冷系统的投资成本和运行成本。扩展储氢罐模型至整个单级氢气加注系统，提出应用于单级加注系统的两级加注速度（平均压力斜坡率）和两级进气温度的两级加注策略，相对于单级加注策略可分别降低最大冷却功率23.8%和16.3%；扩展单级氢气加注系统至三级梯级加注系统，提出基于遗传算法和 Pareto 优化的多目标优化方法，优化低压、中压和高压梯级储罐的初始压力和容积配置，可降低冷却能耗 11.43%；提出应用于三级梯级加注系统的三级进气温度策略，相对于单级温度加注可降低最大冷却功率 16.69%～17.38%。

为了提高氢气加注系统的安全性，提出 SAE J2601 氢气加注协议中 MC 法的两个改进方案，提高目标压力的计算精度和加注过程的控制精度。方案一提出 MC 参数的人工神经网络（ANN）模型和修正公式，ANN 模型可克服 MC 参数原始公式不适用于最终加注时间小于 30 s 的问题，且可降低与 0D1D 模型的相对误差 13.8%～58.8%，MC 参数的修正公式可降低相对误差 16.6%～82.3%；方案二将原始 MC 法的双区单温模型改进为双区双温模型，推导最终氢气温度的修正公式，同样可克服原始公式不适用于最终加注时间小于 30 s 的问题，且可降低与 0D1D 模型的误差 2～7 ℃。

最后，基于储氢罐的双区集总参数热力学模型，推导最终加注时间和最终氢气温度的解析解，探索更为简洁的基于解析解的氢气加注新方法。对比新加注方法与 0D1D 模型的最终氢气温度、压力和 SOC 模拟结果，证明新加注方法的有效性。

本论文有助于理解加氢站加注过程的机制，并提供提高加氢系统效率和安全性的途径，已发表 6 篇论文:

关键词：氢气加注，高压储氢，氢安全，加注协议，优化

Résumé de la thèse en français

L'hydrogène offre des possibilités intéressantes en tant que carburant alternatif dans le contexte de la transition énergétique, en raison de son faible impact sur l'environnement lorsqu'il est utilisé comme combustible et de son large éventail d'utilisations, que ce soit en tant que produit chimique essentiel à l'industrie des procédés ou comme carburant pour une pile à combustible ou un engin thermique. Les véhicules à pile à hydrogène (VPCH) constituent un scénario d'application important de l'hydrogène. Pendant le processus de remplissage, l'effet Joule-Thomson et les processus thermiques liés à la compression de l'hydrogène peuvent provoquer une augmentation significative de la température à l'intérieur du réservoir. À l'heure actuelle, les stations de ravitaillement en hydrogène utilisent généralement des méthodes de pré-refroidissement pour réduire cette augmentation. L'utilisation de systèmes de réfrigération augmente affecte le coût d'investissement des stations de ravitaillement en hydrogène. De plus, la consommation d'énergie requise pour le refroidissement augmente les coûts d'exploitation de ces dernières. À l'heure actuelle, les postes de ravitaillement utilisent une méthode basée sur des tables précompilées et la méthode MC proposées par le protocole SAE J2601, publié par la Society of Automotive Engineers (SAE) pour remplir de façon sécuritaire les véhicules à pile à combustible à l'hydrogène. La précision de la méthode MC pendant le contrôle du remplissage a le potentiel d'être bonifiée en améliorant les modèles des méthodes proposées dans SAE J2601. L'objectif de cette thèse est donc de procéder à une modélisation numérique des processus de remplissages sous différentes conditions d'utilisation, afin d'améliorer les protocoles de remplissage d'hydrogène du point de vue de leur efficacité et de leur sécurité.

Dans cette thèse, le modèle thermodynamique à paramètres amalgamés, des modèles analytiques et numériques du réservoir de stockage d'hydrogène sont établis et validés, et le domaine d'application de chaque modèle est déterminé. Sur la base de la conservation de la masse, de la conservation de l'énergie et de l'équation d'état du

gaz (EOS), les modèles thermodynamiques à paramètres amalgamés des réservoirs de stockage d'hydrogène sont établis pour des approches à une zone, deux zones et trois zones en considérant la paroi du réservoir comme unidimensionnelle et le gaz comme étant amalgamé (« à zéro dimension » - une approche dite 0D1D). Les modèles analytiques correspondants de la température de l'hydrogène dans une seule zone, de la température de l'hydrogène dans deux zones et de la température de la paroi du réservoir sont obtenus en résolvant les équations des modèles thermodynamiques dans une seule zone et dans deux zones. Le modèle analytique correspondant de la pression de l'hydrogène est obtenu en combinant la température de l'hydrogène avec l'équation d'état de Redlich-Kwong. Les équations des modèles thermodynamiques à zone unique, à deux zones, à trois zones et 0D1D sont implémentés dans Matlab/Simulink pour les résoudre numériquement. Ces modèles sont alors validés à l'aide de données expérimentales et de résultats de simulation de mécanique des fluides computationnelles.

Les différents types de modèles d'équations d'états de gaz et de coefficients de transfert de chaleur ont été comparés pour déterminées lesquelles étaient les plus appropriées pour les fins de ce travail. La solution numérique du modèle du réservoir de stockage d'hydrogène utilise la base de données du National Institute of Standards and Technology (NIST) pour calculer la température et la pression de l'hydrogène, alors que le modèle analytique utilise l'équation d'état modifiée de Redlich-Kwong. La nouvelle méthode de remplissage proposée dans le chapitre 6 utilisera plutôt une équation d'états polynômiale. Le coefficient de transfert de chaleur est modélisé à l'aide d'une formule empirique qui est fonction du nombre de Reynolds. En utilisant comme point de comparaison l'estimation de la pression de l'hydrogène calculée à partir de l'équation d'état du NIST, l'erreur relative de l'équation d'états polynômiale est de 0.30 %, celle de l'équation d'états de Redlich-Kwong est de 1.83 % et celle de l'équation d'états du gaz de van der Waals est de 17.90 %. En d'autres termes, la précision de l'approche polynômiale est la plus élevée, suivie de celle de Redlich-Kwong. L'équation de van der Waals offre les résultats les moins précis. Une analyse numérique montre que le coefficient de transfert de chaleur de la formule empirique basée sur le nombre de Reynolds affiche une erreur plus faible par rapport au modèle

de coefficient de transfert de chaleur standard basé sur la conservation de l'énergie pour les plages de paramètres thermodynamiques d'intérêt au problème.

Afin d'améliorer l'efficacité du système de remplissage d'hydrogène, nous avons cherché à optimiser la configuration d'un réservoir de stockage en cascade ainsi que la stratégie de remplissage du réservoir, de façon à réduire la demande maximale de puissance de refroidissement et la consommation d'énergie de refroidissement, pour réduire les coûts d'investissement et d'exploitation du système de réfrigération. Des stratégies de remplissage en deux étapes sont proposées plutôt qu'une stratégie en une étape, dont une approche avec deux vitesses de remplissage (c'est-à-dire deux taux de rampe de pression) et deux spécifications successives de la température à l'entrée. Ces approches, une fois les paramètres optimisés, peuvent réduire la puissance de refroidissement maximale de 23.8% et de 16.3%, respectivement. La stratégie de remplissage à une étape est étendue à une approche de remplissage en cascade à trois étapes. Une méthode d'optimisation multi-objectifs, basée sur un algorithme génétique et une approche d'optimisation de Pareto est proposée pour optimiser la pression initiale et la configuration du volume du réservoir de stockage en cascade basse pression, moyenne pression et haute pression, ce qui permet de réduire la consommation d'énergie de refroidissement de 11.43%. Une stratégie de températures d'entrée spécifiée en trois étapes pour le système de remplissage en cascade à trois stades est proposée, ce qui peut réduire la puissance de refroidissement maximale de 16.69% à 17.38% par rapport au remplissage à température spécifiée en une étape.

Afin d'améliorer la sécurité du processus de remplissage, nous examinons deux améliorations à la méthode MC du protocole proposé dans SAE J2601, dans l'objectif d'améliorer la précision du calcul de la pression désirée et du contrôle du processus de remplissage. Dans un premier temps (Plan I), nous proposons l'utilisation d'un réseau de neurones (ANNN) et d'une formule modifiée pour le paramètre MC. L'usage d'une approche par réseau de neurones permet de surmonter le problème que la formule originelle du paramètre MC n'est pas applicable pour un temps de remplissage final de moins de 30 secondes et permet de réduire l'erreur relative sur le paramètre MC en utilisant par rapport aux prédictions du modèle 0D1D d'un facteur variant entre 13.8 et 58.8%. La formule modifiée du paramètre MC permet de réduire l'erreur relative sur

la valeur du paramètre d'entre 16.6% et 82.3% par rapport au modèle 0D1D. Dans un second temps (Plan II), nous améliorons l'approche originale MC à deux zones et une température en utilisant plutôt une approche à deux zones et deux températures. Nous obtenons une formule modifiée de la température finale de l'hydrogène dans le réservoir. Cette stratégie permet également de surmonter le problème que l'approche originelle ne fonctionne pas pour des temps de remplissage de moins de 30 secondes. Elle permet aussi de réduire l'erreur sur la température finale d'une valeur entre 2 Celsius et 7 degrés Celsius par rapport à la formule originelle.

Finalement, sur la base du modèle thermodynamique à paramètres amalgamés à deux zones du réservoir de stockage d'hydrogène, des solutions analytiques pour le temps de remplissage et pour la température finale de l'hydrogène comprimé sont dérivées, et une nouvelle méthode de remplissage plus concise est examinée à l'aide des solutions analytiques. La température finale de l'hydrogène, la pression et les résultats de simulation de l'état de charge (SOC) de la nouvelle méthode de remplissage et du modèle 0D1D sont comparés pour examiner son efficacité.

Cette thèse, qui a contribué à une meilleure compréhension des mécanismes de remplissage de stations de ravitaillement et qui propose des stratégies pour améliorer l'efficacité et la sécurité des systèmes de remplissage d'hydrogène, a mené à la publication de 6 articles dans des revues scientifiques:

[1] **Luo H**, Xiao J S, Bénard P, Yang T Q, Tong L, Chahine R, Yuan Y P, Yuan C Q, Yao C L. Improvement of MC method in SAE J2601 hydrogen refuelling protocol using dual-zone dual-temperature model. *Journal of Energy Storage*, 2024, 81: 110416. (**JCR Q1, IF=9.4**)

[2] **Luo H**, Xiao J S, Bénard P, Zong Y, Chahine R, Tong L, Yuan C Q, Yang T Q, Yuan Y P. Optimal estimation of MC parameter in SAE J2601 hydrogen refuelling protocol based on modified formula and artificial neural networks. *Fuel,* 2024, 365: 131315. (**JCR Q1, IF=7.4**)

[3] **Luo H**, Xiao J S, Bénard P, Chahine R, Yang T Q. Multi-objective optimization of cascade storage system in hydrogen refuelling station for minimum cooling energy and maximum state of charge. *International Journal of Hydrogen Energy*, 2022,

47: 10963-10975. (**JCR Q1, IF=7.2**)

[4] **Luo H**, Xiao J S, Bénard P, Chahine R, Yang T Q. Effects of filling strategies on hydrogen refueling performance. *International Journal of Hydrogen Energy*, 2024, 51: 664-675. (**JCR Q1, IF=7.2**)

[5] **Luo H**, Xiao J S, Bénard P, Yuan C Q, Tong L, Chahine R, Yuan Y P, Yang T Q, Yao C L. Thermodynamic modeling and analysis of cascade hydrogen refuelling with three-stage pressure and temperature for heavy-duty fuel cell vehicles. *International Journal of Hydrogen Energy*, 2024, 63: 103-113. (**JCR Q1, IF=7.2**)

[6] **Luo H**, Yuan C Q, Wang L, Yang T Q, Tong L, Ye F, Yuan Y P, Bénard P, Chahine R, Xiao J S. Heat transfer analysis methodology for compression hydrogen storage tank during charge-discharge cycle. *International Journal of Energy Research*, 2024, Second review. (**JCR Q1, IF=4.6**)

Mots clés: remplissage d'hydrogène, stockage à haute pression de l'hydrogène, sécurité de l'hydrogène, protocole de ravitaillement, optimisation.

Abstract

Hydrogen energy offers tantalizing opportunities as an alternative fuel for the energy transition due to its low impact on the environment when used and wide range of applications. Hydrogen fuel cell vehicles (HFCVs) are an important hydrogen application scenario. During the filling process, hydrogen's Joule-Thomson effect and compression effect will cause the temperature inside the tank to rise significantly. At present, hydrogen refuelling stations (HRS) generally use precooling filling methods to reduce temperature rise. The use of refrigeration devices directly increases the investment cost of HRS. Meanwhile, cooling energy consumption will increase the operating costs of refuelling stations. Currently, HRSs use a lookup table method and the MC method in the SAE J2601 protocol issued by the Society of Automotive Engineers (SAE) to fill HFCV. The accuracy of the MC method during filling control has great potential for improvement. Therefore, it is necessary to carry out numerical modelling, energy consumption and power optimization and protocol improvement research on the hydrogen filling system to improve its efficiency and safety.

In this thesis, the lumped parameter thermodynamic model, analytical model and numerical model of the hydrogen storage tank are established and verified, and each model's application scope is determined. Based on mass conservation, energy conservation and gas equation of state (EOS), the single-zone, dual-zone, triple-zone and zero-dimensional gas one-dimensional tank wall (0D1D) lumped parameter thermodynamic models of hydrogen storage tanks are established. The corresponding analytical models of single-zone hydrogen temperature, dual-zone hydrogen temperature and tank wall temperature are obtained by solving the equations of the single-zone and dual-zone thermodynamic models. The corresponding analytical model of hydrogen pressure is obtained by combining hydrogen temperature with the Redlich-Kwong gas EOS. Based on the equations of the single-zone, dual-zone, triple-zone and 0D1D thermodynamic models, the corresponding numerical models are established in Matlab/Simulink. The accuracy of these models is verified by using

available experimental data and CFD simulation results from the literature.

The optimal gas EOS type and heat transfer coefficient model are determined. That is, the numerical model of the hydrogen storage tank uses the National Institute of Standards and Technology (NIST) database to calculate the hydrogen temperature and pressure, the analytical model uses the Redlich-Kwong modified gas EOS, and the new filling method in Chapter 6 adopts polynomial gas EOS. The heat transfer coefficient adopts an empirical formula model based on Reynolds number. The calculation results of different types of gas EOS and heat transfer coefficient models are compared. Using the hydrogen pressure calculated based on the NIST database as the standard, the relative error of the polynomial gas EOS is 0.30%, the Redlich-Kwong gas EOS is 1.83%, and the van der Waals gas EOS is 17.90%. That is, the accuracy of the polynomial is the highest, followed by Redlich-Kwong, and van der Waals is the lowest. Compared with the heat transfer coefficients of the empirical formula based on real-time pressure and filling time, the heat transfer coefficient of the empirical formula based on the Reynolds number has a smaller error relative to the standard heat transfer coefficient based on energy conservation.

To improve the efficiency of the hydrogen filling system, we optimize the cascade storage tank configuration and filling strategy to reduce the maximum cooling power demand and cooling energy consumption to reduce the investment cost and operating cost of the refrigeration system. The hydrogen storage tank model is extended to include the entire hydrogen filling system. Two-stage filling strategies for the single-stage filling system are proposed, including a two-stage filling speed (average pressure ramp rate) and a two-stage inlet temperature. These filling strategies can reduce the maximum cooling power by 23.8% and 16.3%, respectively. The single-stage hydrogen filling system is expanded to a three-stage cascade filling system. A multi-objective optimization method based on genetic algorithm and Pareto optimization is proposed to optimize the initial pressure and volume configuration of the low-pressure, medium-pressure and high-pressure cascade storage tank, which can reduce cooling energy consumption by 11.43%. A three-stage inlet temperature strategy for the three-stage cascade filling system is proposed, which can reduce the maximum cooling power by 16.69% to 17.38% compared with the single-stage temperature filling.

To improve the safety of the hydrogen filling system, we propose two improvements to the MC method in the SAE J2601 hydrogen refuelling protocol to improve the calculation accuracy of the target pressure and the control accuracy of the filling process. Plan I proposes an artificial neural network (ANN) model and modified formula for the MC parameter. The ANN model can overcome the problem that the original formula of the MC parameter is unsuitable for the final filling time of less than 30 s. The MC parameter calculated by the 0D1D model is used as the standard, and then the errors between the MC parameter's original formula, the ANN model and the modified formula relative to the 0D1D model are calculated. Compared to the original formula, the ANN model can reduce the relative error by 13.8% to 58.8%, and the modified formula can reduce the relative error by 16.6% to 82.3%. Plan II improves the dual-zone single-temperature model of the original MC method into a dual-zone dual-temperature model and derives the modified formula of the final hydrogen temperature, which can also overcome the problem that the original formula is unsuitable for the final filling time of less than 30 s. The final hydrogen temperature calculated by the 0D1D model is used as the standard. The errors of the final hydrogen temperature's original formula and the modified formula relative to the 0D1D model are calculated. Compared to the original formula, the modified formula can reduce the error by 2 to 7 °C.

Finally, based on the dual-zone lumped parameter thermodynamic model of the hydrogen storage tank, the analytical solutions of the final filling time and the final hydrogen temperature are derived, and a more concise new filling method is explored based on the analytical solutions. The final hydrogen temperature, pressure and state of charge (SOC) of the new filling method and the 0D1D model are compared to prove the effectiveness of the new filling method.

This thesis, which has contributed to the understanding of the mechanisms of filling processes of refuelling stations and offers pathways to improving the efficiency and safety of hydrogen filling systems, has led to the publication of 6 papers:

[1] **Luo H**, Xiao J S, Bénard P, Yang T Q, Tong L, Chahine R, Yuan Y P, Yuan C Q, Yao C L. Improvement of MC method in SAE J2601 hydrogen refuelling protocol

using dual-zone dual-temperature model. *Journal of Energy Storage*, 2024, 81: 110416. (**JCR Q1, IF=9.4**)

[2] **Luo H**, Xiao J S, Bénard P, Zong Y, Chahine R, Tong L, Yuan C Q, Yang T Q, Yuan Y P. Optimal estimation of MC parameter in SAE J2601 hydrogen refuelling protocol based on modified formula and artificial neural networks. *Fuel,* 2024, 365: 131315. (**JCR Q1, IF=7.4**)

[3] **Luo H**, Xiao J S, Bénard P, Chahine R, Yang T Q. Multi-objective optimization of cascade storage system in hydrogen refuelling station for minimum cooling energy and maximum state of charge. *International Journal of Hydrogen Energy*, 2022, 47: 10963-10975. (**JCR Q1, IF=7.2**)

[4] **Luo H**, Xiao J S, Bénard P, Chahine R, Yang T Q. Effects of filling strategies on hydrogen refueling performance. *International Journal of Hydrogen Energy*, 2024, 51: 664-675. (**JCR Q1, IF=7.2**)

[5] **Luo H**, Xiao J S, Bénard P, Yuan C Q, Tong L, Chahine R, Yuan Y P, Yang T Q, Yao C L. Thermodynamic modeling and analysis of cascade hydrogen refuelling with three-stage pressure and temperature for heavy-duty fuel cell vehicles. *International Journal of Hydrogen Energy*, 2024, 63: 103-113. (**JCR Q1, IF=7.2**)

[6] **Luo H**, Yuan C Q, Wang L, Yang T Q, Tong L, Ye F, Yuan Y P, Bénard P, Chahine R, Xiao J S. Heat transfer analysis methodology for compression hydrogen storage tank during charge-discharge cycle. *International Journal of Energy Research*, 2024, Second review. (**JCR Q1, IF=4.6**)

Keywords: Hydrogen filling, High-pressure hydrogen storage, Hydrogen safety, Refuelling protocol, Optimization

Content

Chapter 1 Introduction

1.1 Problem statement and motivation

Hydrogen energy offers tantalizing opportunities as an alternative fuel for the energy transition due to its low impact on the environment when used and its wide range of applications. It is an important carrier to achieve the ambitious goal of "carbon peaking and carbon neutrality" and to implement the national energy security strategy [1, 2]. Hydrogen Fuel Cell Vehicle (HFCV) is an important application scenario for hydrogen energy. In recent years, the marketization process of HFCV has accelerated significantly. In 2021, China's HFCV production and sales increased by 48.21% and 34.75%, respectively, compared with that of 2020. From January to October 2022, the production and sales of HFCV were 2,700 and 2,400, respectively, a year-on-year increase of 1.8 times and 1.5 times, respectively [3]. From January to October 2023, HFCV production and sales were approximately 4,000 and 4,000, respectively, with year-on-year increases of 39.8% and 54.0%, respectively [4].

HFCV usually uses 35 MPa or 70 MPa high-pressure storage tanks to store hydrogen. Safe and efficient hydrogen filling is the key to large-scale deployment of HFCV. Compared with filling gasoline and diesel vehicles, there are unique requirements when filling HFCV: the filling time of light-duty HFCV should be 3 to 5 minutes, the maximum pressure of the storage tank should be below 125% of the rated working pressure, and the maximum temperature should be below 85 ℃ [5, 6]. Research shows that four main factors cause changes in hydrogen temperature inside storage tanks. First, the compression effect caused by continued hydrogen filling. Second, the Joule-Thomson effect caused by hydrogen passing through the reduction valve. Third, the kinetic energy of the high-speed gas flow is converted into internal energy when the hydrogen passes through the injector at the tank inlet. Fourth, heat exchange occurs between hydrogen and the tank wall [7]. Excessively high temperatures can cause irreversible damage to tank wall materials or even cracking leakage and explosions.

Meanwhile, it will cause the density of the gas in the tank to decrease at the same target pressure and reduce the total mass of hydrogen. Therefore, it is necessary to conduct experimental and numerical studies on the hydrogen filling process to reveal the thermal effect mechanism and then achieve safe hydrogen filling.

The hydrogen refuelling station (HRS) is the link between the hydrogen consumption end and the production end. The high energy consumption of the hydrogen filling process is a significant problem faced by HRS. Due to the rise in temperature during the hydrogen filling process, HRS currently generally adopts the precooling filling method. That is, a refrigeration system is used to precool the hydrogen before filling it into the onboard tank. Data from HRS show that each kilogram of hydrogen consumes up to 10kW·h of cooling energy. In addition, the current utilization rate of HRS is generally low, and the daily filling amount is low, resulting in cooling energy consumption accounting for approximately 80% of the total energy consumption of HRS [8]. In addition to high operating costs such as cooling energy consumption, the investment cost of HRS is also high due to the high costs of subsystems such as compressors, refrigeration systems and dispensers. A typical HRS consists of a compressor, hydrogen storage tank, dispenser, refrigeration system and control equipment. The cost of the refrigeration system accounts for approximately 10% of the total equipment cost of the HRS [9]. Therefore, it is necessary to study the impact of different filling strategies and HRS configurations on operating costs and investment costs to achieve efficient hydrogen filling.

A safe and effective refuelling protocol is required to ensure fast and safe refuelling of HFCV, which stipulates the safety limits and control methods of the filling process, mainly controlling the pressure ramp rate (PRR) and pressure target. Currently, the hydrogen refuelling protocols commonly used in the world include the SAE J2601 refuelling protocol of the United States [5], the EN 17127 refuelling protocol of the European Union [10], the JPEC-S003 refuelling protocol of Japan [11] and the GB/T 42855-2023 refuelling protocol of China [12]. The most widely used is the SAE J2601 protocol, published by the Society of Automotive Engineers (SAE). This protocol contains two standard hydrogen filling methods: the lookup table method and the MC

method [5]. The lookup table method tabulates the relationship between the initial filling conditions and the filling control parameters in advance. In an actual hydrogen filling event, the HRS selects the required table based on the capacity category of the storage tank, the precooling temperature level of the HRS, and whether communication is needed. Then, the average pressure ramp rate (APRR) and pressure target in the table are determined based on the ambient temperature and initial pressure. APRR is used to control the filling speed, and the pressure target is used to control the filling stop [5]. PRR is a measure of the hydrogen filling speed and is used in statements related to the MC method, because the filling speed in the MC method changes dynamically during the filling process. APRR is the average value of PRR and is used in statements related to the lookup table method, because the filling speed in the lookup table method remains constant. Honda originally proposed the MC method. This method realizes the processing of the lumped heat capacity (MC) of the tank wall. The filling speed is dynamically controlled using the ambient temperature measured at the HRS, the initial pressure and initial temperature of the hydrogen in the storage tank, and the temperature and pressure of the delivered gas, making the filling speed faster. These refuelling protocols have been implemented for a shorter period. For example, the MC method in the SAE J2601 protocol was officially released in 2016, and the GB/T 42855-2023 protocol was released in 2023. Therefore, it is necessary to study and improve the hydrogen refuelling protocol and then improve the control accuracy of the filling process to achieve safe hydrogen filling.

1.2 Research background

1.2.1 Storage tank model of hydrogen filling system

The thermal effect mechanism of the hydrogen filling process can be studied through experimental and numerical methods, and the results of experimental studies can be used to verify the numerical model. In order to study the temperature changes inside and on the surface of the storage tank during the hydrogen filling process, the research team inserted a thermocouple into the storage tank through the end plug hole to measure the hydrogen temperature and installed the thermocouple on the surface of the storage tank to measure the tank wall temperature [13]. The thermocouples inside the tank are

secured to the frame with several spring steel wires, allowing each thermocouple to reach a specific location. The thermocouple wires are led out of the tank through end plugs and connected to the data acquisition system [14]. Ref. [15] developed a test device named GasTeF to test the thermal effects in high-pressure onboard hydrogen or natural gas storage tanks. Based on the GasTeF test device of Ref. [15], Ref. [16] conducted experiments on the charging-discharging cycles of onboard type III and IV high-pressure hydrogen storage tanks and measured different points inside the tanks during different charging-discharging cycles. The hydrogen temperature and the outer surface temperature of the storage tank were used to study the evolution of the hydrogen temperature during the entire cycle and the thermal response of the outer surface of the storage tank under different cycle conditions. In summary, the experimental study is to obtain hydrogen pressure and temperature data during the filling process through sensors installed inside and on the surface of the storage tank to analyze the impact of filling conditions on thermal effects. Experimental study is time-consuming, expensive and dangerous. Meanwhile, due to the diversity of HFCV, differences in the physical parameters of hydrogen storage tanks, and the complexity of the external environment, it is still necessary to establish a thermodynamic model for the hydrogen storage tank to carry out the numerical study.

Many simplified zero-dimensional lumped parameter thermodynamic models of hydrogen storage tanks have been reported in the literature for evaluating pressure and temperature changes in storage tanks [17]. Using a zero-dimensional thermodynamic model, Ref. [18] studied the effects of conditions such as initial temperature and pressure on exergy damage and exergy efficiency in the filling process based on energy and exergy methods. Refs. [19, 20] studied the influence of filling parameters such as precooling temperature, mass flow rate, ambient temperature and filling time on the thermal effect in the storage tank, respectively. Experimental studies have shown that the hydrogen temperature in the tank is relatively uniform during the filling process [14]. Therefore, for the gas zone in the storage tank, it is reasonable to use a zero-dimensional model for simulation during the hydrogen filling process. Due to the multi-layer structure of the tank wall liner and shell, the temperature distribution within the tank wall is uneven, so Ref. [21] established a one-dimensional model of the tank wall.

The one-dimensional model is more consistent with the actual situation and improves the accuracy of the model.

Experimental studies have shown that during the holding and emptying process, the buoyancy effect within the tank will lead to obvious thermal stratification, that is, the existence of local high-temperature areas and low-temperature areas [14]. At this time, the average hydrogen temperature obtained using the simplified zero-dimensional model will not be consistent with the actual situation. An effective way to solve this problem is to use computational fluid dynamics (CFD) models, including two-dimensional axisymmetric models and three-dimensional models. Ref. [22] used a two-dimensional axisymmetric model to simulate the rapid filling and holding process of 150 L onboard type III and IV storage tanks and studied the temperature rise of different types of storage tanks in different areas. Ref. [23] performed a two-dimensional axisymmetric simulation on the filling process of a 74 L hydrogen storage tank with aspect ratios of 2.4 to 8, analyzed the flow field and temperature field in the tank during the filling process, and studied the influence of tank aspect ratio on gas temperature and flow field. Ref. [24] established a two-dimensional finite volume model, studied the solution of introducing porous fillers into the storage tank to slow down the heat transfer between the gas and the tank wall and simulated and compared the spatial distribution of temperature under four different filling conditions. Compared with the two-dimensional axisymmetric model, the three-dimensional model can describe the thermal behaviour inside the tank in more detail. Ref. [25] used a CFD three-dimensional model to simulate the impact of the initial temperature on the evolution of gas temperature inside the onboard tank during the filling process to gain a deeper understanding of the impact of related phenomena such as gas compression, gas mixing and heat transfer on the evolution of gas temperature. In addition, some literature has studied the effects of injector direction, injector diameter, ambient temperature [26, 27], tank wall liner material thermal properties [28] and different turbulence models [29] on the thermal effect of hydrogen filling based on CFD models. The CFD three-dimensional model can present the fluid flow behaviour and temperature distribution in the internal space of the storage tank in more detail, but the calculation is expensive and time-consuming.

1.2.2 Parametric study of hydrogen filling system

Based on experimental and numerical studies of the hydrogen filling process, some teams have studied the impact of initial and boundary conditions on the thermal effects of the filling process. These initial and boundary conditions include ambient temperature, initial temperature, inlet temperature, initial pressure, filling speed (mass flow rate), tank type and size, etc.

Ambient temperature and initial temperature: The ambient temperature and initial temperature have a non-negligible impact on the final hydrogen temperature of the filling process. At the beginning of filling, if the initial temperature is consistent with the ambient temperature, the final hydrogen temperature will change in the same trend as the ambient temperature and have a linear relationship. For every 1 °C increase in ambient temperature, the final hydrogen temperature will increase by 0.3 °C [30]. If changes in ambient temperature do not affect the initial hydrogen temperature, they will have no significant effect on the final hydrogen temperature. Even if the ambient temperature increases by 30 °C, the final hydrogen temperature only increases by 2 °C [31]. In summary, the degree of influence of the initial temperature on the final hydrogen temperature depends on whether it changes with changes in ambient temperature.

Inlet temperature: Precooling filling technology has been widely used in the hydrogen filling process to prevent the final hydrogen temperature from exceeding the upper limit. The specific method of precooling filling is to reduce the inlet temperature through the refrigeration system. Research in Ref. [32] shows that a higher inlet temperature corresponds to a higher final hydrogen temperature, and there is a linear relationship between the inlet temperature and the final hydrogen temperature. Inlet temperature also has an impact on the average mass flow rate and the total mass of hydrogen charged. Because the higher the inlet temperature, the lower the gas density, and the smaller the amount of gas the tank can hold under the same pressure conditions. Research in Ref. [33] shows that the final state of charge (SOC) in the storage tank is strongly dependent on the inlet temperature. The reason is that the inlet temperature directly affects the incoming gas enthalpy and, thus, the final hydrogen temperature. If the main concern

is hydrogen filling safety and practical filling requirements, i.e. not exceeding the temperature limit of 85 °C and greater than 90% SOC, the lowest inlet temperature should not always be used. By adjusting the inlet temperature during the filling process, minimal cooling energy consumption and a safe SOC range can be achieved.

Initial pressure: When the HFCV returns to the HRS for refuelling, a certain amount of hydrogen will remain in the tank. The pressure of the remaining gas has an impact on the rise in temperature during the filling process. In order to better understand the impact of initial pressure, Ref. [30] simulated the hydrogen filling process with initial pressures of 2, 5, 10, 15, 20 and 25 MPa. The results show that as the initial pressure increases, the maximum temperature rise decreases. For every 1 MPa increase in initial pressure, the maximum temperature rise decreases by 2.2 °C. Ref. [14] simulated the hydrogen filling process with initial pressures of 2, 5, 10, 15, 20 and 30 MPa. The results show that the temperature rise in the storage tank is the largest when the initial pressure is 2 MPa, and the temperature rise is the smallest when the initial pressure is 30 MPa. Ref. [34] studied the temperature rise at initial pressures of 5, 15 and 25 MPa. The results show that filling with an initial pressure of 5 MPa shows the largest temperature rise while filling with an initial pressure of 25 MPa shows the smallest temperature rise. In summary, there is a linear relationship between the initial pressure and the rise in the maximum temperature. That is, the final hydrogen temperature decreases approximately linearly as the initial pressure increases.

Filling speed: SAE J2601 hydrogen refuelling protocol stipulates that the filling time of light-duty HFCV should be 3 to 5 minutes. The filling speed directly affects the filling time. Increasing the filling speed can significantly reduce the filling time, but it will shorten the time of heat transfer from hydrogen to the tank wall, thereby increasing the temperature rise in the storage tank. Therefore, a suitable filling speed is the guarantee for fast and safe hydrogen filling. Ref. [35] studied the influence of gradually increasing, constant and gradually decreasing mass flow rates on the filling effect during the filling process. The results show that the filling method with a gradually decreasing mass flow rate can reduce the maximum hydrogen temperature to a certain extent. Higher mass flow rates will lead to higher pressure losses and Joule-Thomson

effect heat, resulting in higher energy consumption and higher performance requirements for the pipeline. Ref. [36] studied the process of filling the storage tank from 10 MPa to the rated working pressure, using mass flow rates corresponding to the total filling time of 40, 190 and 370 s to study the impact of filling speed. The results show that the faster the filling speed, the higher the final hydrogen temperature, which is due to the reduced time for heat transfer between the hydrogen and the tank wall. Meanwhile, slower filling will produce significant temperature stratification in the vertical direction due to the greater effect of buoyancy at slower filling speeds. Research in Ref. [37] shows that the largest temperature rise occurs at the beginning of filling because, at this time, the pressure drop at the reduction valve is the largest, and the Joule-Thomson effect produced by throttling is the most significant. The temperature rise mainly occurs in the first stage of the filling process, so the filling process can be optimized by using a lower filling speed initially and then a larger filling speed without sacrificing the average filling mass flow rate.

Hydrogen storage tank type and size: Currently, HFCV generally uses type III and IV hydrogen storage tanks. The liner material of the type III storage tank is aluminum alloy, which has high thermal conductivity. The liner material of type IV storage tanks is plastic, which has low thermal conductivity. The shell material of both tanks is carbon fibre composite. Ref. [25] used type III and type IV storage tanks, respectively, to carry out filling experiments under three different initial temperature conditions of 20, 40 and 50 °C. The results show that the temperature change trend in the two tanks is the same, but because the thermal conductivity of the aluminum alloy liner is much higher than that of the plastic, the final hydrogen temperature in the type III tank is lower. Ref. [33] used two different types of storage tanks, type III and type IV, to conduct filling experiments with different inlet temperatures and mass flow rates. The results show that the final SOC of type III tanks is higher than that of type IV. The effects of mass flow rate and inlet temperature on SOC are stronger in type IV tanks than in type III tanks. The reason is that the liner material of type III storage tanks is aluminum alloy with stronger thermal conductivity, so its final hydrogen temperature is lower than that of type IV storage tanks. In order to study the influence of storage tank size on the thermal effect inside the storage tank, Ref. [14] selected a 150 L large-

volume storage tank with a length of 1652 mm and an inner diameter of 376 mm for comparison with a 74 L small-volume storage tank. The results show that the hydrogen temperature distribution in the large-volume 150 L storage tank is uneven, gradually increasing along the axial direction, with the highest temperature at the tail and the lowest temperature near the inlet. The temperature uniformity in the small-volume 74 L storage tank is good. Therefore, a large-volume storage tank with an excessively large aspect ratio will cause local temperatures to be too high, while a small-volume storage tank with a smaller aspect ratio is more conducive to the safe filling of hydrogen.

Some teams have focused on analyzing the factors that influence hydrogen filling performance, including the total mass of hydrogen in the storage tank, storage density, SOC, and cooling energy consumption of the refrigeration system.

Ref. [38] studied the influence of various filling parameters on the total mass of hydrogen. The results show that the initial pressure, precooling temperature and mass flow rate of the onboard tank are the most important factors affecting the total mass of hydrogen. There is a linear or inverse relationship between the total mass of hydrogen and these three factors. Ref. [39] studied the impact of various filling parameters on the storage density of onboard tanks, further analyzed the root causes, and discussed the impact of various filling parameters on improving storage density. The results show that filling time, inlet temperature and initial pressure have significant effects on storage density, while the effects of initial temperature and filling speed are negligible. Ref. [33] studied the effects of inlet temperature and mass flow rate on onboard tank SOC. The results show that SOC strongly depends on the inlet temperature, especially for type IV tanks. In addition, it is unnecessary to use a minimum precooling temperature of −40 °C throughout the filling process to prevent the final hydrogen temperature from being higher than the upper limit. Ref. [40] established a comprehensive model of HRS to evaluate energy consumption. The results show that compared with using one station-side storage tank, using three cascade storage tanks in an HRS can save about 34% of total energy consumption. The total energy consumption of the three-stage cascade HRS increases linearly with the increase in the initial pressure of the high-pressure storage tank. Ref. [41] conducted an optimization

study with the hydrogen utilization rate and filling time of the station-side storage tank as the optimization objectives and proposed a multi-objective optimization filling algorithm to improve the hydrogen utilization rate and filling speed. Ref. [42] proposed a unique cascade-filling control mechanism. By alternately using three cascade storage tanks in the order of pressure reduction, the daily filling capacity of the HRS can be increased by 5%. Ref. [43] summarized the impact of hydrogen filling parameters on filling performance and measures to reduce temperature rise.

1.2.3 Filling strategy optimization of hydrogen filling system

In addition to filling initial/boundary conditions such as ambient temperature, initial temperature, inlet temperature, initial pressure, filling speed (mass flow rate), tank type and size, etc., different filling strategies will also affect the performance of hydrogen filling.

Variable filling speed strategy: Hydrogen filling research generally adopts a constant mass flow rate, but the impact of variable mass flow rate on the thermal effects of filling has also aroused the interest of some teams. Ref. [35] explored the effect of variable mass flow rate on the temperature of hydrogen in the onboard tank based on the CFD model. The results showed that the filling strategy with a gradually increasing mass flow rate had the lowest temperature rise compared with a gradually decreasing or constant mass flow rate. Ref. [44] analyzed the thermal effects of the tank emptying process. The lowest temperature in the tank using the "first slow and then fast" emptying mode is lower than that of the "constant speed" emptying mode. The lowest temperatures of the " first fast and then slow" and " constant speed" emptying modes are close. The temperature curve of the "alternative" emptying mode oscillates around the temperature curve of the "constant speed" emptying mode. Changing the emptying pattern may not be an effective way to reduce hydrogen temperature and tank wall temperature. Ref. [7] proposed a two-stage delayed filling method to reduce the temperature rise in the storage tank and reduce the filling time. The results show that if the total pause delay duration during filling is constant, the moment of the two pauses has a negligible effect on the final hydrogen temperature. Compared with the constant mass flow rate filling strategy, this strategy can complete filling within 155 seconds,

saving 62% of filling time.

Variable filling pressure strategy: During the filling process, the filling speed can be controlled by the mass flow rate or pressure ramp rate (PRR). Different PRRs will produce different filling pressures. Ref. [45] studied the effects of variable filling pressure and inlet temperature on the maximum hydrogen temperature, cooling energy and SOC. The results show that compared with precooling during the entire filling process, the cooling energy can be reduced by 60% by adopting a filling strategy of precooling in the second stage and approximately linear pressure rise. Ref. [46] studied the effect of variable PRR on the final hydrogen temperature in the onboard tank. The results show that different variable PRRs affect the temperature profile but do not reduce the final hydrogen temperature and pressure during the filling process, so the final filling mass does not change significantly. The variable filling pressure strategy that changes the PRR can be achieved by controlling the opening of the reduction valve in the dispenser. Another variable filling pressure strategy is to change the pressure of the hydrogen source, that is, the cascade filling method. Single-stage filling means that the HRS uses a single storage tank to provide hydrogen for filling HFCV, while cascade filling means that the HRS uses multiple station-side storage tanks. Cascade filling first uses a low-pressure storage tank to provide hydrogen filling, then a medium-pressure storage tank, and finally a high-pressure storage tank. Ref. [47] studied the performance of single-stage, two-stage and three-stage cascade filling. Compared with single-stage filling, the hydrogen circulation amount of two-stage and three-stage filling can be reduced by 24.5% and 29.7%, respectively. In terms of energy consumption of the refrigerator, the three-stage cascade filling saves more than 20% of energy. In terms of energy consumption of the compressor, since single-stage filling adopts the method of complete decompression and then compression, the energy consumption is the largest, while two-stage and three-stage filling can save energy by 39.3% and 55.2%, respectively. Increasing the number of station-side cascade storage tanks can significantly reduce energy consumption, but considering the complexity of the system, the number of station-side cascade storage tanks generally does not exceed three.

Variable precooling temperature strategy: Precooling filling is an effective means to

ensure that the final hydrogen temperature is within a safe range. During a single hydrogen filling process, the precooling temperature is usually kept constant, and the precooling temperature is set lower than the actual demand to reserve a certain safety margin, thus resulting in excessive cooling energy consumption. Ref. [45] considered four precooling strategies. That is, during the hydrogen filling process, the time to precool the hydrogen to −40 °C was set to the first 10 s (Case A), the first 30 s (Case B), the first 100 s (Case C) and the last 100 s (Case D), respectively. The results show that in cases A and B, once the hydrogen precooling is stopped, the temperature of the hydrogen in the storage tank will rise rapidly, and eventually, the hydrogen temperature will exceed the allowed maximum value. In Case C, extending the precooling to the first 100 s will be enough to limit the final hydrogen temperature from exceeding the allowed maximum. If precooling is performed within the last 100 s (Case D), the final hydrogen temperature is close to Case C. Comparison of precooling energy consumption in various cases shows that maintaining −40 °C precooling during the entire filling process is unnecessary. Precooling for half the time is sufficient, which can significantly reduce cooling energy. Precooling is more effective in the second half of filling than in the first half.

1.2.4 Configuration optimization of hydrogen filling system

Some teams have further established a more comprehensive model of HRS [48], including models of compressors, single-stage/cascade storage tanks, refrigerators and reduction valves, to optimize the configuration of HRS from the system level and then reduce the energy consumption of HRS and achieve efficient hydrogen filling.

The research in Ref. [49] shows that in the cascade filling system, many factors will affect the cooling energy consumption. Cooling energy consumption is a function of the number of cascade tanks, initial pressure and volume. As the number of cascade storage tanks increases, the total energy consumption of the system decreases [49, 50]. However, to simplify system design, the number of cascade tanks should be less than or equal to three. The initial pressure of the cascade storage tank is also an important factor affecting cooling energy consumption, but the impact of low-pressure, medium-pressure and high-pressure cascade storage tanks on cooling energy consumption is

different. High-pressure cascade storage tanks have a greater impact on cooling energy consumption [40, 51]. As the initial pressure of high-pressure cascade storage tanks increases, the total energy consumption increases almost linearly [40]. Research in Ref. [47] shows that in the range of 1 to 4 m^3 and 20 to 50 MPa, the use of smaller volume low-pressure tanks can reduce cooling energy consumption. In the range of 1 to 3 m^3 and 45 to 60 MPa, medium-pressure storage tanks have little impact on energy consumption. The total volume of cascade tanks is another important factor affecting cooling energy consumption [52, 53]. Research in Ref. [21] shows that as the total volume of cascade storage tanks increases, cooling energy consumption increases. For the cascade storage tanks with the best and worst volume configurations, the energy savings are approximately 12% and 20%, respectively, when the average ambient temperature is 20 °C and 30 °C. In addition, other factors also affect cooling energy consumption, such as pressure losses on the vehicle side and pressure switching coefficients of cascade tanks in HRS. Research in Refs. [54, 55] shows that vehicle-side pressure loss is the main factor that determines cooling requirements, and using cascade storage tanks instead of a single storage tank can reduce cooling energy consumption by about 12%. Research in [56] shows that the entropy increase of a single-stage hydrogen filling system is 55% greater than that of a cascade hydrogen filling system. Therefore, the cascade filling system is more promising than the single-stage filling system.

The above optimization study generally adopts the generalized optimization method of parametric study. The specific implementation process is to change the parameter variables from one level to another level, thereby forming multiple test cases, measuring the objective function under each test case, and finally drawing general conclusions. Some teams have pioneered the introduction of machine learning methods to optimize processes such as hydrogen filling and hydrogen production.

Ref. [41] established a three-stage cascade hydrogen filling system model and proposed an optimization algorithm to improve the filling speed and hydrogen utilization rate. The results show that the optimization algorithm can significantly improve hydrogen utilization and allow filling to be completed within an acceptable time range. Ref. [57]

proposed a multi-objective iterative optimization algorithm to optimize the two controllable variables of pressure switching coefficient and precooling temperature. The results show that this optimization algorithm can significantly reduce energy consumption and increase SOC within an acceptable filling time range. Ref. [58] built a numerical model of a hydrogen storage tank based on the Matlab/Simulink software platform, simulated the hydrogen filling process, and then used the results of the numerical model of the hydrogen storage tank to train artificial neural networks (ANN), and obtained the corresponding regression model. Finally, a nonlinear programming method was used to determine the optimal ranges of precooling temperature, filling time, initial pressure and initial temperature with the goal of reducing precooling energy consumption. The results show that when the filling time is less than 183 s, and the inlet temperature is 259.99 to 266.58 K, the energy consumption can be effectively reduced by about 2.5%. Ref. [59] established the ANN-based relationship between the decision variables (reactor temperature and St/Cu molar ratio) and the objective function (hydrogen production operating cost and exergy efficiency). Then, the genetic algorithm (GA) is used to optimize decision variables, minimize hydrogen production operating costs and maximize exergy efficiency. Ref. [60] conducted an economic evaluation of a four-step Mg-Cl hydrogen production cycle and used a genetic algorithm to optimize the cycle process to reduce the cost of hydrogen production and determine the optimal decision variables. Refs. [61, 62] used a genetic algorithm to optimize the four-step Cu-Cl hydrogen production cycle to reduce the cost of hydrogen production.

1.2.5 Hydrogen refuelling protocol

Although the thermal effects of the hydrogen filling process have been intensively studied experimentally and numerically, it is not feasible to build a model of the actual tank in the field to determine the appropriate filling speed during an actual hydrogen filling event. Because the environmental conditions, dimensions of onboard storage tanks, and physical properties of materials in real-life scenarios are complex and uncertain. Therefore, a standard and reliable hydrogen refuelling protocol is needed.

In 2010, SAE introduced the light-duty HFCV hydrogen refuelling protocol SAE J2601

[63], which introduced a table-based filling approach, named the lookup table method, that became standardized in 2014. Based on the capacity levels of onboard tanks (2 to 4, 4 to 7, and 7 to 10 kg), dispenser interface type (communicative or not), precooling temperature categories of the HRS (*T*40, *T*30, and *T*20), and delivery pressure categories (70 and 35 MPa), 54 distinct tables (42 standard tables and 12 optional cold dispenser tables) were predetermined. Subsequently, the average pressure ramp rate (APRR) within the selected table, employed to regulate filling speed, was determined according to the ambient temperature, while the pressure target within the selected table, utilized to govern the filling cessation, was established based on the ambient temperature and initial pressure. The lookup table method is categorized into non-communication and communication methods. Both methods utilize the same APRR, differing only in their utilization of hydrogen temperature and pressure data measured by sensors to calculate SOC for communication filling, which halts filling under pressure conditions corresponding to 95 to 100% SOC. Conversely, non-communication filling utilizes the pressure target chosen from the table to cease filling.

Communication filling encompasses top-off filling, fallback procedures, and cold dispenser filling techniques. When the initial pressure within the onboard tank falls below 5 MPa, the dispenser initially employs a higher APRR for filling until the tank pressure reaches the intermediate level. Subsequently, the dispenser switches to a lower APRR until a higher top pressure target is achieved. The pressure drop between the dispenser outlet and the onboard tank is directly proportional to the mass flow rate. Consequently, employing a lower APRR towards the end of filling brings the tank pressure closer to that at the dispenser outlet, thereby enhancing the final SOC. The fallback procedure serves as a filling alternative for specific circumstances. For instance, for an HRS with a precooling category of *T*40, if the precooling temperature falls within the anticipated range of −40 to −33 °C after 30 s of filling, the initial APRR continues to regulate the filling process. Otherwise, initiation of the fallback procedure occurs, with a switch to a lower APRR for filling control. The cold dispenser filling method is utilized when the HRS consistently refills HFCVs, with temperatures of each HRS component sufficiently low. Here, the cold dispenser optional table aids in identifying a higher APRR for filling control, thus optimizing filling time [5].

The SAE J2601 hydrogen refuelling protocol, introduced in 2014, released a non-standardized approach known as the MC method [64], which underwent standardization in 2016 [65]. Initially developed by Honda, this method utilizes the parameter MC to denote the mathematical structure or lumped heat capacity of the tank wall's characteristic volume. Utilizing formulas and coefficients established through the zero-dimensional gas one-dimensional tank wall (0D1D) model, the MC method computes both the pressure ramp rate (PRR) and pressure target. The PRR of the MC method varies based on the hydrogen temperature at the HRS outlet. Employing an adaptive control strategy, the MC method dynamically calculates the PRR within the precooling temperature range of −40 to −17.5 °C without requiring division into specific temperature categories such as *T*40 (−40 to −33 °C), *T*30 (−33 to −26 °C), and *T*20 (−26 to −17.5 °C), thereby enhancing the flexibility in HRS design [66]. For both communication and non-communication refuelling, the MC method employs identical formulas and coefficients for PRR calculation, albeit utilizing distinct methodologies for determining the pressure target. In communication refuelling, the pressure target determination method mirrors that of the lookup table method, while in non-communication refuelling, it combines the calculated final hydrogen temperature with the SOC target. Essentially, the MC method employs a simplified hydrogen storage tank model to derive the formula for the final hydrogen temperature, incorporating the parameter MC. Through extensive analysis of MC simulation data derived from the 0D1D model under various initial and boundary conditions, two formulas for the parameter MC were proposed by SAE, with the latter demonstrating improved accuracy over the former [5, 67]. The precision of the parameter MC holds significance as it directly influences the accuracy of calculating the final hydrogen temperature and pressure target, thereby impacting the control precision of the filling process and, consequently, the safety of refuelling.

Both the lookup table method and MC method underwent validation via simulation and field testing [68, 69], albeit development occurred under the two most extreme operational conditions: high-temperature and low-temperature environments. For instance, in developing the MC method, simulations utilized a 25 L type III storage tank, known as a cold tank, to determine the coefficients of the MC parameter formula

[5]. The cold tank possesses a small volume-to-area ratio, and its aluminum alloy liner exhibits high thermal conductivity. Consequently, heat influx is minimal, while the dissipation area is substantial, leading to rapid heat dissipation and limited temperature elevation within the cold tank. When applying the MC method, developed using a cold tank, to regulate actual filling processes, the outcome tends to be conservative due to the lower heat dissipation capacity of typical onboard tanks compared to cold tanks. In the case of the non-communication MC method, the pressure target derives from the final hydrogen temperature obtained through a simplified tank model, necessitating several assumptions throughout the calculation process. Variations in initial tank temperature and ambient temperature, induced by factors like sunlight exposure or tank depletion, necessitate the incorporation of hot soak or cold soak assumptions to guard against worst-case scenarios, thereby introducing a safety margin concerning temperature and pressure and resulting in a conservative filling outcome.

Limited research exists on hydrogen refuelling protocols, particularly regarding the MC method within the SAE J2601 protocol, possibly due to its official release occurring only in 2016. As of the current writing, merely two studies have addressed both the lookup table method and the MC method. In 2017, Ref. [70] employed the H2SCOPE model to compare the SOC and filling time associated with these two methods. Subsequently, in 2020, Ref. [71] assessed the filling time, SOC, and overall energy consumption pertaining to the lookup table method and MC method. Additionally, several teams have endeavoured to devise novel refuelling protocols. For instance, Ref. [72] utilized a real-time response approach to develop a communication-based hydrogen refuelling protocol, optimizing filling time, precooling requirement, and energy consumption.

1.3 Summary of research status

To sum up, although some teams have carried out extensive and in-depth research on hydrogen storage tank modelling, parameter studies of initial/boundary conditions, filling strategy optimization, system configuration optimization, hydrogen refuelling protocol, etc., there are still problems in the following aspects.

In terms of parametric study on hydrogen filling system: existing research generally focuses on the impact of the initial and boundary conditions of hydrogen filling (ambient temperature, initial temperature, inlet temperature, initial pressure, filling speed, tank type and size) on thermal effects, while there are few studies on the influence of the gas equation of state (EOS) on the thermal effects of hydrogen filling. There are many types of gas EOS, such as ideal gas EOS, Abel-Nobel gas EOS, van der Waals gas EOS and their modified forms of Redlich-Kwong, Soave and Peng-Robinson, etc. Research on the impact of different types of gas EOS on the thermal effects of hydrogen filling needs to be strengthened. According to relevant knowledge of heat transfer, the heat transfer coefficient between hydrogen in the storage tank and the tank wall has a greater impact on the thermal effect in the storage tank, but there are few studies on the heat transfer coefficient model. Therefore, it is necessary to study the impact of different types of gas EOS and heat transfer coefficient models on the thermal effect of hydrogen filling to determine the optimal gas EOS type and heat transfer coefficient model to improve the accuracy of the hydrogen filling system model established in this thesis, improve the efficiency and safety of hydrogen filling.

In terms of study on filling strategy optimization: existing filling strategy optimization generally focuses on reducing the temperature rise in the storage tank, increasing the SOC in the storage tank, reducing the filling time and reducing the energy consumption of the compressor and refrigeration system. The energy consumption of the compressor and refrigeration system is an operating cost, and the purchase cost of the equipment itself is an investment cost. Literature research shows that there are few studies on reducing the maximum cooling power demand of the refrigeration system to reduce the investment cost of HRS. Therefore, it is necessary to study efficient hydrogen filling strategies to reduce the maximum cooling power demand of the refrigeration system, reduce the investment cost of HRS, and improve the efficiency of hydrogen filling.

In terms of study on configuration optimization of hydrogen filling system: Literature research shows that the cascade hydrogen filling system consumes less energy than the single-stage filling system and is more promising. Some teams have studied the optimal number of cascade tanks, initial pressure, and volume configuration using a generalized

optimization method of the parametric study. The parametric study method generally can only obtain qualitative conclusions. Some teams have introduced optimization methods such as machine learning and artificial intelligence, but they are generally single-objective optimization and cannot find the optimal solution to two objective functions at the same time. This thesis will establish a regression model of the hydrogen filling system based on machine learning methods and then combine it with artificial intelligence algorithms to carry out multi-objective optimization, which can quantitatively find the optimal cascade tank volume and initial pressure configuration to minimize cooling energy consumption and maximize the SOC of the storage tank and then improve the efficiency of hydrogen filling.

In terms of hydrogen refuelling protocol: For the MC method in the existing SAE J2601 hydrogen refuelling protocol, the accuracy of the MC parameter is very important, which determines the calculation accuracy of the final hydrogen temperature and pressure target and then determines the accuracy of the filling control process. During the development process of the MC method, SAE determined two formulas for MC parameters by fitting simulation data. However, the goodness of fit obtained when fitting the first term of the formula was relatively small, so the MC parameter formula has the potential to be improved. Meanwhile, in the development process of the MC method, a dual-zone single-temperature model was used. That is, it was assumed that the hydrogen temperature and the tank wall temperature were equal. In the actual hydrogen filling process, there is a significant difference between the hydrogen temperature and the tank wall temperature. Therefore, it is necessary to improve the MC method by using a dual-zone dual-temperature model that distinguishes hydrogen temperature and tank wall temperature. In the development and use of the lookup table method and MC method, a large number of tables, formulas and coefficients are involved, so it is also necessary to develop a more concise filling method.

1.4 Research contents and methods

In view of the current lack of research on hydrogen filling system modelling, optimization and protocols, combined with our team's early research on hydrogen filling [20, 58, 73, 74], this thesis takes the hydrogen filling system as the study object.

Then, it conducts in-depth research on the modelling, parametric study, filling strategy, system configuration optimization, and hydrogen refuelling protocols to improve the efficiency and safety of hydrogen filling.

(1) Hydrogen storage tank model of hydrogen filling system: The single-zone, dual-zone, triple-zone and zero-dimensional gas one-dimensional tank wall (0D1D) lumped parameter thermodynamic models of hydrogen storage tanks were established. In order to be more convenient in engineering applications, we solved the mathematical and physical equations of the lumped parameter thermodynamic model of the hydrogen storage tank, derived the corresponding analytical models of the hydrogen storage tank, and used M language to write the analytical models in the Matlab Function module. Then, based on the mathematical and physical equations of the hydrogen storage tank thermodynamic models, we established the corresponding numerical models in the Matlab/Simulink platform. Finally, we verified the accuracy of the analytical models and numerical models of the hydrogen storage tank based on the experimental data and CFD simulation results of the references. The applicability of each hydrogen storage tank model in this thesis was determined by combining the model's accuracy with actual needs. Please see Chapter 2.

(2) Parametric study on the hydrogen filling system: In order to improve the accuracy of the established hydrogen storage tank model, the initial/boundary conditions that affect the thermal effects in the storage tank during the hydrogen filling process, the different gas EOS and heat transfer coefficient models used in the modelling process were studied. The critical point experimental value was used to identify the parameters in the gas EOS. The Joule-Thomson inverse curve was used to test the accuracy of the modified gas EOS in the form of Redlich-Kwong, Soave and Peng-Robinson. The influence of polynomial gas EOS, van der Waals gas EOS and its modified forms on the thermal effect in the storage tank was compared. The calculation method of the heat transfer coefficient based on energy conservation was used to identify the parameters in the heat transfer coefficient of the empirical formula. The influence of different heat transfer coefficient models based on Reynolds number, real-time pressure and filling time on the thermal effect in the storage tank was compared. The influence of

constant/variable mass flow rate and heat transfer coefficient on the thermal effect in the storage tank was compared. The optimal gas EOS and the heat transfer coefficient model applicable to each research content in this thesis were determined. Please see Chapter 3.

(3) Optimization study on single-stage and cascade hydrogen filling systems: We established reduction valve, heat exchanger and pressure drop models to extend the hydrogen storage tank model to the entire hydrogen filling system, including single-stage and three-stage cascade filling systems. For a single-stage hydrogen filling system, a two-stage average pressure ramp rate (APRR) filling strategy is proposed under the condition that the inlet temperature is set constant, and a two-stage inlet temperature filling strategy is proposed under the condition that the APRR is set constant. For the three-stage cascade hydrogen filling system, we first used a machine learning artificial neural network (ANN) to establish the ANN model of the hydrogen filling system. Then, we used genetic algorithm (GA) and Pareto to conduct multi-objective optimization, including optimizing initial pressure and volume configuration of low-pressure, medium-pressure and high-pressure cascade storage tanks. When generating the data set for training ANN, an orthogonal experiment method is used to reduce the number of runs of the Simulink model. A three-stage inlet temperature filling strategy was proposed. The performance of the single-stage and cascade filling methods was compared. This part of the research will help improve the efficiency of the hydrogen filling system. Please see Chapter 4.

(4) Research on hydrogen refuelling protocol: Two improvements to the MC method in the SAE J2601 refuelling protocol are proposed. One is to improve the calculation formula of the MC parameter in the MC method, and the second is to improve the calculation formula of the final hydrogen temperature in the MC method. For the proposed ANN model of the MC parameter, in order to ensure the randomness and accuracy of generating ANN training set data, Latin hypercube sampling (LHS) is used to sample the filling conditions randomly. The artificial intelligence GA is used to optimize the initial weight and bias of the ANN to improve the prediction accuracy of the ANN model. In order to determine the importance of each filling condition to the

MC parameter, the Sobol sensitivity analysis method based on variance is used. For the calculation formula of the final hydrogen temperature in the MC method, the dual-zone dual-temperature model, which distinguishes the hydrogen temperature and tank wall temperature, is used to replace the dual-zone single-temperature model of the original MC method to derive the correction formula for the final hydrogen temperature. Meanwhile, the simulation data of the 0D1D model is used to fit the correction factor. This part of the research will help improve the safety of the hydrogen filling system. Please see Chapter 5.

Based on the dual-zone lumped parameter thermodynamic model of the hydrogen storage tank, the analytical solution of the final hydrogen temperature and filling time is derived, and a new filling method based on the analytical solution is proposed. The simulation results of the new filling method are compared with the results of the 0D1D model to verify the effectiveness of the new filling method. Please see Chapter 6.

Combined with the research content, the technology roadmap of this thesis is shown in Fig. 1.1.

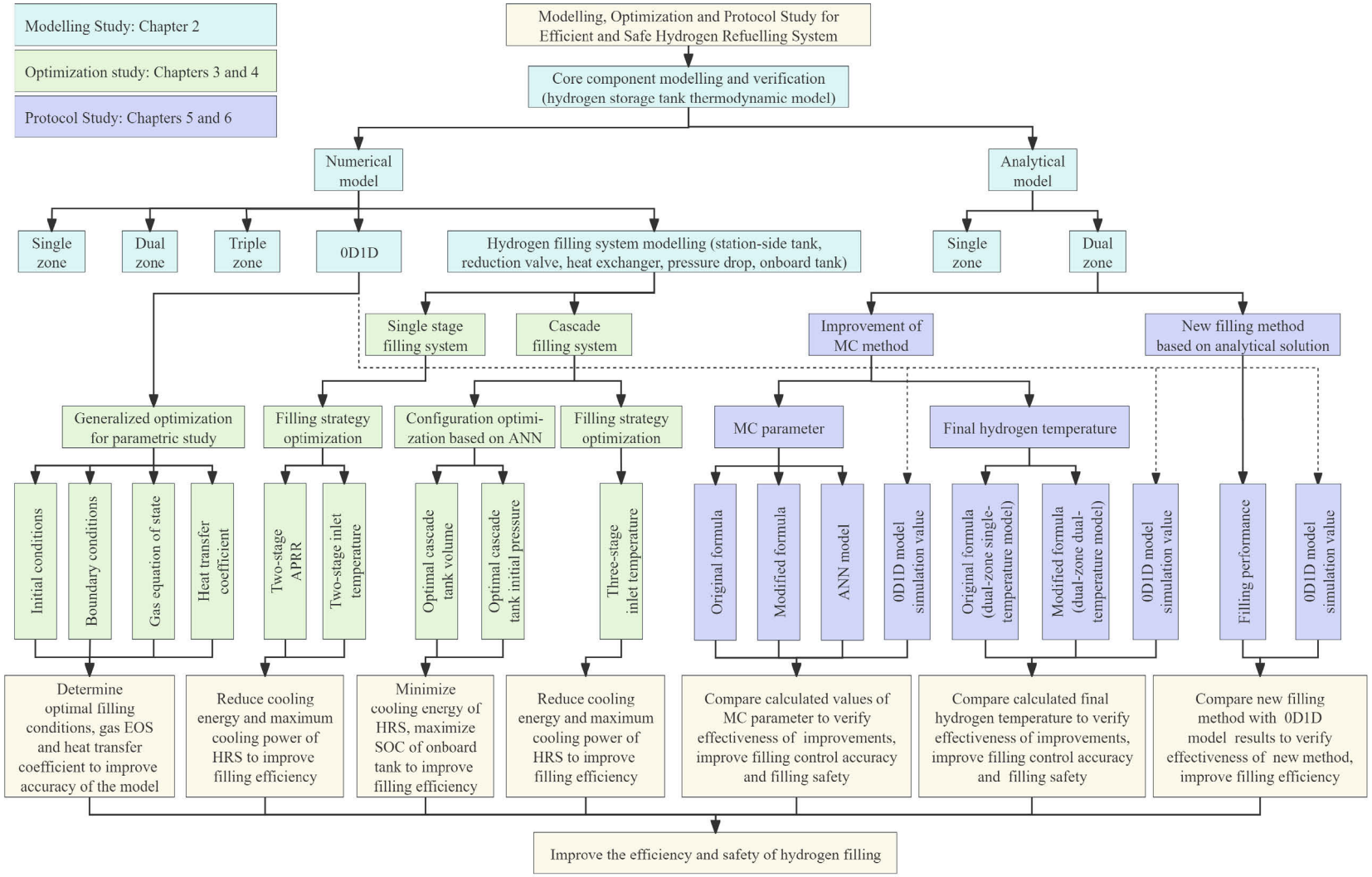

Fig. 1.1 Technology roadmap of this thesis.

Chapter 2 Hydrogen storage tank model of hydrogen filling system

The literature study in the previous chapter shows that the thermal effects of the hydrogen filling process have been extensively studied experimentally. However, considering the differences in hydrogen storage tank parameters and the complexity of the environment, it is still necessary to establish the hydrogen storage tank models to conduct research in more scenarios. Meanwhile, the hydrogen storage tank models established in this chapter are applicable to both onboard tanks and station tanks and will be the basis for research in subsequent chapters. This chapter will establish the thermodynamic model, analytical model and numerical model of the hydrogen storage tank during the hydrogen filling process based on the mass and energy conservation equations of hydrogen, the energy conservation equation of the tank wall and the real gas equation of state (EOS).

2.1 Thermodynamics and heat transfer model of hydrogen storage tank

According to the principle from simple to complex and ideal to practical, the structure of the hydrogen storage tank is simplified into four types. The first is only to consider the hydrogen zone and consider the temperature distribution in the hydrogen zone to be uniform. That is, we ignore the impact of the tank wall on the temperature of the hydrogen in the tank and consider that the hydrogen directly exchanges heat with the environment. At this time, the thermodynamic model is defined as a single-zone single-temperature model. The second is to consider both the hydrogen zone and the tank wall zone, considering that the temperature distribution in the hydrogen zone is uniform and that the tank wall is a single-layer zone with uniform temperature distribution. At this time, the thermodynamic model is defined as a dual-zone dual-temperature model. The third is to consider that the hydrogen storage tank wall has a two-layer structure of liner and shell. The temperature distribution of each layer of the liner and shell is uniform. At this time, the model has a hydrogen zone, a tank wall liner zone, and a tank wall

shell zone, and it is defined as a triple-zone triple-temperature model. The fourth is that the tank wall is a multi-layer structure, and heat is conducted in each layer along the radial direction. The temperature distribution of each cylindrical layer is uniform. At this time, the thermodynamic model is defined as a zero-dimensional gas one-dimensional tank wall model (0D1D).

2.1.1 Single-zone lumped parameter thermodynamic model

It is assumed that the influence of the tank wall on the hydrogen is ignored. That is, the hydrogen directly exchanges heat with the environment. The experimental study in Ref. [14] shows that the temperature in the storage tank is relatively uniform during the hydrogen filling process. Therefore, it is reasonable to consider the hydrogen temperature to be uniform during hydrogen filling. The structure of the single-zone single-temperature lumped parameter model of the storage tank is shown in Fig. 2.1.

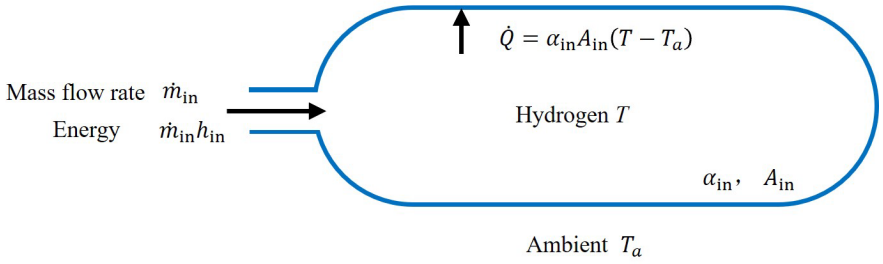

Fig. 2.1 Single-zone single-temperature lumped parameter thermodynamic model of hydrogen storage tank.

The mass conservation of hydrogen in the single-zone lumped parameter thermodynamic model can be expressed as [73]

$$\frac{\mathrm{d}m}{\mathrm{d}t} = \dot{m}_{\mathrm{in}} \tag{2.1}$$

where m is the mass of hydrogen in the storage tank (kg). $\dot{m}_{\mathrm{in}}$ the mass flow rate of hydrogen (kg/s).

During the hydrogen filling process, four factors will cause the temperature of the hydrogen in the tank to change. First, the continuous filling of hydrogen causes the gas in the tank to compress. Secondly, the Joule-Thomson effect caused by throttling when hydrogen passes through the reduction valve. Third, when the hydrogen passes through the injector at the inlet of the hydrogen storage tank, the kinetic energy of the high-

speed gas flow is converted into internal energy. Fourth, heat exchange occurs between hydrogen and the inner wall of the storage tank. Therefore, the energy conservation of hydrogen can be expressed as [73]

$$\frac{\mathrm{d}(mu)}{\mathrm{d}t} = \dot{m}_{\mathrm{in}} h_{\mathrm{in}} - \dot{Q} \tag{2.2}$$

where u is the specific internal energy of hydrogen (J/kg). h_{in} is the specific enthalpy of hydrogen inflow (J/kg). $\dot{Q}$ is the heat exchange rate between hydrogen and the ambient (W). The single-zone model considers hydrogen to exchange heat with the ambient directly, that is, ignoring the impact of the tank wall on the hydrogen in the tank. According to Newton's law of cooling, it can be expressed as

$$\dot{Q} = \alpha_{\mathrm{in}} A_{\mathrm{in}} (T - T_a) \tag{2.3}$$

Substituting Eq. (2.3) into Eq. (2.2), the energy conservation of hydrogen in the single-zone lumped parameter thermodynamic model can be expressed as [73]

$$\frac{\mathrm{d}(mu)}{\mathrm{d}t} = \dot{m}_{\mathrm{in}} h_{\mathrm{in}} - \alpha_{\mathrm{in}} A_{\mathrm{in}} (T - T_a) \tag{2.4}$$

where $\dot{m}_{\mathrm{in}}$ is the mass flow rate of hydrogen inflow (kg/s). h_{in} is the specific enthalpy of hydrogen inflow (J/kg). T and T_a are the temperatures of hydrogen and the ambient (K), respectively. A_{in} is the surface area of the inner wall of the storage tank (m^2). α_{in} is the heat transfer coefficient between hydrogen and the ambient ($W/m^2/K$).

2.1.2 Dual-zone lumped parameter thermodynamic model

In actual situations, both hydrogen and air will exchange heat with the tank wall through thermal convection. The heat inside the tank wall will be transferred by thermal conduction. It is assumed that there is no temperature gradient inside the hydrogen storage tank wall. That is, the tank wall temperature is uniform. The model at this time includes the hydrogen zone and the tank wall zone. There are two temperatures: hydrogen temperature and tank wall temperature. The model is defined as a dual-zone dual-temperature model, as shown in Fig. 2.2. The mass conservation of hydrogen in the dual-zone lumped parameter thermodynamic model is consistent with the single-

zone lumped parameter thermodynamic model.

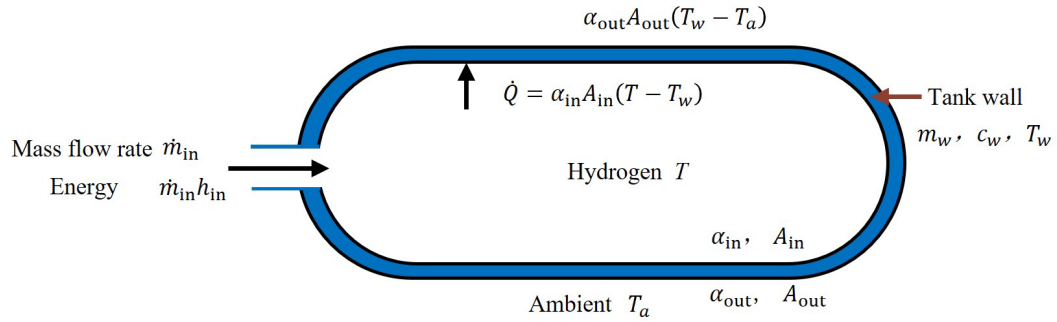

Fig. 2.2 Dual-zone dual-temperature lumped parameter thermodynamic model of hydrogen storage tank.

At this time, the hydrogen and the inner wall of the storage tank will exchange heat through thermal convection. The energy conservation of hydrogen can be expressed as [74]

$$\frac{\mathrm{d}(mu)}{\mathrm{d}t} = \dot{m}_{in}h_{in} - \alpha_{in}A_{in}(T - T_w) \tag{2.5}$$

where $\dot{m}_{in}$ is the mass flow rate of hydrogen inflow (kg/s). h_{in} is the specific enthalpy of hydrogen inflow (J/kg). T and T_w are the temperatures of hydrogen and the tank wall (K), respectively. A_{in} is the surface area of the inner wall of the storage tank (m^2). α_{in} is the heat transfer coefficient between hydrogen and the inner wall of the storage tank ($W/m^2/K$).

At this time, on the one hand, the tank wall and hydrogen conduct convective heat exchange, and on the other hand, the tank wall and air conduct convective heat exchange. The energy conservation of the tank wall can be expressed as [74]

$$\frac{\mathrm{d}(m_w c_w T_w)}{\mathrm{d}t} = \alpha_{in}A_{in}(T - T_w) - \alpha_{out}A_{out}(T_w - T_a) \tag{2.6}$$

where c_w is the specific heat capacity of the tank wall (J/kg/K). m_w is the mass of the tank wall (kg). T, T_w and T_a are the temperatures of hydrogen, the storage tank wall and the ambient (K), respectively. α_{in} is the heat transfer coefficient between hydrogen and the inner wall of the storage tank ($W/m^2/K$). α_{out} is the heat transfer coefficient

between the outer wall of the storage tank and the air (W/m^2/K). A_{in} is the surface area of the inner wall of the storage tank (m^2). A_{out} is the surface area of the outer wall of the storage tank (m^2).

2.1.3 Triple-zone lumped parameter thermodynamic model

In actual situations, the liner material of the tank wall of a type III hydrogen storage is aluminum alloy, and the shell material is carbon fibre composite material. The liner material of the tank wall of a type IV hydrogen storage tank is plastic, and the shell material is the same as that of a type III hydrogen storage tank. Because of the difference in materials of the liner and shell of the hydrogen storage tank, there are also differences in thermal conductivity, which will cause a temperature gradient along the radial direction of the tank wall. Therefore, the liner and shell can be considered separately as two zones. At this time, there is a hydrogen zone, a tank wall liner zone, and a tank wall shell zone. Assuming that the temperatures in the liner and shell zones are uniform, the model at this time is a triple-zone triple-temperature model, as shown in Fig. 2.3. The mass conservation and energy conservation equations of hydrogen in the triple-zone lumped parameter thermodynamic model are the same as those in the dual-zone lumped parameter thermodynamic model.

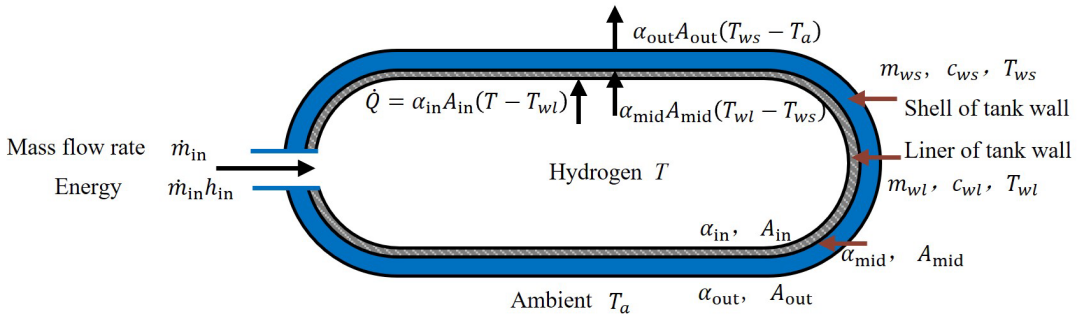

Fig. 2.3 Triple-zone triple-temperature lumped parameter thermodynamic model of hydrogen storage tank.

The energy conservation of the tank wall liner in the triple-zone lumped parameter thermodynamic model can be expressed as [75]

$$\frac{\mathrm{d}\left(m_{wl}c_{wl}T_{wl}\right)}{\mathrm{d}t}=\alpha_{in}A_{in}\left(T-T_{wl}\right)-\alpha_{ls}A_{ls}\left(T_{wl}-T_{ws}\right) \tag{2.7}$$

where c_{wl} is the specific heat capacity of the tank wall liner (J/kg/K). m_{wl} is the mass of the tank wall liner (kg). T, T_{wl} and T_{ws} are the temperatures of hydrogen, the tank wall liner and the tank wall shell (K). α_{ls} is the heat transfer coefficient between the tank wall liner and shell (W/m^2/K). α_{in} is the heat transfer coefficient between hydrogen and the tank's inner wall (W/m^2/K). A_{in} is the inner surface area of the tank wall (m^2). A_{ls} is the area of the contact surface between the liner and the shell (m^2).

The energy conservation of the tank wall shell in the triple-zone lumped parameter thermodynamic model can be expressed as [75]

$$\frac{\mathrm{d}\left(m_{ws}c_{ws}T_{ws}\right)}{\mathrm{d}t}=\alpha_{ls}A_{ls}\left(T_{wl}-T_{ws}\right)-\alpha_{\text{out}}A_{\text{out}}\left(T_{ws}-T_{a}\right) \tag{2.8}$$

where c_{ws} is the specific heat capacity of the tank wall shell (J/kg/K). m_{ws} is the mass of the tank wall shell (kg). T_{wl}, T_{ws} and T_a are the temperatures of the tank wall liner, the tank wall shell and the ambient (K), respectively. α_{out} is the heat transfer coefficient between the outer wall of the tank and the ambient (W/m^2/K). α_{ls} is the heat transfer coefficient between the tank wall liner and shell (W/m^2/K). A_{out} is the outer surface area of the tank wall (m^2). A_{ls} is the area of the contact surface between the liner and the shell (m^2).

2.1.4 Zero-dimensional gas one-dimensional tank wall thermodynamic model

In order to more accurately express the heat conduction in the hydrogen storage tank wall and thus more accurately calculate the hydrogen temperature, we established a zero-dimensional gas one-dimensional tank wall (0D1D) thermodynamic model of a hydrogen storage tank, as shown in Fig. 2.4. In cylindrical layers of the same radius, the temperature distribution is assumed to be uniform. In addition, since the thickness of the hydrogen storage tank wall is much smaller than the inner diameter of the tank, the cylindrical layer can be simplified to a flat layer. At this time, the one-dimensional heat conduction equation and boundary conditions along the radial direction of the tank wall can be expressed as [21]

$$k\frac{\partial^2 T_w}{\partial x^2}=\rho_w c_w\frac{\partial T_w}{\partial t} \tag{2.9}$$

$$-k\frac{\partial T_w}{\partial x}\Big|_{x=0}=\alpha_{\text{in}}\left(T-T_w\big|_{x=0}\right) \tag{2.10}$$

$$-k\frac{\partial T_w}{\partial x}\Big|_{x=L}=\alpha_{\text{out}}\left(T_w\big|_{x=L}-T_a\right) \tag{2.11}$$

where T is the temperature of hydrogen (K). T_w is the temperature of the hydrogen storage tank wall (K). L is the thickness of the hydrogen storage tank wall (m). ρ_w is the density of the tank wall material (kg/m^3). c_w is the specific heat capacity of the tank wall material (J/kg/K). k is the thermal conductivity of the tank wall material (W/m/K). α_{in} is the heat transfer coefficient between hydrogen and the inner wall of the storage tank (W/m^2/K). α_{out} is the heat transfer coefficient between the outer wall of the storage tank and the air (W/m^2/K).

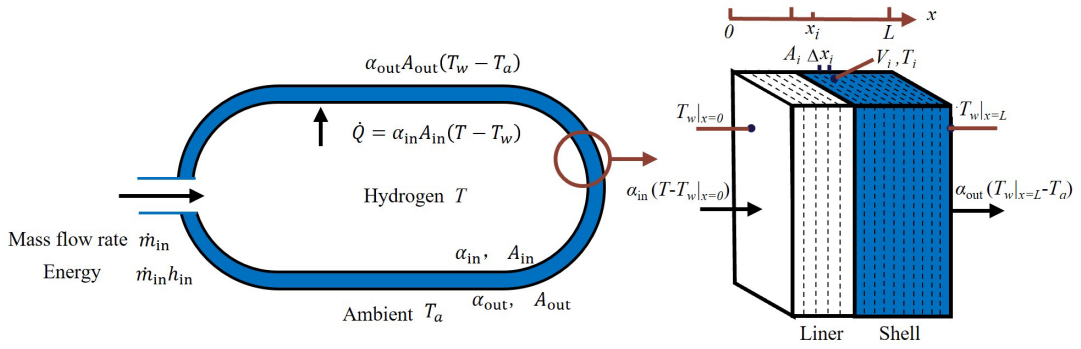

Fig. 2.4 Zero-dimensional gas one-dimensional tank wall (0D1D) thermodynamic model of a hydrogen storage tank.

The numerical solution of the one-dimensional heat conduction partial differential Eq. (2.9) can be solved using the capacitance-resistance method, which corresponds to finite volume analysis. Therefore, the partial differential Eq. (2.9) can be simplified into an ordinary differential equation [21]:

$$\dot{Q}_i=-\left(\rho_w c_w\Delta V\right)_i\frac{\mathrm{d}T_i}{\mathrm{d}t} \tag{2.12}$$

where i is the i-th layer of element in the tank wall. $\dot{Q}_i$ is the heat transfer rate between

the *i*-th layer of element and its two adjacent elements. $\dot{Q}_i$ can be further expressed as

$$\dot{Q}_i = \dot{Q}_{i-1} + \dot{Q}_{i+1} \tag{2.13}$$

$$\dot{Q}_{i-1} = \frac{T_i - T_{i-1}}{R_{i-1}} \tag{2.14}$$

$$\dot{Q}_{i+1} = \frac{T_i - T_{i+1}}{R_{i+1}} \tag{2.15}$$

where R_i is the thermal resistance of the tank wall (K/W), $R_i = \Delta x_i / (A_i k)$. Δx_i is the thickness of the *i*-th layer of element (m). A_i is the cylindrical layer area of the *i*-th layer of element (m^2).

For various thermodynamic models of hydrogen storage tanks, the pressure of hydrogen can be calculated by the real gas EOS after calculating the temperature of hydrogen in the tank. For the analytical models of the hydrogen storage tank in Section 2.2, the real gas EOS in the form of Redlich-Kwong will be used to calculate the hydrogen pressure. The reasons for choosing the Redlich-Kwong form of the real gas EOS and the effects of different forms of gas EOS on the thermal effect of hydrogen filling will be introduced in Section 3.2. For the numerical models of the hydrogen storage tank in Section 2.3, the real gas EOS (2.16) will be used to calculate the hydrogen pressure.

$$p = \frac{Zm\mathrm{R}T}{V\mathrm{M}_{\mathrm{H}_2}} \tag{2.16}$$

where R is the universal gas constant, its value is 8.314 (J/mole/K). $\mathrm{M}_{\mathrm{H}_2}$ is the molar mass of hydrogen, its value is 2.0159×10^{-3} (kg/mole). m is the mass of hydrogen in the tank (kg). T is the temperature of hydrogen in the tank (K). p is the pressure of hydrogen in the tank (Pa). V is the volume of the hydrogen tank (m^3). Z is the compressibility factor, which can be obtained through the database of the National Institute of Standards and Technology (NIST).

2.2 Analytical model of hydrogen storage tank

According to the mathematical and physical equations of the thermodynamic model of the hydrogen storage tank in Section 2.1, the analytical models of hydrogen temperature, hydrogen pressure and tank wall temperature can be derived. Analytical models can be more easily applied to engineering applications such as the development of hydrogen refuelling protocol. Since the process of solving and deriving the triple-zone lumped parameter analytical model of a hydrogen storage tank is very difficult, this thesis currently only studies the single-zone and dual-zone lumped parameter analytical models.

2.2.1 Single-zone lumped parameter analytical model

For the single-zone lumped parameter model of the hydrogen storage tank, it is assumed that the mass flow rate of the filling process is constant, and we can define that $\dot{m}_{\text{in}} = \dot{m}$. Integrating Eq. (2.1), the mass of hydrogen can be expressed as

$$m = m_0 + \dot{m}t \tag{2.17}$$

Substituting Eq. (2.17) into the energy conservation Eq. (2.4) of hydrogen, we can get

$$\left(m_0 + \dot{m}t\right)\frac{\mathrm{d}u}{\mathrm{d}t} + \dot{m}u = \dot{m}h - \alpha_{\text{in}} A_{\text{in}} \left(T - T_a\right) \tag{2.18}$$

Substituting $u = c_v T$, $h = c_p T_c$ into Eq. (2.18), we can get

$$c_v \left(m_0 + \dot{m}t\right)\frac{\mathrm{d}T}{\mathrm{d}t} = \dot{m}\left(c_p T_c - c_v T\right) - \alpha_{\text{in}} A_{\text{in}} \left(T - T_a\right) \tag{2.19}$$

where c_v is the constant-volume specific heat capacity of hydrogen (J/kg/K). c_p is the constant-pressure specific heat capacity of hydrogen (J/kg/K). T is the temperature of hydrogen (K). T_c is the inlet/precooling temperature (K). T_a is the ambient temperature (K).

We can define the characteristic filling time $t^* = m_0/\dot{m}$, define the dimensionless heat transfer coefficient $\alpha = \alpha_{\text{in}} A_{\text{in}}/(\dot{m}c_v)$, and define the ratio of the constant-pressure and

constant-volume specific heat capacity of hydrogen $\gamma = c_p / c_v$. Substituting them into Eq. (2.19), we can get

$$\frac{\mathrm{d}T}{\mathrm{d}t} = \frac{\gamma T_c + \alpha T_a - (1+\alpha)T}{t^* + t} \tag{2.20}$$

We define the characteristic temperature $T^* = (\gamma T_c + \alpha T_a)/(1+\alpha)$ and substitute it into Eq. (2.20) to get

$$\frac{\mathrm{d}T}{\mathrm{d}t} = (1+\alpha)\left(\frac{T^* - T}{t^* + t}\right) \tag{2.21}$$

We define the initial mass fraction $\mu = m_0 / m$, substitute it into Eq. (2.21) and solve it. The analytical model of the single-zone lumped parameter hydrogen temperature can be obtained as

$$T = T^* - (T^* - T_0)\mu^{1+\alpha} \tag{2.22}$$

The M language is used to write the single-zone lumped parameter analytical model of the hydrogen storage tank during the hydrogen filling process in the Matlab Function module.

2.2.2 Dual-zone lumped parameter analytical model

For the dual-zone lumped parameter model of the hydrogen storage tank, the hydrogen energy conservation equation Eq. (2.5) and the tank wall energy conservation equation Eq. (2.6) are coupled. It is necessary to use the element reduction method to simplify and solve the differential equations of hydrogen and tank wall temperatures. When solving for hydrogen temperature, we can first assume that the tank wall temperature is constant. At this time, by replacing the ambient temperature in the single-zone hydrogen temperature analytical model with the tank wall temperature, the dual-zone hydrogen temperature analytical model can be obtained. That is, the ambient temperature in the characteristic temperature in Eq. (2.22) needs to be replaced by the tank wall temperature. At this time, the characteristic temperature applied to the dual-zone model is $T^* = (\gamma T_c + \alpha T_w)/(1+\alpha)$.

Expressing Eq. (2.22) in the form of a "mixture rule":

$$T = f_g T_0 + \left(1 - f_g\right) T^* \tag{2.23}$$

where $f_g = \mu^{1+\alpha}$ is the weight of the mixing rule. We can define the dimensionless heat transfer coefficient $\alpha_{w\text{in}} = \alpha_{\text{in}} A_{\text{in}} / \left(m_w c_w\right)$, $\alpha_{w\text{out}} = \alpha_{\text{out}} A_{\text{out}} / \left(m_w c_w\right)$ and substitute them into the tank wall energy conservation Eq. (2.6) of the dual-zone lumped parameter model of the hydrogen storage tank to get

$$\frac{\mathrm{d}T_w}{\mathrm{d}t} = \alpha_{w\text{in}}(T - T_w) - \alpha_{w\text{out}}(T_w - T_a) \tag{2.24}$$

In order to solve the tank wall temperature, it can be assumed that the hydrogen temperature is constant. At this time, solving the differential Eq. (2.24) can be obtained

$$\frac{\alpha_{w\text{in}}\left(T - T_w\right) - \alpha_{w\text{out}}\left(T_w - T_a\right)}{\alpha_{w\text{in}}\left(T - T_{w0}\right) - \alpha_{w\text{out}}\left(T_{w0} - T_a\right)} = e^{-\left(\alpha_{w\text{in}} + \alpha_{w\text{out}}\right)t} \tag{2.25}$$

We can define $\delta_{\text{in}} = \alpha_{w\text{in}} \big/ \left(\alpha_{w\text{in}} + \alpha_{w\text{out}}\right)$, $\delta_{\text{out}} = \alpha_{w\text{out}} \big/ \left(\alpha_{w\text{in}} + \alpha_{w\text{out}}\right)$ and substitute them into Eq. (2.25) to get

$$T_w = f_w T_{w0} + \left(1 - f_w\right)\left(\delta_{\text{in}} T + \delta_{\text{out}} T_a\right) \tag{2.26}$$

where $f_w = e^{-\left(\alpha_{w\text{in}} + \alpha_{w\text{out}}\right)t}$ is the weight of the mixing rule. Solving Eqs. (2.23) and (2.26), the analytical models of dual-zone lumped parameters hydrogen and tank wall temperature can be obtained:

$$T = \frac{f_g T_0 + \dfrac{\alpha}{1+\alpha}\left(1 - f_g\right) f_w T_{w0} + \dfrac{\gamma}{1+\alpha}\left(1 - f_g\right) T_c + \dfrac{\alpha}{1+\alpha}\left(1 - f_g\right)\left(1 - f_w\right)\delta_{\text{out}} T_a}{1 - \dfrac{\alpha}{1+\alpha}\delta_{\text{in}}\left(1 - f_g\right)\left(1 - f_w\right)} \tag{2.27}$$

$$T_w = \frac{\delta_{\text{in}}\left(1 - f_w\right) f_g T_0 + f_w T_{w0} + \dfrac{\gamma}{1+\alpha}\left(1 - f_g\right)\left(1 - f_w\right)\delta_{\text{in}} T_c + \delta_{\text{out}}\left(1 - f_w\right) T_a}{1 - \dfrac{\alpha}{1+\alpha}\delta_{\text{in}}\left(1 - f_g\right)\left(1 - f_w\right)} \tag{2.28}$$

The M language is used to write in the Matlab Function module to realize the dual-

zone lumped parameter analytical model of the hydrogen storage tank during the hydrogen filling process.

2.2.3 MC analytical model

In 2014, the SAE J2601 hydrogen refuelling protocol published by SAE mentioned a non-standard protocol called the MC method, which was standardized in 2016. The MC method was developed by Honda, where the parameter MC represents the lumped heat capacity of the characteristic volume of the hydrogen storage tank. As shown in Fig. 2.5, the hydrogen storage tank model used by the MC method distinguishes the hydrogen zone and the tank wall zone, but it assumes that the hydrogen temperature and the tank wall temperature are equal. Therefore, the hydrogen storage tank model used by the MC method is essentially a dual-zone single-temperature model, which is a special case of the dual-zone dual-temperature model.

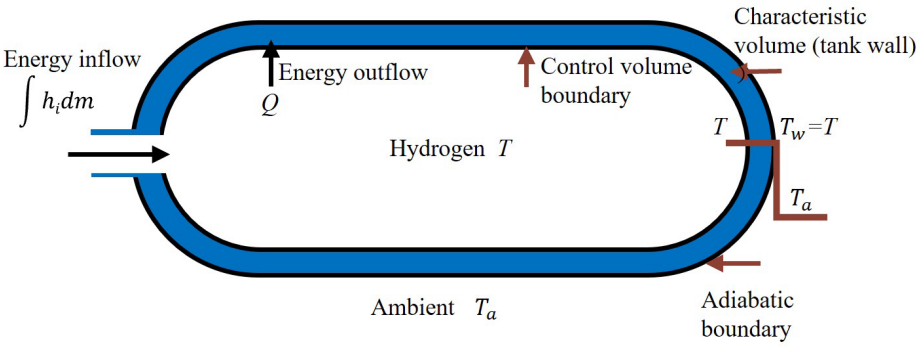

Fig. 2.5 MC model of hydrogen storage tank.

For the hydrogen in the control volume shown in Fig. 2.5, the energy conservation of hydrogen during the hydrogen filling time from t_{initial} to t_{final} can be expressed as

$$m_{\text{final}}c_v T_{\text{final}} - m_{\text{initial}}c_v T_{\text{initial}} = \int_{t_{\text{initial}}}^{t_{\text{final}}} \dot{m}_{\text{in}} h_{\text{in}} \mathrm{d}t - Q \tag{2.29}$$

where m_{final} is the final hydrogen mass (kg). m_{initial} is the initial hydrogen mass (kg). T_{initial} is the initial hydrogen temperature (K). T_{final} is the final hydrogen temperature (K). c_v is the constant-volume specific heat capacity of hydrogen (J/kg/K). $\dot{m}_{\text{in}}$ is the mass flow rate of hydrogen inflow (kg/s). h_{in} is the specific enthalpy of hydrogen inflow (J/kg). Q is the total amount of heat transferred from hydrogen to the tank wall during the filling process (J).

The MC method assumes that the outer boundary of the tank wall is adiabatic. That is, the heat transferred from the tank wall to the ambient is ignored. At this time, the energy conservation of the tank wall can be expressed as

$$\mathrm{MC}\left(T_{\mathrm{final}}-T_{\mathrm{initial}}\right)=Q \tag{2.30}$$

where MC is the total heat capacity of the tank wall characteristic volume (J/K).

Solving Eqs. (2.29) and (2.30), we can get

$$\mathrm{MC}=\frac{m_{\mathrm{initial}}c_v T_{\mathrm{initial}}+\int_{t_{\mathrm{initial}}}^{t_{\mathrm{final}}}\dot{m}_{\mathrm{in}}h_{\mathrm{in}}\mathrm{d}t-m_{\mathrm{final}}c_v T_{\mathrm{final}}}{T_{\mathrm{final}}-T_{\mathrm{initial}}} \tag{2.31}$$

Assuming that it is adiabatic between the hydrogen in the tank and the tank wall. In this case, the energy conservation of hydrogen can be expressed as

$$m_{\mathrm{final}}c_v T_{\mathrm{adiabatic}}=m_{\mathrm{initial}}c_v T_{\mathrm{initial}}+\int_{t_{\mathrm{initial}}}^{t_{\mathrm{final}}}\dot{m}_{\mathrm{in}}h_{\mathrm{in}}\mathrm{d}t \tag{2.32}$$

where $T_{\mathrm{adiabatic}}$ is the final hydrogen temperature assuming adiabatic conditions (K).

Substituting Eq. (2.32) into Eq. (2.31), the analytical models of the final hydrogen temperature and the MC parameter in the MC method can be obtained:

$$T_{\mathrm{final}}=\frac{m_{\mathrm{final}}c_v T_{\mathrm{adiabatic}}+\mathrm{MC}T_{\mathrm{initial}}}{\mathrm{MC}+m_{\mathrm{final}}c_v} \tag{2.33}$$

$$\mathrm{MC}=\frac{m_{\mathrm{final}}c_v\left(T_{\mathrm{adiabatic}}-T_{\mathrm{final}}\right)}{T_{\mathrm{final}}-T_{\mathrm{initial}}} \tag{2.34}$$

The MC method obtains a large amount of simulation data of the MC parameter by simulating under various initial/boundary conditions and then substituting the obtained simulation data into Eq. (2.34). Based on the observation of MC parameter simulation data and using multiple linear regression to test the significance of each parameter, the MC method proposed two formulas for the MC parameter [5, 67]:

$$\mathrm{MC}=AC+BC\frac{U_{\mathrm{adiabatic}}}{U_{\mathrm{initial}}}+GC\left(1-e^{-KC\Delta t_1}\right)^{JC} \tag{2.35}$$

$$\mathrm{MC} = AC + BC \ln \sqrt{\frac{U_{\text{adiabatic}}}{U_{\text{initial}}}} + GC\left(1 - e^{-KC\Delta t_2}\right)^{JC} \tag{2.36}$$

where U_{initial} is the initial hydrogen internal energy (J). $U_{\text{adiabatic}}$ is the final hydrogen internal energy assuming adiabatic conditions (J). Δt_1 is the time after the start of filling 180s (s), $\Delta t_1 = t_{\text{final}} - 180$. Δt_2 is the time after the start of filling 30s (s), $\Delta t_2 = t_{\text{final}} - 30$. *AC*, *BC*, *GC*, *KC*, and JC are the coefficients in the formula, which were obtained through simulation using a 1kg type III storage tank. This content will be introduced in detail in Chapter 5. The analytical model of the MC method will be used in Chapter 5.

2.3 Numerical model of hydrogen storage tank

Section 2.1 establishes the single-zone, dual-zone, triple-zone and zero-dimensional gas one-dimensional tank wall (0D1D) thermodynamic models of the hydrogen storage tank during the hydrogen filling process. Then, Section 2.2 derives the single-zone and dual-zone lumped parameter analytical model based on the mathematical and physical equations of the thermodynamic models. This section will use the Matlab/Simulink software platform to implement the numerical models of the hydrogen filling process based on the mathematical and physical equations of the thermodynamic models of the hydrogen storage tank. Finally, the results of the numerical model, analytical model, references' experimental data and CFD model were compared to verify the accuracy of the thermodynamic model, analytical model and numerical model of the hydrogen storage tank.

2.3.1 Single-zone lumped parameter numerical model

According to the hydrogen mass and energy conservation Eqs. (2.1) and (2.4) and the real gas EOS Eq. (2.16), the single-zone lumped parameter numerical model of a hydrogen storage tank for the hydrogen filling process was established based on the Matlab/Simulink software platform, as shown in Fig. 2.6.

In order to verify the accuracy of the single-zone analytical model and numerical model of the hydrogen storage tank during the hydrogen filling process, the physical properties of the type IV 29 L onboard tank in Ref. [25] were used for comparison with

the results of the CFD model in Ref. [25]. The numerical or experimental conditions and results provided by many references are not sufficient, which is not conducive to comparison. However, the tank parameters and CFD model results in Ref. [25] are relatively detailed, so they are selected for comparison. The physical properties of the hydrogen storage tank are shown in Table 2.1, and the initial and boundary conditions for hydrogen filling are shown in Table 2.2.

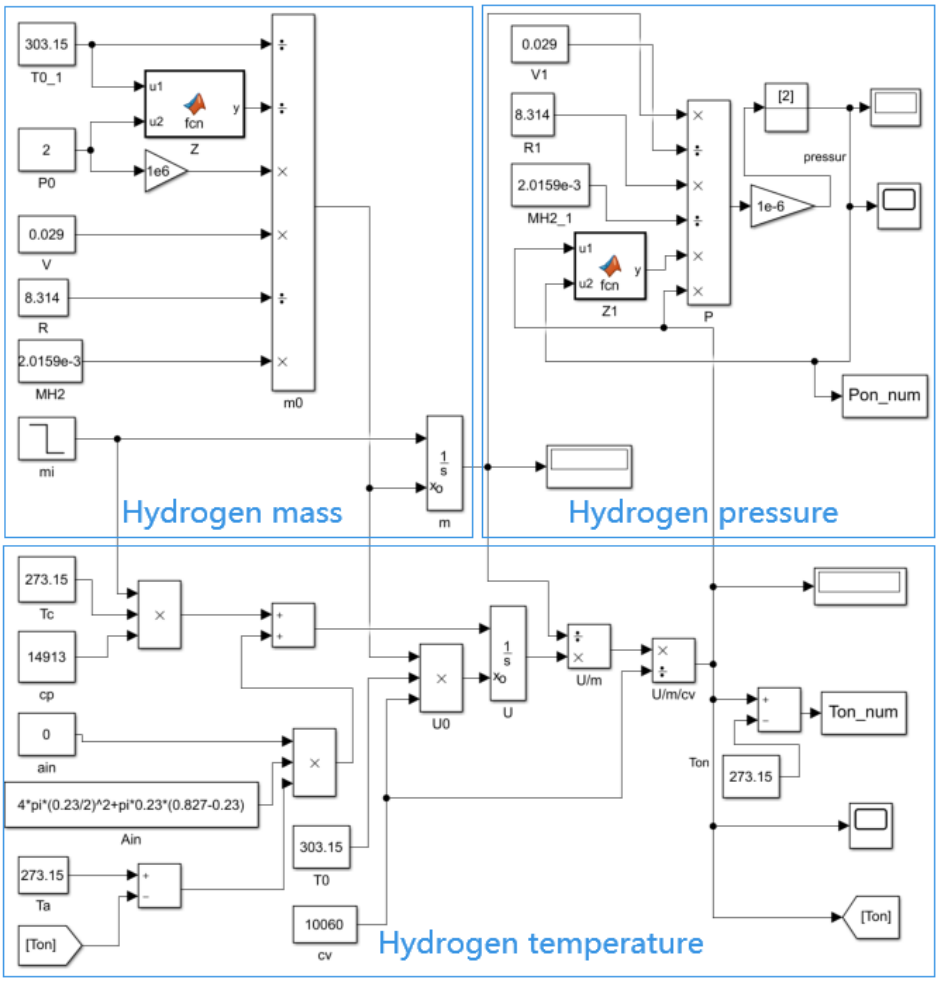

Fig. 2.6 Single-zone lumped parameter numerical model of hydrogen storage tank during hydrogen filling process.

Table 2.1 Physical properties of hydrogen storage tanks in Ref. [25]

Parameter	Physical definition	Value
NWP	Nominal working pressure (MPa)	70
V	Tank volume (m^3)	0.029
L	Tank length (m)	0.827
D_{in}	Tank inner diameter (m)	0.230

Table 2.2 Initial and boundary conditions in Ref. [25]

Parameter	Physical definition	Value
T_0	Initial temperature (℃)	−20/0/30
T_a	Ambient temperature (℃)	0
T_c	Inlet/Precooling temperature (℃)	0
p_0	Initial pressure (MPa)	2
$\dot{m}$	Mass flow rate (kg/s)	0.005

Fig. 2.7 shows the comparison between the simulation results of the numerical and analytical models of the single-zone lumped parameter of the hydrogen storage tank and the CFD model results in Ref. [25] when the initial hydrogen temperatures are −20 °C, 0 °C and 30 °C, respectively. Fig. 2.7(a) shows that in the early and middle stages of hydrogen filling, the maximum error between the hydrogen temperature calculated by the single-zone lumped parameter analytical and numerical models and the CFD model result is about 10 °C, but the error in the final hydrogen temperature is only about 5 °C, which is an acceptable error range. In the early and middle stages of hydrogen filling, the hydrogen pressure calculated by the single-zone lumped parameter analytical and the numerical models are relatively consistent, but the error in the final hydrogen pressure is about 2 MPa. The reason is that the numerical model in this thesis uses a calculation method based on the NIST database, while the analytical model uses a gas EOS in the Redlich-Kwong form, and its accuracy is lower than that calculated based on the NIST database. The error patterns of hydrogen temperature and pressure calculated by various models in Figs. 2.7 (b) and (c) are similar to Fig. (a). The comparison between Figs. 2.7 (a), (b) and (c) show that under different initial hydrogen temperature conditions, the final hydrogen temperatures are close to the same, indicating that the initial temperature has little effect on the final hydrogen temperature. The reason is that the initial hydrogen temperature only determines the initial hydrogen internal energy, and the initial pressure, in this case, is only 2 MPa, so the initial hydrogen internal energy accounts for a small proportion of the final hydrogen internal energy. Only when the initial pressure is large, that is, when the initial hydrogen internal energy accounts for a large proportion, will the initial hydrogen temperature

have a greater impact on the final hydrogen temperature. In summary, the single-zone analytical and numerical models of the hydrogen storage tank in this thesis have a certain ability to express the results of the CFD model.

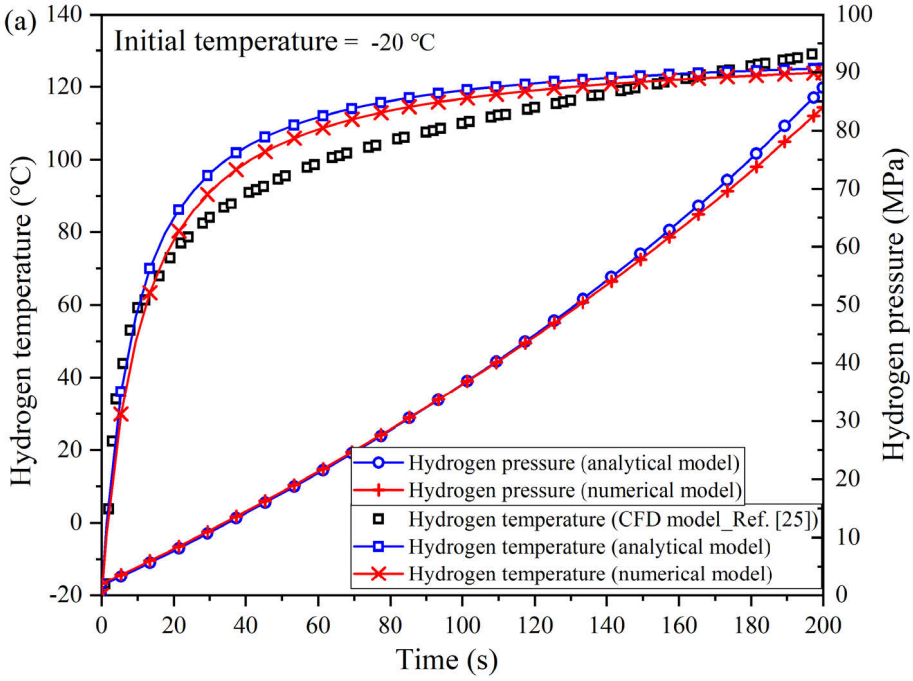

(a) Initial temperature −20 ℃

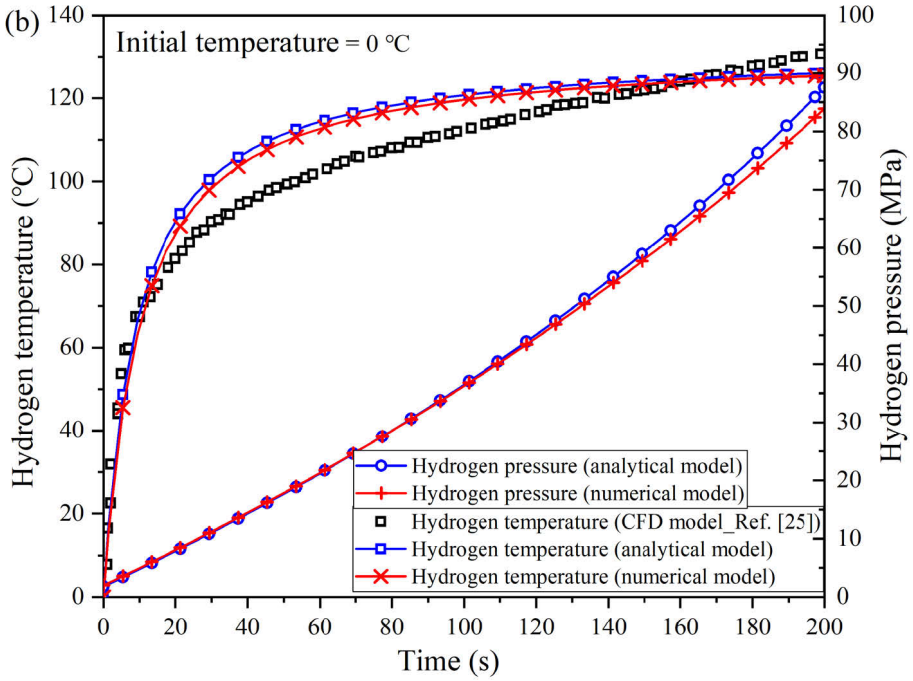

(b) Initial temperature 0 ℃

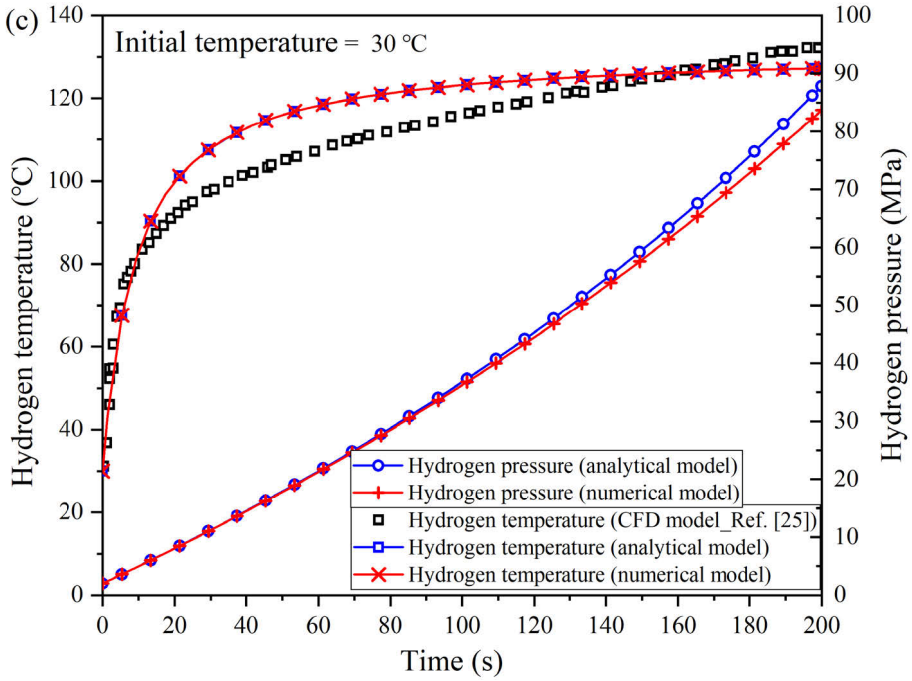

(c) Initial temperature 30 ℃

Fig. 2.7 Comparison between the simulation results of the single-zone numerical and analytical models of the hydrogen storage tank and the results of Ref. [25] under different initial temperature conditions [75].

2.3.2 Dual-zone lumped parameter numerical model

According to the mass and energy conservation Eqs. (2.1) and (2.5) of hydrogen, the energy conservation Eq. (2.6) of the tank wall and the real gas EOS Eq. (2.16), the dual-zone lumped parameter numerical model of the hydrogen storage tank during the hydrogen filling process was established based on the Matlab/Simulink software platform, as shown in Fig. 2.8.

In order to verify the accuracy of the dual-zone lumped parameter analytical model and numerical model of the hydrogen storage tank during the hydrogen filling process, the physical properties and experimental data of the type IV 72 L onboard tank in Ref. [13] were used for comparative verification. The physical properties of the hydrogen storage tank are shown in Table 2.3, and the initial/boundary conditions of the filling process are shown in Table 2.4. Table 2.3 shows the mass and specific heat capacity of the tank wall liner and shell, respectively. For the overall lumped heat capacity of the tank wall, we use the mass average heat capacity method to calculate. Three cases were used to

carry out simulation verification. The mass flow rate, initial pressure, and filling time were different in different cases. The mass flow rate of case 1 is 0.0047 kg/s, and the initial pressure is 10 MPa. Ref. [13] provides the experimental and CFD simulated hydrogen temperatures in this case, but the data of hydrogen pressure and tank wall temperature are not provided. The mass flow rate of case 2 is 0.0041 kg/s, and the initial pressure is 15 MPa. Ref. [13] provides the experimental and CFD simulated hydrogen pressure in this case, but the data of hydrogen and tank wall temperatures are not provided. The mass flow rate of case 3 is 0.00376 kg/s, and the initial pressure is 20 MPa. The data provided in Ref. [13] is the same as that of case 1.

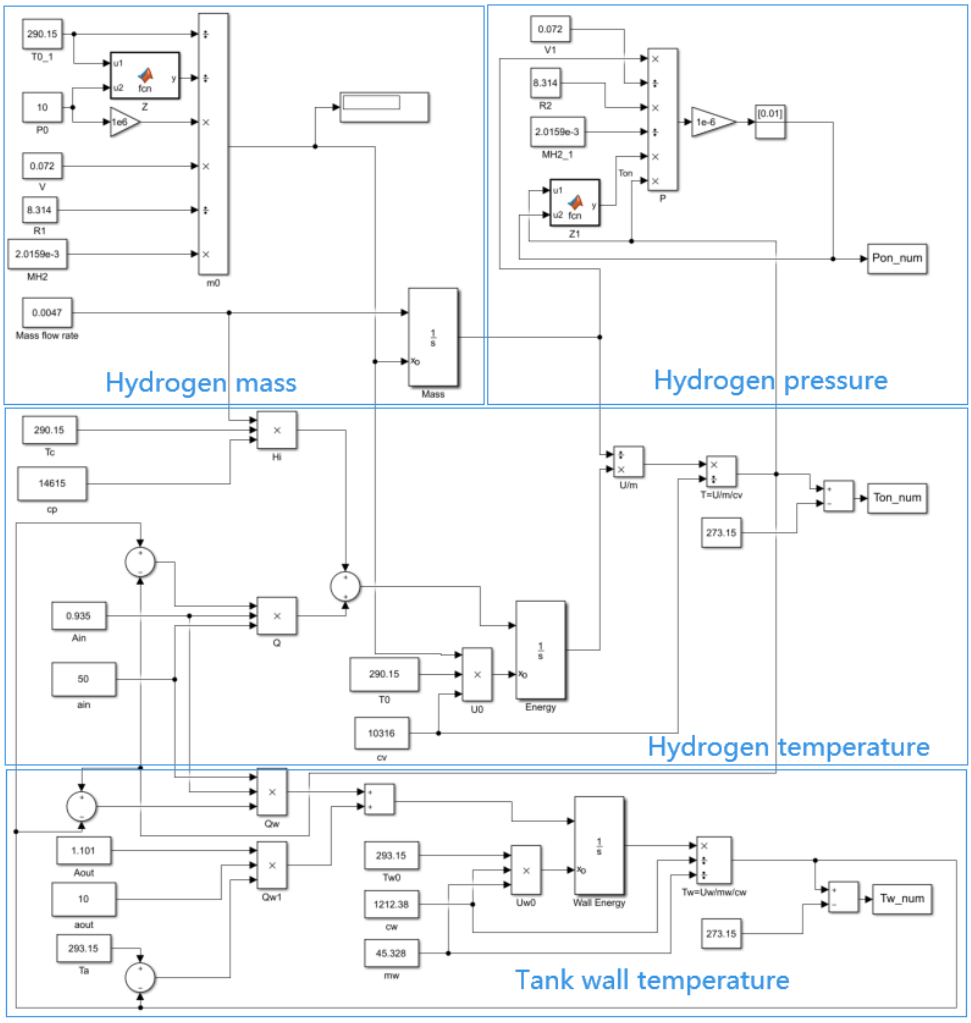

Fig. 2.8 Dual-zone lumped parameter numerical model of hydrogen storage tank during hydrogen filling process.

Table 2.3 Physical properties of the hydrogen storage tank in Ref. [13]

Parameter	Physical definition	Value
NWP	Nominal working pressure (MPa)	35
V	Tank volume (m^3)	0.072
m_{wl}	Mass of liner (kg)	4.273
c_{wl}	Specific heat capacity of liner (J/kg/K)	2100
m_{ws}	Mass of shell (kg)	41.055
c_{ws}	Specific heat capacity of shell (J/kg/K)	1120
A_{in}	Internal surface area of tank (m^2)	0.935
A_{out}	External surface area of tank (m^2)	1.101

Table 2.4 Initial and boundary conditions in Ref. [13]

Parameter	Physical definition	Value
T_0	Initial hydrogen temperature (°C)	17
Tw_0	Initial tank wall temperature (°C)	20
T_a	Ambient temperature (°C)	20
T_c	Inlet temperature (°C)	17
p_0	Initial pressure (MPa)	10/15/20
$\dot{m}$	Mass flow rate (kg/s)	0.0047/0.0041/0.00376

For case 1, Fig. 2.9(a) shows that during the filling process, the CFD results of the hydrogen temperature in Ref. [13] are at most about 10 °C lower than the experimental results, but they are consistent at the end of the filling. The reason is that Ref. [13] used a variable mass flow rate when conducting experiments but used a constant average mass flow rate when conducting CFD simulations, that is, the total mass filled during the experiment was divided by the filling time. The effects of variable versus constant mass flow rates on hydrogen filling will be further discussed in Chapter 3. A constant mass flow rate was also used in this case. Therefore, the hydrogen temperatures calculated by the dual-zone lumped parameter analytical and numerical models are at most about 10 °C lower than the experimental value in Ref. [13] during the filling process but are consistent at the end of the filling. Throughout the filling process, the

hydrogen temperatures simulated by the analytical and numerical models were in good agreement. Ref. [13] does not provide tank wall temperature and hydrogen pressure data for case 1, so only the analytical and numerical model results of tank wall temperature and hydrogen pressure are shown in Figs. 2.9 (a) and (b). Throughout the filling process, the analytical and numerical model results of the tank wall temperature were in good agreement. In the early stage of filling, the analytical and numerical model results of hydrogen pressure are consistent, while the analytical model result is about 1 MPa higher than that of the numerical model at the end of filling. The reason is that when calculating hydrogen pressure, the analytical model uses the Redlich-Kwong gas EOS, while the numerical model uses a calculation method based on the NIST database, also reflecting the potential for further optimization of the Redlich-Kwong gas EOS.

For case 2, Ref. [13] does not provide relevant data on hydrogen temperature and tank wall temperature. Therefore, only the results of the analytical model and the numerical model are shown in Fig. 2.9(c). The results of the analytical model and the numerical model of hydrogen temperature and tank wall temperature are in good agreement. Ref. [13] provides experimental and CFD simulated hydrogen pressure data for case 2. Fig. 2.9(d) shows that during the filling process, the experimental hydrogen pressure is up to about 2 MPa higher than the CFD simulation result, but they are consistent at the end of the filling. The reason is that, as mentioned in case 1, a variable mass flow rate was used in the experiment. That is, the mass flow rate started from 0 and slowly increased to the maximum value, then slowly decreased. Therefore, the increase rate of the experimental hydrogen pressure first increases and then decreases during the filling process. However, the CFD model of Ref. [13], the analytical model and the numerical model of this thesis all use a constant mass flow rate, so the increase rate of the hydrogen pressure remains unchanged. During the entire filling process, the maximum error between the hydrogen pressure calculated by the analytical model, the numerical model and the CFD model is about 2 MPa.

For case 3, the overall changing pattern is the same as that of cases 1 and 2. The comparison of the three cases shows that as the initial pressure increases from 10 MPa to 20 MPa, the total filling time decreases by about 80 s, the final hydrogen temperature

decreases by about 20 °C, and the final tank wall temperature decreases to a certain extent. The reason is that the greater the initial pressure, the smaller the net increment of hydrogen in the tank when filling is terminated, and therefore, the smaller the inlet enthalpy, resulting in a lower hydrogen temperature rise. The comparison of the results in Fig. 2.9 and Fig. 2.7 shows that the initial pressure affects the final hydrogen temperature to a greater extent than the initial temperature.

Intuitively, compared with the single-zone lumped parameter model, the hydrogen temperature and pressure of the dual-zone lumped parameter model are more consistent with the results of the CFD model and experimental values. Moreover, the dual-zone lumped parameter model can solve the temperature of the tank wall. Overall, the dual-zone lumped parameter model of the hydrogen storage tank during the filling process improves the single-zone lumped parameter model.

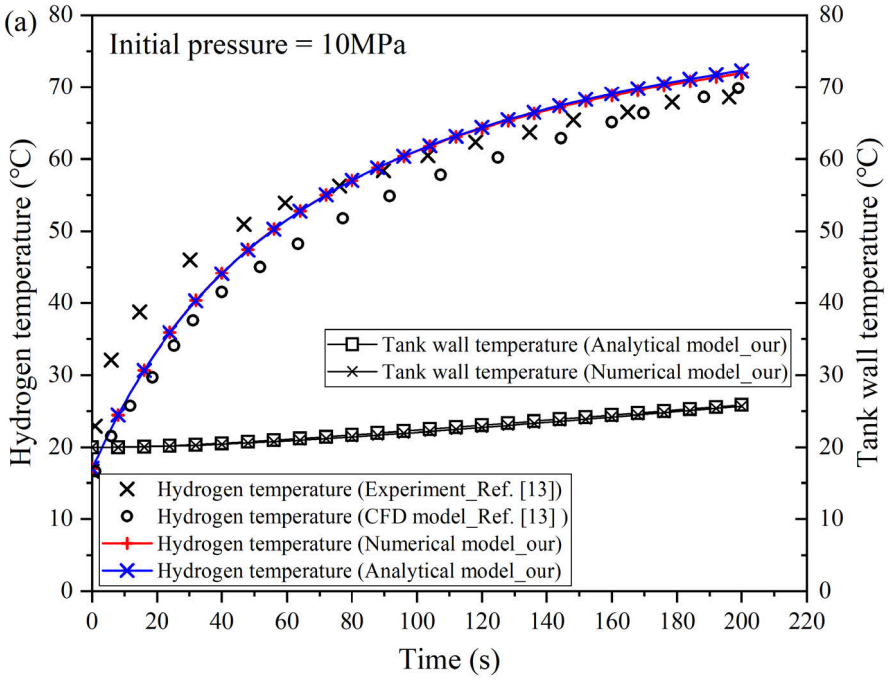

Case 1: (a) Hydrogen and tank wall temperatures

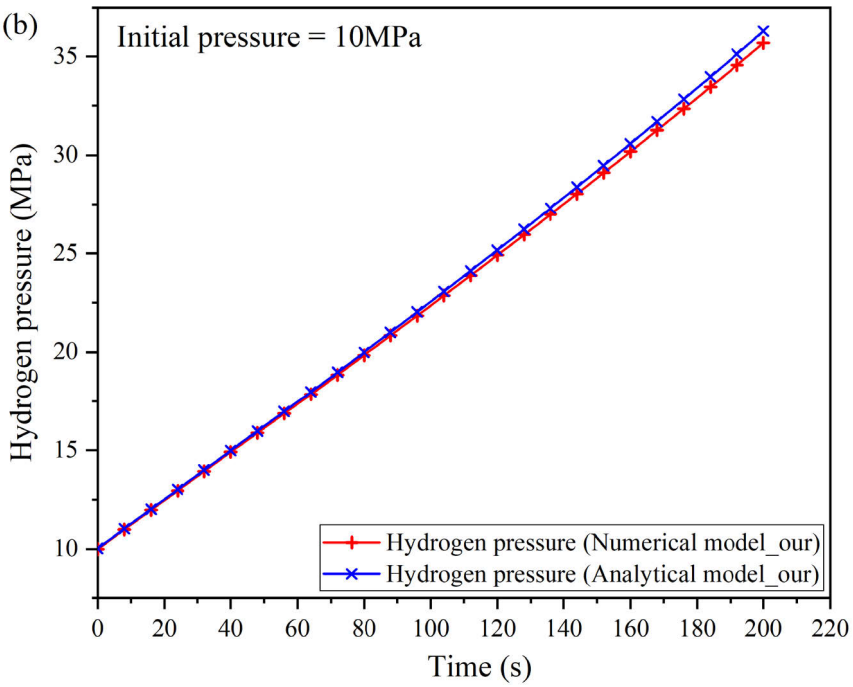

Case 1: (b) Hydrogen pressure

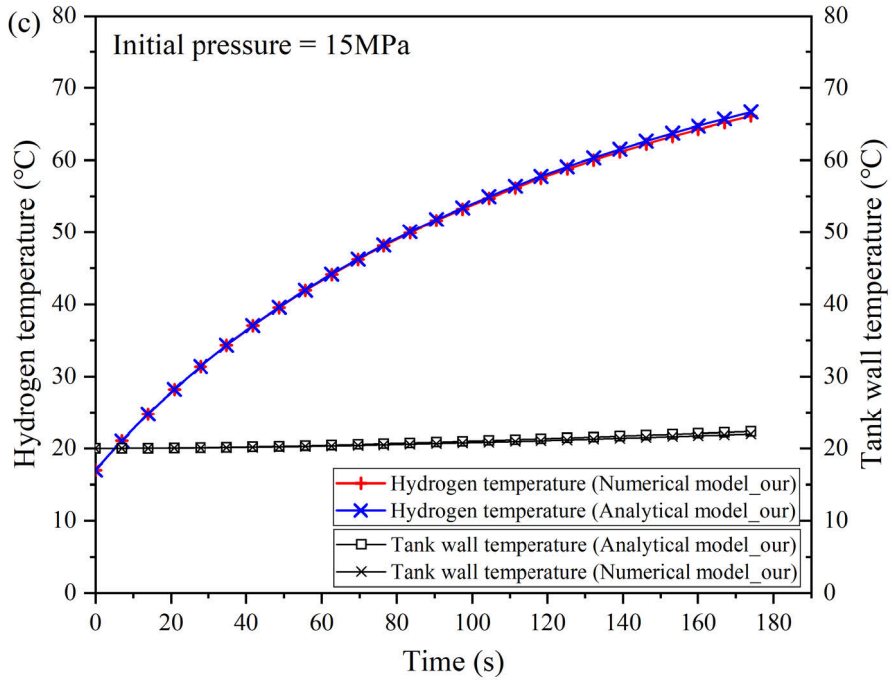

Case 2: (c) Hydrogen and tank wall temperatures

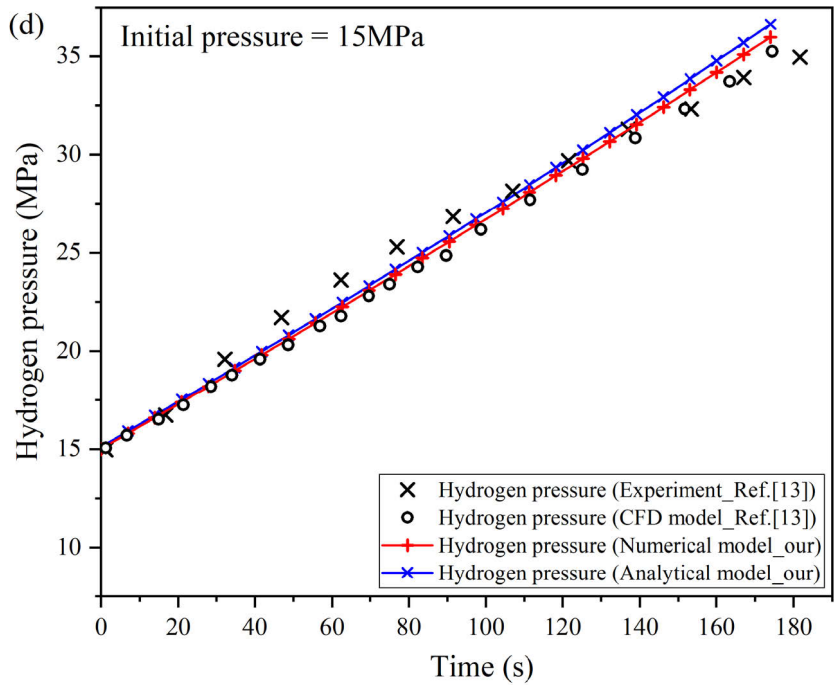

Case 2: (d) Hydrogen pressure

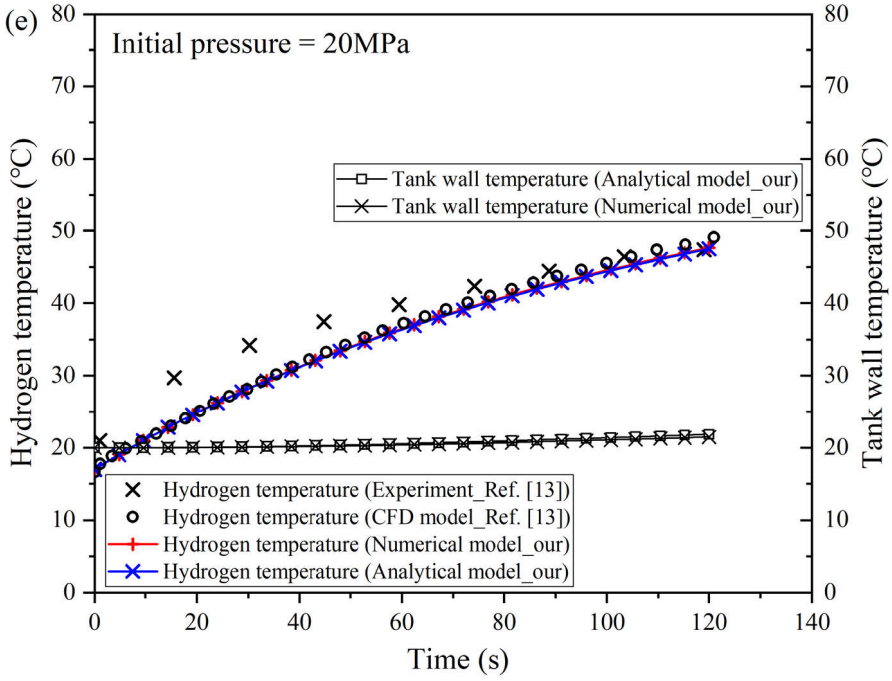

Case 3: (e) Hydrogen and tank wall temperatures

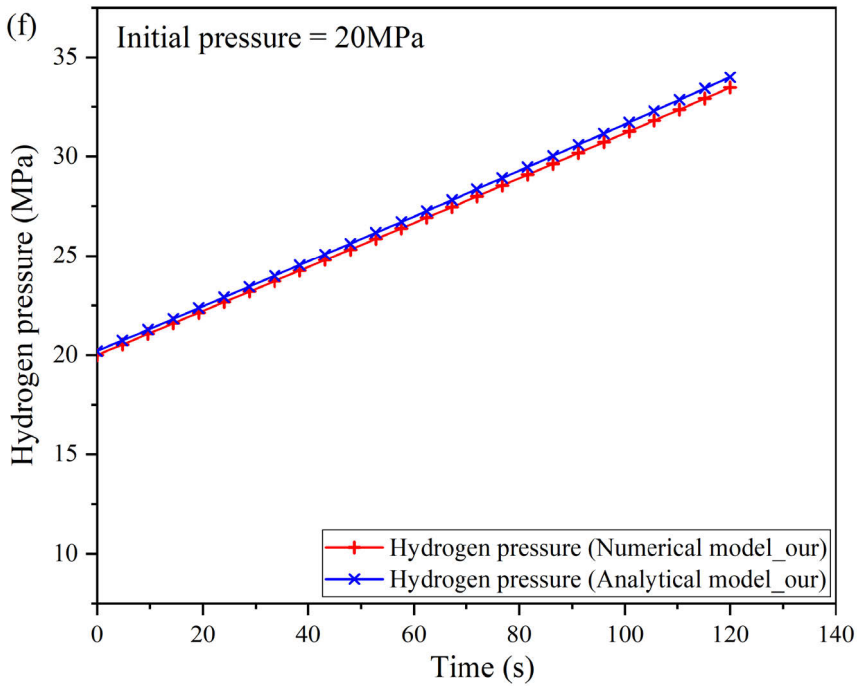

Case 3: (f) Hydrogen pressure

Fig. 2.9 Comparison between the numerical and analytical model results of the dual-zone lumped parameters of the hydrogen storage tank with the results of Ref. [13].

2.3.3 Triple-zone lumped parameter numerical model

According to the mass and energy conservation Eqs. (2.1) and (2.5) of hydrogen, the energy conservation Eqs. (2.7) and (2.8) of the tank wall, and the real gas EOS Eq. (2.16), a triple-zone lumped parameter numerical model of the hydrogen storage tank during the hydrogen filling process was established based on the Matlab/Simulink software platform, as shown in Fig. 2.10.

In order to verify the accuracy of the triple-zone lumped parameter numerical model of the hydrogen storage tank during the hydrogen filling process, the physical properties and CFD model results of the type IV hydrogen storage tank with a volume of 150 L and a nominal working pressure of 70 MPa in Ref. [22] were used to carry out comparative verification. The physical properties of the hydrogen storage tank are shown in Table 2.5, and the initial and boundary conditions of the filling process are shown in Table 2.6.

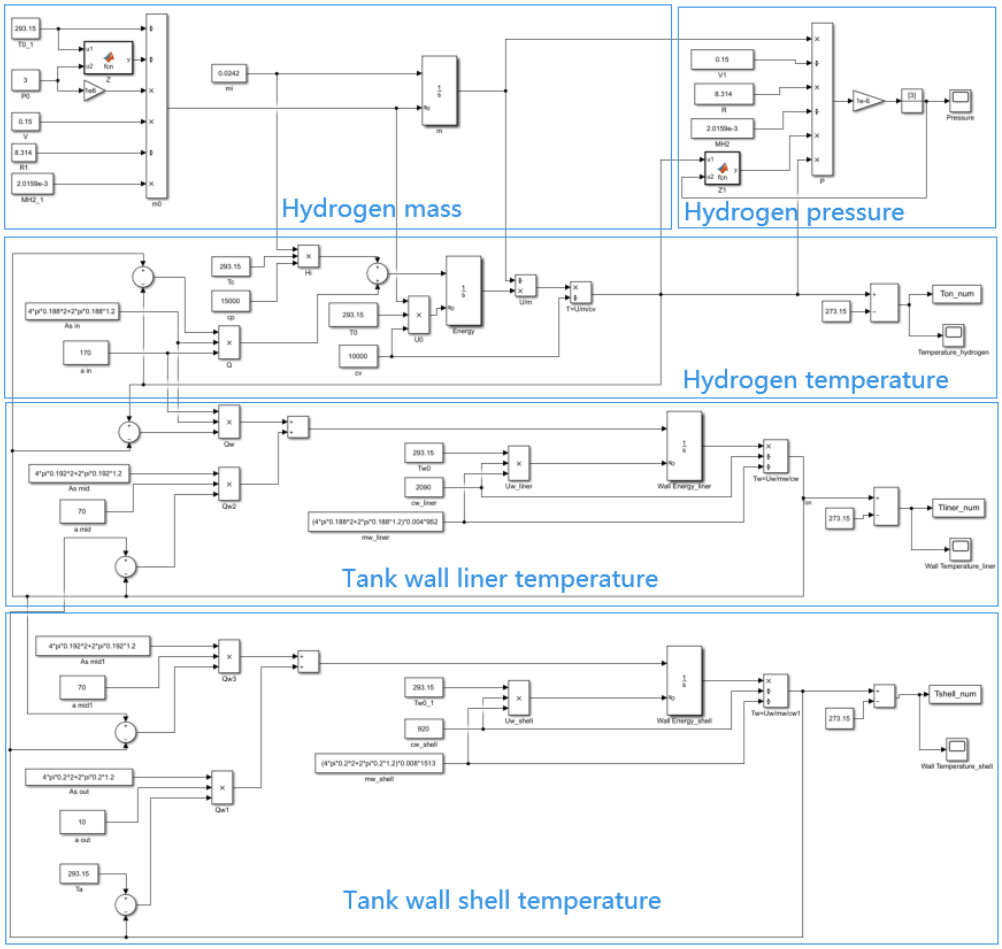

Fig. 2.10 Triple-zone lumped parameter numerical model of the hydrogen storage tank during the hydrogen filling process.

Table 2.5 Physical properties of hydrogen storage tanks in Ref. [22]

Parameter	Physical definition	Value
NWP	Nominal working pressure (MPa)	70
V	Tank volume (m^3)	0.15
L	Length of horizontal part of tank (m)	1.2
D_{in}	Tank inner diameter (m)	0.376
D_{out}	Tank outer diameter (m)	0.4
l_{wl}	Thickness of tank liner (m)	0.004
l_{ws}	Thickness of tank shell (m)	0.009
c_{wl}	Specific heat capacity of tank liner (J/kg/K)	2090
c_{ws}	Specific heat capacity of tank shell (J/kg/K)	920
ρ_{wl}	Density of tank liner (kg/m^3)	952
ρ_{ws}	Density of tank shell (kg/m^3)	1513

Table 2.6 Initial and boundary conditions in Ref. [22]

Parameter	Physical definition	Value
T_0	Initial hydrogen temperature (℃)	20
Tw_0	initial tank wall temperature (℃)	20
T_a	Ambient temperature (℃)	20
T_c	Inlet temperature (℃)	20
p_0	Initial pressure (MPa)	3
$\dot{m}$	Mass flow rate (kg/s)	0.0242

Fig. 2.11(a) compares the hydrogen temperature of the triple-zone lumped parameter numerical model of the hydrogen storage tank with the results of the CFD model in Ref. [22]. It can be seen that around the 30th s of hydrogen filling, there is an error of up to about 3 °C between them, but they are in good agreement at the end of the filling. The reason is that the simulation of this case uses an average heat transfer coefficient, but the actual heat transfer coefficient is highly correlated with the mass flow rate, which will be discussed in Chapter 3. So, the actual heat transfer coefficient should first increase and then decrease. Around the 30s, because the average heat transfer coefficient is smaller than the actual one, the hydrogen temperature simulated in this case is higher than the CFD model results in Ref. [22]. Ref. [22] does not provide hydrogen pressure data, so Fig. 2.11(a) only shows the hydrogen pressure of the numerical model. The maximum value is close to 70 MPa, which reaches the nominal working pressure of the storage tank.

Fig. 2.11(b) compares the temperature results of the tank wall liner and shell of the triple-zone lumped parameter numerical model with the CFD model. It can be seen that during the entire process, the shell temperatures of the two are basically the same. As for the liner temperature, the results of the triple-zone lumped parameter numerical model are about 5 °C lower than the results of the CFD model, but the overall upward trend is consistent. The reason is that the triple-zone lumped parameter model divides the tank wall into the liner and the shell, which is more realistic. However, it assumes that the temperatures of the liner and the shell are uniform, which is inconsistent with reality and leads to errors in the tank wall temperature. Comparing Fig. 2.9 and Fig. 2.11, intuitively, the triple-zone lumped parameter numerical model can better express

the results of the CFD model than the dual-zone numerical model and can more accurately express the temperature of the tank wall liner and shell. In summary, the triple-zone lumped parameter numerical model improves the dual-zone numerical model.

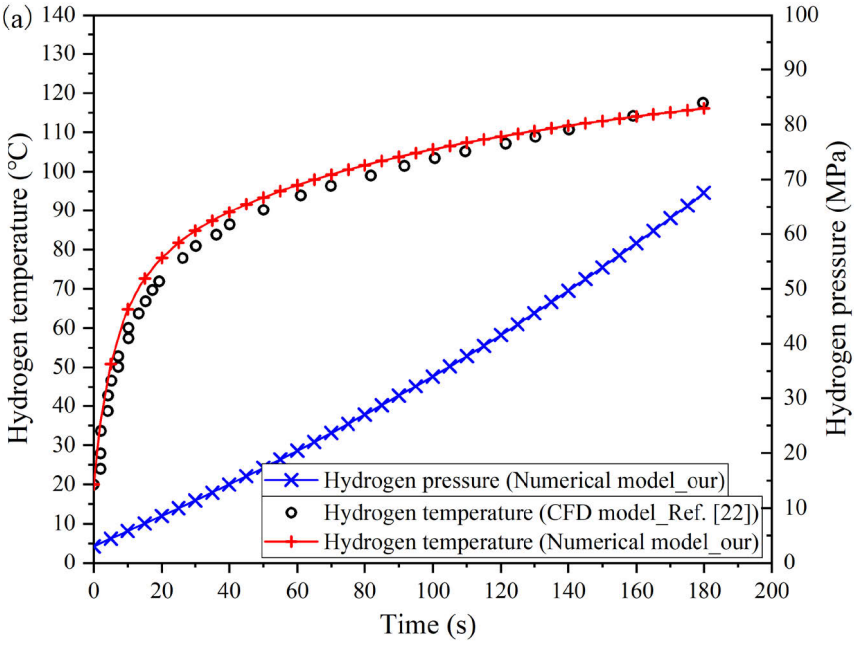

(a) Hydrogen temperature and pressure

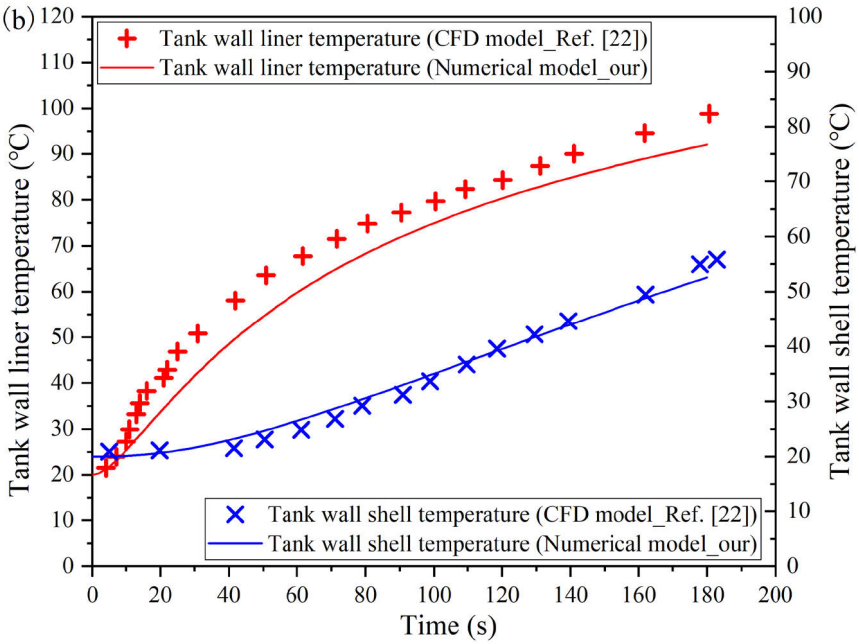

(b) Tank wall liner and shell temperatures

Fig. 2.11 Comparison between the simulation results of the triple-zone lumped parameter numerical model of the hydrogen storage tank and the results of Ref. [22].

2.3.4 Zero-dimensional gas one-dimensional tank wall numerical model

According to the mass conservation Eq. (2.1) and energy conservation Eq. (2.5) of hydrogen and energy conservation Eq. (2.9) -(2.15) of the tank wall, a zero-dimensional gas one-dimensional tank wall (0D1D) numerical model of the hydrogen storage tank during hydrogen filling process was established based on the Matlab/Simulink software platform, as shown in Fig. 2.12. We divide the liner zone of the tank wall into 5 parts on average and divide the shell zone of the tank wall into 10 parts on average. The division results of the physical model are shown in Fig. 2.4, and the implementation process of the Simulink numerical model is shown in Fig. 2.13. For the innermost tank wall, heat is transferred between the tank wall and the hydrogen by heat convection. For the innermost tank wall and the second layer of the tank wall, heat is transferred by heat conduction, as shown in Fig. 2.14. For the outermost tank wall, heat transfer occurs through convection between the outside of the tank wall and the air, and heat transfer occurs between the layers of the tank wall through heat conduction, as shown in Fig. 2.15.

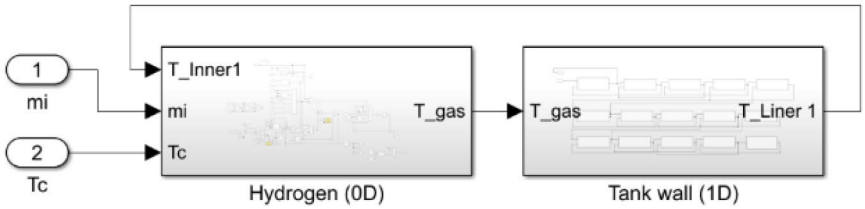

Fig. 2.12 Zero-dimensional gas one-dimensional tank wall (0D1D) numerical model.

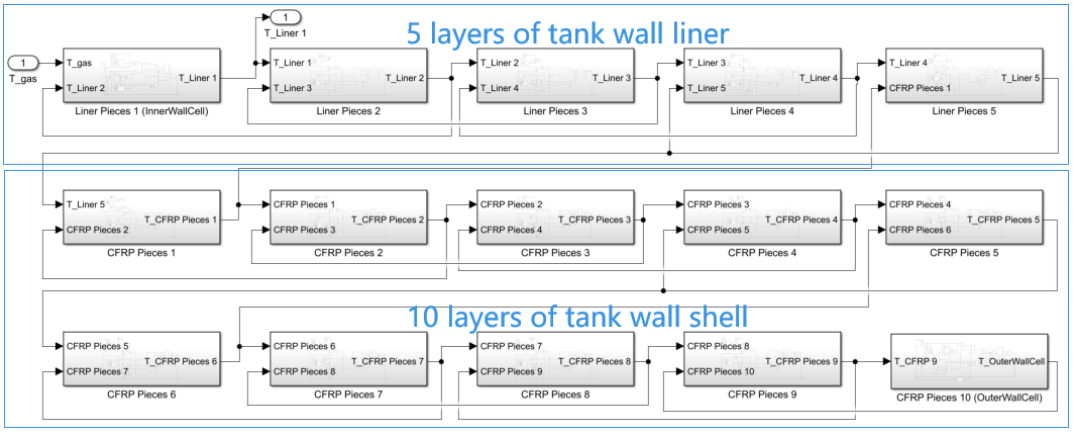

Fig. 2.13 One-dimensional tank wall numerical model.

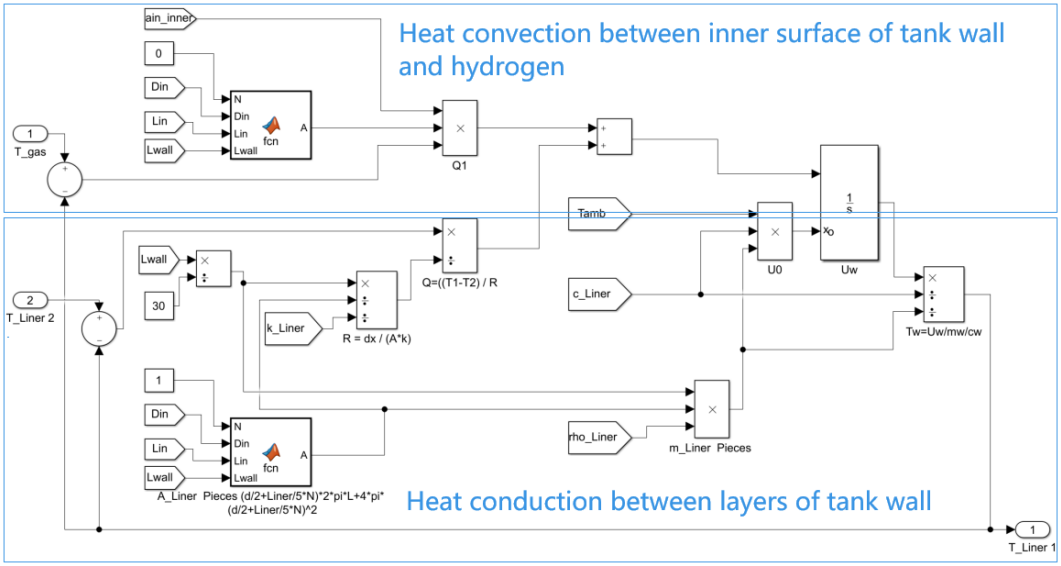

Fig. 2.14 Energy conservation of the innermost tank wall.

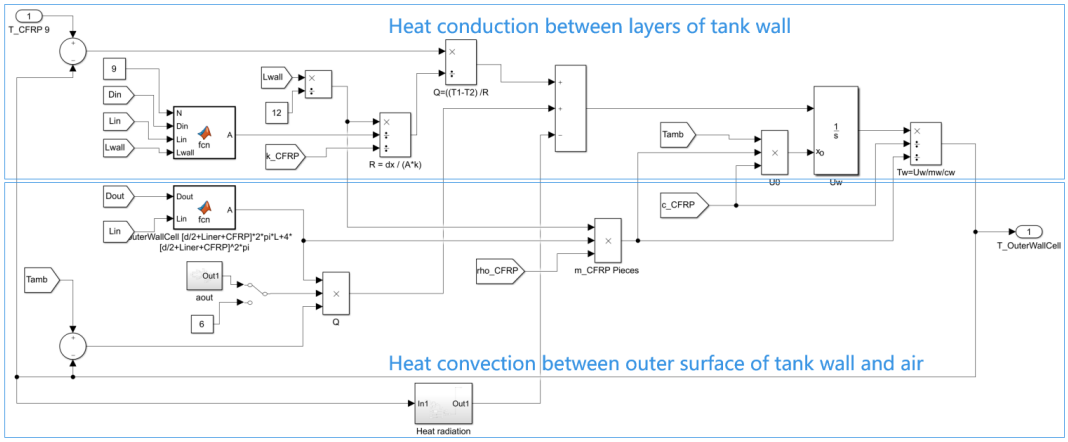

Fig. 2.15 Energy conservation of the outermost tank wall.

In order to verify the accuracy of the 0D1D numerical model of the hydrogen storage tank during the hydrogen filling process, the physical properties and experimental data of the hydrogen storage tank with a volume of 90.5 L and a nominal working pressure of 70 MPa in Ref. [17] were used for comparative verification. The physical properties of the storage tank are shown in Table 2.7, and the initial and boundary conditions are shown in Table 2.8.

The hydrogen temperature experimental data provided in Ref. [17] is a large number of discrete data points. In order to ensure the accuracy and repeatability of the extracted data, this thesis uses WebPlotDigitizer software (version: 4.6, set to the average window algorithm, X=5Px and Y=5Px) to automatically extract the data points in the

Ref. [17] and combine them Plotted together with the simulation results of the 0D1D numerical model, as shown in Fig. 2.16. Fig. 2.16 shows that the simulation results of hydrogen temperature, filling pressure and heat transfer coefficient between hydrogen and tank wall are consistent with the results of Ref. [17]. Comparing Fig. 2.7, Fig. 2.9, Fig. 2.11 and Fig. 2.16, intuitively, the 0D1D numerical model of the hydrogen storage tank can express the experimental data more accurately, and it is more consistent with the structure and heat transfer of the actual storage tank. Therefore, in the research on the hydrogen refuelling protocol in Chapters 5 and 6, the simulation results of the 0D1D numerical model will be used as the standard to verify the accuracy of the hydrogen refuelling protocol.

Fig. 2.16 shows that at the beginning of hydrogen filling, the heat transfer coefficient increases rapidly to a maximum value of about 140 W/m^2/K, and then gradually decreases, indicating that the heat transfer coefficient is not constant. In this section, we use the empirical formula heat transfer coefficient based on the Reynolds number to improve the calculation accuracy of the model. The relevant content of the heat transfer coefficient will be discussed in Chapter 3.

Table 2.7 Physical properties of the hydrogen storage tank in Ref. [17]

Parameter	Physical definition	Value
NWP	Nominal working pressure (MPa)	70
V	Tank volume (m^3)	0.0905
L	Length of horizontal part of tank (m)	0.58
D_{in}	Tank inner diameter (m)	0.434
D_{out}	Tank outer diameter (m)	0.484
k_{wl}	Thermal conductivity of tank liner (W/m/K)	0.4
k_{ws}	Thermal conductivity of tank shell (W/m/K)	0.53
c_{wl}	Specific heat capacity of tank liner (J/kg/K)	1917
c_{ws}	Specific heat capacity of tank shell (J/kg/K)	942
ρ_{wl}	Density of tank liner (kg/m^3)	954
ρ_{ws}	Density of tank shell (kg/m^3)	1442
d_{in}	Injector diameter at tank inlet (m)	0.006

Table 2.8 Initial and boundary conditions in Ref. [17]

Parameter	Physical definition	Value
T_0	Initial hydrogen temperature (℃)	1.9
Tw_0	Initial tank wall temperature (℃)	1.9
T_a	Ambient temperature (℃)	1.9
T_c	Inlet temperature (℃)	7.9
p_0	Initial pressure (MPa)	3
APRR	Average pressure ramp rate (filling speed) (MPa/s)	0.07

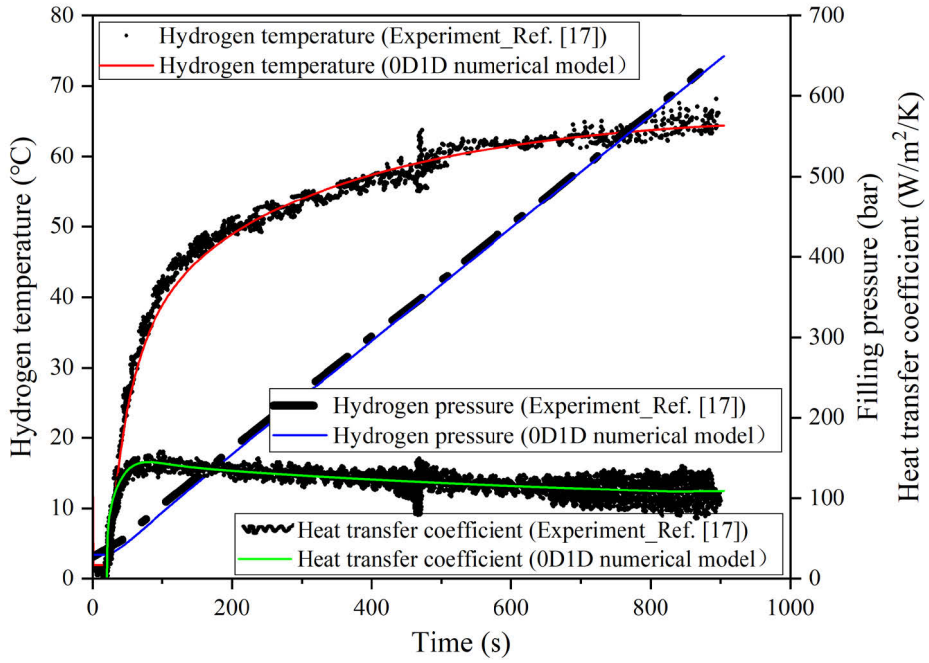

Fig. 2.16 Comparison between the results of the zero-dimensional gas one-dimensional tank wall (0D1D) model and the experimental results of Ref. [17].

2.4 Conclusion

This chapter established and verified the lumped parameter thermodynamic model, analytical model, and numerical model of the hydrogen storage tank, as well as determined the application scope of each model.

Based on mass conservation, energy conservation and the real gas EOS, the single-zone, dual-zone, triple-zone and zero-dimensional gas one-dimensional tank wall (0D1D) lumped parameter thermodynamic models of the hydrogen storage tank were established.

Solving the mathematical and physical equations of the single-zone and dual-zone thermodynamic models, we obtained the corresponding analytical models of single-zone hydrogen temperature, dual-zone hydrogen temperature and tank wall temperature. Combined with Redlich-Kwong gas EOS, we obtained the corresponding analytical model of hydrogen pressure.

Based on the mathematical and physical equations of single-zone, dual-zone, triple-zone and 0D1D thermodynamic models, the corresponding numerical models were established using the Matlab/Simulink software platform.

The experimental data and CFD model results in the reference were used to verify the accuracy of the single-zone and dual-zone analytical models, as well as the single-zone, dual-zone, triple-zone and 0D1D numerical models.

The 0D1D numerical model will be applied to the parametric study in Chapter 3, the optimization study in Chapter 4, and the protocol research in Chapters 5 and 6. The analytical model will be applied to the protocol research in Chapters 5 and 6.

Chapter 3 Parametric study of hydrogen filling system

This section has been submitted in:

Luo H, Yuan C Q, Wang L, Yang T Q, Tong L, Ye F, Yuan Y P, Bénard P, Chahine R, Xiao J S. Heat transfer analysis methodology for compression hydrogen storage tank during charge-discharge cycle. International Journal of Energy Research, 2024, Second review. (JCR Q1, IF=4.6)

My specific contribution of this work was to determine the optimal gas EOS and heat transfer coefficient model in order to improve further the accuracy of the established hydrogen storage tank model of the hydrogen filling system.

During the verification process of the analytical model and numerical model of the hydrogen storage tank in the previous chapter, we found that parameters such as mass flow rate, heat transfer coefficient, and real gas equation of state (EOS) will affect the accuracy of the simulation results. For example, in Section 2.3.2, Ref. [13] used a constant mass flow rate, which resulted in errors between the simulated hydrogen temperature and pressure and the experimental values. There is an error between the hydrogen temperature simulated using a constant heat transfer coefficient and the reference CFD model results in Section 2.3.3, while the hydrogen temperature simulated using an empirical formula heat transfer coefficient based on Reynolds number is consistent with the reference experimental data in Section 2.3.4. In Sections 2.3.1 and 2.3.2, there is a difference between the hydrogen pressure calculated by the analytical model and the numerical model when using different gas EOS. Therefore, this chapter will carry out generalized optimization of the parametric study and systematically study the impact of various initial/boundary conditions, different gas EOS and heat transfer coefficient models on the thermal effects in the storage tank to determine the optimal gas EOS and heat transfer coefficient model and further improve the accuracy of the hydrogen storage tank model.

3.1 Effect of initial and boundary conditions on hydrogen filling

The simulation study in this section uses the zero-dimensional gas one-dimensional tank wall (0D1D) model established and verified in Section 2.3.4. The technical parameters of the filling system are shown in Table 2.7. The initial and boundary conditions used are shown in Table 3.1. During the filling process, the initial conditions are generally the initial temperature and pressure of hydrogen in the storage tank, and the boundary conditions are generally ambient temperature, inlet temperature and mass flow rate. The control variable method is adopted. That is, when studying the impact of a specific condition, the condition under study adopts the changing value in Table 3.1, while the condition not studied adopts the basic value in Table 3.1. The basic values are the same as in Table 2.8. The filling time of all cases was set to 3 min, which is the appropriate filling time for light-duty HFCV recommended by the SAE J2601 hydrogen refuelling protocol.

Table 3.1 Initial and boundary conditions used in this section of the study

Parameter	Physical definition	Basic value	Changing value
p_0	Initial hydrogen pressure (MPa)	3	2，4，6，8
T_0	Initial hydrogen temperature (℃)	1.9	−10，0，10，20
T_a	Ambient temperature (℃)	1.9	−10，0，10，20
T_c	Inlet temperature (℃)	7.9	−10，0，10，20
$\dot{m}$	Filling speed (mass flow rate) (g/s)	10	10，12，14，16

3.1.1 Initial pressure and initial temperature

According to the energy conservation of hydrogen, the final energy of hydrogen is equal to the sum of the initial energy of hydrogen, the entering enthalpy of hydrogen, and the heat lost from the hydrogen to the tank wall. The initial pressure and temperature of the hydrogen in the storage tank directly affect the initial energy of the hydrogen, thereby affecting the final energy of the hydrogen, as well as the final temperature and pressure of the hydrogen.

Fig. 3.1 shows that the final hydrogen temperature decreases as the initial pressure

increases. The final hydrogen temperature and initial pressure can be fitted as $T=-1.17p_0+77.42$, that is, for every 1 MPa increase in initial pressure, the final hydrogen temperature decreases by approximately 1.17 °C. The final hydrogen pressure increases with the initial pressure. The final hydrogen pressure and the initial pressure can be fitted as $p=1.66p_0+34.16$, that is, for every 1 MPa increase in the initial pressure, the final hydrogen pressure increases by about 1.66 MPa. The reason is that the mass flow rate, filling time, inlet temperature and ambient temperature are the same when filling at different initial pressures, so the total mass of hydrogen added and the total enthalpy of hydrogen added are the same, respectively. The heat lost from hydrogen to the tank wall is relatively small, so the increment of hydrogen energy in the tank is approximately equal. When the initial pressure is higher, the mass of the initially lower-temperature hydrogen is greater, so when an equal increment of hydrogen energy is distributed to more of the initially lower-temperature hydrogen, the average temperature will be lower. Under different initial pressure conditions, the increment of hydrogen mass is the same, so the final hydrogen pressure increases as the initial pressure increases.

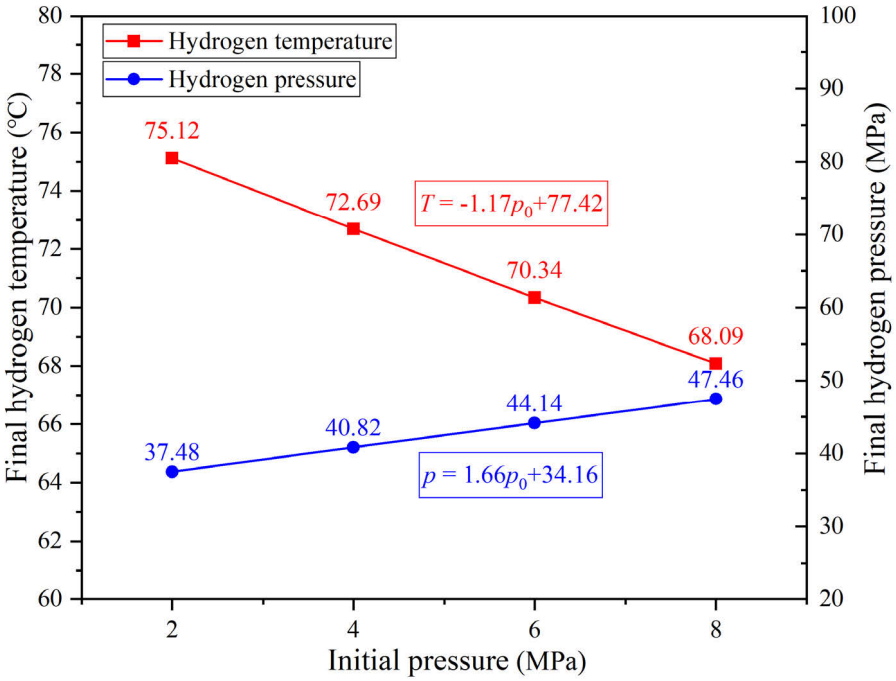

Fig. 3.1 Effect of initial pressure on final hydrogen temperature and pressure.

Fig. 3.2 shows the changes in the final hydrogen temperature and pressure in the tank

as the initial temperature changes. Fig. 3.2 shows an interesting phenomenon that the initial temperature increases from −10 °C to 20 °C with an increment of 30 °C, but the final hydrogen temperature and pressure are almost equal. The reason is that when filling under different initial temperature conditions, the mass flow rate, filling time and inlet temperature are the same, so the total mass of hydrogen added and the inlet enthalpy are equal. Although the initial hydrogen temperature differs by 30 °C, the initial hydrogen pressure is low. That is, the initial hydrogen mass and energy are very small, and they account for a small proportion of the final hydrogen mass and energy. Therefore, the initial temperature has little impact on the final hydrogen temperature and pressure at this time. Meanwhile, it can be seen from the gas EOS that the higher the initial temperature, the less the initial mass under the same initial pressure and volume conditions, resulting in less final hydrogen mass in this case. It can also be seen from the gas EOS that the final hydrogen pressure may be lower.

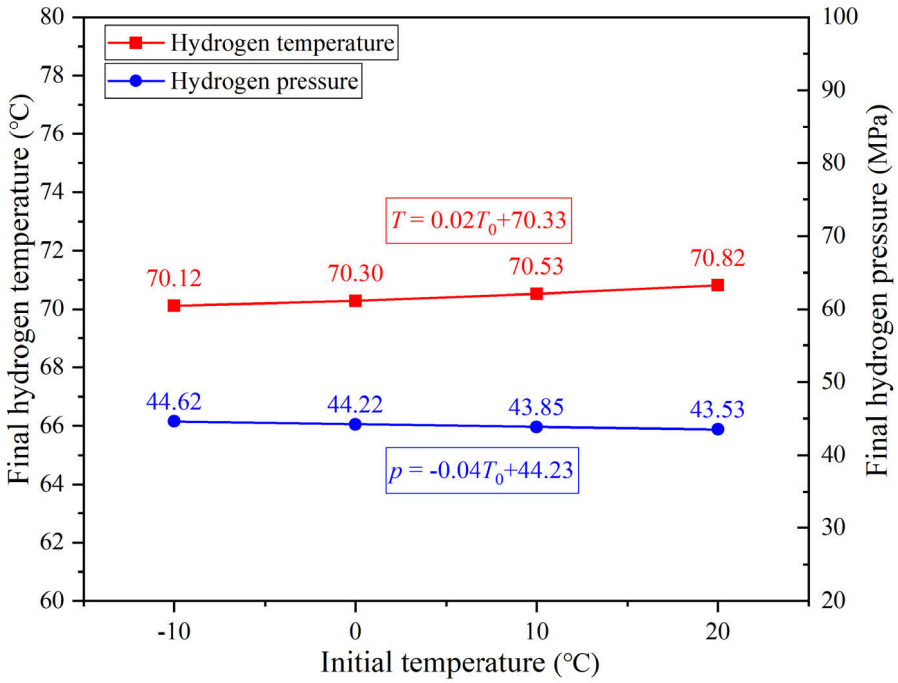

Fig. 3.2 Effect of initial temperature on final hydrogen temperature and pressure.

3.1.2 Ambient temperature and inlet temperature

Ambient temperature affects the rate of heat transfer between the tank wall and the ambient. The greater the difference between the tank wall temperature and the ambient temperature, the stronger the heat transfer between the two and the higher the heat

transfer rate, which affects the changing trend of hydrogen energy and hydrogen temperature in the storage tank. The inlet temperature directly affects the enthalpy of hydrogen entering the storage tank and the hydrogen temperature in the storage tank.

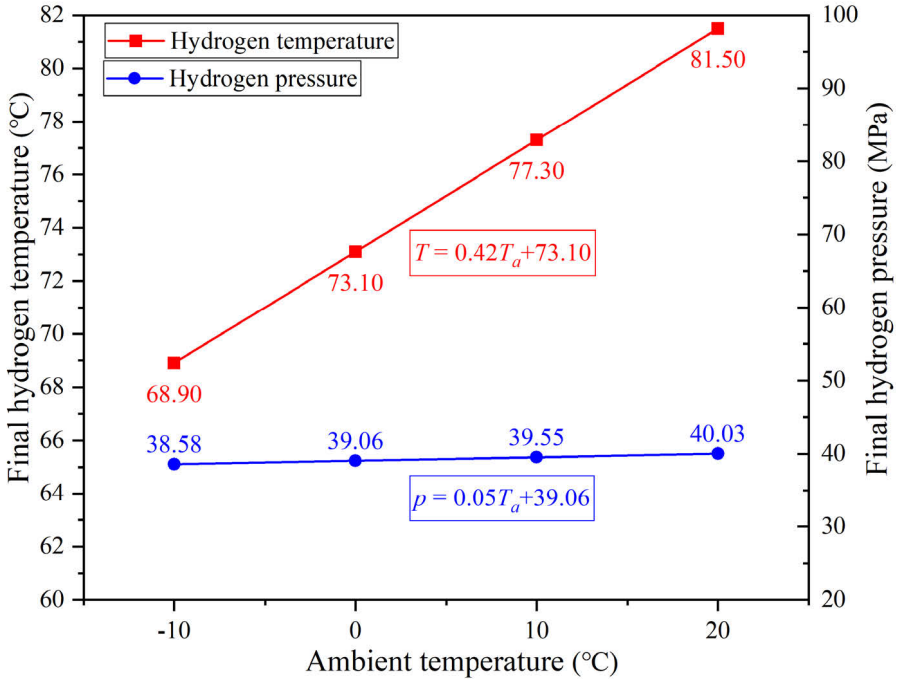

Fig. 3.3 Effect of ambient temperature on final hydrogen temperature and pressure.

Fig. 3.3 shows the changes in the final hydrogen temperature and pressure when the ambient temperature changes. It can be seen that the final hydrogen temperature increases with the increase in ambient temperature. The final hydrogen temperature and ambient temperature can be fitted as $T = 0.42T_a + 73.10$, that is, for every 1 °C increase in ambient temperature, the final hydrogen temperature increases by approximately 0.42 °C. The final hydrogen pressure increases slowly with the increase of ambient temperature. When the ambient temperature increases by 30 °C, the final hydrogen pressure only increases by about 1.45 MPa. The reason is that the higher the ambient temperature, the lower the temperature difference between the tank wall and the ambient, and the less heat transferring from the tank wall to the ambient, resulting in a higher energy of the hydrogen in the tank and, therefore, a higher final hydrogen temperature. The mass flow rate, filling time, inlet temperature, initial pressure and initial temperature when filling at different ambient temperatures are the same, so the final total mass of hydrogen is equal. According to the real gas EOS, when the mass of hydrogen

in the tank is equal, the higher the hydrogen temperature, the greater the hydrogen pressure.

Fig. 3.4 shows the changes in final hydrogen temperature and pressure when the inlet temperature changes. It can be seen that the final hydrogen temperature increases significantly with the increase in inlet temperature. The final hydrogen temperature and the inlet temperature can be fitted as $T = 0.81T_c + 67.45$, that is, for every 1 °C increase in the inlet temperature, the final hydrogen temperature increases by about 0.81 °C. The sensitivity of the inlet temperature to the final hydrogen temperature is higher than the initial temperature and ambient temperature. The reason is that the inlet temperature directly affects the enthalpy of hydrogen entering the storage tank. Therefore, currently, hydrogen refuelling stations (HRS) generally use the precooling filling method to fill HFCV to reduce the final hydrogen temperature in the storage tank and ensure its safety. The final hydrogen pressure increases slowly as the inlet temperature increases. When the inlet temperature increases by 30 °C, the final hydrogen pressure only increases by about 2.82 MPa. The reason is the same as the impact of ambient temperature on the final hydrogen pressure, which can also be analyzed based on the real gas EOS.

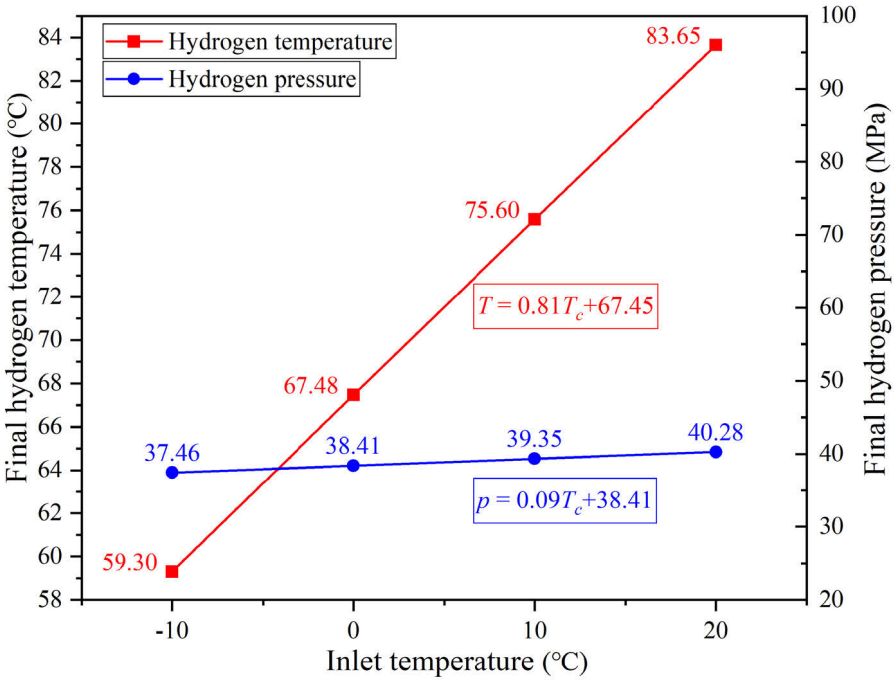

Fig. 3.4 Effect of inlet temperature on final hydrogen temperature and pressure.

3.1.3 Filling speed

The filling speed affects the rate of energy entering the tank and the total time for the heat transfer from hydrogen to the tank wall. The faster the filling speed, the more energy enters the storage tank per unit time, and the faster the hydrogen temperature rises. Meanwhile, the faster the filling speed, the shorter the total filling time, and the less heat the hydrogen transfers to the tank wall, resulting in more hydrogen energy accumulating in the tank and thus increasing the final hydrogen temperature.

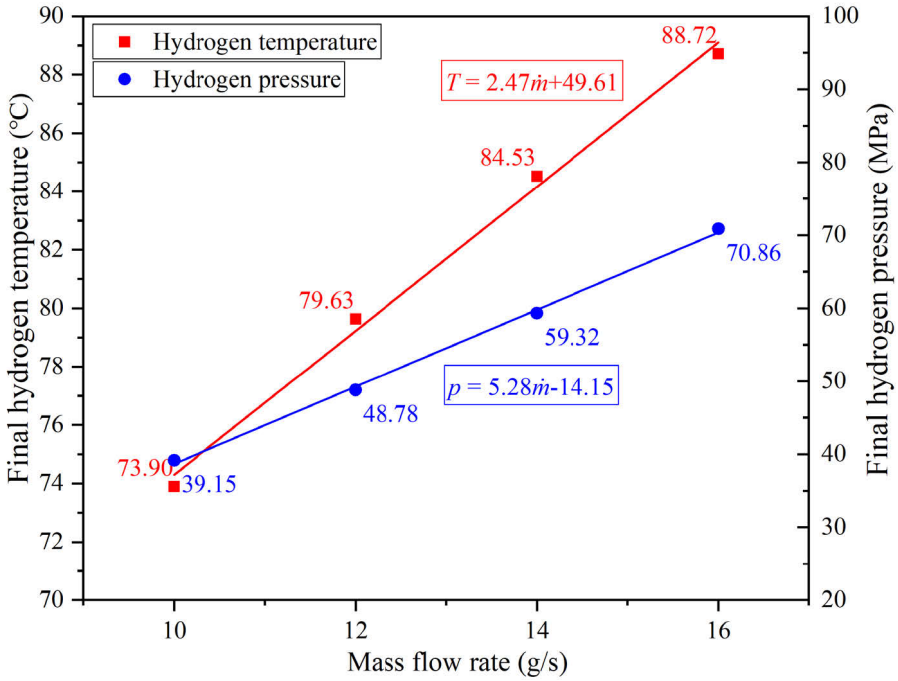

Fig. 3.5 Effect of filling speed (mass flow rate) on final hydrogen temperature and pressure.

Fig. 3.5 shows the changes in the final hydrogen temperature and pressure in the tank when the filling speed (mass flow rate) is changed. It can be seen that the greater the mass flow rate, the greater the final hydrogen temperature and pressure. The final hydrogen temperature and pressure and the mass flow rate can be fitted as $T = 2.47\dot{m} + 49.61$, $p = 5.28\dot{m} - 14.15$, respectively. That is, for every 1 g/s increase in the mass flow rate, the final hydrogen temperature and pressure increase by 2.47 °C and 5.28 MPa, respectively. The reason is that when the total filling time is equal, the greater the mass flow rate, the more enthalpy entering the storage tank, the higher the final hydrogen internal energy, and the higher the final hydrogen temperature. According to the real gas EOS, the greater the final hydrogen pressure.

Comparing Figs. 3.1-3.5, we can find that for the sensitivity of the final hydrogen

temperature and pressure, when the initial temperature, ambient temperature and inlet temperature increase by 1 ℃, the changes in the final hydrogen temperature are 0.02 ℃, 0.42 ℃ and 0.81 ℃, the changes in the final hydrogen pressure are −0.04 MPa, 0.05 MPa and 0.09 MPa. That is, the sensitivity of the inlet temperature to the final hydrogen temperature is higher than the initial temperature and ambient temperature. The initial temperature, ambient temperature and inlet temperature have a smaller effect on the final hydrogen pressure. When the mass flow rate increases by 1 g/s, the hydrogen pressure changes as high as 5.28 MPa, which is higher than 1.66 MPa when the initial pressure increases by 1 MPa. Therefore, the mass flow rate is relatively more sensitive to the final hydrogen pressure. The conclusions here will be used to determine the filling conditions in Section 3.2.4. Earlier studies by our team have shown that there is a coupling relationship between multiple initial and boundary conditions [19, 20], but this thesis does not further discuss and summarize the coupling relationship of multiple parameters because the focus of the parametric study in this thesis is on the gas EOS and heat transfer coefficient model.

3.2 Effect of gas equation of state on hydrogen filling

During the hydrogen filling process, the pressure of hydrogen in the storage tank is high. At this time, if the ideal gas EOS ($p = \mathrm{R}T/v$) is used, errors will occur, and the real gas EOS should be used. The simplest real gas EOS is the Abel-Nobel EOS:

$$p = \frac{\mathrm{R}T}{v - b} \tag{3.1}$$

where b is the volume parameter, which takes into account the non-zero volume factor of the molecule. The pressure becomes infinite when the molar specific volume v needs to be compressed to b rather than when the molar specific volume v needs to be compressed to 0 as described in the ideal gas EOS. This equation solves the accuracy problem at high pressure to a certain extent.

In order to further improve the accuracy of the gas EOS, many forms of real gas EOS have been proposed, among which the most famous and far-reaching one is the van der Waals real gas EOS:

$$p = \frac{RT}{v-b} - \frac{a}{v^2} \tag{3.2}$$

where a/v^2 is the gravitational term, which further considers the factor that reduces the pressure caused by the attraction effect between molecules based on the Abel-Nobel EOS.

The real gas EOS also includes modified forms developed on the basis of the van der Waals gas EOS, such as the Redlich-Kwong, Soave, and Peng-Robinson real gas EOS. The numerical model of hydrogen filling in Chapter 2 of this thesis uses the real gas EOS Eq. (2.16) that introduces the compressibility factor *Z* when calculating the hydrogen pressure. *Z* was queried from the physical property database developed by the National Institute of Standards and Technology (NIST). This method is defined as a method based on the NIST database calculation in this thesis. The analytical model of hydrogen filling in Chapter 2 uses the Redlich–Kwong real gas EOS when calculating hydrogen pressure. The new filling method proposed in Chapter 6 will use a polynomial gas EOS.

3.2.1 van der Waals gas equation of state

The van der Waals gas EOS Eq. (3.2) contains parameters *a* and *b*. In this section, the experimental values of the temperature and pressure of hydrogen at the critical point will be used to calculate parameters *a* and *b*. Fig. 3.6 is the van der Waals isotherm. In the figure, based on the critical temperature T_c, critical pressure p_c and critical molar specific volume v_c, each state variable is expressed as a dimensionless form of reduced temperature T_r ($T_r = T/T_c$), reduced pressure p_r ($p_r = p/p_c$) and reduced molar specific volume v_r ($v_r = v/v_c$). At the critical point of substance, that is, at (1,1) of the isotherm T_r=1 in Fig. 3.6, the slope and curvature of the curve T_r=1 are both zero. Therefore, for Eq. (3.2), $(\partial p/\partial v)_T = 0$ and $\left(\partial^2 p/\partial v^2\right)_T = 0$ when T=T_c, p=p_c and v=v_c. According to van der Waals gas EOS Eq. (3-2), it can be calculated:

$$\left(\frac{\partial p}{\partial v}\right)_T = -\frac{RT}{(v-b)^2} + \frac{2a}{v^3} \tag{3.3}$$

$$\left(\frac{\partial^2 p}{\partial v^2}\right)_T = \frac{2RT}{(v-b)^3} - \frac{6a}{v^4} \tag{3.4}$$

When T=T_c, p=p_c and v=v_c, the above two equations are equal to zero, and the solution can be

$$p_c = \frac{a}{27b^2} \tag{3.5}$$

$$v_c = 3b \tag{3.6}$$

$$T_c = \frac{8a}{27Rb} \tag{3.7}$$

For two unknowns, a and b, there are three equations Eqs. (3.5), (3.6) and (3.7). Solving Eq. (3.6) gives $b = v_c/3$, and solving simultaneous Eqs. (3.5) and (3.7) gives $b = \mathrm{R}T_c/8p_c$. When the experimental values of p_c, v_c and T_c are substituted into the $b = v_c/3$ and $b = \mathrm{R}T_c/8p_c$, two different b values can be obtained, which is inconsistent with the actual situation. Since critical volume is more difficult to measure accurately than critical pressure and critical temperature, $b = \mathrm{R}T_c/8p_c$ is used to determine the values of a and b. Combining the experimental critical parameters of hydrogen $T_c = 33.3$ K, $p_c = 1.28\times10^6$ Pa and $v_c = 6.5\times10^{-5}$ m^3/mole [76], it can be calculated that a=25.2 J·m^3/kilomole^2, b=0.027 m^3/kilomole.

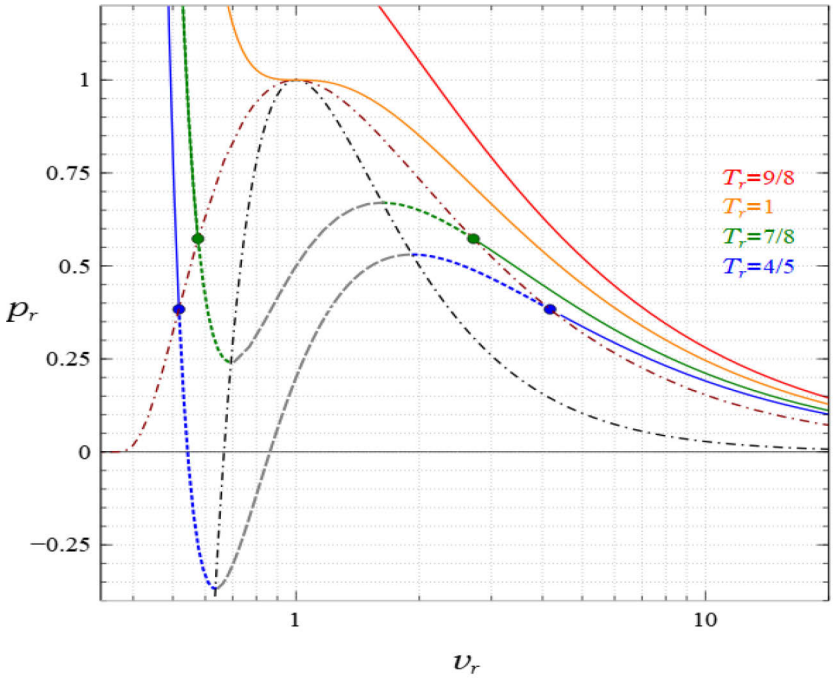

Fig. 3.6 Van der Waals isotherm ($T_r = T/T_c$, $p_r = p/p_c$, $v_r = v/v_c$).

3.2.2 Modified gas equation of state

In order to further improve the accuracy of the gas EOS, many modified van der Waals gas EOS have been proposed, among which the modified forms of Redlich-Kwong, Soave and Peng-Robinson are widely used.

The modified gas EOS in Redlich-Kwong form can be expressed as [77]

$$p = \frac{\mathrm{R}T}{v-b} - \frac{a}{\sqrt{T}v\left(v+b\right)} \tag{3.8}$$

The modified gas EOS in Soave form can be expressed as [77]

$$p = \frac{\mathrm{R}T}{v-b} - \frac{a\alpha}{v\left(v+b\right)} \tag{3.9}$$

where $\alpha = 1.202e^{\left(-0.30288T_r\right)}$.

The modified gas EOS in Peng-Robinson form can be expressed as [77]

$$p = \frac{\mathrm{R}T}{v-b} - \frac{a}{v^2+2bv-b^2} \tag{3.10}$$

According to the relevant knowledge of the isotherm in Fig. 3.6, we project the gas EOS Eqs. (3.8), (3.9) and (3.10) on the *p*-*v* plane, then the slope and curvature are both 0 at the critical point (v_c, p_c) of the isotherm. At this time, the first-order and second-order partial derivatives of *p* versus *v* are both 0. The expressions of parameters *a* and *b* in the Redlich-Kwong, Soave and Peng-Robinson gas EOS can be solved, as shown in Table 3.2. By substituting the critical temperature $T_c = 33.3$ K, critical pressure $p_c = 1.28\times10^6$ Pa and critical molar specific volume $v_c = 6.5\times10^{-5}$ m^3/mole of hydrogen obtained experimentally into the expressions of parameters *a* and *b* in Table 3.2, the experimental values of *a* and *b* can be calculated. The method for obtaining the experimental values of hydrogen critical T_c, p_c and v_c can be found in Ref. [76].

The Joule-Thomson inverse curve is a very sensitive test method for the gas EOS (near critical point). Therefore, it can be used to evaluate parameters in different forms of gas EOS. The Joule-Thomson inverse curve data for hydrogen comes from NASA Technical Note D-6807 (1972) [78]:

$$p_r = \sum_{i=0}^{6} A_i T_r^i \tag{3.11}$$

where A_0=−15.5988252, A_1=26.0321395, A_2=−9.7459013, A_3=2.4207304, A_4=−0.49105816, A_5=0.05932495 and A_6=−0.002913248.

Table 3.2 Parameters in different forms of the modified gas equation of state

Form	Parameter *a*			Parameter *b*			R^2
	Expressions	Experimental	Fitted	Expressions	Experimental	Fitted	
R-K	$0.42748R^2T_c^{2.5}/p_c$	1.477e-1	1.690e-1	$0.08662RT_c/p_c$	1.874e-5	1.874e-5	0.99
Soave	$0.427487T_c^2/p_c$	3.703e-4	3.239e-2	$0.08664RT_c/p_c$	1.874e-5	1.874e-5	0.99
P-R	$0.45724R^2T_c^2/p_c$	2.738e-2	2.249e-2	$0.07780RT_c/p_c$	1.683e-5	1.683e-5	0.99

We set the value range of T_r as 0.9 to 6.28 and the increasing step to 0.01. This range can ensure that the hydrogen temperature and pressure calculated by Eq. (3.11) are both positive numbers. The Joule-Thomson inverse curve can be calculated by Eq. (3.11). Combining the critical temperature $T_c = 33.3$ K, critical pressure $p_c = 1.28\times10^6$ Pa and critical molar specific volume $v_c = 6.5\times10^{-5}$ m^3/mole of hydrogen obtained through experiments, the corresponding Joule-Thomson inverse curve can be calculated. And because $T = T_r T_c$, $p = p_r p_c$ and $v = v_r v_c$, we can finally draw a three-dimensional space curve for (p, v, T), as shown in the black curve in Fig. 3.7(a), which can be regarded as the standard data of the real gas EOS. The modified gas EOS in the form of Redlich-Kwong, Soave and Peng-Robinson are used to fit the black curve in Fig. 3.7(a), respectively. During the fitting process, the value of parameter *b* is fixed to the experimental value in Table 3.2 to facilitate a comparison of the fitted value and experimental value of parameter *a*. The parameter values determined by the fitting are shown in Table 3.2.

Table 3.2 shows that the R^2 fitted by the three modified gas EOS are all greater than or equal to 0.99, indicating that the fitting process is accurate and reliable. The comparison between the fitted value and experimental value of parameter *a* in Table 3.2 shows that the relative error between the fitted value and experimental value of parameter *a* in

Redlich-Kwong form is smaller, indicating that compared with Soave and Peng-Robinson forms, Redlich-Kwong form can more accurately characterize the thermal behaviour of gases. Fig. 3.7(b) intuitively shows that the fitting curve in the Redlich-Kwong form is closer to the standard Joule-Thomson inverse curve. Meanwhile, the Redlich-Kwong form has been widely used due to its simple form. Therefore, the Redlich-Kwong form of the gas EOS is used in the analytical model of hydrogen filling in Chapter 2. Using the experimental values of parameters *a* and *b*, we can determine the specific form of the Redlich-Kwong EOS as

$$p = \frac{RT}{v - 1.874\times10^{-5}} - \frac{1.477\times10^{-1}}{\sqrt{T}v\left(v + 1.874\times10^{-5}\right)} \tag{3.12}$$

where p is the pressure of hydrogen (Pa). T is the temperature of hydrogen (K). v is the molar specific volume of hydrogen (m^3/mole). R is the universal gas constant, whose value is 8.314 J/mole/K.

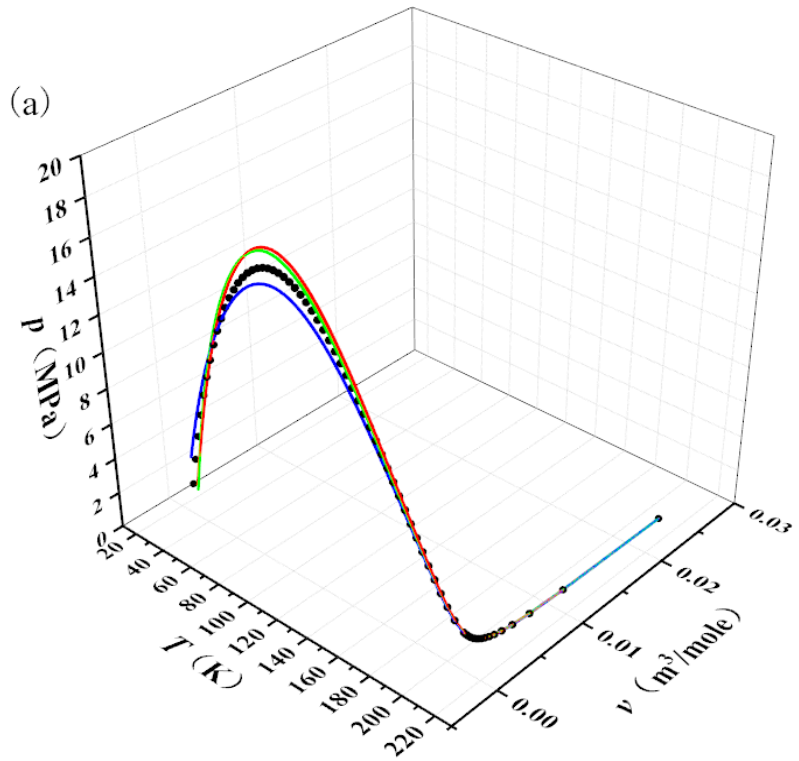

(a) Fitting curve in three-dimensional space.

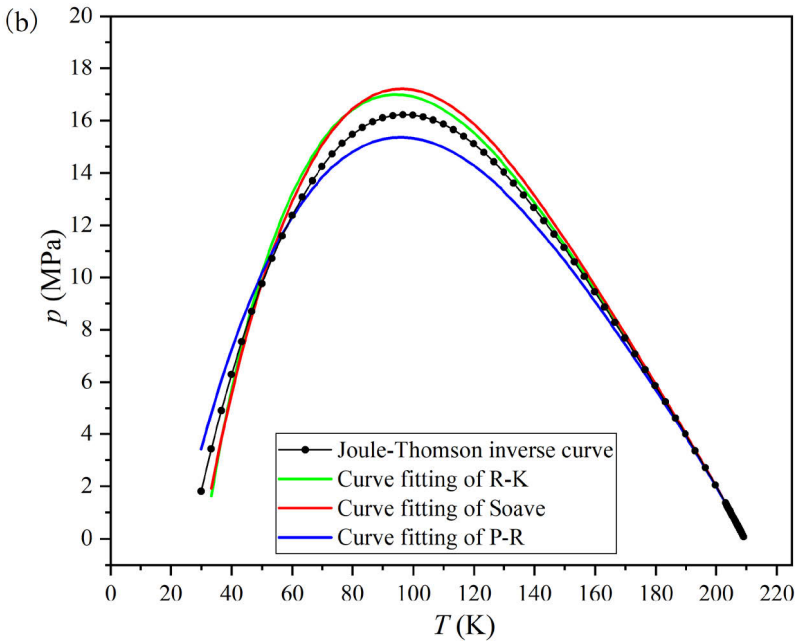

(b) Projection of the fitting curve in the three-dimensional space on the plane *p*-*T*.

Fig. 3.7 Using the Joule-Thomson inverse curve to fit different forms of the modified gas equation of state.

3.2.3 Polynomial gas equation of state

Bourgeois and his collaborators believe that calculations based on the NIST database appear to be more suitable for simulating the high-pressure hydrogen filling process than any other type of gas EOS [79]. Therefore, it is necessary to explore a reliable EOS that directly represents the NIST data in a simplified form to meet the computational accuracy requirements of engineering applications. This EOS can be expressed as a polynomial equation using different coefficients to represent the different thermophysical properties of hydrogen. The coefficients can be determined by fitting data generated based on the NIST database. The polynomial gas EOS determined in this section will be used in Chapter 6.

First, we determine the polynomial form of the real gas EOS as

$$p = \sum_{i=0}^{N}\sum_{j=0}^{N-i} a_{ij} T^i \rho^j \tag{3.13}$$

where ρ is the density of hydrogen (mole/L). T is the temperature of hydrogen (K). p is the pressure of hydrogen (MPa). When N=5, the specific form of the polynomial gas EOS Eq. (3.13) is

$$
\begin{aligned}
p = {} & a_{00}T^0\rho^0 + a_{01}T^0\rho^1 + a_{02}T^0\rho^2 + a_{03}T^0\rho^3 + a_{04}T^0\rho^4 + \\
& a_{05}T^0\rho^5 + a_{10}T^1\rho^0 + a_{11}T^1\rho^1 + a_{12}T^1\rho^2 + a_{13}T^1\rho^3 + \\
& a_{14}T^1\rho^4 + a_{20}T^2\rho^0 + a_{21}T^2\rho^1 + a_{22}T^2\rho^2 + a_{23}T^2\rho^3 + \\
& a_{30}T^3\rho^0 + a_{31}T^3\rho^1 + a_{32}T^3\rho^2 + a_{40}T^4\rho^0 + a_{41}T^4\rho^1 + a_{50}T^5\rho^0 + d
\end{aligned}
\tag{3.14}
$$

We set the change range of hydrogen temperature as 223.15 K to 373.15 K and the increasing step to 2 K. The hydrogen pressure changes in the range of 0.1 MPa to 100.1 MPa, and the increasing step is 2 MPa. By combining different temperatures and pressures, 3876 data sets of different hydrogen temperatures and pressures were obtained. Calculations were performed based on the NIST database to obtain 3876 different groups (p, T and ρ). These data are used to fit the polynomial gas EOS Eq. (3.14), and the coefficients obtained are shown in Table 3.3.

Table 3.3 Parameter values in the polynomial gas equation of state

Coefficient value (R^2=0.998)				
a_{00}: 0.000e+00	a_{01}: −1.185e+02	a_{02}: 3.744e+00	a_{03}: −8.399e−02	a_{04}: 1.157e−03
a_{05}: −6.779e−06	a_{10}: −3.512e+01	a_{11}: 1.325e+00	a_{12}: −2.807e−02	a_{13}: 3.811e−04
a_{14}: −2.353e−06	a_{20}: 2.094e−01	a_{21}: −5.506e−03	a_{22}: 7.174e−05	a_{23}: −4.348e−07
a_{30}: −6.217e−04	a_{31}: 1.026e−05	a_{32}: −6.150e−08	a_{40}: 9.188e−07	a_{41}: −7.177e−09
a_{50}: −5.408e−10	d: 2.346e+03			

3.2.4 Effect of gas equation of state on hydrogen filling

This section compared the temperature and pressure of hydrogen calculated by the van der Waals real gas EOS, the Redlich-Kwong modified real gas EOS, the polynomial real gas EOS, and the NIST database. The hydrogen storage tank model in Section 3.1 was used, and only the gas EOS in the model was changed. According to the research in Section 3.1, the inlet temperature has a greater impact on the final hydrogen temperature, and the mass flow rate has a greater impact on the final hydrogen pressure. In order to highlight the influence of different gas EOS on the thermal effect of hydrogen filling, extreme filling conditions are adopted. That is, the inlet temperature and mass flow rate adopt the upper and lower boundary values in Table 3.1, respectively, and other filling conditions adopt the basic value in Table 3.1.

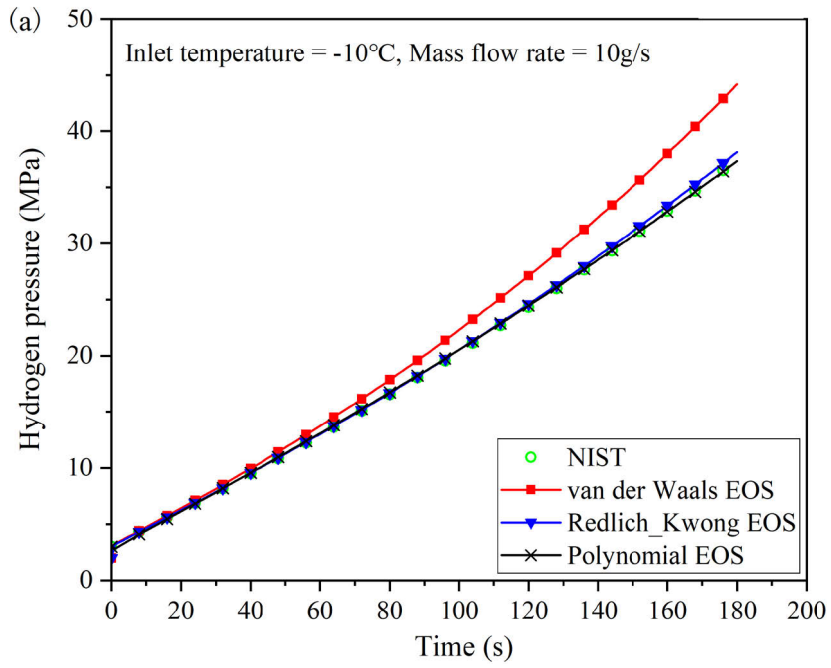

(a) Inlet temperature −10 °C, mass flow rate 10 g/s

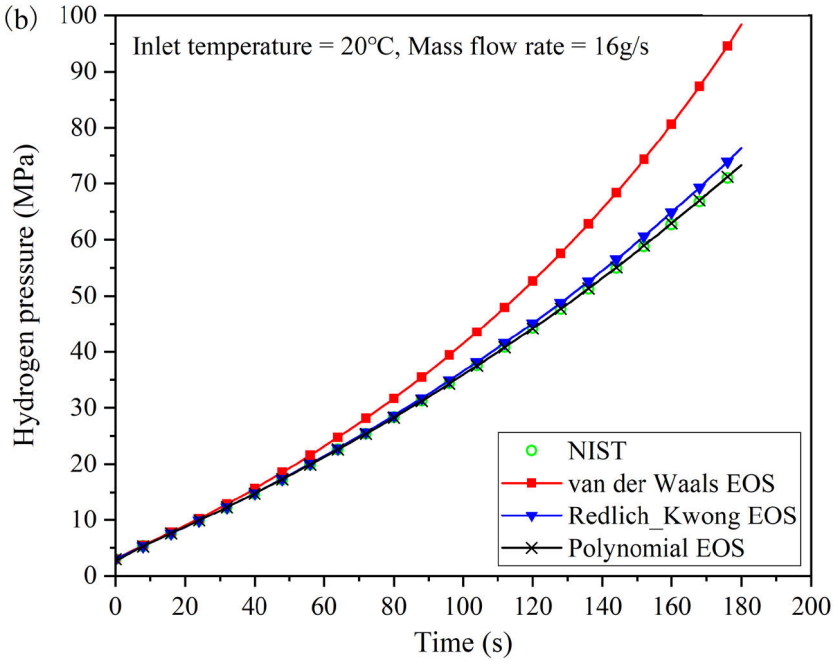

(b) Inlet temperature 20 °C, mass flow rate 16 g/s

Fig. 3.8 Hydrogen pressure calculated using different gas equations of state at different inlet temperatures and mass flow rates.

The calculation results show that different gas EOS have a negligible impact on the calculation results of hydrogen temperature but have a more significant impact on the

calculation results of hydrogen pressure. Fig. 3.8 compares the hydrogen pressure calculated using different forms of the gas EOS. Fig. 3.8(a) shows that if the final hydrogen pressure calculated based on the NIST database is used as the standard, the relative error of the final hydrogen pressure calculated by the polynomial gas EOS is 0.30%, the Redlich-Kwong gas EOS is 1.83%, and the van der Waals gas EOS is 17.90%. That is, the polynomial gas EOS is most consistent with the one calculated based on the NIST database, while the van der Waals gas EOS is less accurate. The accuracy of the modified gas EOS in the Redlich-Kwong form is higher than that of van der Waals. That is, the modified gas EOS improves the van der Waals gas EOS to a certain extent. Fig. 3.8(b) has a similar pattern to Fig. 3.8(a), but the final hydrogen pressure is higher in Fig. 3.8(b). The relative error between the van der Waals gas EOS and NIST is 34.57 %, which is higher than the error in Fig. 3.8(a). That is, the higher the hydrogen pressure in the storage tank, the greater the deviation of the hydrogen pressure calculated using the van der Waals gas EOS. In short, because the hydrogen pressure is relatively high during the hydrogen filling process, real gas EOS based on NIST database calculations or polynomials can be used in order to reduce calculation errors. The calculation method based on the NIST database is applied to the numerical model of the hydrogen storage tank in Chapter 2. Although the polynomial real gas EOS is very accurate, there are many coefficients in the equation, and the form is relatively complex, so it is only used in Chapter 6. The Redlich-Kwong form of the modified gas EOS has a relatively high accuracy, few parameters, and a simple form, so it is applied to the analytical model of the hydrogen storage tank in Chapter 2.

3.3 Effect of heat transfer coefficient on hydrogen filling

According to the hydrogen mass flow rate, the diameter of the injector at the tank inlet and the aspect ratio of the tank, the heat transfer form in the tank during the hydrogen filling process can be divided into natural convection, forced convection and mixed convection. Mixed convection refers to the simultaneous existence of natural convection and forced convection. The heat transfer coefficient in the storage tank is a key parameter in heat transfer analysis, and some studies treat it as a constant [33]. However, sometimes, a more accurate heat transfer coefficient is needed to simulate a

more accurate actual hydrogen filling process. Ignoring the accuracy of the heat transfer coefficient may lead to an inaccurate prediction of the hydrogen temperature in the tank, adversely affecting the safety of the tank. Some studies choose to use a constant heat transfer coefficient to simulate the heat transfer between hydrogen in the tank and the tank wall. This method seems to be inaccurate. Research in Ref. [80] shows that as the mass flow rate of hydrogen (2 to 8 g/s) and the diameter of the injector at the tank inlet change (3 to 10 mm), the heat transfer coefficient between hydrogen and the tank wall changes from 200 to 1000 W/m^2/K. Currently, there is no single standard method for calculating the heat transfer coefficient between hydrogen and the tank wall. The heat transfer coefficient is generally calculated based on experimental studies and is strongly dependent on the aspect ratio of the tank, the orientation of the tank and the nature of the internal flow.

3.3.1 Heat transfer coefficient based on empirical formula

Some dimensionless parameters are often used in heat transfer analysis, such as the Nusselt number Nu, which is an important indicator of the intensity of convective heat transfer. There is a relationship between the Nusselt number and the heat transfer coefficient in the storage tank [17]:

$$\mathrm{Nu} = \frac{\alpha_{\mathrm{in}} L}{\lambda} \tag{3.15}$$

where α_{in} is the heat transfer coefficient between hydrogen and the tank wall (W/m^2/K). L is the characteristic length (m), which is equal to the inner diameter of the storage tank D_{in} during the filling process. λ is the thermal conductivity coefficient of hydrogen (W/m/K).

Refs. [81, 82] expresses the heat transfer correlation during hydrogen filling as

$$\mathrm{Nu} = a\mathrm{Ra}_{D_{\mathrm{in}}}^{b} + c\,\mathrm{Re}_{d_{\mathrm{in}}}^{d} \tag{3.16}$$

where $\mathrm{Ra}_{D_{\mathrm{in}}}$ is the Rayleigh number in the storage tank. $\mathrm{Re}_{d_{\mathrm{in}}}$ is the Reynolds number at the inlet of the storage tank. d_{in} is the diameter of the injector at the inlet of the storage tank (m). a, b, c and d are parameters, and their values are determined by

experiments. Eq. (3.16) considers both the effects of forced convection and natural convection on heat transfer during hydrogen filling.

Research in Ref. [17] shows that for a compact tank (the ratio of length to diameter is small), forced convection is the main form in the tank during the hydrogen filling process, and natural convection can be ignored. Because all parts of the tank are close to the inlet, they are affected by the turbulence of the inlet airflow. Therefore, the Nusselt number at this time can be expressed as

$$\mathrm{Nu} = 0.14\,\mathrm{Re}_{d_{\mathrm{in}}}^{0.67} \tag{3.17}$$

where $\mathrm{Re}_{d_{\mathrm{in}}} = \left(\rho v d_{\mathrm{in}}\right)/\mu = \left(4\dot{m}\right)/\left(\pi\mu d_{\mathrm{in}}\right)$. ρ is the density of hydrogen (kg/m^3). v is the kinematic viscosity of hydrogen (m^2/s). $\dot{m}$ is the mass flow rate of hydrogen (kg/s). μ is the dynamic viscosity of hydrogen (Pa·s). This heat transfer coefficient formula does not contain parameters and is widely used.

Research in Ref. [83] shows that during the hydrogen filling process, due to the significant mass flow rate of hydrogen, the intensity of forced convection is significant, and the intensity of natural convection is slight. Therefore, forced convection is mainly considered during the filling process, and natural convection can be ignored. Under forced convection conditions, the Nusselt number can be expressed in terms of Prandtl number and Reynolds number:

$$\mathrm{Nu} = a\left[\mathrm{Re}_{d_{\mathrm{in}}}\,\mathrm{Pr}\left(\frac{{d_{\mathrm{in}}}^2}{L_{\mathrm{in}} D_{\mathrm{in}}}\right)\right]^{0.632} \tag{3.18}$$

where a is a parameter. Pr is Prandtl number. L_{in} is the internal length of the hydrogen storage tank (m).

In order to further improve the calculation accuracy of the empirical formula heat transfer coefficient, Eqs. (3.17) and (3.18), SOC can be further introduced for correction [84]. SOC can be expressed as

$$\mathrm{SOC} = \frac{\rho_{\mathrm{H_2}}(p,T)}{\rho_{\mathrm{H_2}}\left(\mathrm{NWP},15^{\circ}\mathrm{C}\right)} \tag{3.19}$$

where $\rho_{H_2}\left(\mathrm{NWP},15^{\circ}\mathrm{C}\right)$ and $\rho_{H_2}(p,T)$ respectively represent the hydrogen density under nominal working pressure and 15 °C, and the real-time hydrogen density during the filling process (kg/m^3).

Combining the Eqs. (3.15), (3.17), (3.18) and (3.19), the heat transfer coefficient between hydrogen and the inner wall of the tank during the filling process can be expressed as

$$\alpha_{\mathrm{in}}=\frac{0.14\lambda\left(\mathrm{Re}_{d_{\mathrm{in}}}/\mathrm{SOC}\right)^{0.67}}{D_{\mathrm{in}}} \tag{3.20}$$

$$\alpha_{\mathrm{in}}=a\frac{\lambda}{D_{\mathrm{in}}}\left[\frac{\mathrm{Re}_{d_{\mathrm{in}}}\,\mathrm{Pr}}{\mathrm{SOC}}\left(\frac{{d_{\mathrm{in}}}^2}{L_{\mathrm{in}}D_{\mathrm{in}}}\right)\right]^{0.632} \tag{3.21}$$

Ref. [57] believes that the heat transfer coefficient is related to the hydrogen mass flow rate and the real-time pressure in the storage tank and can be expressed as a function of them. That is, the heat transfer coefficient during the filling process can be expressed as

$$\alpha_{\mathrm{in}}=a\dot{m}\frac{p_N}{p_{\mathrm{on}}} \tag{3.22}$$

where a is the correction factor. $\dot{m}$ is the hydrogen mass flow rate (kg/s). p_N is the nominal working pressure of the onboard tank (Pa). p_{on} is the real-time pressure in the onboard tank (Pa).

Ref. [85] empirically determined the heat transfer coefficient between hydrogen and the tank wall as the exponential function of filling time:

$$\alpha_{\mathrm{in}}=ae^{-bt}+c \tag{3.23}$$

where t is the filling time (s). a, b and c are parameters, and their values are determined by experiments.

In practical applications, the thermal conductivity λ, dynamic viscosity μ, hydrogen density ρ, kinematic viscosity v, compressibility factor Z, specific heat capacity c_v and c_p in the above equations can be queried through the NIST database [86].

3.3.2 Heat transfer coefficient based on energy conservation

According to the energy conservation Eq. (2.5) of hydrogen in the hydrogen filling process in Chapter 2, the heat transfer coefficient between the hydrogen in the tank and the tank wall can be expressed as

$$\alpha_{\text{in}} = \frac{\dot{m}_{\text{in}} h_{\text{in}} - \mathrm{d}(mu)/\mathrm{d}t}{A_{\text{in}} \left(T - T_w\right)} \tag{3.24}$$

Since the hydrogen temperature and tank wall temperature are unknown parameters, Eq. (3.24) is a reverse calculation. That is, the temperatures of hydrogen and tank wall are first measured experimentally, and then the heat transfer coefficient can be calculated through Eq. (3.24). Theoretically, this method can accurately calculate the heat transfer coefficient between hydrogen and the tank wall, and its calculation results can be used as standard values to identify parameters in the empirical formula heat transfer coefficient.

When calculating the heat transfer coefficient through Eq. (3.24), it is also necessary to determine the mass flow rate. However, sometimes, the reference literature does not provide experimental mass flow rate data. In this case, the mass flow rate can be calculated inversely through the real gas EOS. That is, the experimental data of hydrogen temperature and pressure are substituted into the real gas EOS Eq. (2.16) to calculate the hydrogen mass, $m = pV\mathrm{M}_{\mathrm{H}_2} / \left(Z\mathrm{R}T\right)$. Finally, the mass flow rate can be calculated by differentiating the hydrogen mass.

3.3.3 Effect of heat transfer coefficient on hydrogen filling

In order to use the energy conservation heat transfer coefficient to identify the parameters in the empirical formula heat transfer coefficient and compare the impact of different calculation methods of heat transfer coefficient on the hydrogen filling process, this section uses type IV 19 L and 29 L hydrogen storage tanks and their corresponding experimental data in Ref. [16] to conduct the study. The 19 L storage tank was used as an experimental group to determine the parameters in the different heat transfer coefficient models, and the 29 L storage tank was used as a control group to verify the applicability of the determined parameters. The filling conditions of Ref.

[16] are shown in Table 3.4, and the physical properties of the hydrogen storage tank are shown in Table 3.5.

Table 3.4 Filling conditions in Ref. [16]

Parameter	19 L type IV	29 L type IV
Filling time (s)	290	260
Ambient temperature T_a (K)	298	289
Initial hydrogen pressure p_0 (MPa)	3	2
Initial hydrogen temperature T_0 (K)	271	267
Mass flow rate $\dot{m}$ (kg/s)	0.0024	0.0039
Initial tank wall temperature at measuring point T_{w0} (K)	281	277

Table 3.5 Physical properties of hydrogen storage tanks in Ref. [16]

Parameter	19 L type IV	29 L type IV
Mass of tank wall liner m_{wl} (kg)	1.1	2.0
Mass of tank wall shell m_{ws} (kg)	17.2	30.9
Total mass of tank wall m_w (kg)	18.3	32.9
External length of tank L_{out} (m)	0.904	0.827
Internal length of tank L_{in} (m)	0.856	0.778
External diameter of tank D_{out} (m)	0.228	0.279
Internal diameter of tank D_{in} (m)	0.18	0.23
Specific heat capacity of liner c_{wl} (J/kg/K)	1580	1580
Specific heat capacity of shell c_{ws} (J/kg/K)	1120	1120

When calculating the heat transfer coefficient based on energy conservation, the variable mass flow rate needs to be determined first. Ref. [16] only provides a constant average mass flow rate, so we first substitute the experimental data of hydrogen temperature and pressure into the real gas EOS to calculate the hydrogen mass and then calculate the variable mass flow rate through the differentiation of the hydrogen mass. Fig. 3.9 shows the mass flow rate and total mass of the 19 L and 29 L IV storage tanks during hydrogen filling. There is a significant difference between constant and variable mass flow rates during hydrogen filling. The variable mass flow rate curve oscillates

around the constant mass flow rate curve. The differential calculation of the hydrogen mass causes the oscillations of the variable mass flow rate curve. The total mass curves are consistent at the filling endpoint but have some differences at other times. The convective heat transfer during the filling process is mainly forced convection, and its intensity can be characterized by Reynolds number. Since there is a specific relationship between the Reynolds number and mass flow rate, the mass flow rate should not be regarded as a constant value when studying the change of heat transfer coefficient during hydrogen filling. Otherwise, it will lead to large errors in the heat transfer coefficient.

We use the heat transfer coefficient based on energy conservation, Eq. (3.24), to calculate the heat transfer coefficient between hydrogen and the tank wall. Then, we use them as the standard values to determine the parameter values in the empirical formula heat transfer coefficients, Eqs. (3.21), (3.22) and (3.23), as shown in Table 3.6.

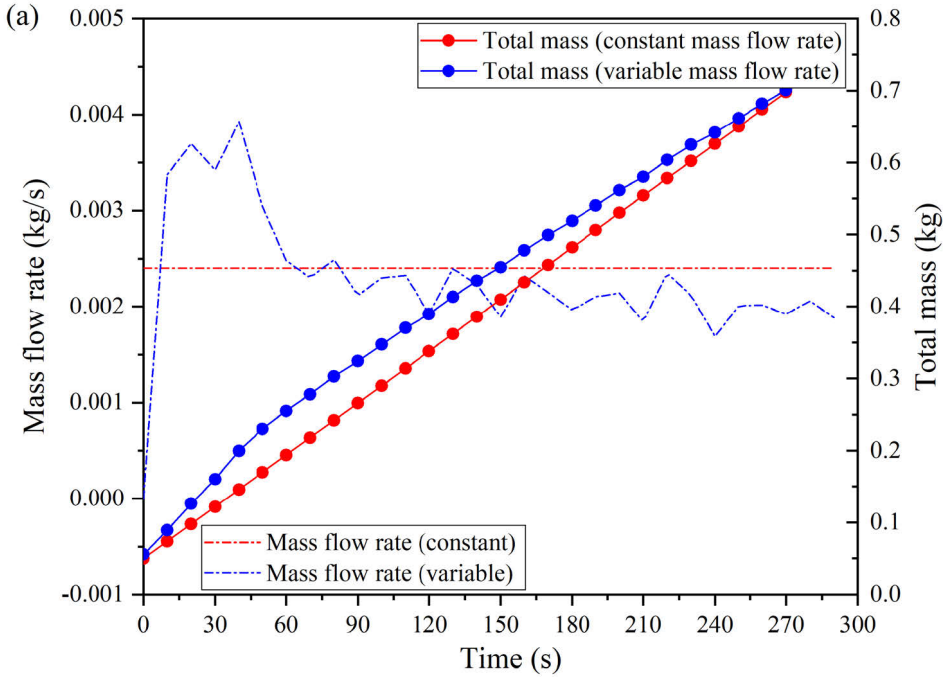

(a) 19 L type IV hydrogen storage tank

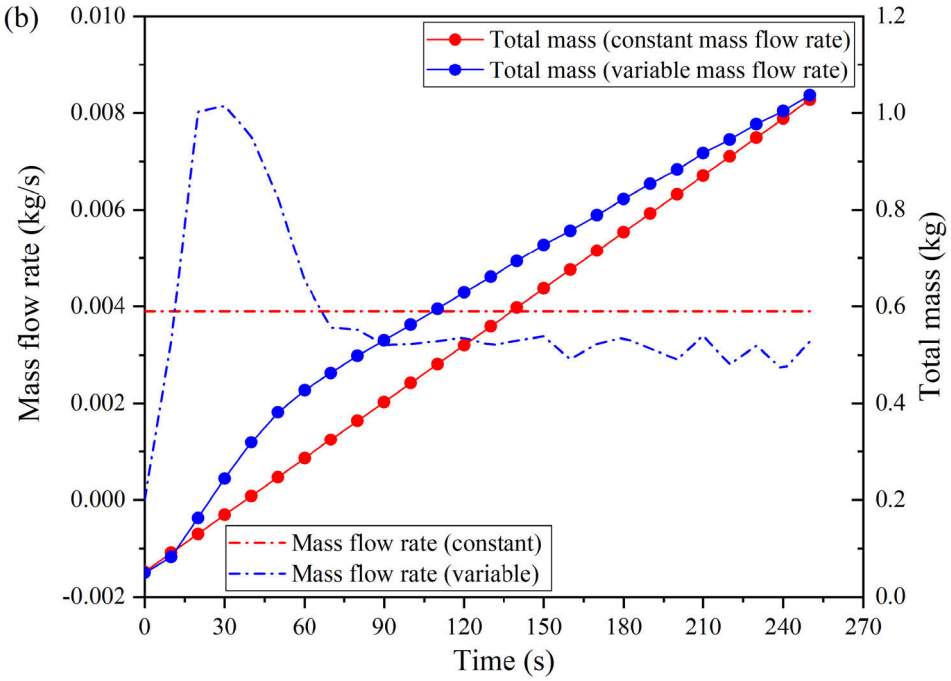

(b) 29 L type IV hydrogen storage tank

Fig. 3.9 Constant/variable mass flow rate and corresponding total hydrogen mass during hydrogen filling.

Table 3.6 Parameter values in different forms of empirical formula heat transfer coefficients obtained using the heat transfer coefficient calculated by the energy conservation method as the standard for fitting (using data from type IV 19 L storage tanks)

Form	Formula	Parameter		
		a	*b*	*c*
Reynolds number [83]	$\alpha_{in} = a\frac{\lambda}{D_{in}}\left[\frac{\mathrm{Re}_{d_{in}}\,\mathrm{Pr}}{\mathrm{SOC}}\left(\frac{d_{in}^{\,2}}{L_{in}D_{in}}\right)\right]^{0.632}$	9.575	/	/
Real-time pressure [57]	$\alpha_{in} = a\dot{m}\frac{p_N}{p_{on}}$	3926.384	/	/
Filling time [85]	$\alpha_{in} = ae^{-bt} + c$	117.568	0.00457	−11.314

Fig. 3.10 shows the results of fitting the heat transfer coefficients based on Reynolds number [83], based on real-time pressure [57] and based on filling time [85] when using the heat transfer coefficient based on energy conservation as the standard. Intuitively, the heat transfer coefficient based on the Reynolds number has good fitting consistency with the one based on energy conservation during the entire filling process. Within 0 to 30 s of filling, the peak value of the heat transfer coefficient based on the filling time is lower than that of energy conservation, and the peak value of the heat transfer

coefficient based on real-time pressure is higher than that of energy conservation. Within 30 to 290 s of filling, the heat transfer coefficient based on filling time is more consistent with the one based on energy conservation, while the one based on real-time pressure is significantly lower than the one based on energy conservation. Overall, for the accuracy of the empirical formula heat transfer coefficients, the one based on Reynolds number is better, the one based on filling time is second, and the one based on real-time pressure is poor.

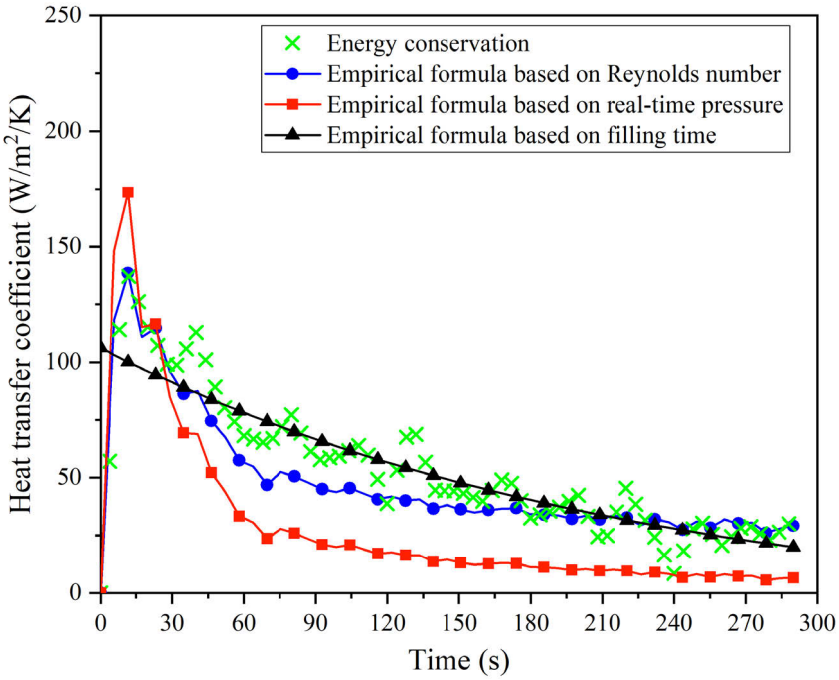

Fig. 3.10 The results of fitting the heat transfer coefficient of different forms of empirical formulas using the heat transfer coefficient calculated by the energy conservation method as the standard (using data from a type IV 19 L storage tank).

In order to further verify the accuracy of various heat transfer coefficient models, we apply them to the 29 L storage tank after the specific parameters have been determined by fitting the 19 L storage tank data. Fig. 3.11 shows that throughout the filling process, the heat transfer coefficient based on the Reynolds number is still relatively consistent with the one based on energy conservation, illustrating the accuracy of the parameters obtained by fitting in Table 3.6. Within 0 to 30 s of filling, the peak value of the heat transfer coefficient based on the filling time is still lower than that of energy conservation, and the peak value of the heat transfer coefficient based on real-time pressure is still higher than that of energy conservation. Within 30 to 260 s of filling,

the one based on the filling time is more consistent with energy conservation.

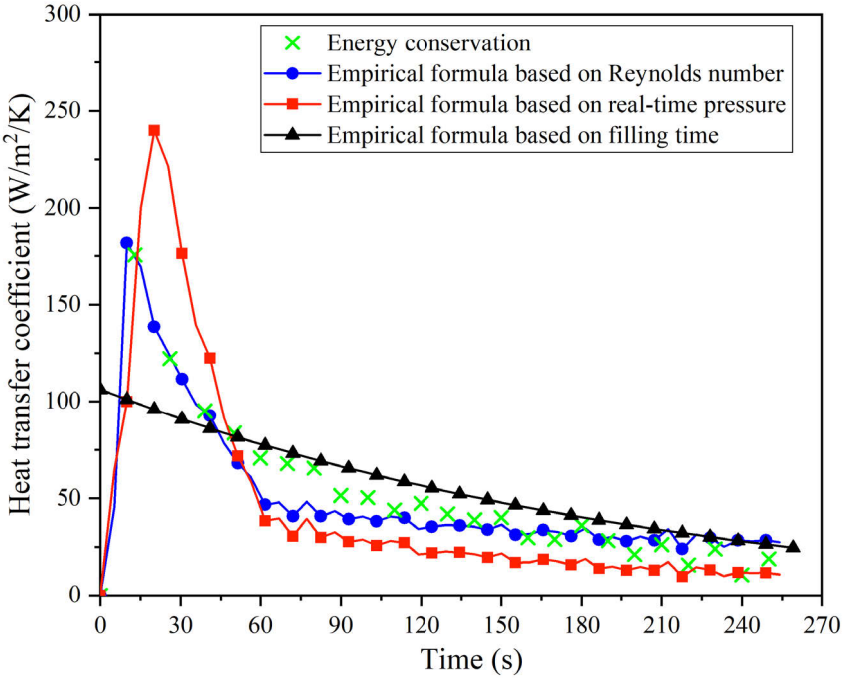

Fig. 3.11 Applying the heat transfer coefficient models with determined parameters in Table 3.6 to the type IV 29 L storage tank.

To sum up, the heat transfer coefficient based on Reynolds number, Eq. (3.21), is a relatively high-precision heat transfer coefficient model, while the ones based on real-time pressure, Eq. (3.22), and based on filling time, Eq. (3.23), are less accurate, especially in the early stages of filling. The empirical formula heat transfer coefficient models based on the Reynolds number also include Eq. (3.20), which does not contain unknown parameters and has a simple structure. Below, we will compare the effects of the different heat transfer coefficient models based on Reynolds number, namely Eqs. (3.20) and (3.21).

When studying the impact of filling speed on the thermal effect of hydrogen filling in Section 3.1.3, a constant mass flow rate was used. However, the mass flow rate generally changes during the actual hydrogen filling process, as shown in the filling experiment in Ref. [16]. The variable mass flow rate curve shown in Fig. 3.9 is just what was actually used in the filling experiment.

Combining constant/variable mass flow rate and constant/variable heat transfer coefficient, we define three cases, as shown in Table 3.7. On the premise that the

simulated value of the final hydrogen temperature at the end of filling is equal to the experimental value, we determine the value of the constant heat transfer coefficient: 42 W/m^2/K for the 19 L type IV storage tank and 38 W/m^2/K for the 29 L type IV storage tank. We use the variable and constant mass flow rate data from Fig. 3.9.

Table 3.7 Filling conditions with different constant/variable mass flow rates and heat transfer coefficients

Cases	Mass flow rate	Heat transfer coefficient
Case 1	Constant	19 L：42 W/m^2/K 29 L：38 W/m^2/K
Case 2	Variable	$\alpha_{\text{in}} = a\frac{\lambda}{D_{\text{in}}}\left[\frac{\text{Re}_{d_{\text{in}}}\text{Pr}}{\text{SOC}}\left(\frac{{d_{\text{in}}}^2}{L_{\text{in}}D_{\text{in}}}\right)\right]^{0.632}$
Case 3	Variable	$\alpha_{\text{in}} = \frac{0.14\lambda\left(\text{Re}_{d_{\text{in}}}/\text{SOC}\right)^{0.67}}{D_{\text{in}}}$

Figs. 3.12 (a) and (b) compare the simulated hydrogen temperature using constant/variable mass flow rate and heat transfer coefficient with the experimental values in Ref. [16] during the hydrogen filling process, respectively. In general, for the three cases using two storage tanks, the final hydrogen temperatures simulated are in good agreement with the experimental values at the end of filling. However, at other filling moments, the hydrogen temperature simulated in Case 3 using variable mass flow rate and heat transfer coefficient Eq. (3.20) is in better agreement with the experimental value. The maximum error for the 19 L storage tank is about 7 °C, and the maximum error for the 29 L storage tank is about 5 °C. Case 1, using a constant mass flow rate and constant heat transfer coefficient to simulate, has the largest error. The maximum error for the 19 L storage tank is about 20 °C, and the maximum error for the 29 L storage tank is about 18 °C. The error of case 2 is between cases 1 and 3. In the first 60 s of filling, when a constant heat transfer coefficient is used in Case 1, the average temperature rise rate is greater, about 1.3 °C/s for the 19 L storage tank and about 1.5 °C/s for the 29 L storage tank. When the variable heat transfer coefficient is used in Case 2, the average temperature rise rate is relatively lower, about 1.1 °C/s for the 19 L storage tank and about 1.4 °C/s for the 29 L storage tank. The reason can be

seen in Fig. 3.10 and Fig. 3.11. In the first 60 s of filling, the variable heat transfer coefficient produced a peak value. The reason is that the mass flow rate has a peak value during this period, and the heat transfer coefficient is positively related to the mass flow rate. A larger heat transfer coefficient near the peak will result in a lower temperature rise rate. Therefore, the variable mass flow rate and heat transfer coefficient used in Cases 2 and 3 are more consistent with the actual situation and can simulate the changing trend of hydrogen temperature that is more consistent with reality. Meanwhile, because the heat transfer coefficient Eq. (3.20) is more concise than Eq. (3.21), the heat transfer coefficient model of Eq. (3.20) will be selected in the following sections of this thesis.

Figs. 3.13 (a) and (b) compare the simulated hydrogen pressure using constant/variable mass flow rate and heat transfer coefficient with the experimental data of Ref. [16] during the hydrogen filling process. In general, for the three cases using two storage tanks, the final hydrogen pressures simulated are in good agreement with the experimental values at the end of filling. However, at other filling moments, the hydrogen pressure simulated using variable mass flow rates and heat transfer coefficients in Cases 2 and 3 is in better agreement with the experimental values, with a maximum error of only about 1 MPa. In case 1, the simulation result using constant mass flow rate and constant heat transfer coefficient has a larger error, with the maximum error of the 19 L storage tank being about 5 MPa and the maximum error of the 29 L storage tank being about 10 MPa. A comparison of the hydrogen pressure curve in Fig. 3.13 and the total hydrogen mass curve in Fig. 3.9 shows that the changing trends of the two are consistent, indicating that the hydrogen pressure in the storage tank is mainly affected by the mass flow rate, which is consistent with the conclusion in Section 3.1.3. Therefore, in order to simulate more accurately the changing trend of hydrogen pressure in the hydrogen storage tank, the actual variable mass flow rate should be used.

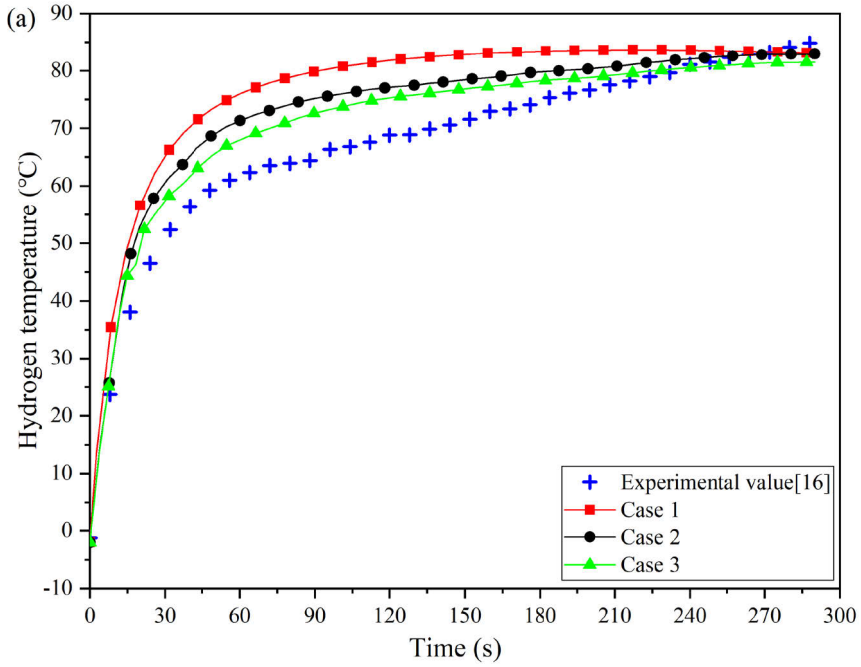

(a) 19 L type IV hydrogen storage tank

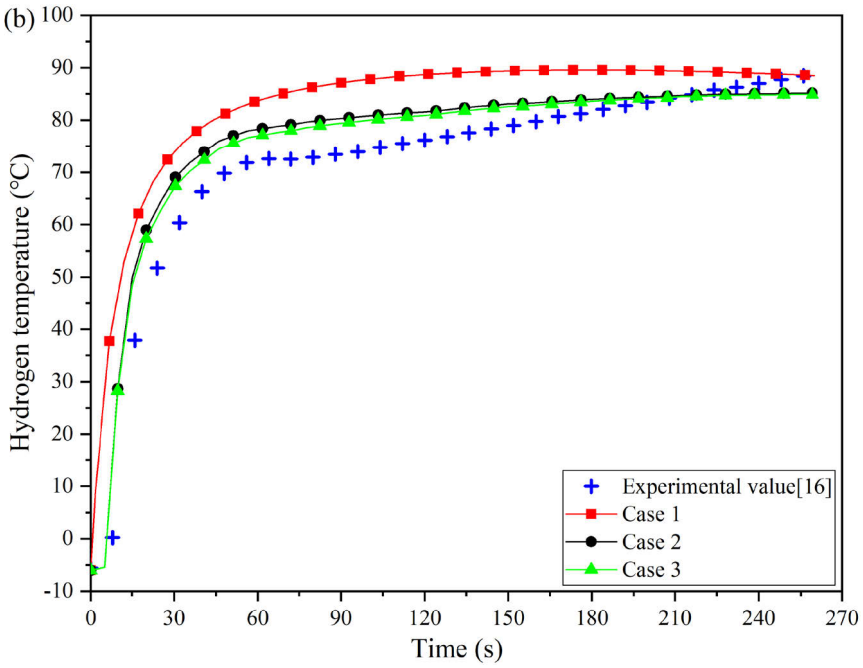

(b) 29 L type IV hydrogen storage tank

Fig. 3.12 Comparison of the simulated hydrogen temperature using different mass flow rates and heat transfer coefficients with the experimental values of Ref. [16].

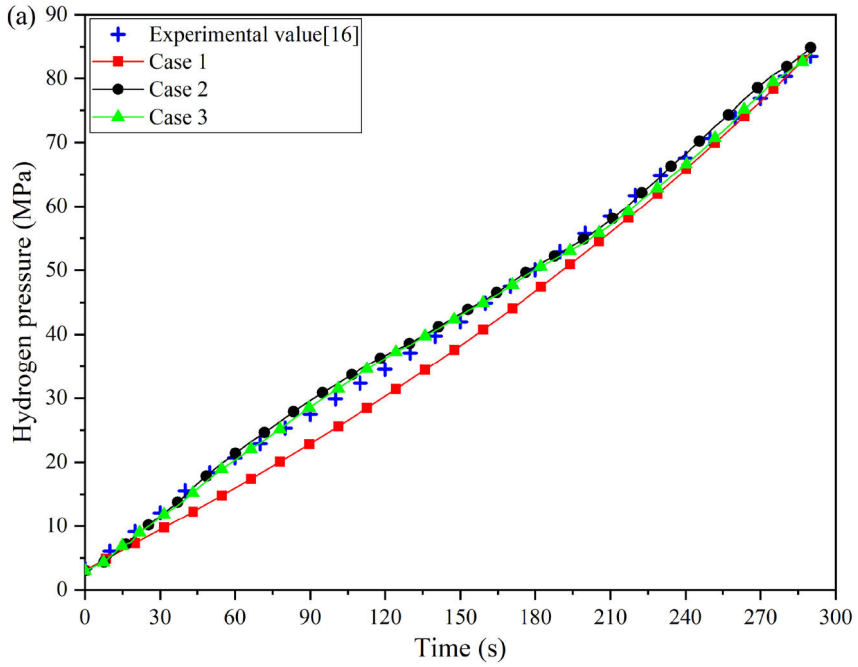

(a) 19 L type IV hydrogen storage tank

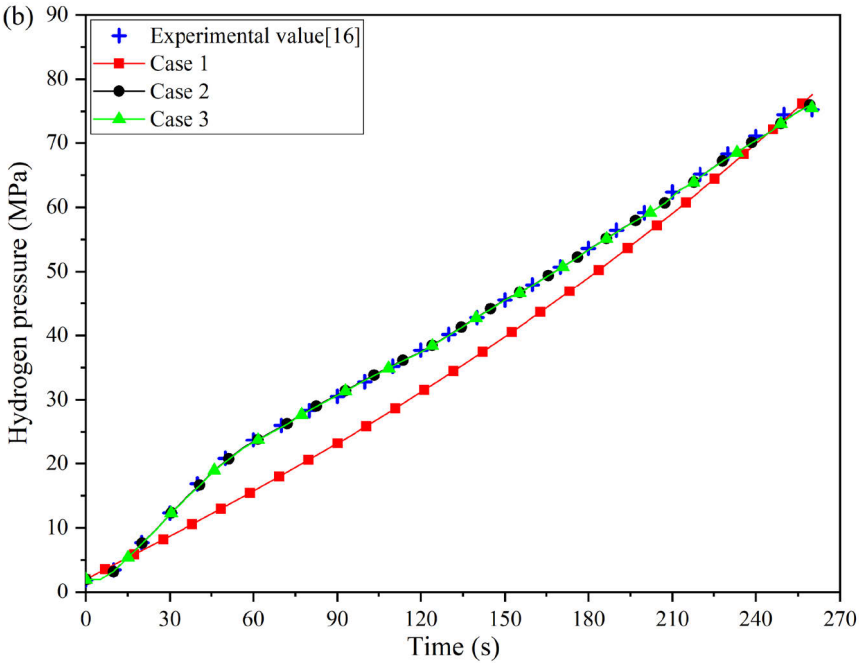

(b) 29 L type IV hydrogen storage tank

Fig. 3.13 Comparison of the simulated hydrogen pressure using different mass flow rates and heat transfer coefficients with the experimental values of Ref. [16].

3.4 Conclusion

This chapter determines the optimal gas EOS and heat transfer coefficient model applicable to each research content of this thesis.

The accuracy of the modified van der Waals gas EOS in Redlich-Kwong, Soave and Peng-Robinson forms was tested using the Joule-Thomson inverse curve. The results show that the fitting curve of the Redlich-Kwong EOS is closer to the Joule-Thomson inverse curve. That is, the Redlich-Kwong EOS is more accurate.

A polynomial gas EOS was constructed. The van der Waals gas EOS, the Redlich-Kwong modified gas EOS, the polynomial gas EOS and the calculation based on the NIST database were compared. The results show that using the final hydrogen pressure calculated based on the NIST database as the standard, the relative error of the polynomial gas EOS is 0.30%, the Redlich-Kwong gas EOS is 1.83%, and the van der Waals gas EOS is 17.90%. That is, the accuracy of the polynomial gas EOS is higher, followed by the Redlich-Kwong gas EOS, and the van der Waals gas EOS is lower.

A calculation method of heat transfer coefficient based on energy conservation was proposed, which was used as a standard to identify the parameters in the empirical formula heat transfer coefficients. The hydrogen filling process was simulated using different forms of heat transfer coefficients. The results show that compared with the empirical formula heat transfer coefficients based on real-time pressure and the one based on filling time, the error between the heat transfer coefficient based on Reynolds number and the one based on energy conservation is smaller. That is, the heat transfer coefficient based on Reynolds number is more accurate.

In Chapter 2, the numerical model of the hydrogen storage tank uses the NIST database to calculate the hydrogen temperature and pressure. The analytical model of the hydrogen storage tank uses the modified gas EOS in the form of Redlich-Kwong. The new filling method in Chapter 6 uses a polynomial gas EOS. The heat transfer coefficient adopts the empirical formula model based on Reynolds number.

Chapter 4 Optimization study of single-stage and cascade hydrogen filling systems

This section has been published in:

[1] Luo H, Xiao J S, Bénard P, Chahine R, Yang T Q. Multi-objective optimization of cascade storage system in hydrogen refuelling station for minimum cooling energy and maximum state of charge. International Journal of Hydrogen Energy, 2022, 47: 10963-10975. (JCR Q1, IF=7.2)

[2] Luo H, Xiao J S, Bénard P, Chahine R, Yang T Q. Effects of filling strategies on hydrogen refueling performance. International Journal of Hydrogen Energy, 2024, 51: 664-675. (JCR Q1, IF=7.2)

[3] Luo H, Xiao J S, Bénard P, Yuan C Q, Tong L, Chahine R, Yuan Y P, Yang T Q, Yao C L. Thermodynamic modeling and analysis of cascade hydrogen refuelling with three-stage pressure and temperature for heavy-duty fuel cell vehicles. International Journal of Hydrogen Energy, 2024, 63: 103-113. (JCR Q1, IF=7.2)

My specific contribution in this work was to to extend the hydrogen storage tank model to the entire single-stage hydrogen filling system, based on which the filling strategies of two-stage filling speed and inlet temperature are proposed. Then, the single-stage hydrogen filling system was expanded to a three-stage cascade hydrogen filling system, based on which the initial pressure and volume of the low-pressure, medium-pressure and high-pressure cascade storage tanks were optimized, and a three-stage inlet temperature filling strategy was proposed.

The previous chapter determined the optimal gas EOS and heat transfer coefficient model with higher accuracy, which improved the accuracy of the storage tank models in Chapter 2. However, the storage tank is only the terminal of the hydrogen filling system. The main components of the complete hydrogen filling system also include ① Compressor, which is used to compress hydrogen from hydrogen sources such as tube trailers to the station-side storage tank. ② Station-side storage tank, which is used to store hydrogen at the HRS. Depending on the number of station-side storage tanks and the initial pressure, the hydrogen filling system can be divided into a single-stage filling

system and a cascade filling system. The cascade filling system uses multiple station-side storage tanks with different initial pressures and volumes. ③ Reduction valve, which is used to adjust the pressure of hydrogen output from the HRS to control the filling speed. ④ Heat exchanger, which is used to adjust the temperature of hydrogen output from the HRS. During the hydrogen filling process, due to the compression effect and the Joule-Thomson effect, the temperature of the hydrogen in the onboard tank will increase significantly. At present, HRS generally uses a heat exchanger to precool hydrogen to reduce the rise in temperature. Research shows that precooling filling will result in higher cooling energy consumption. Meanwhile, due to the high cost of the refrigeration equipment itself, the investment cost of the HRS is high. Therefore, this chapter will extend the storage tank model to the entire hydrogen filling system, optimize the tank configuration and filling strategy of the filling system, reduce operating costs and investment costs, and improve the efficiency of hydrogen filling.

4.1 Single-stage hydrogen filling system

When there is only one station-side storage tank in an HRS, the hydrogen filling system at this time is called a single-stage hydrogen filling system. Fig. 4.1 shows the single-stage hydrogen filling system model established in this thesis. From left to right are the station-side storage tank, reduction valve, heat exchanger and onboard tank. For the station side, the pressure drops caused by pipes and valves are aggregated and calculated as Δp_1 . For the vehicle side, the pressure drops caused by pipes and valves are aggregated and calculated as Δp_2 . Neglecting the pressure drop at the inlet of the onboard tank, the pressure at the inlet of the onboard tank is equal to the pressure inside, that is $p_{in} = p_{on}$ [24].

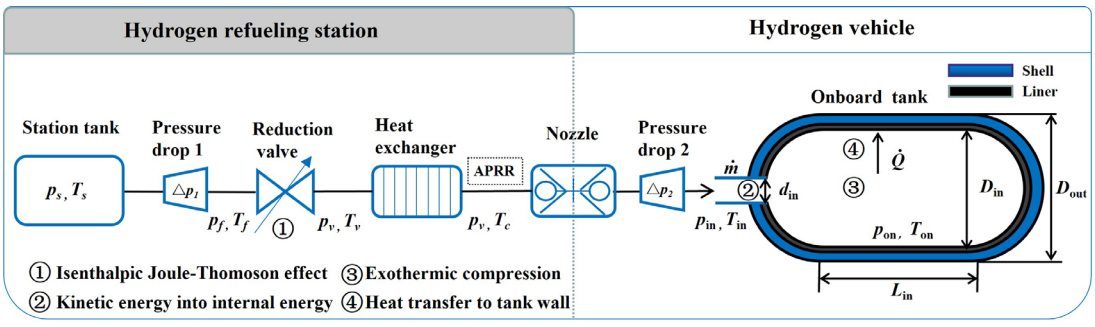

Fig. 4.1 Simplified structure of a single-stage hydrogen filling system.

4.1.1 Single-stage hydrogen filling system model

(1) Reduction valve and Joule-Thomson effect

During the modelling process, the reduction valve can be considered as an adiabatic throttle valve. Due to the isenthalpic throttling of the real gas, the pressure and temperature before and after the reduction valve will change, and the degree of change depends on the Joule-Thomson coefficient. Some groups have studied the Joule-Thomson effect caused by throttling during hydrogen filling. Ref. [87] observed that the temperature downstream of the reduction valve changes with time, and the temperature rises by about 3 °C. Ref. [55] found that when the hydrogen temperature is higher than 200 K, the temperature rise caused by the Joule-Thomson effect is about −0.4 °C/MPa. Ref. [25] found that in the pressure range of 2 to 78 MPa, the Joule-Thomson coefficient value at 0 °C is approximately −0.264 to −0.505 °C/MPa. When the pressure drop is 10 MPa, the potential temperature rise is about 2.64 to 5.05 ℃. Therefore, the Joule-Thomson effect needs to be considered during the modelling process. The temperature change of hydrogen passing through the reduction valve can be expressed as

$$\Delta T = T_v - T_f = \int_{p_f}^{p_v} \mu_{JT} \mathrm{d}p = \left(\frac{\mu_{JT(T_f, p_f)} + \mu_{JT(T_v, p_v)}}{2} \right) \left(p_v - p_f \right) \tag{4.1}$$

where $\mu_{JT} = \left(\partial T / \partial P \right)_h$ and μ_{JT} is the Joule-Thomson coefficient, which describes the temperature change (∂T) during isenthalpic expansion (∂P)$_h$ [88].

(2) Heat exchanger (refrigeration system)

To lower the hydrogen temperature within the onboard tank, hydrogen undergoes precooling via the heat exchanger. The pressure drop caused by one-way resistance within the heat exchanger is negligible and thus disregarded [47]. The energy conservation of hydrogen inside the heat exchanger is

$$\frac{\mathrm{d}U}{\mathrm{d}t} = \dot{U}_{\mathrm{in}} - \dot{U}_{\mathrm{out}} = \dot{m} \left(u_{\mathrm{in}} - u_{\mathrm{out}} \right) = \dot{m} \left(c_{vv} T_v - c_{vc} T_c \right) \tag{4.2}$$

where T_v and T_c are the hydrogen temperature at the inlet and outlet of the heat

exchanger (K), respectively. T_c is also the precooling temperature required by the HRS.

The energy consumption required by the heat exchanger for precooling hydrogen is

$$W = \frac{U}{\mathrm{COP}} \tag{4.3}$$

where COP is the coefficient of performance for the refrigeration facility [8].

(3) Pressure loss

The pressure losses mainly occur in the valve, tube, filter and flowmeter. The pressure loss caused by the valve is [89]

$$\Delta p_{\mathrm{valve}} = \frac{\rho_{\mathrm{H_2}}}{\rho_{\mathrm{water}} \left(k_v / \dot{V} \right)^2} \tag{4.4}$$

where $\rho_{\mathrm{H_2}}$ and ρ_{water} are the density of hydrogen and water (kg/m^3), respectively. $\dot{V}$ is the volumetric flow rate (m^3/s), and k_v is the flow coefficient of the valve (m^3/h).

The pressure loss caused by the tube is [90]

$$\Delta p_{\mathrm{tube}} = f \frac{L}{d} \frac{\rho_{\mathrm{H_2}}}{2} \left(\frac{\dot{V}}{A_{\mathrm{tube}}} \right)^2 \tag{4.5}$$

where f is the friction factor between the hydrogen flow and the tube. L is the length (m), d is the diameter (m), and A_{tube} is the cross-sectional area of tube (m^2).

The pressure loss caused by the flowmeter or the filter is [91]

$$\Delta P_{\mathrm{flowmeter/filter}} = 0.5 k_p \rho_{\mathrm{H_2}} \dot{V}^2 \tag{4.6}$$

where k_p is the pressure loss constant.

By observing Eqs. (4.4) -(4.6), it can be found that all pressure losses can be expressed as

$$\Delta p = k \rho_{\mathrm{H_2}} \dot{V}^2 = k \frac{\dot{m}^2}{\rho_{\mathrm{H_2}}} \tag{4.7}$$

Therefore, In Fig. 4.1, it is reasonable for the pressure loss at the station side to be aggregated as Δp_1 , which may include the pressure losses of valves and filters. The pressure losses at the vehicle side are calculated as a lumped value ΔP_2 , which may include the pressure losses of tubes and flowmeters.

(4) Mass flow rate

Certain research groups employ a constant mass flow rate to investigate hydrogen refilling [22, 33, 73]. As per the SAE J2601 protocol, refilling velocity is regulated by the pressure ramp rate (PRR), contingent upon ambient temperature [5]. Utilizing a constant mass flow rate rather than the PRR may introduce discrepancies in the actual mass flow rate pattern. Illustrated in Fig. 4.2, the temperature elevation within the onboard tank exhibits a gentler ascent with a constant PRR in contrast to a constant mass flow rate. Under a constant PRR, the mass flow rate initially ascends gradually, resulting in a slower temperature increase. Subsequently, as the mass flow rate surpasses its peak, its decline is gradual, thereby facilitating a gradual stabilization of the temperature curve and simplifying the regulation of the final hydrogen temperature within the onboard tank. A survey of the literature indicates two primary approaches for computing variable mass flow rates.

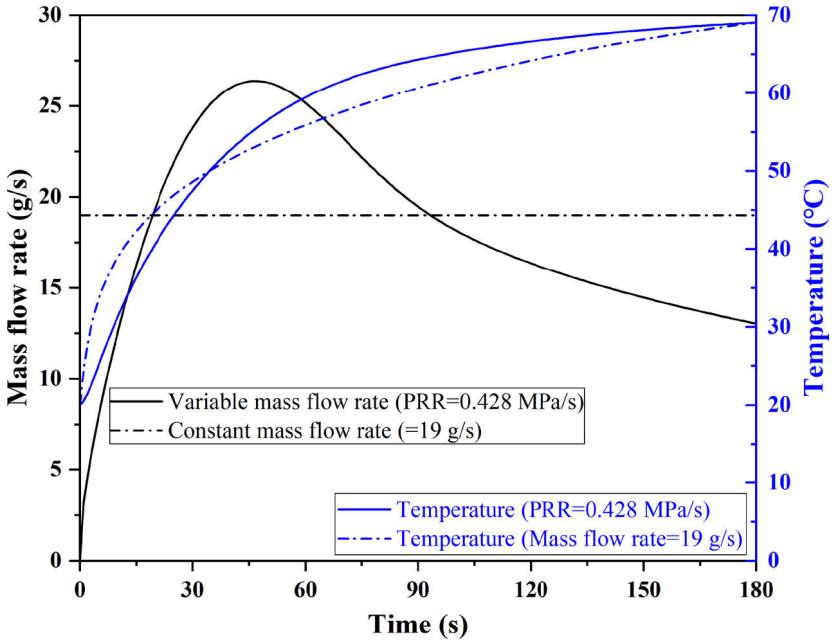

Fig. 4.2 Hydrogen temperature and mass flow rate in the onboard tank using constant PRR or constant mass flow rate, respectively.

1) Calculation based on isenthalpic expansion of gas passing through orifice plate [56, 57]

According to the theoretical formula for the mass flow rate of the orifice plate, the hydrogen mass flow rate through the valve can be calculated.

When $\frac{p_{\text{on}}}{p_s} > \left(\frac{2}{k+1}\right)^{k/k-1}$,

$$\dot{m} = C\rho S_{or}\left(\frac{p_{\text{on}}}{p_s}\right)^{1/k}\left\{\left(\frac{2k}{k-1}\right)\left(\frac{p_{\text{on}}}{p_s}\right)\left[1-\left(\frac{p_{\text{on}}}{p_s}\right)^{k-1/k}\right]\right\}^{1/2} \tag{4.8}$$

When $\frac{p_{\text{on}}}{p_s} \le \left(\frac{2}{k+1}\right)^{k/k-1}$,

$$\dot{m} = C\left(k\rho p_s\right)^{1/2} S_{or}\left(\frac{2}{k+1}\right)^{k+1/2(k-1)} \tag{4.9}$$

where p_{on} and p_s are the pressures of the onboard tank and the HRS storage tank, respectively (Pa). C is the flow coefficient of the valve orifice. ρ is the density of hydrogen (kg/m^3). S_{or} is the cross-sectional area of the valve orifice (m^2). k is the ratio of the specific heat capacity of hydrogen, $k = c_p / c_v$. c_p and c_v are the specific heat capacity of hydrogen at constant pressure and constant volume (J/kg/K), respectively. Eqs. (4.8) and (4.9) are suitable for subsonic and sonic conditions of hydrogen flow, respectively.

2) Calculated based on pressure loss [92, 93]

According to the SAE J2601 hydrogen refuelling protocol, the mass flow rate filled into the onboard tank depends on the pressure loss at the vehicle side [5]. Therefore, the mass flow rate can be rewritten from Eq. (4.7) as

$$\dot{m} = \left(\frac{\Delta p \rho}{k_p}\right)^{1/2} \tag{4.10}$$

where Δp is the pressure loss, $\Delta p = p_v - p_{\text{on}}$, $p_v = p_0 + \text{PRR} * t$. p_v is the outlet pressure of the dispenser (Pa). p_0 is the initial pressure in the onboard tank (Pa). k_p is

the pressure loss coefficient. In the following thesis, this method will be used to calculate the mass flow rate in the filling system. That is, PRR is directly used as the input parameter to control the filling speed, and then Eq. (4.10) is used to calculate the mass flow rate in the hydrogen filling system.

4.1.2 Optimization of filling strategy for single-stage hydrogen filling system

In the actual hydrogen filling process, the lookup table method in the SAE J2601 hydrogen refuelling protocol uses the average pressure ramp rate (APRR) to control the filling speed and uses the inlet/precooling temperature to control the final hydrogen temperature. At present, HRS generally uses constant single-stage APRR and inlet temperature to control the hydrogen filling process. That is, APRR and inlet temperature are determined before the filling starts and then remain unchanged throughout the filling process. Based on the single-stage hydrogen filling system model shown in Fig. 4.1, this section will study the impact of different filling strategies of constant and variable APRR and inlet temperature on the thermal effect of hydrogen filling. The filling time under each filling strategy is set to 180 s, which is the filling time recommended by the SAE J2601 refuelling protocol and is suitable for light-duty HFCV.

(1) Constant average pressure ramp rate (APRR) and inlet temperature

We examined the refuelling performance of various constant APRRs and inlet temperatures. Figs. 4.3(a)-(c) demonstrate that APRR exerts a greater influence on both maximum pressure and SOC compared to maximum temperature. This is because APRR regulates filling in our investigation, making the maximum pressure of the onboard tank more closely tied to APRR. Inlet temperature minimally affects maximum pressure but significantly impacts maximum SOC and most notably affects maximum temperature. This is due to the increase in hydrogen enthalpy upon entering the tank with inlet temperatures, resulting in an elevation of the maximum temperature within the tank. In several instances, the maximum temperature of the storage tank surpasses the upper limit of 85 ℃ when the inlet temperature exceeds 0 ℃, necessitating hydrogen precooling.

Figs. 4.3(d) and 4(e) illustrate that maximum cooling energy and cooling power increase nearly linearly with APRR increments or inlet temperature reductions. APRR

demonstrates a more pronounced impact on maximum cooling energy and cooling power at lower inlet temperatures. With higher APRR values, the influence of inlet temperature on maximum cooling energy and cooling power becomes more evident. Consequently, for lower precooling or faster filling requirements, careful attention should be directed towards controlling inlet temperature and APRR, taking into consideration both energy conservation and the safe operation of the refrigeration system.

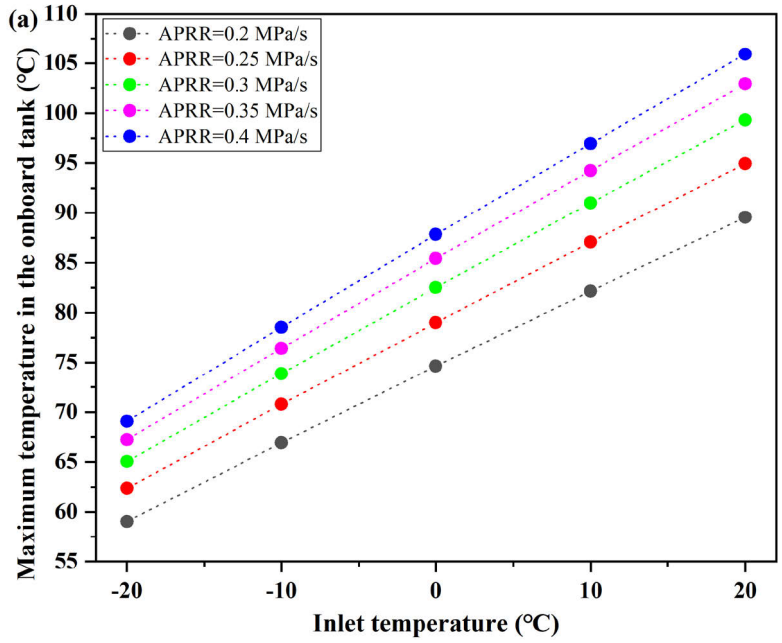

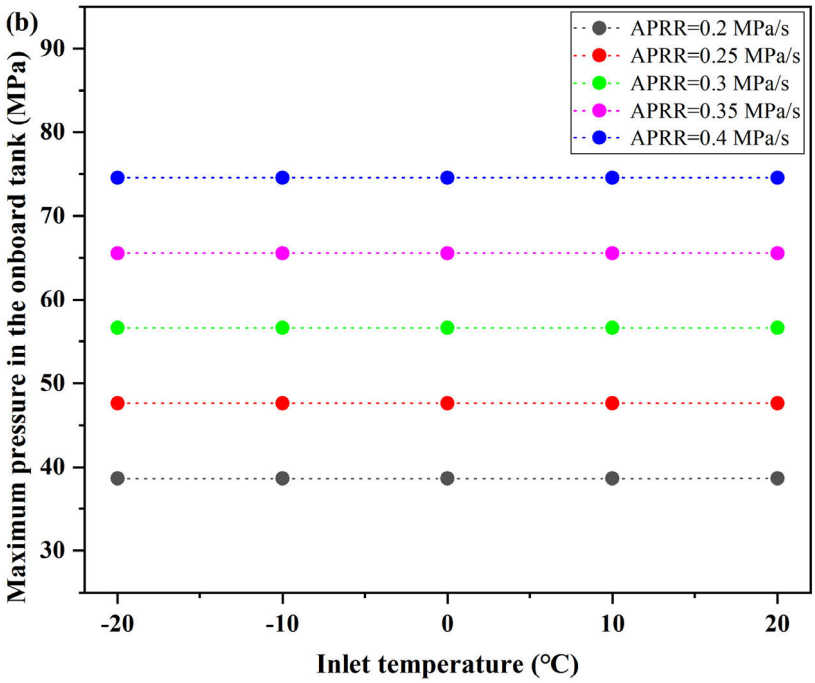

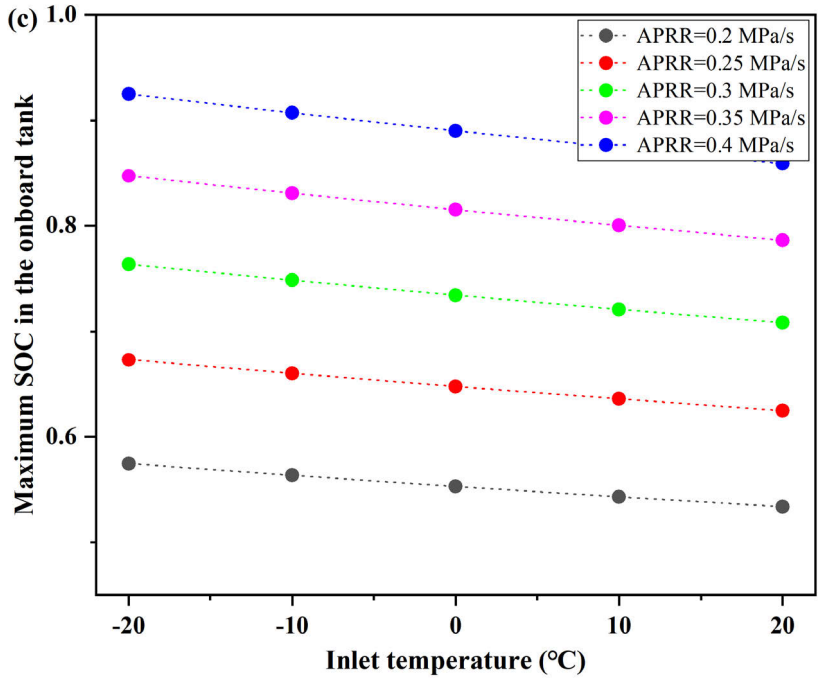
(c)
Maximum SOC in the onboard tank
1.0
0.8
0.6
APRR=0.2 MPa/s
APRR=0.25 MPa/s
APRR=0.3 MPa/s
APRR=0.35 MPa/s
APRR=0.4 MPa/s
-20
-10
0
10
20
Inlet temperature (°C)

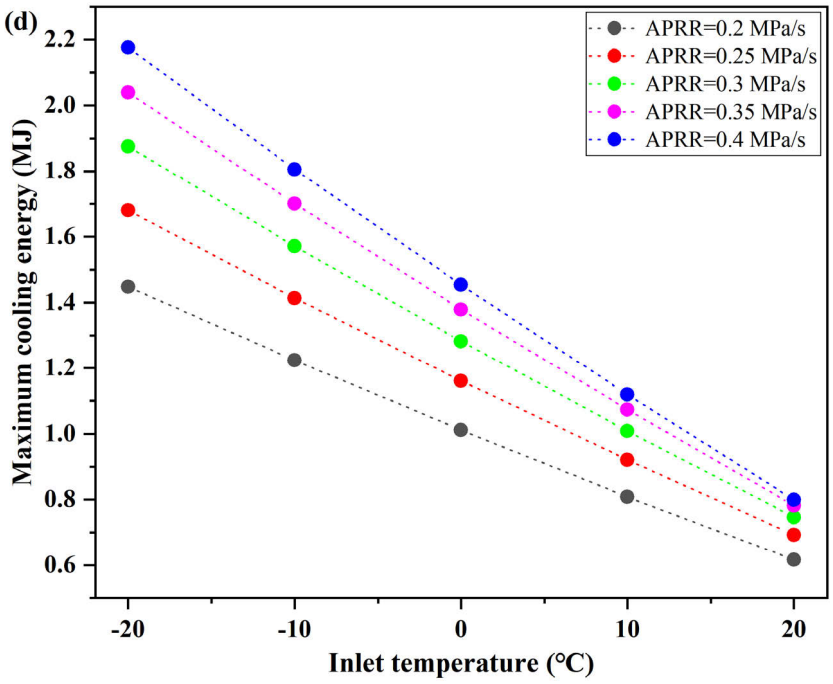
(d)
Maximum cooling energy (MJ)
2.2
2.0
1.8
1.6
1.4
1.2
1.0
0.8
0.6
APRR=0.2 MPa/s
APRR=0.25 MPa/s
APRR=0.3 MPa/s
APRR=0.35 MPa/s
APRR=0.4 MPa/s
-20
-10
0
10
20
Inlet temperature (°C)

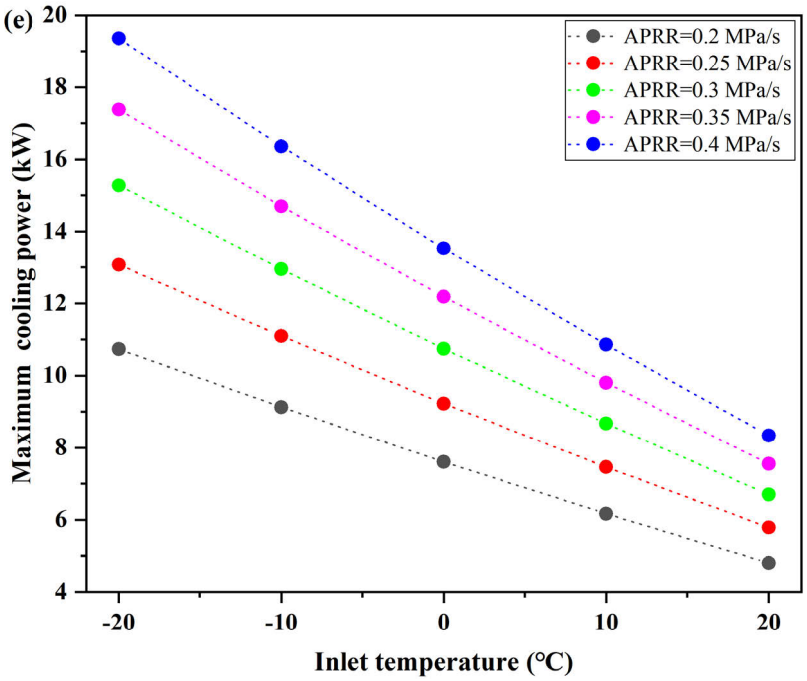

Fig. 4.3 Effects of different constant APRRs and inlet temperatures on maximum temperature (a), pressure (b), SOC (c), cooling energy (d) and cooling power (e).

(2) Two-stage average pressure ramp rate (APRR) and inlet temperature

Fig. 4.2 in Section 4.1.1 illustrates the hydrogen temperature in the onboard tank, exhibiting an initial rapid rise followed by a gradual increase. Consequently, a two-stage APRR filling approach can be implemented: initially filling at a slow pace, then accelerating to manage temperature elevation. Presently, precooling filling stands as the most efficient means to counter excessive tank temperatures. Nevertheless, due to substantial variations in filling's initial and boundary conditions, it becomes imperative to ascertain the necessity of precooling and define precise precooling temperature parameters. This section will further propose a two-stage inlet temperature filling strategy.

1) Two-stage average pressure ramp rate (APRR)

We examined the filling performance of various two-stage APRRs at inlet temperatures ranging from −20 to 20 ℃. Fig. 4.4 depicts the results solely at −20 ℃, indicative of the outcomes across different inlet temperatures, as the change pattern remains consistent. The ultimate filling pressure stabilizes at approximately 80 MPa across all scenarios through adjustments to APRR1 and APRR2.

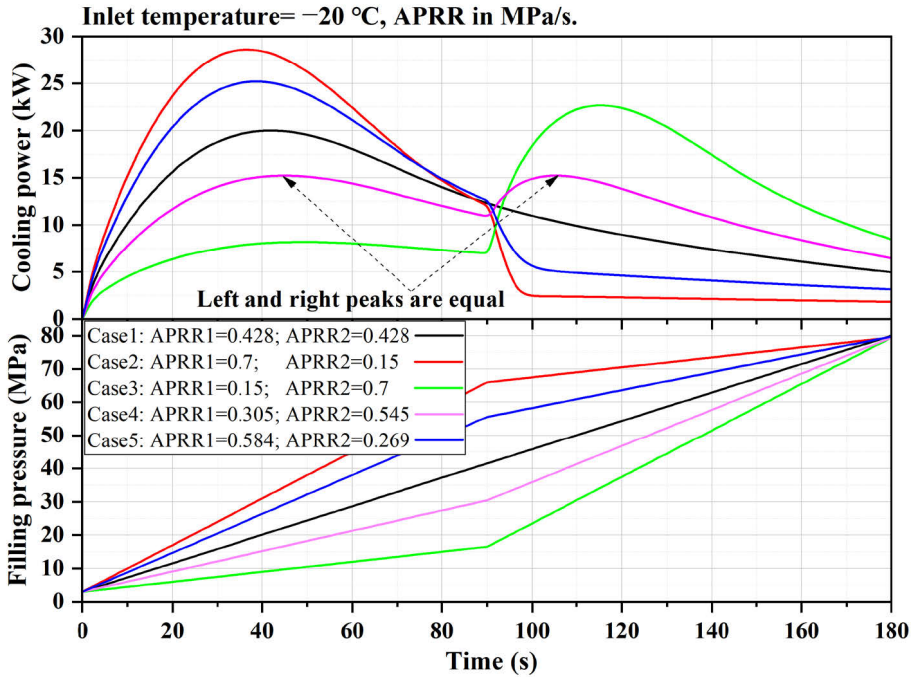

Fig. 4.4 Effects of different two-stage APRRs on cooling power at an inlet temperature of −20 °C.

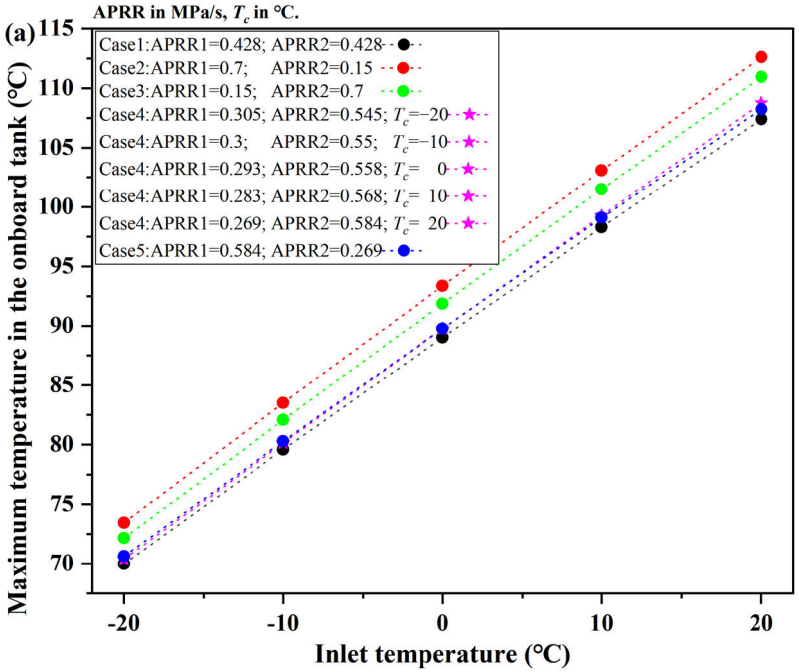

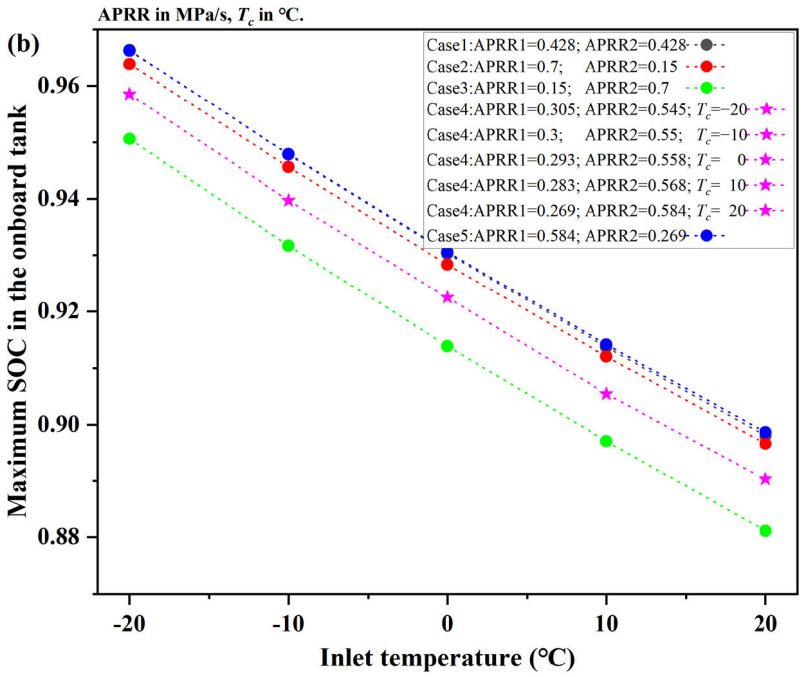
APRR in MPa/s, T_c in °C.
(b)
Maximum SOC in the onboard tank
0.96
0.94
0.92
0.90
0.88
-20
-10
0
10
20
Inlet temperature (°C)
Case1:APRR1=0.428; APRR2=0.428
Case2:APRR1=0.7; APRR2=0.15
Case3:APRR1=0.15; APRR2=0.7
Case4:APRR1=0.305; APRR2=0.545; T_c=−20
Case4:APRR1=0.3; APRR2=0.55; T_c=−10
Case4:APRR1=0.293; APRR2=0.558; T_c= 0
Case4:APRR1=0.283; APRR2=0.568; T_c= 10
Case4:APRR1=0.269; APRR2=0.584; T_c= 20
Case5:APRR1=0.584; APRR2=0.269

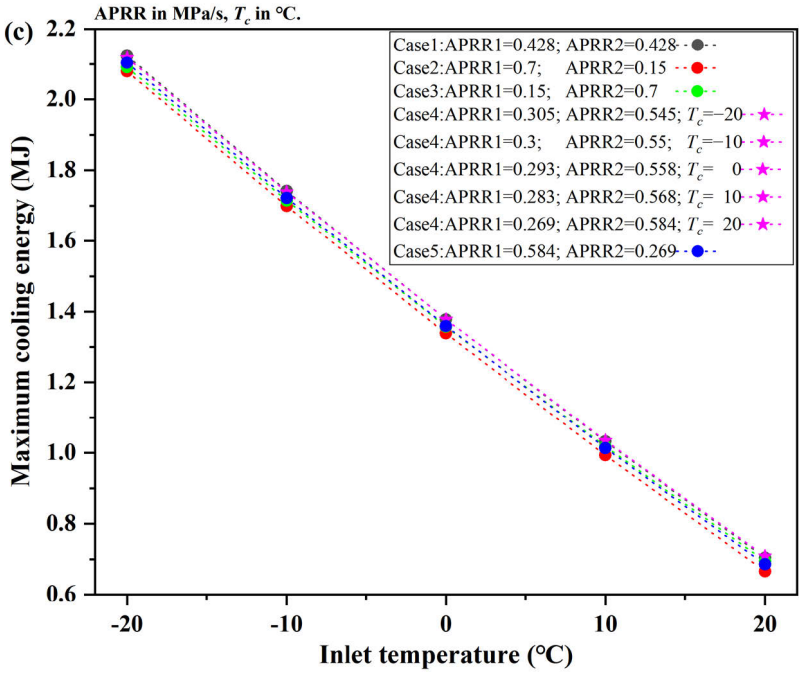
APRR in MPa/s, T_c in °C.
(c)
Maximum cooling energy (MJ)
2.2
2.0
1.8
1.6
1.4
1.2
1.0
0.8
0.6
-20
-10
0
10
20
Inlet temperature (°C)
Case1:APRR1=0.428; APRR2=0.428
Case2:APRR1=0.7; APRR2=0.15
Case3:APRR1=0.15; APRR2=0.7
Case4:APRR1=0.305; APRR2=0.545; T_c=−20
Case4:APRR1=0.3; APRR2=0.55; T_c=−10
Case4:APRR1=0.293; APRR2=0.558; T_c= 0
Case4:APRR1=0.283; APRR2=0.568; T_c= 10
Case4:APRR1=0.269; APRR2=0.584; T_c= 20
Case5:APRR1=0.584; APRR2=0.269

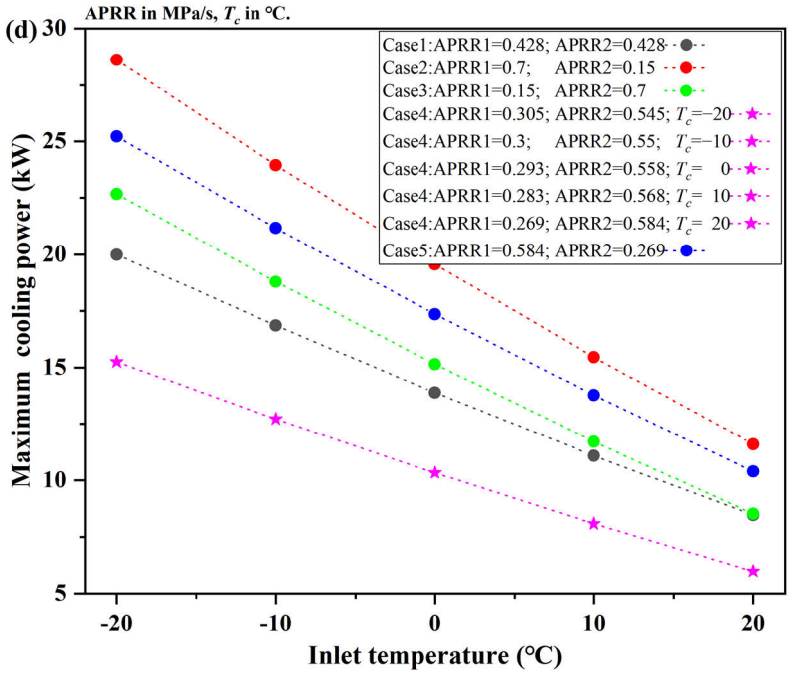

Fig. 4.5 Effects of different two-stage APRRs on maximum temperature (a), SOC (b), cooling energy (c) and cooling power (d) at different inlet temperatures.

Fig. 4.5 presents the maximum temperature, SOC, cooling energy, and cooling power at each inlet temperature. These maximum values exhibit nearly linear variations with inlet temperature, maintaining consistent trends across all conditions, suggesting the applicability of conclusions derived at −20 °C to other temperatures. Figs. 4.5(a)-(c) highlight inferior performance in temperature for Cases 2 and 3, with Case 3 exhibiting subpar SOC performance. Changes in APRR yield comparable effects on maximum cooling energy across all cases, as well as similar impacts on maximum temperature and SOC for Cases 1 and 5. However, Fig. 4.5(d) reveals that Case 1 trails Case 5 in terms of cooling power. Excluding Case 4, linear pressure rise (Case 1) aligns with recommendations in Ref. [45] as the optimal choice. Table 4.1 indicates a 23.8% reduction in maximum cooling power for Case 4 compared to Case 1, with marginal changes in other maximum values, suggesting Case 4's superiority over Case 1. In Fig. 4.4, the equality of left and right peaks in Case 4 denotes the attainment of minimum cooling power. At alternative inlet temperatures, similar two-stage APRR1 and APRR2 configurations can be identified to achieve equivalent left-right peak and minimum cooling power. The specific APRR1 and APRR2 values for minimal cooling power at various inlet temperatures are delineated in Case 4 of Fig. 4.5.

2) Two-stage inlet temperature

In the preceding examination of two-stage APRRs, Case 4 emerges as the optimal filling strategy; however, the most effective two-stage APRRs differ across various inlet temperatures. To streamline analysis, Case 1, characterized by a constant APRR of 0.428 MPa/s, is selected as the foundational model for further exploration of two-stage inlet temperature filling strategies. Since APRR remains consistent across cases, the final filling pressure remains unchanged. By adjusting the two-stage inlet temperatures, T_{c1} and T_{c2}, the maximum temperature within the onboard tank can be maintained at approximately 80 ℃ across all scenarios. The configuration of T_{c1}, T_{c2}, and their respective switching points in each case is illustrated in Fig. 4.6. Fig. 4.7 depicts the maximum cooling energy and cooling power corresponding to the six cases outlined in Fig. 4.6. Notably, Case 3 exhibits higher cooling energy consumption compared to other cases, accompanied by the highest cooling power output.

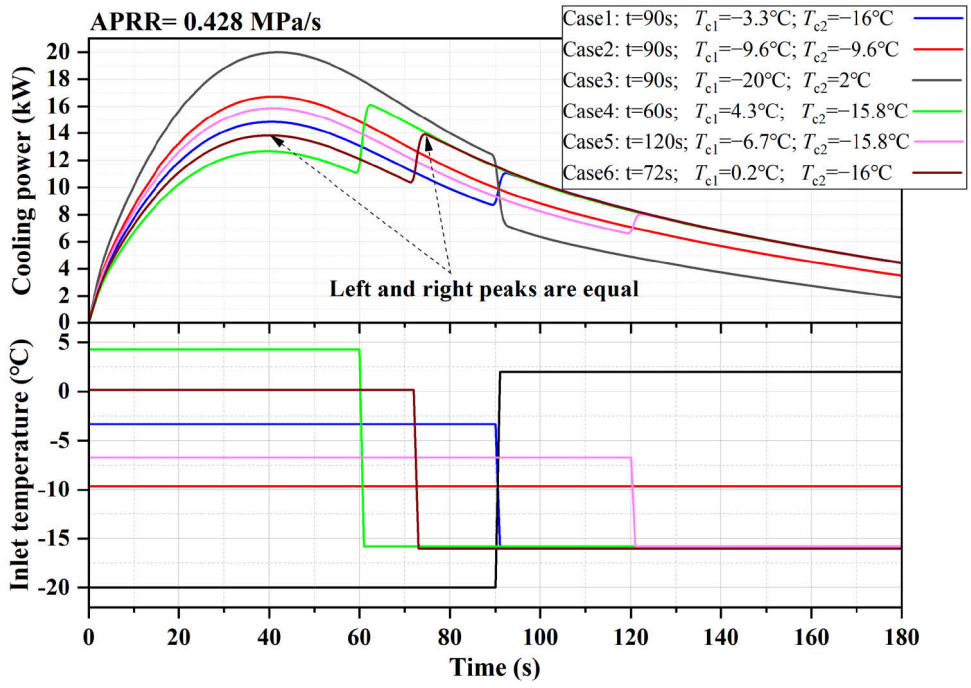

Fig. 4.6 Effects of different two-stage inlet temperatures on cooling power at APRR of 0.428 MPa/s.

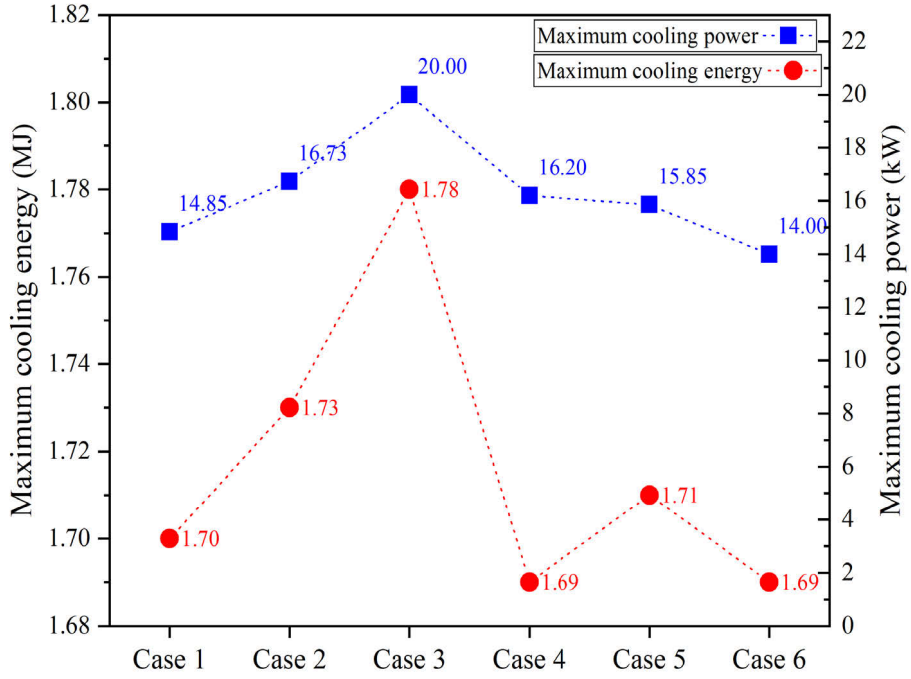

Fig. 4.7 Effects of different two-stage inlet temperature filling strategies on the maximum cooling energy and power when the APRR is 0.428 MPa/s.

In Fig. 4.6, it's observed that Case 3 undergoes robust precooling during the initial stage, followed by a weaker precooling phase in the second stage. Figs. 4.6 and 4.7 demonstrate that for Cases 2, 5, 1, 6, and 4, prolonging the cooling duration in the second stage leads to reduced maximum cooling energy. It can be inferred that second-stage precooling yields greater benefits compared to the initial stage, a finding consistent with Ref. [45]. Referring to Table 4.1, Case 2 serves as a benchmark against which to compare the maximum results of Cases 1, 4, 5, and 6. Given the comparable final onboard tank temperature and filling pressure across all cases, their SOC remains consistent. Cases 1 and 5 exhibit inferior cooling energy and cooling power performance compared to Case 6. Despite Case 6 boasting 0.3% higher cooling energy than Case 4, its cooling power is 13.1% lower than that of Case 4. Hence, Case 6 is deemed superior to Case 4. In Fig. 4.6, it's noted that the equality of left and right peaks in Case 6 signifies the attainment of minimum cooling power.

Table 4.1 Maximum results and relative rate of change for typical cases.

Case		Max T_{on} (℃)	Max SOC	Max cooling energy (MJ)	Max cooling power (kW)
Inlet temperature = −20 ℃	Case 1	69.988	0.966	2.124	19.999
	Case 4	70.379 (+0.5%)	0.959 (−0.7%)	2.118 (−0.3%)	15.246 (−23.8%)
APRR = 0.428 MPa/s	Case 1	79.987	0.947	1.697 (−1.7%)	14.846 (−11.3%)
	Case 2	79.983	0.947	1.727	16.730
	Case 4	80.001	0.947	1.687 (−2.3%)	16.199 (−3.2%)
	Case 5	79.929	0.947	1.709 (−1.0%)	15.854 (−5.2%)
	Case 6	79.937	0.947	1.693 (−2.0%)	13.999 (−16.3%)

In synthesis, the research in Ref. [45] suggests that a single-stage constant APRR proves optimal, whereas the findings in this section indicate the potential efficacy of employing a two-stage APRR approach. Consistently, two-stage APRR1 and APRR2 configurations can be identified to further diminish cooling power without augmenting cooling energy consumption. For instance, at an inlet temperature of −20 °C, adopting a two-stage APRR filling strategy can achieve a 23.8% reduction in maximum cooling power. Additionally, the investigation herein reveals that employing two-stage inlet temperatures, T_{c1} and T_{c2}, can yield a further reduction in cooling power without a concurrent increase in cooling energy usage. For instance, with an APRR of 0.428 MPa/s, employing the two-stage inlet temperature filling strategy can lead to a 16.3% reduction in maximum cooling power.

Approximately 15% of the total expenditure on HRS equipment is allocated to refrigeration equipment [53], making the reduction in maximum cooling power consequential for curtailing refrigeration equipment investment. Ref. [94] underscores the necessity for in-depth research and analysis on refrigeration equipment performance, energy consumption, and design optimization to mitigate HRS costs. Regarding the filling strategies proposed, achieving a two-stage APRR can be facilitated by dynamically controlling the reduction valve through the dispenser. For high-pressure gas-storage HRS, two-stage inlet temperatures can be attained by

dynamically adjusting the hydrogen mixing ratio pre and post precooling [33]. Conversely, for liquid-storage HRS, two-stage inlet temperatures can be realized by blending low-temperature hydrogen pressurized by the cryopump with normal-temperature hydrogen heated by the heat exchanger [95]. Integration of aluminum heat exchange blocks in refrigeration systems can serve as thermal mass, absorbing heat during filling. Consequently, determining the rated power of refrigeration equipment based on the average power demand of precooling hydrogen rather than its maximum power demand becomes feasible [51].

4.2 Cascade hydrogen filling system

4.2.1 Cascade hydrogen filling system model

Depending on the number of storage tanks at HRS, the hydrogen filling system is divided into single-stage and cascade filling systems. The currently commonly used cascade filling systems are two-stage and three-stage cascade filling systems. Refs. [96, 97] reported on the European 3Emotion project. This project studied a two-stage cascade HRS in Aalborg, Denmark, without a precooling system, as shown in Fig. 4.8. The hydrogen filling system uses electrolysers to produce hydrogen, with a production capacity of 100 kg per day. The hydrogen is first stored in a 3.5 MPa low-pressure buffer tank, then compressed by a compressor into a 30 MPa medium-pressure storage tank and a 45 MPa high-pressure storage tank, and finally filled sequentially through the medium-pressure and high-pressure storage tanks.

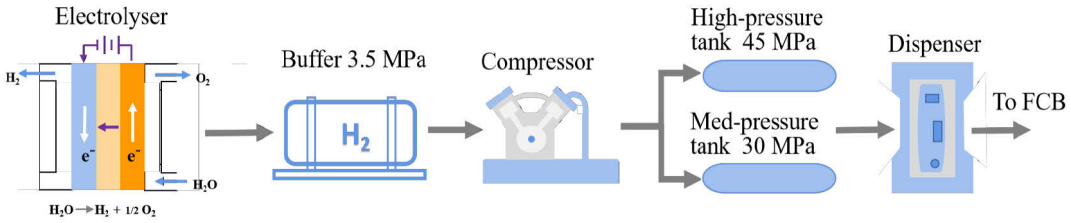

Fig. 4.8 Structural diagram of the hydrogen filling system using two-stage pressure filling for fuel cell buses in Aalborg.

Sinopec built a three-stage cascade HRS in Wuhan in November 2021, equipped with a hydrogen precooling system. The capacity of hydrogen filling is 500kg per day, providing filling services for buses, sanitation vehicles and logistics vehicles. Fig. 4.9 shows the structure of the three-stage cascade hydrogen filling system established in

this section. It includes three station-side cascade storage tanks, a reduction valve, a heat exchanger and an onboard tank. The reduction valve and heat exchanger adopt the model established in Section 4.1. The temperature and pressure in the onboard tank are the focus of this section, so the onboard tank adopts the zero-dimensional gas one-dimensional tank wall (0D1D) lumped parameter model established in Section 2.3.4. The cascade storage tank in the HRS is not the focus of the study, so it is simplified, and the single-zone lumped parameter model established in Section 2.3.1 is used. That is, the influence of the tank wall is ignored, and it is assumed that there is a direct heat exchange between hydrogen and air. We further assume that the geometry of the cascade storage tank is a standard sphere, then its surface area can be derived from its volume, which is beneficial to the configuration optimization study of the cascade storage tank volume and initial pressure in the following.

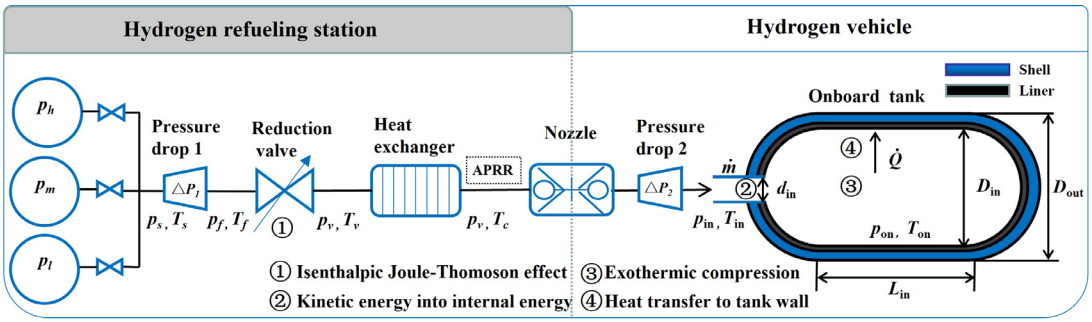

Fig. 4.9 Structure of the three-stage cascade hydrogen filling system established in this thesis.

In order to verify the accuracy of the three-stage cascade filling system model, the results in Ref. [21] were used for comparison and verification. The geometric and physical properties of the onboard tank are shown in Table 4.2. The volume is 173 L, and the initial pressure is 2 MPa. The initial pressures of the low-pressure, medium-pressure and high-pressure cascade storage tanks of the HRS are 45 MPa, 65 MPa and 90 MPa, respectively. Their volumes are the same, and they are all 1000 L. The hydrogen precooling temperature is −40 °C, and the ambient temperature is 25 °C. The average pressure ramp rate (APRR) during filling is constant at 28.2 MPa/min.

Table 4.2 Parameters of the onboard tank in this study [36].

Parameter	Physical definition	Value
L_{wl}	Thickness of tank wall liner (mm)	3
k_{wl}	Thermal conductivity of tank wall liner (W/m/K)	1.17
c_{wl}	Specific heat capacity of tank wall liner (J/kg/K)	1578
ρ_{wl}	Density of tank wall liner (kg/m^3)	1286
L_{ws}	Thickness of tank wall shell (mm)	22
k_{ws}	Thermal conductivity of tank wall shell (W/m/K)	1.14
c_{ws}	Specific heat capacity of tank wall shell (J/kg/K)	1075
ρ_{ws}	Density of tank wall shell (kg/m^3)	1375

As shown in Fig. 4.10(a), the P_s , P_f , P_v and P_{on} represent the pressure inside the cascade tanks, before the reduction valve, behind the reduction valve, and inside the onboard tank, respectively. In summary, the simulation values agree with the reference values. The pressure P_v increases linearly because a constant APRR is set. There is a certain difference between the pressure P_s and P_f , which is caused by the pressure loss ΔP_1 . There is a certain difference between the pressure P_{on} and P_v , which is caused by the pressure loss ΔP_2 .

As shown in Fig. 4.10(b), the T_s , T_v , T_c , T_{in} and T_{on} represent the temperature inside the cascade tanks, behind the reduction valve, behind the heat exchanger, before the onboard tank, and inside the onboard tank, respectively. In summary, the simulation values T_c and T_{in} agree with the reference values. The simulation values T_s and T_v are basically consistent with the reference values, and the simulation values are about 1-2 °C higher than the reference values only in the later stages of refuelling at each level. The simulation value T_{on} is consistent with the changing trend of the reference value, but there is a deviation of about 1-5 °C in the middle and last stages. The deviations of T_s , T_v and T_{on} are caused by the assumption that the cascade tanks established in this thesis are a zero-dimensional single-zone model leading to the deviation of heat transfer rate $\dot{Q}$. There is a noticeable temperature difference between T_v and T_s , which is

mainly caused by the Joule-Thomson effect. As the pressure difference between P_f and P_v gradually decreases, the Joule-Thomson effect gradually weakens, and the temperature difference between T_v and T_s gradually decreases. At the beginning of refuelling, the mass flow rate increases rapidly, and the temperature T_{on} rises rapidly due to the compression effect. With the decrease of mass flow rate, the curve of T_{on} gradually becomes flat.

In Figs. 4.10(c) and (d), the mass flow rate and cooling demand are depicted, respectively, exhibiting initial consistency between simulation and reference values during refuelling commencement. However, slight discrepancies emerge towards the end. This variance may stem from disparities in vehicle-side pressure losses between the current model and those outlined in Ref. [21]. Notably, vehicle-side pressure losses dictate the system's mass flow rate [55], with deviations therein influencing cooling demand variation. Furthermore, deviations between this study and the reference material are evident at peak points in Fig. 4.10(d). These deviations are caused by the assumption that there is no pressure loss in the heat exchanger, and P_v is used to replace the pressure behind the heat exchanger P_c. In fact, P_v is greater than P_c, causing a large c_{vc}. The c_{vc} as a function of P and T is calculated using the NIST database in real-time. As shown in Eq. (4.2), the increase of c_{vc} leads to the decrease in cooling demand, while the other parameters are consistent with the reference at the peak points.

In summary, the model of the three-stage cascade hydrogen filling system we established is accurate. The three-stage cascade hydrogen filling system has low-pressure, medium-pressure and high-pressure tanks. The different tank configurations of initial pressure and volume have a significant impact on the energy consumption and power of the filling system and the thermal effect of the onboard tank. Next, we will study the optimal volume and initial pressure configuration of the cascade storage tank based on the established and verified three-stage cascade filling system model so as to achieve lower energy consumption of the filling system, lower temperature rise and higher SOC of the onboard tank.

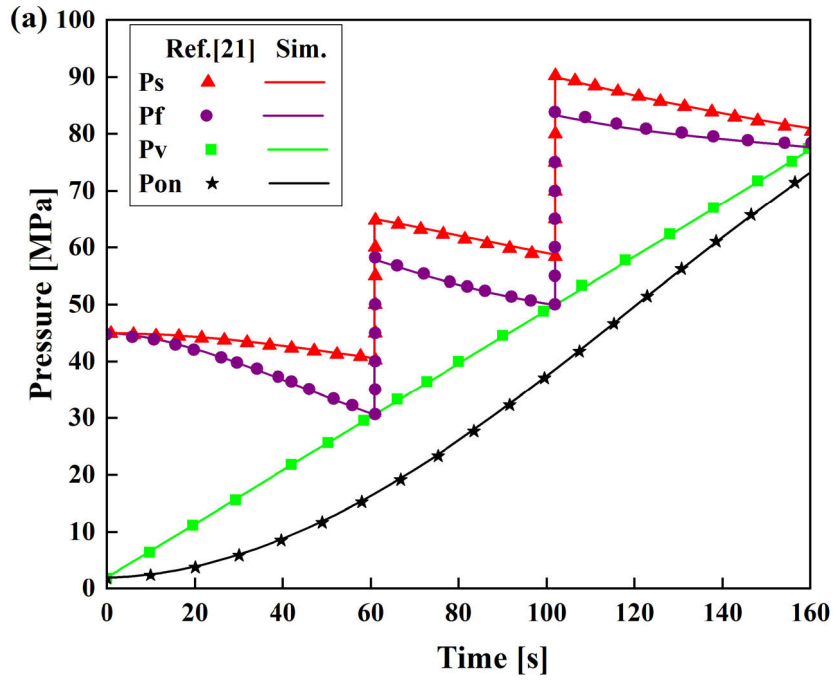
(a)
Ref.[21] Sim.
Ps
Pf
Pv
Pon
Pressure [MPa]
Time [s]
0
10
20
30
40
50
60
70
80
90
100
0
20
40
60
80
100
120
140
160

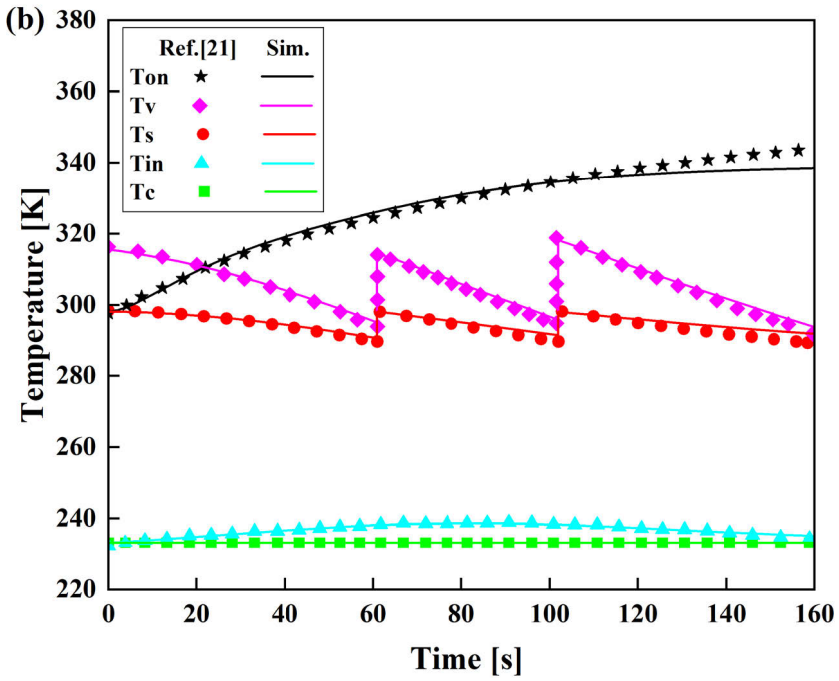
(b)
Ref.[21] Sim.
Ton
Tv
Ts
Tin
Tc
Temperature [K]
Time [s]
220
240
260
280
300
320
340
360
380
0
20
40
60
80
100
120
140
160

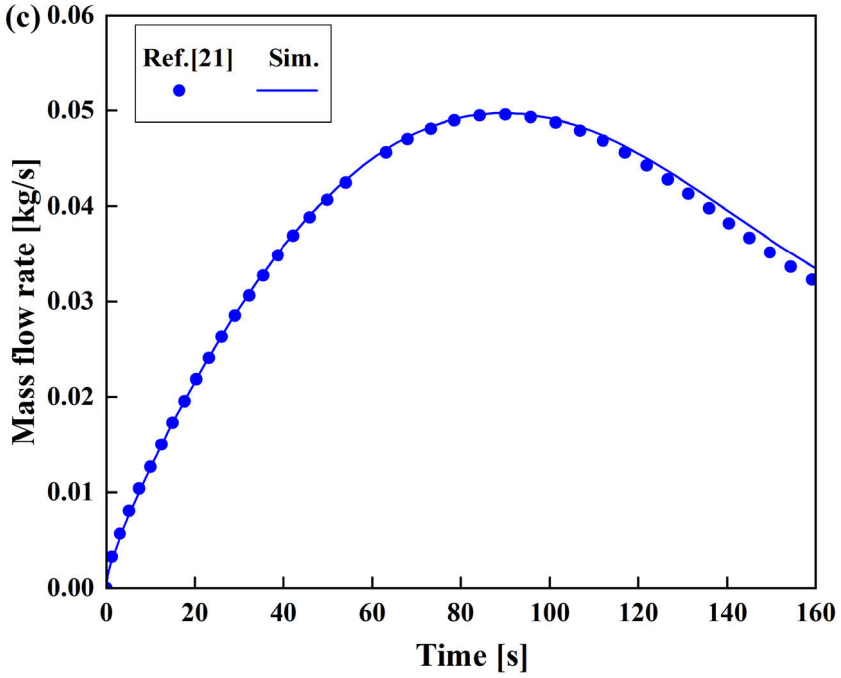

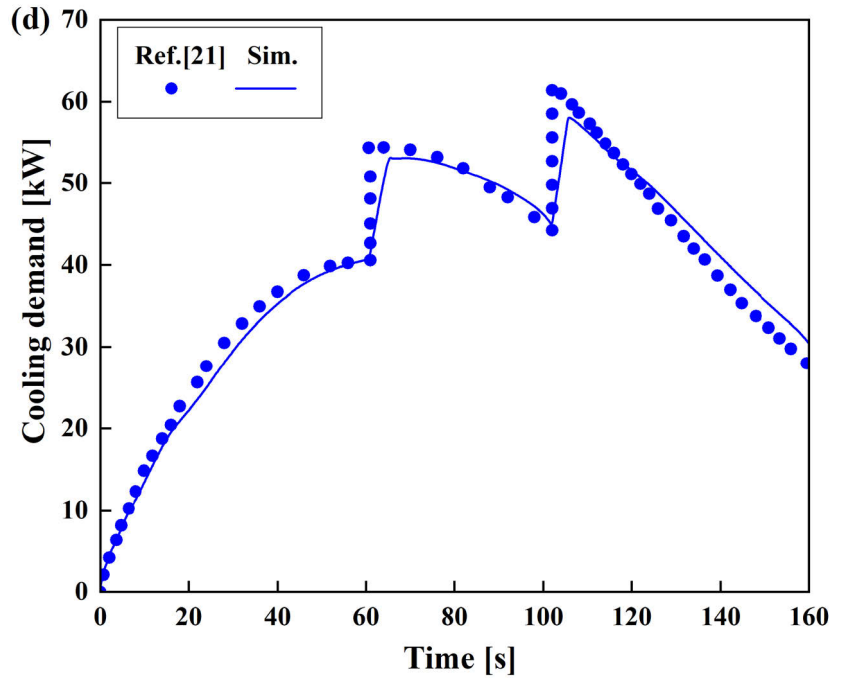

Fig. 4.10 Comparison of the pressure (a), temperature (b), mass flow rate (c), and cooling demand (d) between the simulation results of the current model and the results of Ref. [21].

4.2.2 Optimization of initial pressure and volume of cascade storage tanks

(1) Generating independent variable data set

Cascade filling systems commonly employ multiple cascade storage tanks, with studies indicating that the volume and initial pressure of these tanks significantly influence filling performance [40]. Building upon the verified cascade filling system model from Section 4.2.1, this section investigates the impact of cascade storage tank volume and initial pressure on onboard tank SOC and refrigeration equipment cooling energy. The selected independent variables encompass the volume and initial pressure of low, medium, and high-pressure cascade tanks, while dependent variables include cooling energy and SOC. According to the SAE J2601 hydrogen refuelling protocol, the maximum allowable pressure is 125% of the rated pressure, i.e., 87.5 MPa. Consequently, the initial pressure range for low, medium, and high-pressure cascade tanks ranges from 35 to 95 MPa.

For the cascade tanks, volumes of the low, medium, and high-pressure tanks are uniformly increased from 200 L to 2000 L, while initial pressures are maintained equal and set at 35 MPa, 50 MPa, 65 MPa, 80 MPa, and 95 MPa, respectively. The onboard tank's initial pressure is set to 5 MPa, with a volume of 173 L. Ambient temperature remains at 20 °C, while precooling hydrogen temperature is set to −40 °C. The APRR is established at 21.8 MPa/min as per the SAE J2601 lookup table protocol.

Fig. 4.11 illustrates the impact of total cascade tank volume and initial pressure on cooling energy and SOC. Under an initial pressure of 95 MPa, SOC reaches 1 as the total cascade tank volume increases. Hence, setting the initial pressure range between 35-95 MPa is deemed reasonable. With an initial pressure of 95 MPa, cooling energy exhibits rapid escalation initially with increasing total volume, plateauing once the volume surpasses approximately 3300 L. Thus, the volume range for low, medium, and high-pressure tanks can be defined as 200-1100 L. The independent variable values for this study are outlined in Table 4.3.

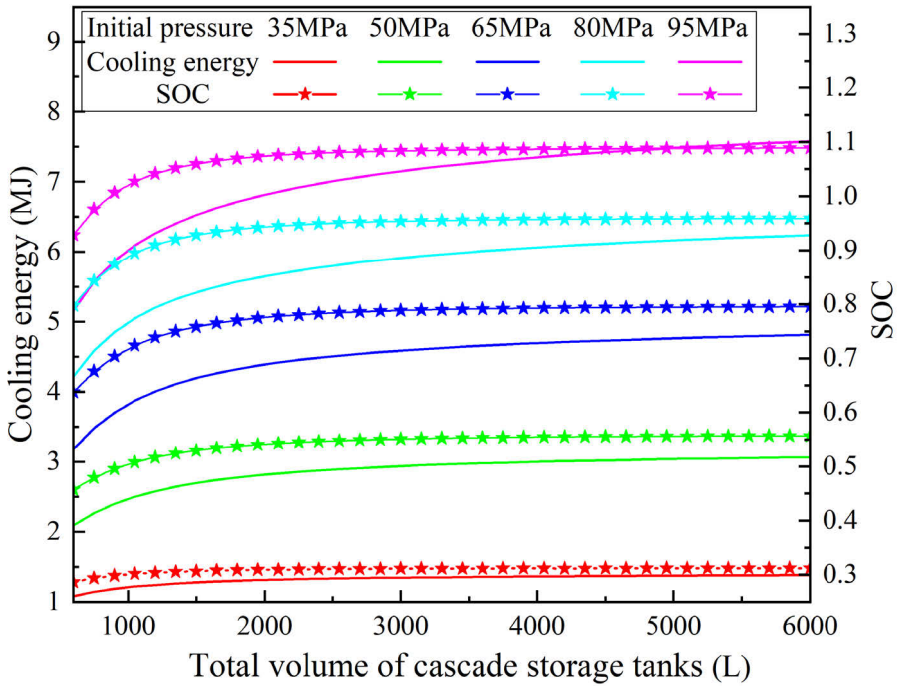

Fig. 4.11 Effect of the total volume of three tanks and initial pressure in cascade tanks on cooling energy and SOC.

Table 4.3 Volume and initial pressure ranges of low, medium and high-pressure cascade storage tanks

Parameter	Physical definition	Value
V_l	Volume of low-pressure tank (L)	From 200 to 1100, step 50
V_m	Volume of med-pressure tank (L)	From 200 to 1100, step 50
V_h	Volume of high-pressure tank (L)	From 200 to 1100, step 50
p_l	Initial pressure of low-pressure tank (MPa)	From 35 to 95, step 5
p_m	Initial pressure of med-pressure tank (MPa)	From 35 to 95, step 5
p_h	Initial pressure of high-pressure tank (MPa)	From 35 to 95, step 5

The independent variables encompass six factors: the volumes and initial pressures of the three storage tanks. Each tank consists of 19 volume levels and 13 initial pressure levels. Conducting a comprehensive experiment without test design would entail a vast number of simulation calculations, rendering actual operation complex. Hence, an orthogonal test design is employed, resulting in the determination of 419 test case sets. These sets effectively encapsulate the comprehensive experiment results, adhering to orthogonal test design principles. Subsequently, these 419 test case sets undergo simulation to calculate corresponding cooling energy and SOC values. Fig. 4.12 depicts

the relationship between the 419 sets of cooling energy and SOC. Notably, each SOC corresponds to multiple cooling energy values, some of which exceed the smallest value by approximately 10%-20%. The red curve in Fig. 4.12 represents cases where cooling energy is minimized, with corresponding optimal volume and initial pressure configurations. Therefore, it is necessary to optimize the initial pressure and volume of the cascade storage tank to find the volume and initial pressure of the cascade storage tank corresponding to the red curve in Fig. 4.12.

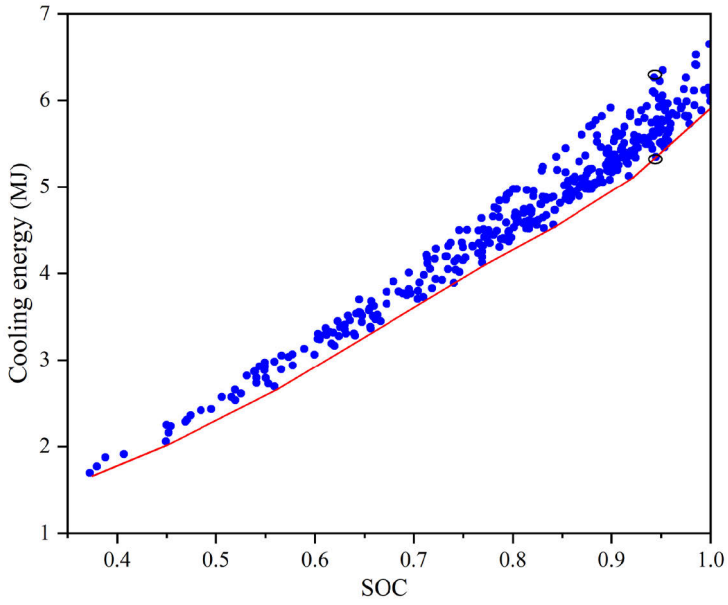

Fig. 4.12 Relationship between 419 sets of cooling energy and SOC.

(2) Multi-objective optimization method

An optimization problem typically comprises three primary elements: objective functions, decision variables, and constraints. In the context of this study, the objective functions encompass cooling energy and SOC, while the decision variables pertain to the volume and initial pressure of low, medium, and high-pressure cascade tanks. As previously analyzed, the volume constraint ranges from 200 to 1100 L, and the initial pressure constraint spans from 35 to 95 MPa. Establishing a connection between the decision variables (V_l, V_m, V_h, P_l, P_m and P_h) and the objective functions (SOC and cooling energy) is imperative. This linkage can be achieved through the utilization of an artificial neural network (ANN).

1) Artificial Neural Network (ANN)

Three common artificial neural network structures are feedforward neural network, feedback neural network and graph network. This section uses a feedforward neural network, as shown in Fig. 4.13, which generally includes an input layer, one or more hidden layers and an output layer. Each node is also called an artificial neuron, and they are connected to another node with associated weights and biases. The main idea is to calculate the error between the output and the target value, then back-propagate the error to each layer in the network, and finally adjust the weight and bias of each neuron to minimize the error [99].

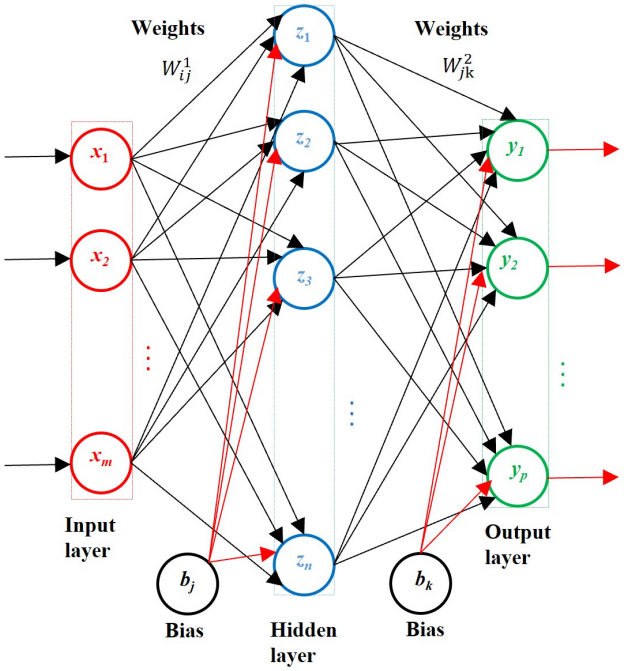

Fig. 4.13 Structure of feedforward backpropagation artificial neural network.

In this study, a feed-forward backpropagation ANN is employed and structured with three layers of neurons. The input layer comprises six parameters: V_l, V_m, V_h, P_l, P_m, and P_h, while the output layer includes cooling energy and SOC. A computational hidden layer houses nine neurons. Training methods utilize mathematical mean square error (MSE) functions to minimize discrepancies between network output and target values. The implementation process revolves around iteratively adjusting weights and biases to reduce error [100]. The dataset of 419 entries is partitioned into training and test data at a 3:1 ratio. The *newff* function in Matlab facilitates training to procure the requisite ANN.

Fig. 4.14 illustrates the correlation coefficient between prediction and simulation results. All correlation coefficients exceed 0.99, with data distribution points closely aligning with the fitted regression line, indicating that the neuron effectively captures the correlation between decision variables and objective functions.

Fig. 4.15 depicts the comparison between prediction and simulation data. Notably, in Figs. 4.15(a) and (b), 104 prediction data points align with simulation counterparts. Conversely, in Figs. 4.15(c) and (d), only 8-10 points exhibit relative errors surpassing 5%. Thus, this ANN satisfactorily meets the requirements for predicting SOC and cooling energy during the fueling process.

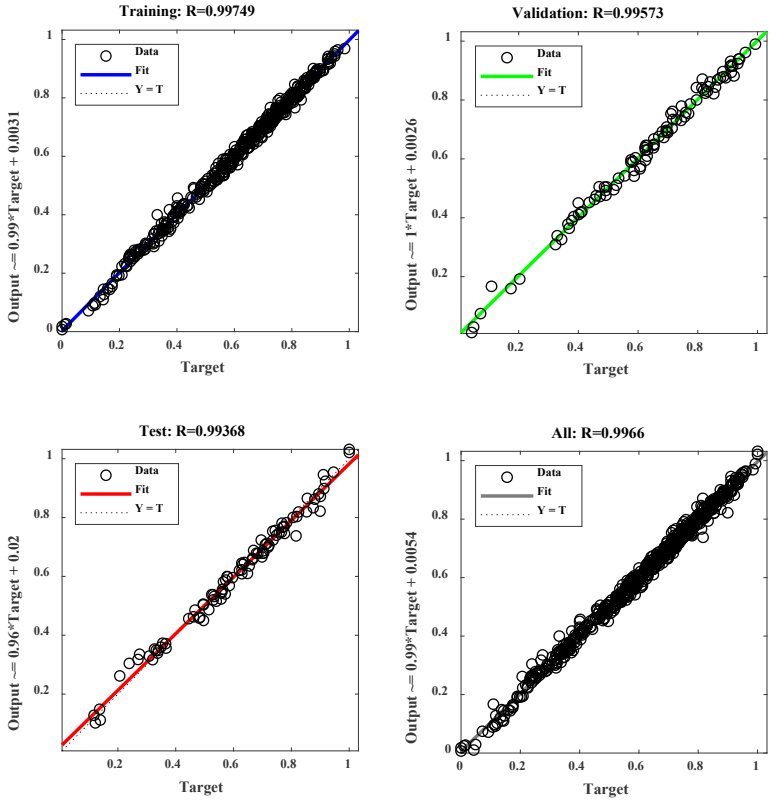

Fig. 4.14 Correlation coefficient between the prediction and simulation results.

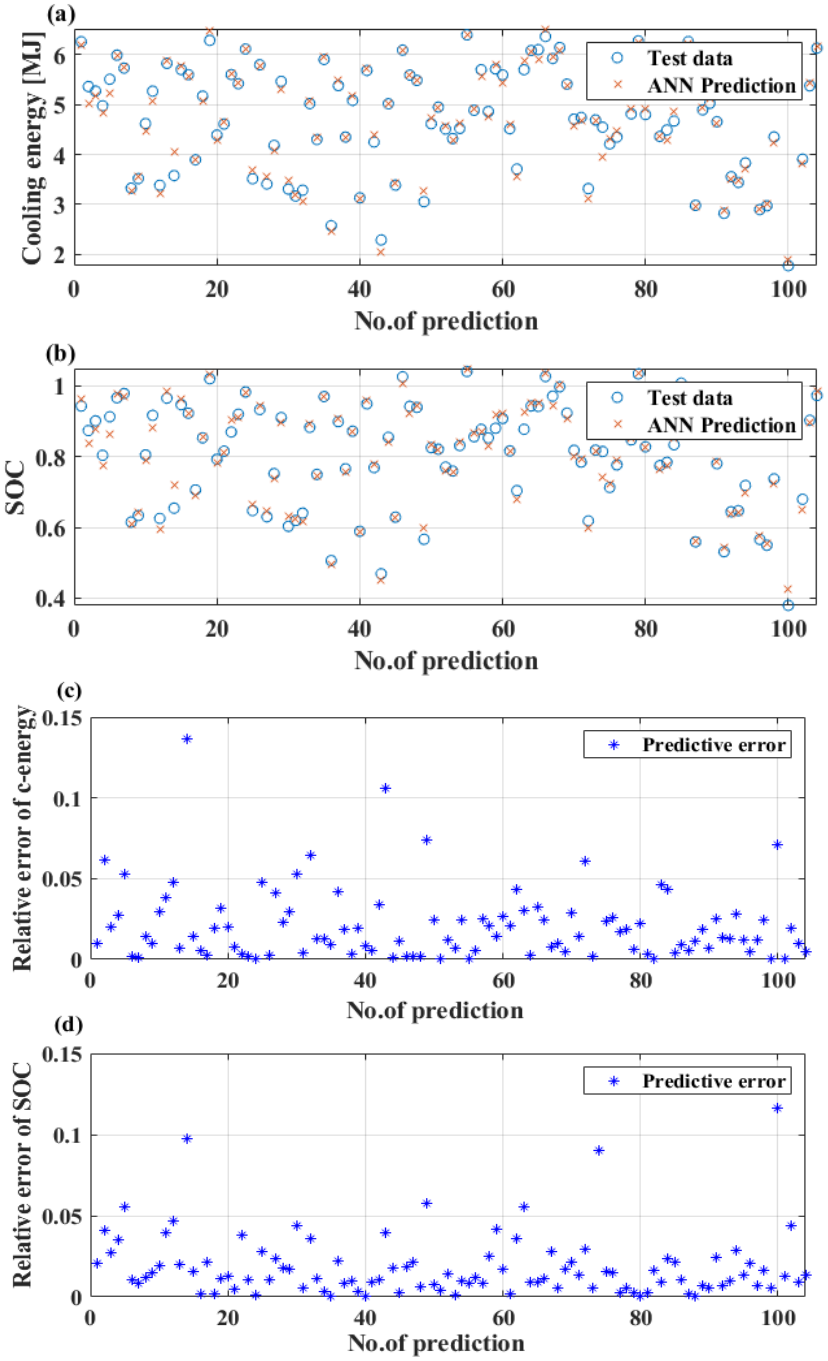

Fig. 4.15 Comparison of the absolute values of cooling energy (a), SOC (b) and the relative error of cooling energy (c), SOC (d) between prediction and simulation.

2) Genetic Algorithm (GA)

After establishing the relationship between the decision variables and the objective function through ANN, an optimization algorithm needs to be used to find the best decision variable values. Optimization algorithms include traditional optimization

algorithms and intelligent optimization algorithms. A genetic algorithm (GA) is a kind of intelligent optimization algorithm that is suitable for dealing with complex nonlinear problems. The relationship between the decision variables and the objective function established in this section is a complex nonlinear relationship, which is suitable for genetic algorithms. In addition, compared with the particle swarm algorithm, the GA that was studied earlier is more mature and stable and is less likely to fall into a locally optimal solution.

The running process of the GA: First, it randomly selects a group of valid candidate individuals to create an initial population, and then the fitness function value for each individual in the initial population is calculated. Then, the genetic operators of selection, crossover, and mutation are applied to the initial population to construct a new generation population, and the fitness function value is calculated for each individual in the new generation population. The selection operation is used to select advantageous individuals in the current population. The crossover operation is used to create offspring from selected individuals, usually by swapping parts of the chromosomes of two selected individuals to create two new chromosomes. The mutation operation is used to randomly change one or more chromosomes of each newly created individual. There are many conditions for controlling the termination of the algorithm. The two most commonly used ones are the one where the maximum number of iterations has been reached and the other where there has been no significant improvement in the individuals of the population in the past few iterations. The specific implementation process is to compare the best fitness function value obtained in each iteration with the best fitness function value obtained previously. If the difference between the two is less than a certain threshold, the algorithm is stopped.

3) Pareto optimization

The relationship $\left(\text{SOC}, \text{Cooling Energy}\right) = f\left(V_l, V_m, V_h, P_l, P_m, P_h\right)$ established by ANN includes two objective functions. The objective function of SOC needs to be maximized, and the objective function of cooling energy needs to be minimized. The two objectives conflict. If a single-objective optimization method is used, the optimal solution to the two objective functions cannot be found simultaneously. Multi-objective optimization problems generally use two types of methods. The first type of method is to simplify

the multi-objective optimization problem into a single-objective optimization problem, mainly by weighting different objective functions and combining them into one objective function. The main idea is to transform it into a single-objective optimization problem. The second type of method is the Pareto optimization method. The main idea is first to clarify the priorities or weights of different objective functions, then find a set of Pareto solutions that are optimal solutions under optimization conditions and different weights, and finally, decide which solution to choose based on the application scenario of the decision maker. When the GA is combined with Pareto optimization suitable for multi-objective processing, the GA can play an effective role in multi-objective optimization [101]. Therefore, the introduction of Pareto optimization can relatively effectively find a representative Pareto optimal solution set [102].

This thesis first substitutes the different values of V_l, V_m, V_h, p_l, p_m and p_h, as well as the corresponding SOC and cooling energy into the ANN as matrices to establish the relationship between the decision variables and the objective function and then conducts a multi-objective optimization based on GA and Pareto. Fig. 4.16 shows the multi-objective optimization steps of this study.

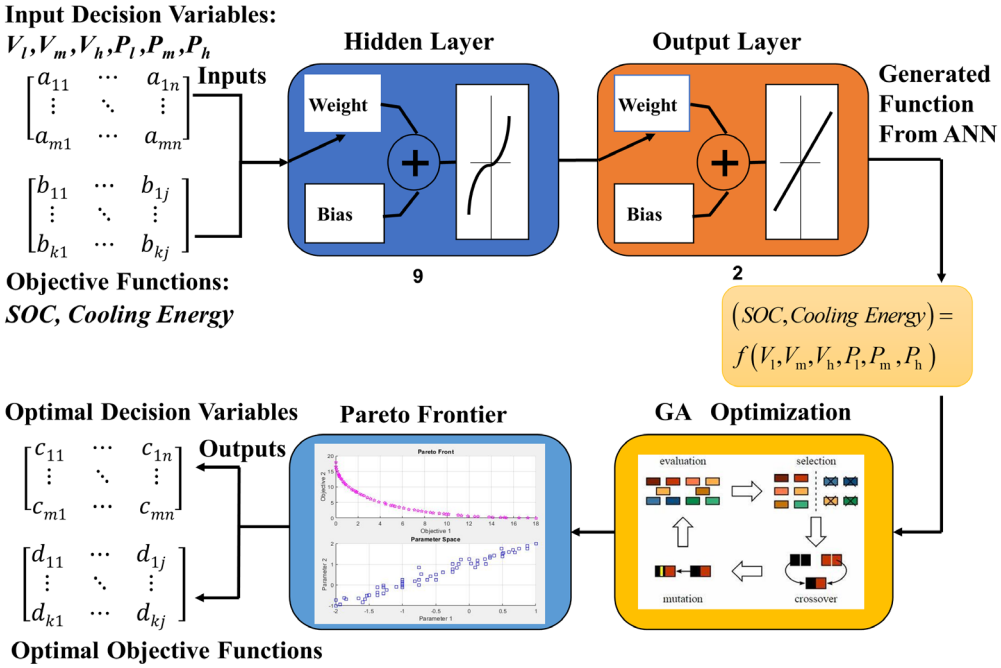

Fig. 4.16 Schematic diagram of multi-objective optimization steps of this study.

(3) Multi-objective optimization results

Fig. 4.17 illustrates the Pareto frontier resulting from a single Pareto optimization. A comparison between Fig. 4.17 and Fig. 4.12 reveals that the Pareto frontier in Fig. 4.17 corresponds directly to the red curve depicted in Fig. 4.12. No further optimization of decision variables is feasible along this Pareto frontier. Optimal points for cooling energy and SOC under single-objective optimization are denoted as Points A and B, respectively. For multi-objective optimization, Point C is selected as it is closest to the ideal point when both objective functions carry equal importance [59, 103]. However, in practical engineering applications, one objective function may outweigh the other. In this study, refilling the onboard tank is necessary if SOC falls below a certain threshold. Typically, refuelling concludes at a pressure equivalent to a SOC of 0.95 to 1 in refuelling processes involving communication [104]. Consequently, points with a SOC ranging from 0.98 to 0.99 on the Pareto frontier are targeted for further investigation. However, as depicted in Fig. 4.17, the scarcity of points with a SOC between 0.98 and 0.99 complicates the elucidation of corresponding initial pressure and volume distributions. Therefore, Pareto optimization was conducted 100 times in this study.

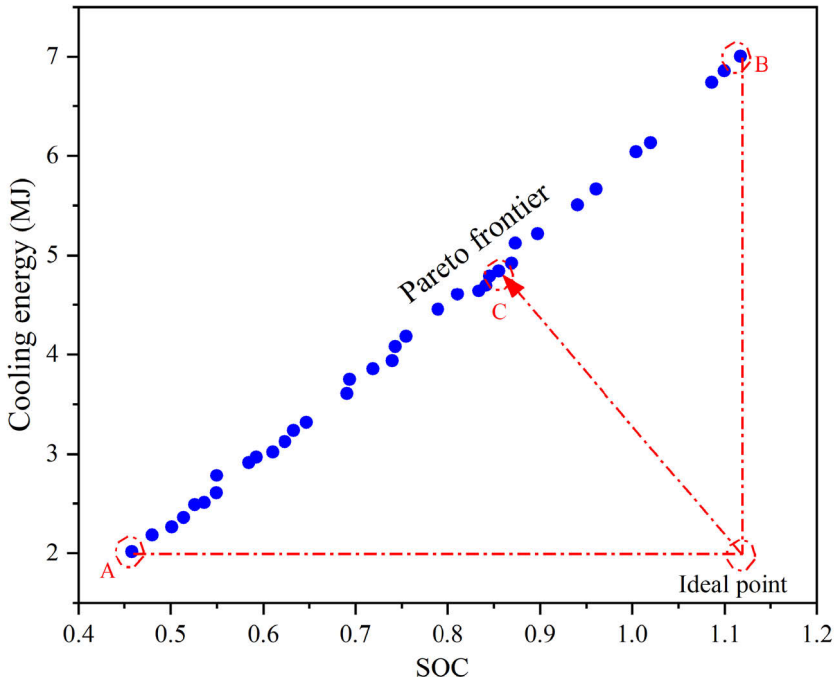

Fig. 4.17 Pareto frontier of a single Pareto optimization.

Fig. 4.18 presents the distribution of V_l, V_m, V_h, P_l, P_m, and P_h following 100 iterations of Pareto optimization with a SOC range of 0.98 to 0.99. The abscissa represents the optimization serial number. At each abscissa position, the corresponding six figures depict the optimal values of V_l, V_m, V_h, P_l, P_m, and P_h obtained in the respective optimization. The red line represents the fitted linear trend line, with data points distributed on both sides of it. Discounting outliers in Fig. 4.18 due to the stochastic nature of genetic algorithms (GAs), optimal values for V_l, V_m, and V_h fall within the range of 600 to 900 L, while P_l ranges from 45 to 75 MPa, P_m from 70 to 85 MPa, and P_h from 85 to 90 MPa. Notably, the distribution of V_l, V_m, and V_h appears relatively scattered, whereas P_l, P_m, and P_h exhibit greater concentration. The sensitivity of initial pressure surpasses that of volume concerning their impact on cooling energy and SOC, suggesting greater significance in optimizing initial pressure when constructing HRS.

As depicted in Figs. 4.18(a)-(e), the distribution of V_l, V_m, V_h, P_l, and P_m shows a degree of scattering, as these decision variables compromise each other to balance the two objective functions. However, single-objective optimization's limitation lies in its inability to fully reflect the constraint relationship between each objective, resulting in suboptimal decision variables [105]. Conversely, Fig. 4.18(f) illustrates that the distribution of P_h is notably concentrated, indicating its heightened sensitivity. Thus, greater emphasis should be placed on the initial pressure of the high-pressure tank when constructing HRS.

The dataset comprises 419 sets of test cases obtained through orthogonal test design, with corresponding SOC and cooling energy values. Sets with a SOC range of 0.98-0.99 are selected as pre-optimization datasets. The average value in each figure serves as the optimal dataset, as depicted in Fig. 4.18. Table 4.4 indicates that cooling energy (kWh/kgH_2) aligns closely with data from Ref. [8] at an ambient temperature of 20 ℃, with a deviation attributed to assumptions regarding heat transfer in the heat exchanger. Compared with the best and worst scenarios pre-optimization, cooling energy can be reduced by 1.37% and 11.43%, respectively, as detailed in Table 4.4.

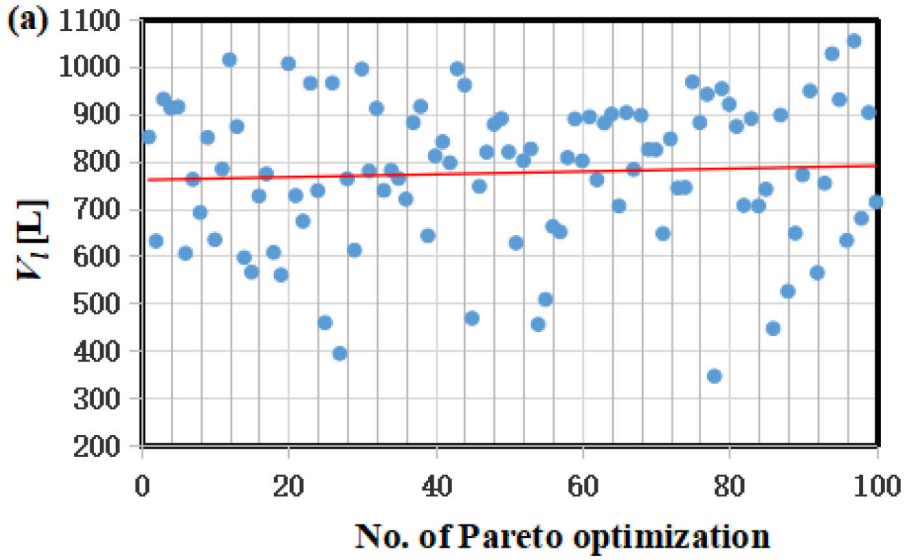
(a)
1100
1000
900
800
700
600
500
400
300
200
V_l [L]
0
20
40
60
80
100
No. of Pareto optimization

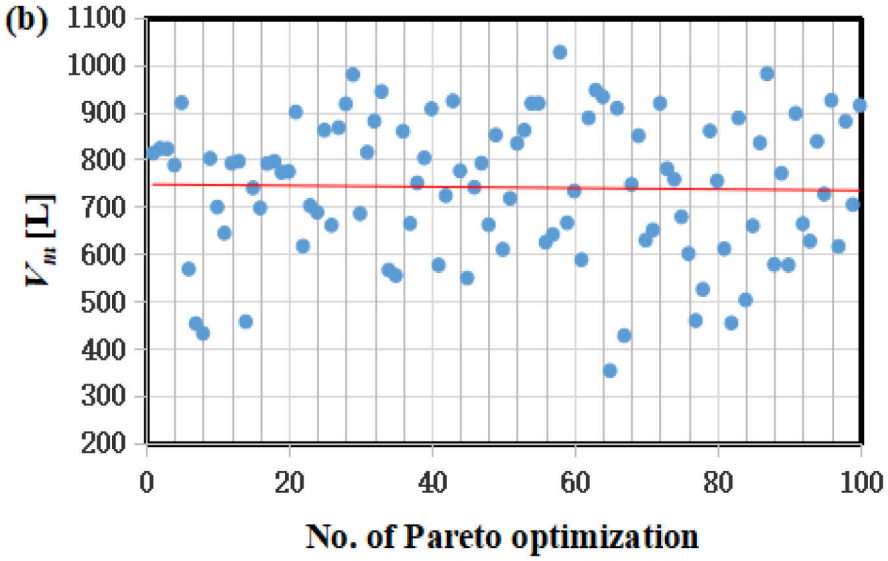
(b)
1100
1000
900
800
700
600
500
400
300
200
V_m [L]
0
20
40
60
80
100
No. of Pareto optimization

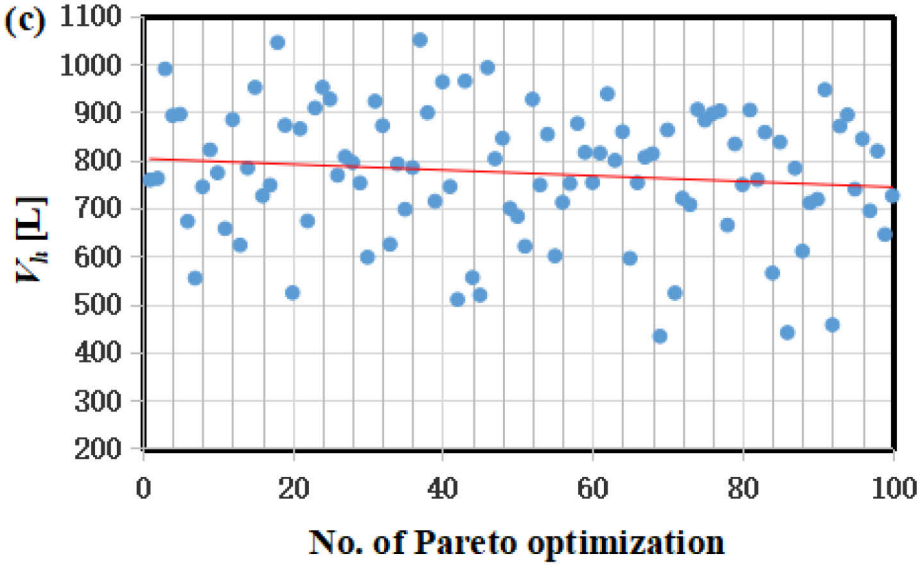
(c)
1100
1000
900
800
700
600
500
400
300
200
V_h [L]
0
20
40
60
80
100
No. of Pareto optimization

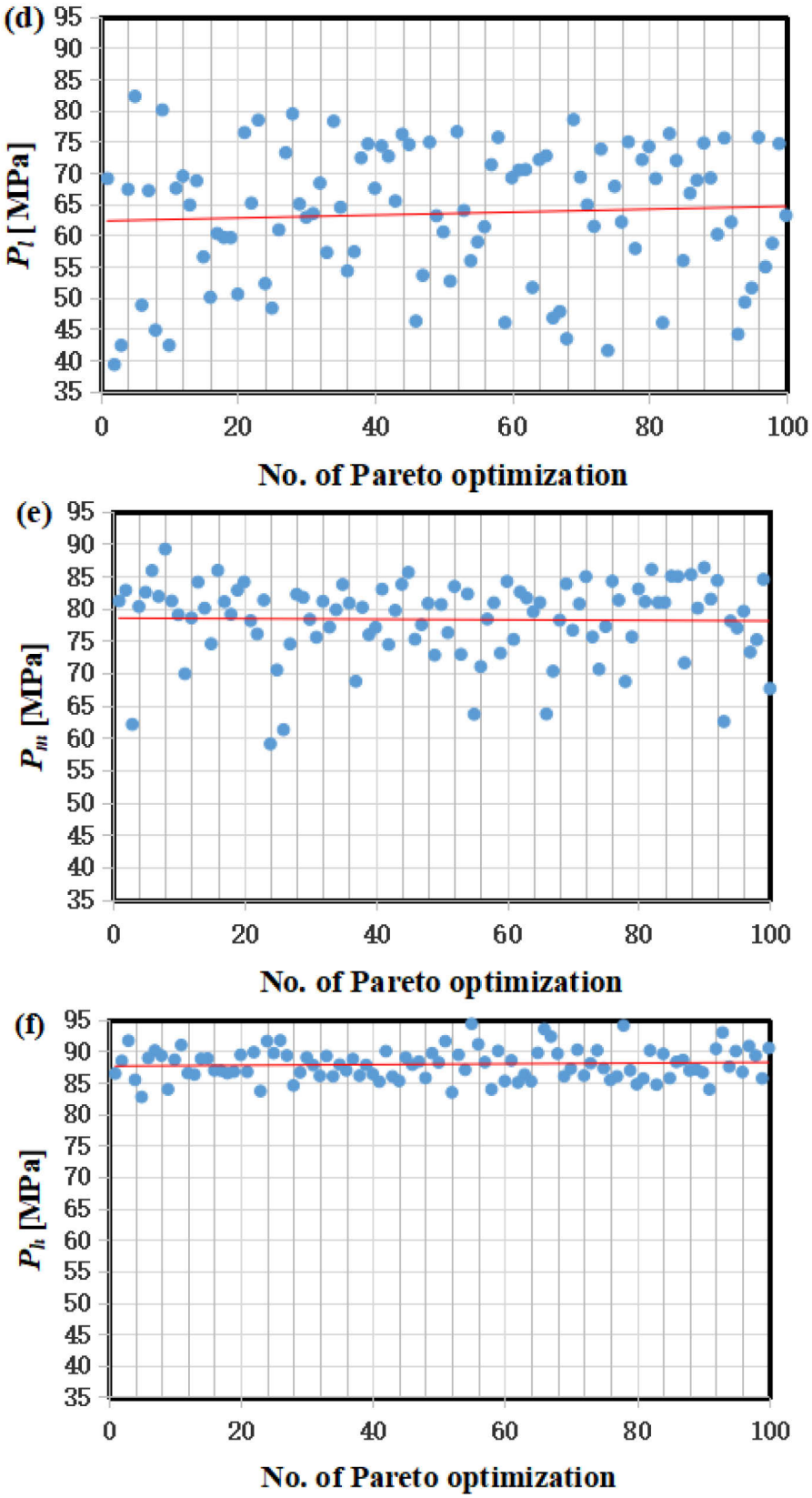

Fig. 4.18 Distribution of V_l (a), V_m (b), V_h (c), P_l (d), P_m (e) and P_h (f) when the SOC is 0.98-0.99 after 100 times Pareto optimization.

Table 4.4 Results before and after optimization

Parameters	V_l L	V_m L	V_h L	P_l MPa	P_m MPa	P_h MPa	T_{on} K	P_{on} MPa	SOC	Cooling Energy kWh/kgH_2
	950	700	550	80	90	45	333.88	79.36	0.983	0.277
	450	950	500	90	90	80	333.89	79.45	0.984	0.269 (1.37%)
Baseline	900	450	200	95	60	95	333.89	79.55	0.985	0.290
	1050	250	500	95	90	65	333.90	79.62	0.985	0.295 (11.43%)
	1100	1000	900	90	75	85	333.90	79.64	0.985	0.289
Optimal	775	740	773	63	78	88	333.93	80.22	0.990	0.263

This section uses a multi-objective optimization algorithm based on GA and Pareto optimization to successfully determine the optimal initial pressure and volume configuration of the cascade storage tank. When the ambient temperature is 20 °C, the SOC is 0.98 to 0.99, and the optimal values of V_l, V_m, V_h, P_l, P_m and P_h are 775 L, 740 L, 773 L, 63 MPa, 78 MPa and 88 MPa, the cooling energy after optimization is reduced by 1.37% and 11.43%, respectively, compared with the best and worst situation before optimization. Among the factors that affect cooling energy and SOC, initial pressure is more sensitive than volume, so optimizing initial pressure seems to be more meaningful than volume.

4.2.3 Optimization of filling strategy for cascade hydrogen filling system

Section 4.2.2 studies the optimal initial pressure and volume configuration of the station-side storage tanks in the three-stage cascade hydrogen filling system. Since the cascade hydrogen filling system sequentially uses three storage tanks with different initial pressures to provide hydrogen for filling, the switching time of these three storage tanks has a certain impact on the energy consumption of the system and the thermal effect of the onboard tank.

Fig. 4.19 illustrates the control process of three-stage pressure filling. Upon connection of the dispenser nozzle in the HRS to the vehicle receptacle, refuelling commences with the low-pressure tank. If the pressure of the low-pressure tank falls short of the expected PRR, the HRS transitions sequentially to the medium-pressure tank and then

to the high-pressure tank. Throughout the filling process, the dispenser monitors real-time attainment of the target condition and ceases filling upon fulfillment. There are two potential cessation scenarios: attainment of the SOC target in the onboard tank or insufficient pressure in the highest pressure-level tank to sustain ongoing filling.

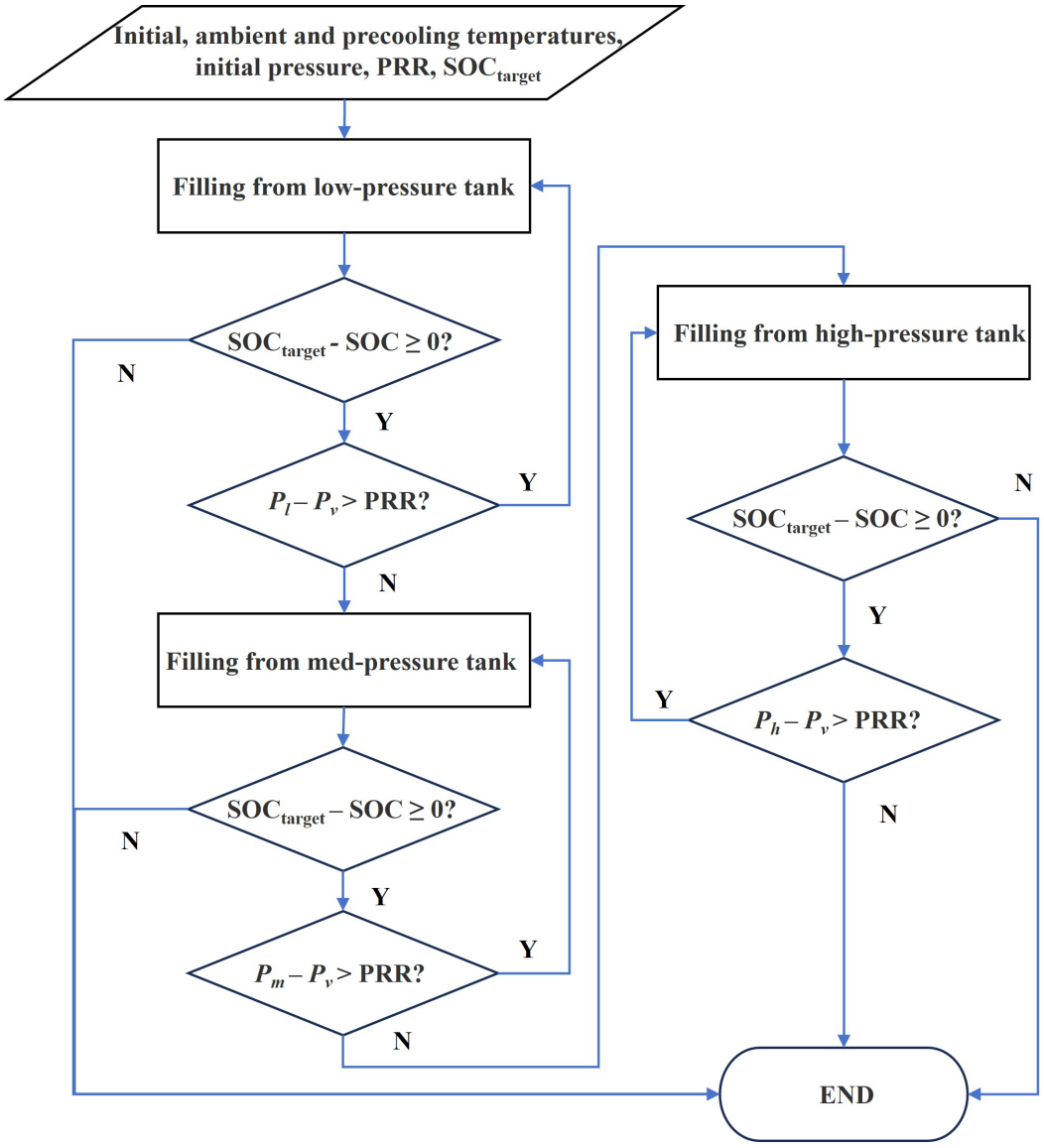

Fig. 4.19 Control process of the three-stage pressure filling.

(1) Different pressure differences at switching points

Generally speaking, when the pressure difference between the station-side tanks and the onboard tank is 0, the switching operation of low, medium and high-pressure storage tanks is performed. However, research shows that this operation is not optimal.

Research in Ref. [106] shows that the pressure difference at the switching point affects the energy consumption of the compressor. When the pressure difference at the switching point is 5.4 MPa, the compressor energy consumption is the lowest.

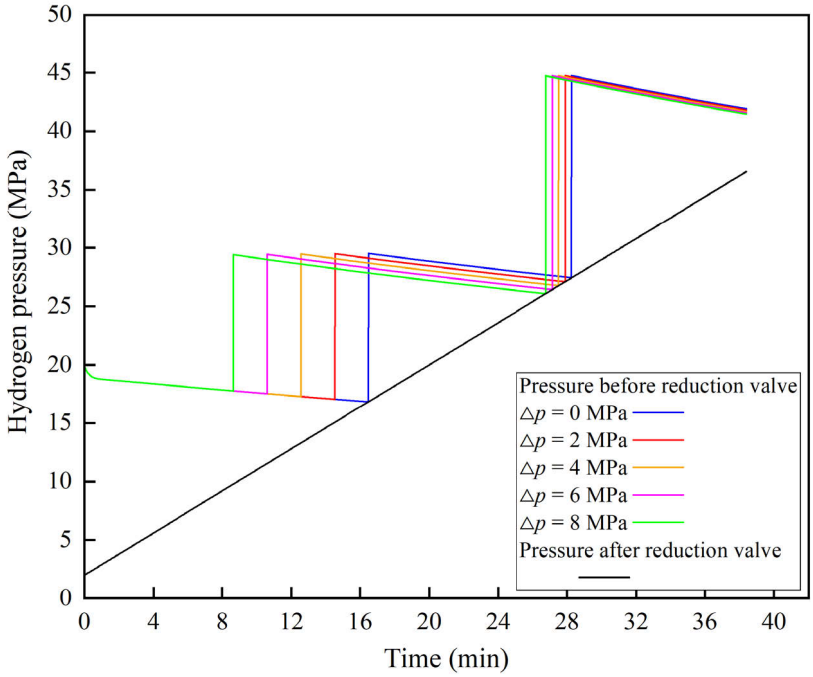

Fig. 4.20 Pressure before and after the reduction valve at the first-level switching point with different pressure differences.

The research object of Ref. [106] is a two-stage cascade HRS. This section will study the switching point pressure difference of the three-stage cascade hydrogen filling system established in Section 4.2.1. We define the switching point of low-pressure and medium-pressure storage tanks as the first-level switching point and the switching point of medium-pressure and high-pressure storage tanks as the second-level switching point. Fig. 4.20 shows that when the pressure difference of the first-level switching point increases from 0 MPa to 8 MPa, and the second-level switching point remains at 0, the low-pressure tank switches to the medium-pressure tank 7.85 minutes ahead of schedule, and then the medium-pressure tank switches to the high-pressure tank 1.52 minutes ahead of schedule. Table 4.5 shows that as the first-level switching point pressure difference increases from 0 MPa to 8 MPa, the hydrogen utilization rate of the low-pressure tank decreases by 45.04%, and the hydrogen utilization rate of the medium-pressure and high-pressure tanks increases by 38.62% and 15.88%, respectively. The cooling energy consumption of the refrigeration system increased by 3.22%. The reason is that the low-pressure tank is switched to the medium-pressure

tank in advance, which increases the average pressure difference before and after the reduction valve, thereby increasing the Joule-Thomson effect caused by the reduction valve throttling and cooling energy consumption.

Assume that the HRS has no hydrogen source to replenish hydrogen and continuously refills multiple vehicles. Table 4.5 shows that as the pressure difference at the first-level switching point increases, the SOC of the third and fourth vehicles becomes lower and lower, which reflects the decrease in the overall hydrogen utilization rate of the HRS and reduces the ability of resistance to risks for the HRS, for example, in some cases, the hydrogen source cannot replenish the HRS in time. We set the pressure difference at the first-level switching point to 0, and we also reached a similar conclusion when the pressure difference at the second-level switching point changed according to the above rules. We also found that the pressure difference at the switching point will not affect the filling time, final hydrogen temperature and pressure because the PRR and inlet temperature are the same under various switching points with different pressures. Therefore, according to the research in Ref. [106], if the switching point pressure difference is determined to be 5.4 MPa based on the minimum energy consumption of the compressor, this may reduce the hydrogen utilization rate and risk resistance of the HRS.

Table 4.5 Filling effect with different pressure differences at the first-level switching point

Performance indicators	0 (MPa)	2 (MPa)	4 (MPa)	6 (MPa)	8 (MPa)
Cooling energy (MJ)	10.26	10.39	10.48	10.55	10.59
Utilization rate of low-pressure tank	8.0%	7.1%	6.2%	5.3%	4.4%
Utilization rate of med-pressure tank	4.5%	5.2%	5.9%	6.6%	7.4%
Utilization rate of high-pressure tank	3.7%	3.8%	4.0%	4.1%	4.3%
SOC of No. 1 HFCV	1	1	1	1	1
SOC of No. 2 HFCV	1	1	1	1	1
SOC of No. 3 HFCV	0.96	0.95	0.94	0.94	0.93
SOC of No. 4 HFCV	0.89	0.88	0.87	0.85	0.84

(2) Three-stage inlet (precooling) temperature

In the traditional three-stage cascade filling system, three storage tanks of low pressure, medium pressure and high pressure are used to fill HFCV in sequence while the precooling (inlet) temperature remains unchanged. This section proposes a three-stage inlet temperature filling strategy. That is, the refrigeration system provides three different inlet temperatures in the three stages of providing hydrogen from low-pressure, medium-pressure and high-pressure storage tanks.

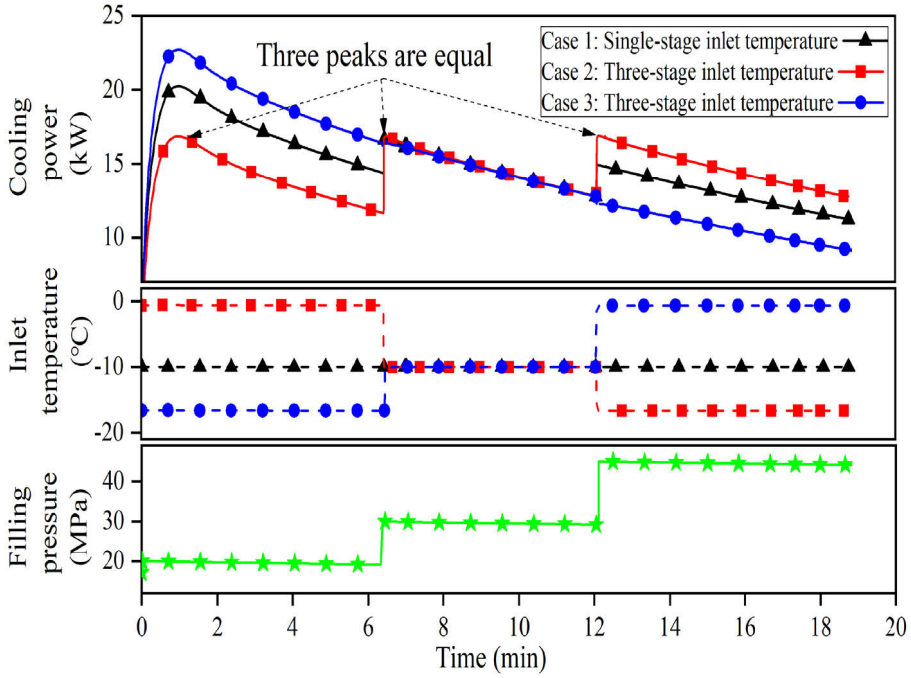

Fig. 4.21 Cooling power of the heat exchanger when using single-stage and three-stage inlet temperature filling strategies, respectively.

In Fig. 4.21, Case 1 depicts the three-stage pressure-filling method employing a constant precooling temperature. Cases 2 and 3 represent three-stage pressure-filling methods utilizing varying precooling temperatures across the stages. A comparison between Cases 2 and 3 indicates that higher precooling temperatures in the initial stage and lower ones in the final stage are more advantageous for minimizing maximum cooling power. Case 2 shows that its three peak points of cooling power are equal, achieving the theoretical minimum. Relative to Case 1's 20.3 kW with single-stage temperature precooling, Case 2's adoption of three-stage temperature precooling reduces maximum cooling power by 16.8% to 16.9 kW, thereby diminishing the heat exchanger's cooling power demand and lowering equipment investment. Eq. (4.2)

reveals an inverse relationship between cooling power and precooling temperature, and a direct proportionality to mass flow rate. While higher precooling temperatures weaken the increase in maximum cooling power despite higher mass flow rates during the initial filling, lower precooling temperatures towards the end of filling can appropriately boost maximum cooling power. Thus, implementing the proposed three-stage precooling temperature method can curtail the cooling system's maximum cooling power without augmenting total cooling energy, consequently reducing equipment investment.

These findings, derived at an ambient temperature of 45 °C, were subjected to verification across various ambient temperatures through an ambient temperature sensitivity analysis. Table 4.6 details the total cooling energy and maximum cooling power of the heat exchanger using single-stage and three-stage precooling temperature methods at ambient temperatures of 5, 15, 25, 35, and 45 °C. Across diverse ambient temperatures, the three-stage precooling temperature method consistently yields lower total cooling energy and maximum cooling power compared to the single-stage method. Within the ambient temperature range specified in this study, the three-stage precooling temperature method reduces maximum cooling power by 16.69% to 17.38% compared to the single-stage method.

Table 4.6 Comparison of single-stage and three-stage temperature precooling methods at different ambient temperatures.

Ambient temperature (°C)	Precooling method	Total cooling energy (MJ)	Maximum peak cooling power (kW)
5	Single-stage	5.20	7.33
	Three-stage	4.87	6.09 (16.92%)
15	Single-stage	8.09	10.82
	Three-stage	7.71	8.94 (17.38%)
25	Single-stage	10.97	14.13
	Three-stage	10.55	11.71 (17.13%)
35	Single-stage	13.83	17.27
	Three-stage	13.36	14.33 (17.02%)
45	Single-stage	16.68	20.25
	Three-stage	16.20	16.87 (16.69%)

Hydrogen refuelling stations (HRS) conventionally maintain a constant precooling temperature. Aluminum heat exchange blocks within the chiller can be employed to regulate cooling power demand, allowing the rated power of the chiller to be aligned with average rather than peak demand [51]. The approach advocated in this thesis necessitates precise control of precooling temperature across three stages during the filling process. Ref. [95] outlines a method involving direct mixing of normal-temperature hydrogen, heated by a heat exchanger, and low-temperature hydrogen, pressurized by a cryopump, to swiftly regulate precooling temperature. Ref. [107] proposes an integrated hydrogen precooling system, merging a two-stage compression refrigeration cycle with a vortex tube. Ref. [108] introduces a novel precooling system utilizing two-temperature evaporation to achieve step cooling within the HRS. These aforementioned methods may be considered for the implementation of the method described in this thesis.

4.3 Performance comparison of single-stage and cascade filling

4.3.1 Final hydrogen temperature and pressure

Based on the three-stage cascade filling system model established in Section 4.2.1, this section compares the performance of single-stage, two-stage cascade and three-stage cascade filling systems. When simulating single-stage filling, we shut down the low-pressure and medium-pressure storage tanks and only used the high-pressure storage tank to provide hydrogen. When simulating two-stage cascade filling, we close the low-pressure storage tank and only use the medium-pressure and high-pressure storage tanks to provide hydrogen. When simulating three-stage cascade filling, we do not shut down any tanks.

Fig. 4.22 shows the real-time pressure of the cascade tank and the onboard tank. When the single-stage filling is used, the pressure in the high-pressure storage tank decreases linearly. When using two-stage cascade filling, the medium-pressure storage tank first provides hydrogen filling and then switches to the high-pressure storage tank. When using three-stage cascade filling, low, medium and high-pressure storage tanks provide hydrogen in sequence. These phenomena are consistent with our assumptions. Fig. 4.22 shows that no matter which method is used to fill HFCV at the HRS, the pressure

change trend in the onboard tank is consistent. Regardless of single-stage, two-stage or three-stage cascade pressure filling, the final hydrogen temperature and pressure in the onboard tank are 65.6 °C and 41.4 MPa, respectively. That is, the final temperature and pressure of the hydrogen in the onboard tank are equal. The reason is that the inlet temperature and PRR are the same during single-stage, two-stage, and three-stage cascade pressure filling. Therefore, the single-stage or cascade filling method does not affect the thermal effect of the onboard tank.

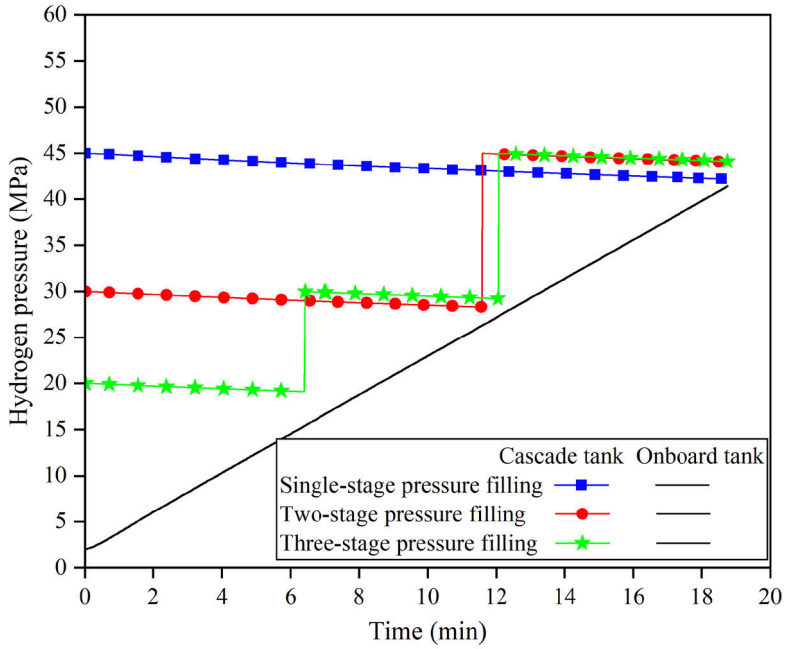

Fig. 4.22 Pressure of the cascade storage tank and the onboard storage tank when using single-stage, two-stage and three-stage cascade pressure filling, respectively.

4.3.2 Cooling energy and cooling power

Fig. 4.23 illustrates the real-time cooling power of the heat exchanger. In single-stage, two-stage, and three-stage cascade pressure filling, the heat exchanger's maximum cooling power measures 24 kW, 21.7 kW, and 20.2 kW, respectively, while the total cooling energy amounts to 18 MJ, 17 MJ, and 16.7 MJ, respectively. Consequently, in terms of maximum cooling power and total cooling energy, single-stage filling ranks highest, followed by two-stage cascade filling, and finally, three-stage cascade filling registers the lowest values. This trend is discernible in Fig. 4.22. Regarding the average pressure difference between the cascade tank and the onboard tank, three-stage cascade pressure filling exhibits the smallest difference, followed by two-stage cascade

pressure filling, and single-stage pressure filling exhibits the largest disparity. A larger average pressure difference leads to increased throttling of the reduction valve, resulting in greater Joule-Thomson effect heat and higher cooling energy consumption by the heat exchanger downstream of the reduction valve. Consequently, compared to single-stage filling, cascade filling can mitigate total cooling energy and maximum cooling power requirements, thereby reducing investment in refrigeration system equipment.

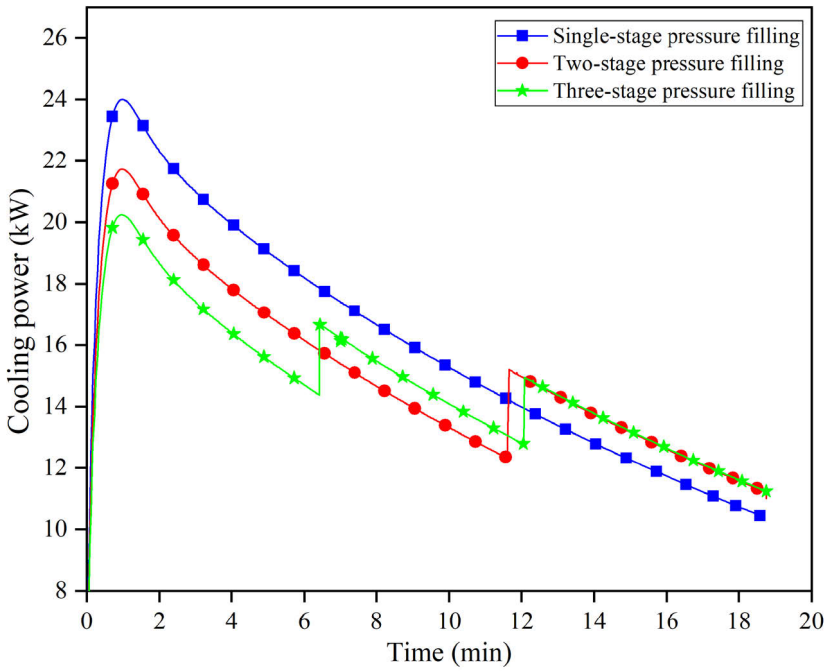

Fig. 4.23 Cooling power of the heat exchanger when single-stage, two-stage and three-stage cascade pressure filling are used, respectively.

4.4 Conclusion

This chapter optimizes the configuration and filling strategy of the filling system to improve the efficiency of the hydrogen filling system.

We extend the hydrogen storage tank model to the entire single-stage hydrogen filling system, including station-side storage tanks, onboard storage tank, reduction valve, heat exchanger, pressure drops, etc. The two-stage average pressure ramp rate (APRR) and inlet temperature filling strategies applied to a single-stage hydrogen filling system were proposed. The results show that when the inlet temperature is −20 °C, the two-stage APRR filling strategy can reduce the maximum cooling power by 23.8%. When

APRR is 0.428 MPa/s, the two-stage inlet temperature filling strategy can reduce the maximum cooling power by 16.3%.

We expand the single-stage hydrogen filling system to a three-stage cascade hydrogen filling system. A multi-objective optimization method based on genetic algorithm and Pareto optimization was proposed to optimize the initial pressure and volume configuration of low-pressure, medium-pressure and high-pressure cascade storage tanks. The results show that when the ambient temperature is 20 °C, and the SOC is 0.98 to 0.99, using the optimized configuration for the cascade storage tanks can reduce cooling energy by 11.43%.

A three-stage inlet temperature filling strategy applied to the three-stage cascade hydrogen filling system was proposed. The results show that when the ambient temperature is 5 to 45 °C, the three-stage inlet temperature filling strategy can reduce the maximum cooling power by 16.69% to 17.38%.

Optimizing the cascade tank configuration and filling strategy can reduce cooling energy and maximum cooling power demand, thereby reducing the operating and investment costs of the refrigeration system and improving the efficiency of the hydrogen filling system.

Chapter 5 Improvement of hydrogen refuelling protocol MC method

This section has been published in:

[1] Luo H, Xiao J S, Bénard P, Yang T Q, Tong L, Chahine R, Yuan Y P, Yuan C Q, Yao C L. Improvement of MC method in SAE J2601 hydrogen refuelling protocol using dual-zone dual-temperature model. Journal of Energy Storage, 2024, 81: 110416. (JCR Q1, IF=9.4)

[2] Luo H, Xiao J S, Bénard P, Zong Y, Chahine R, Tong L, Yuan C Q, Yang T Q, Yuan Y P. Optimal estimation of MC parameter in SAE J2601 hydrogen refuelling protocol based on modified formula and artificial neural networks. Fuel, 2024, 365: 131315. (JCR Q1, IF=7.4)

My specific contribution in this work was to propose two improvements to the MC method in the SAE J2601 hydrogen refuelling protocol to improve the control accuracy and filling safety of the hydrogen filling system.

The previous chapter established and verified the currently widely used single-stage and cascade hydrogen filling system models and optimized the cascade tank configuration and filling strategy. However, when actually filling HFCV, it is not feasible to use a hydrogen filling system model to determine the appropriate filling speed on site. Because the environmental conditions in real scenarios, the geometric dimensions of the onboard tank, the physical properties of the tank material, and the equipment parameters of the HRS are complex and uncertain. Therefore, a standard and reliable hydrogen refuelling protocol is needed. From 2010 to 2020, the Society of Automotive Engineers (SAE) has successively released and updated the SAE J2601 hydrogen refuelling protocol for the light-duty HFCVs, which includes two standard hydrogen filling methods: the lookup table method and the MC method. As mentioned in Section 1.2.5, there is potential for further improving the MC method. Therefore, this chapter proposes two improvements to the MC method to improve the control accuracy and filling safety of the hydrogen filling system.

5.1 Control logic and verification of MC method

Both the lookup table method and the MC method are divided into two categories: communication filling and non-communication filling. Communication filling controls the filling process based on the temperature and pressure in the tank measured by sensors, while non-communication filling is different. For the non-communication lookup table method, different tables were developed in advance based on simulations of a zero-dimensional gas one-dimensional tank wall (0D1D) model similar to Section 2.3.4. The table contains the pressure ramp rate (PRR) that controls the filling speed and the pressure target that controls the filling stop. When actually using the lookup table method, the table was first selected based on the nominal working pressure of the onboard tank and the precooling temperature category of the HRS. Then, the PRR in the selected table was determined based on the ambient temperature. Finally, the pressure target in the selected table was determined based on the initial pressure of the storage tank [5]. The lookup table method basically meets the filling requirements of HFCV. However, the upper limit of the precooling temperature category is always used when developing the PRR in the lookup table, while the precooling temperature during actual filling is not always at the upper limit of the precooling temperature category. Hence, the PRR in the lookup table method has the potential to be further improved.

In order to further improve the PRR in the lookup table method, the MC method was proposed. Like the non-communication lookup table method, the non-communication MC method also includes the PRR to control the filling speed and the pressure target to control the filling stop, but they are not constant at this time. As shown in Fig. 5.1, PRR is calculated based on the final filling time t_{final}. The final filling time is calculated based on the mass average temperature (MAT) of the delivered hydrogen. The calculation formula and coefficients of the final filling time are determined by fitting a large number of simulation data under extreme working conditions. The MAT of delivered hydrogen is calculated based on the temperature, pressure and mass flow rate of hydrogen measured by the dispenser. The pressure target p_{target} is calculated by combining the final hydrogen temperature and the SOC target.

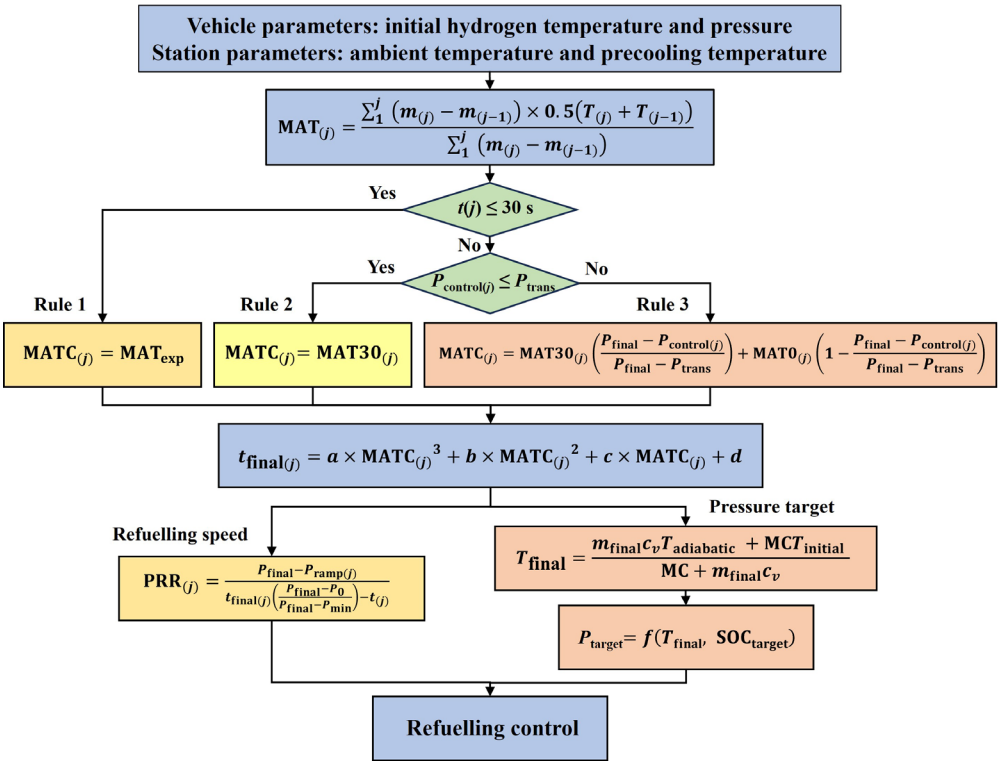

Fig. 5.1 Control logic of the MC method without communication.

5.1.1 Filling speed control of MC method

The filling speed control of the dispenser is managed through the utilization of PRR. Within the PRR calculation, a critical factor termed t_{final} is incorporated, deriving its value from the ambient temperature, initial pressure, tank volume, and the mass average temperature (MAT). MAT is determined by the dispenser's assessment of the temperature during precooling at the outlet. Three guidelines govern this procedure, as illustrated in Fig. 5.2.

(1) Rule 1: if $t(j) \leq 30$ s, $MATC_{(j)} = MAT_{exp}$

(2) Rule 2: if $t(j) > 30$ s and $P_{control(j)} \leq P_{trans}$, $MATC_{(j)} = MAT30_{(j)}$

(3) Rule 3: if $P_{control(j)} > P_{trans}$,

$$MATC_{(j)} = MAT30_{(j)}\left(\frac{P_{final} - P_{control(j)}}{P_{final} - P_{trans}}\right) + MAT0_{(j)}\left(1 - \frac{P_{final} - P_{control(j)}}{P_{final} - P_{trans}}\right) \quad (5.1)$$

The MAT, t_{final} and PRR can be calculated by

$$MAT_{(j)} = \frac{\sum_1^j (m_{(j)} - m_{(j-1)}) \times 0.5(T_{(j)} + T_{(j-1)})}{\sum_1^j (m_{(j)} - m_{(j-1)})} \quad (5.2)$$

$$t_{\text{final}(j)} = a \times \text{MATC}_{(j)}{}^{3} + b \times \text{MATC}_{(j)}{}^{2} + c \times \text{MATC}_{(j)} + d \tag{5.3}$$

$$\text{PRR}_{(j)} = \frac{P_{\text{final}} - P_{\text{ramp}(j)}}{t_{\text{final}(j)}\left(\frac{P_{\text{final}} - P_0}{P_{\text{final}} - P_{\text{min}}}\right) - t_{(j)}} \tag{5.4}$$

where MAT_{exp}, MAT0, MAT30 and MATC are the MATs of expected at the end of the fill, calculated from the beginning of the fill, calculated from the 30th s, and that of the mathematical combination of MAT_{exp}, MAT0 and MAT30, respectively. P_{control} is the pressure that the dispenser control targets during filling. P_{trans} is a parameter in the MATC formula that controls how much MAT0 and MAT30 are weighted. P_{min} and P_{final} are the minimum and final pressures deriving the t_{final} formula coefficients.

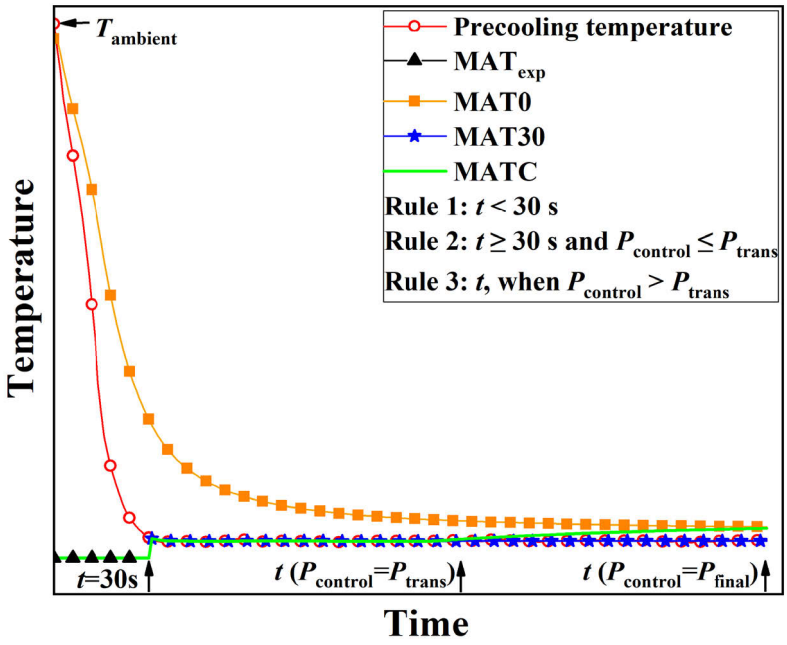

Fig. 5.2 Three rules for the MATC to control filling speed in the MC method.

In Fig. 5.2, it is depicted that upon completion of refuelling, MATC shifts to MAT0, and subsequently, MATC undergoes augmentation. As indicated in Eq. (5.3), the escalation of MATC precipitates an increase in the t_{final}. Consequently, the PRR experiences a gradual decline, as elucidated in Eq. (5.4). The decrement in PRR induces a reduction in the pressure differential between the onboard tank and dispenser, thereby augmenting the final SOC within the onboard tank. This delineates a benefit of the MC method, akin to the Top-off refuelling in the lookup table approach.

The coefficients (a, b, c, and d) in Eq. (5.3) are contingent upon the ambient temperature, tank volume, and initial pressure. The initial values of a, b, c, and d are ascertained for specific ambient temperatures and tank volumes. Utilizing linear interpolation, values for alternative ambient temperatures and tank volumes can be computed.

5.1.2 Pressure target control of MC method

The MC method encompasses communication and non-communication refuelling [5]. In the case of non-communication refuelling, an analytical solution for the final hydrogen temperature within the onboard tank is derived using the MC method, represented by Eq. (5.5). Subsequently, the pressure target is determined by integrating the SOC target with the final hydrogen temperature within the storage tank. Filling ceases once the pressure at the dispenser outlet aligns with the pressure target. Eq. (5.5) incorporates the parameter MC. Through analysis of numerous MC data simulated from the 0D1D model, the MC method ultimately formulates the parameter MC, expressed in Eq. (5.6). $T_{\text{adiabatic}}$ and $U_{\text{adiabatic}}$ can be computed based on the mass average enthalpy observed throughout the entire refuelling process, as measured by the dispenser. The mass average enthalpy is influenced by the gas temperature, pressure, and mass flow rate at the dispenser outlet.

$$T_{\text{final}} = \frac{m_{\text{final}} c_v T_{\text{adiabatic}} + \text{MC} T_{\text{initial}}}{\text{MC} + m_{\text{final}} c_v} \tag{5.5}$$

$$\text{MC} = AC + BC\ln\left(\frac{U_{\text{adiabatic}}}{U_{\text{initial}}}\right)^{1/2} + GC(1 - e^{-KC\Delta t})^{JC} \tag{5.6}$$

where T_{initial} and U_{initial} are the initial hydrogen temperature and internal energy. $T_{\text{adiabatic}}$ and $U_{\text{adiabatic}}$ are the final hydrogen temperature and internal energy, assuming adiabatic. m_{final} and T_{final} are the final hydrogen mass and temperature. Δt is the filling time after 30 s, namely $\Delta t = t_{\text{final}} - 30$. Because Δt is positive, so t_{final} needs to be greater than 30 s. Namely, the original MC method is unsuitable when the final filling time is less than 30 s.

The MC method encompasses the regulation of both the filling speed and pressure target. Filling speed is managed to avert overheating, while the pressure target is adjusted to prevent overfilling. Formulas and coefficients for the pressure ramp rate

(PRR), utilized in controlling filling speed, were devised under Hot Case Tank conditions, whereas this for pressure target was established under Cold Case Tank conditions. The Hot Case Tank and Cold Case Tank serve as benchmarks outlined in Table A3 of the SAE J2601 protocol. This study solely concentrates on enhancing pressure targets and exclusively employs the Cold Case Tank.

The Cold Case Tank, a 25 L tank, is smaller than the actual tank (Toyota 2023 Mirai features three tanks: 64.9 L, 52 L, and 25.3 L). Energy influx during filling correlates with tank volume, while energy dissipation is linked to the inner surface area of the tank wall. With its low volume-to-area ratio, the Cold Case Tank experiences minimal temperature elevation. Presently, two prevalent storage tank types are in use: type III and type IV. Type III tanks feature metal liners with high thermal conductivity, while type IV tanks employ plastic liners with low thermal conductivity. The Cold Case Tank, a type III tank, rapidly dissipates heat, curbing temperature escalation.

When the MC method, derived from Cold Case Tank parameters, governs the filling process, the calculated final hydrogen temperature within the storage tank tends to be lower than the actual value. Given that $P_{\text{target}} = f\left(T_{\text{final}}, \text{SOC}_{\text{target}}\right)$, with fixed $\text{SOC}_{\text{target}}$, the inferred lower final hydrogen temperature leads to a reduced pressure target and premature cessation of filling, thus averting overfilling. Employing the conservative Cold Case Tank for MC method development ensures safety during actual refuelling occurrences. Table 5.1 delineates the parameters of the Cold Case Tank.

5.1.3 Control logic verification of MC method

In this thesis, the control logic for the filling speed of the MC method is programmed into the 0D1D model established in section 2.3.4. The refuelling process is executed using the Simulink software platform. Table 5.1 presents the geometric parameters, thermodynamic properties, ambient temperature, initial pressure, and initial temperature of the actual storage tank utilized to validate the filling speed control logic of the MC method. The precooling (inlet) temperature, depicted as the green point in Fig. 5.3, represents a typical temperature reduction observed in actual refuelling scenarios, transitioning from ambient temperature to the anticipated value within 30 s. The Cold Case Tank specified in Table 5.1 will serve as the basis for improving the MC method in Sections 5.2 and 5.3.

Table 5.1 Parameters of the actual storage tank used to verify the control logic of the MC method and the cold case tank used to develop the original and modified MC methods

Physical definition	Actual tank for MC method validation [5, 70]	Cold Case Tank for MC method development [5]
Type of tanks	Type IV	Type III
Nominal work pressure (MPa)	70	70
Liner/Shell density (kg/m^3)	975/1550	2700/1494
Liner/Shell thermal conductivity (W/m/K)	0.3/0.3	164/0.74
Liner/Shell specific heat capacity (J/kg/K)	1000/500	1106/1120
Internal gas volume (L)	129	25
Total external length (mm)	722	835
Internal liner surface area (m^2)	1.3	0.5
External/Internal diameter (mm)	600/513	240/200
Liner/Shell wall thickness (mm)	5/38.3	3.25/16.7
Liner/Shell mass (kg)	6.0/74.1	4.7/14.9
Ambient temperature (°C)	25	0 to 40
Precooling temperature (°C)	varying	−40 to −20
Initial temperature (°C)	25	Equal to T_a
Initial pressure (MPa)	5	2 to 60

Fig. 5.3 illustrates a comparison between the simulation outcomes of the MC method programmed in this thesis and those reported in Ref. [70]. This thesis utilizes the variable precooling temperature from Ref. [70] as input, enabling the model to autonomously compute the PRR based on the three rules governing filling speed in the MC method. As depicted in Fig. 5.3, the PRR occupies the initial position during the initial 30 s, shifts to the secondary position from 30 s until reaching P_{trans}, and then assumes the tertiary position from P_{trans} to completion, exhibiting a gradual decline. Notably, the MC method dynamically regulates filling speed in response to precooling temperature, distinguishing it from the lookup table approach.

The simulation outcomes, encompassing PRR, mass flow rate, filling pressure at the dispenser outlet, and hydrogen pressure within the onboard tank, align well with those of Ref. [70]. However, the simulated final hydrogen temperature is approximately 5 °C lower compared to Ref. [70]. Nevertheless, this discrepancy falls within an acceptable margin of error. In summary, this section entails the implementation of the control logic governing the filling speed of the MC method.

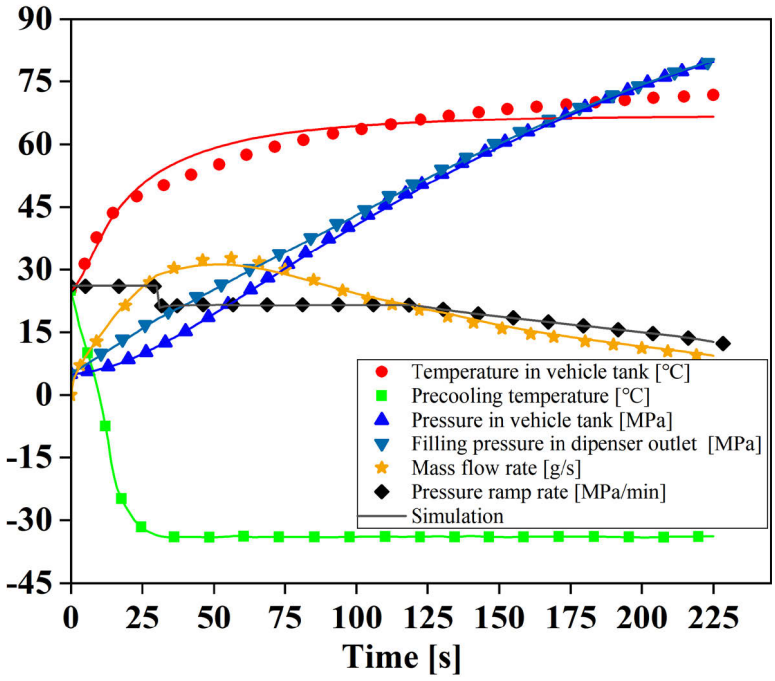

Fig. 5.3 Comparison of simulation results of temperature, pressure, mass flow rate and PRR with Ref. [70] (Line: 0D1D model simulation; Dot: Ref. [70]).

5.2 Improvement of MC parameter in MC method

In the non-communication MC method, the pressure target is calculated using the formula of the final hydrogen temperature derived from the simplified tank thermodynamic model, that is, Eq. (5.5). The Eq. (5.5) for the final hydrogen temperature contains a key parameter MC. The accuracy of the MC parameter is important because it determines the accuracy of the calculation of the final hydrogen temperature and pressure target.

5.2.1 Modified formula of MC parameter

SAE has proposed two formulas for MC parameter, namely Eqs. (5.6) and (5.7)[67]:

$$\mathrm{MC} = AC + BC\frac{U_{\mathrm{adiabatic}}}{U_{\mathrm{initial}}} + GC(1 - e^{-KC\Delta t})^{JC} \tag{5.7}$$

Eq. (5.7) is proposed earlier, and Eq. (5.6) is the revised version later. U_{initial} is the initial hydrogen internal energy, and $U_{\mathrm{adiabatic}}$ is the final one assuming adiabatic. Δt in Eqs. (5.7) and (5.6) are the filling time after 3 min and 30 s, respectively. Therefore, Eqs. (5.7) and (5.6) are only suitable for filling more than 3 min and 30 s, respectively. AC,

BC, *GC*, *KC* and *JC* are the coefficients.

Based on the fitting and analysis of a large amount of MC simulated data, we propose a modified formula for the MC parameter:

$$\mathrm{MC} = AC + BC\mathbf{ln}\left(\ln\sqrt{\frac{U_{\mathrm{adiabatic}}}{U_{\mathrm{initial}}}}\right) + GC(1 - e^{-KC\Delta t})^{JC} \tag{5.8}$$

Based on the original formula of Eq. (5.6), the modified one of Eq. (5.8) calculates the second term's natural logarithm again. The performance of Eq. (5.8) will be verified in Section 5.2.3. Next, an ANN model for the MC parameter will be built.

5.2.2 ANN model of MC parameter

The Artificial Neural Network (ANN) emulates the structure and functionality of actual neural networks, enabling it to approximate functions and capture intricate nonlinear associations. A convoluted nonlinear correlation is evident between initial/boundary conditions (ambient, precooling, initial temperatures, and initial pressure within the storage tank) and fueling performance (final temperature, pressure, and fueling duration). This section will employ the backpropagation (BP) ANN, a specific type utilized in Section 4.2.2. It operates on the gradient descent learning rule, iteratively adjusting the weights and biases of the networks via backpropagation to minimize the sum of squared errors [109].

(1) MC data simulated by 0D1D model

The initial step in training an ANN involves data set preparation. To ensure the randomness and reliability of the data, Latin hypercube sampling (LHS) is utilized for random sampling of initial conditions. Widely employed in ANN training data sampling, LHS operates as a stratified sampling technique, wherein each variable is equally divided based on its value range. The number of partitions corresponds to the required count for each variable. Subsequently, each partition randomly selects a representative individual, effectively covering the entire sample space with a minimal number of samples.

LHS sampling is conducted on ambient temperature, precooling temperature, and initial pressure of the 25 L type III storage tank listed in Table 5.1, resulting in the generation of 50 sample groups. The scatter plot matrix in Fig. 5.4 illustrates the

sampling outcomes. Each diagonal figure displays 7 values corresponding to the data quantity within the abscissa range of each column. Each initial condition is segmented into 7 parts within its value range, demonstrating a uniform distribution overall. Off-diagonal figures depict the scenarios when three initial conditions are paired. The fitted trend lines of the two variables in each figure are nearly horizontal, indicating minimal correlation. Thus, the results of LHS sampling are deemed reliable.

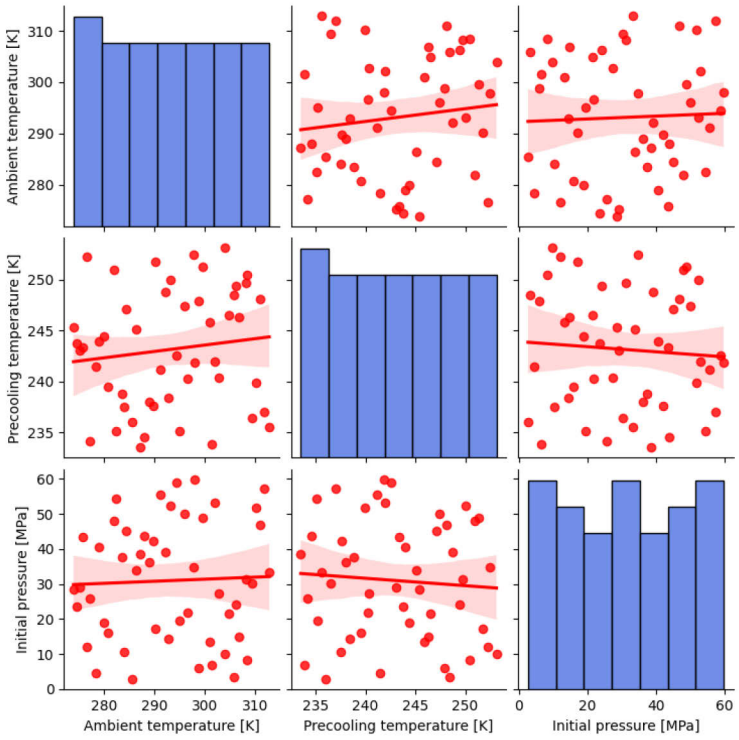

Fig. 5.4 Scatter plot matrix of LHS sampling results for ambient temperature, precooling temperature and initial pressure.

The 25 L type III storage tank from Table 5.1 serves as the simulation basis, mirroring the tank utilized in MC method development. By integrating 50 sets of initial conditions generated through LHS sampling with varied PRRs (ranging from 0.1 to 2.5 MPa/s with a step of 0.1), a total of 1250 distinct fueling scenarios are derived. Simulations are executed using the 0D1D model, each concluding upon the attainment of 100% SOC within the tank. Subsequently, 1250 sets of outcomes are obtained and substituted into Eq. (5.5), which can be transformed into $\mathrm{MC} = m_{\mathrm{final}} c_v \left(T_{\mathrm{adiabatic}} - T_{\mathrm{final}}\right) / \left(T_{\mathrm{final}} - T_{\mathrm{initial}}\right)$. Consequently, 1250 simulated data points for the MC parameter are generated. Through observation of the MC simulated data and employing multiple linear regression to assess the significance of various fueling conditions, SAE scrutinizes

numerous potential physical models delineating the relationship between MC and fueling time alongside fueling conditions. Ultimately, SAE formulates the equation for the MC parameter, as detailed in Eqs. (5.6) and (5.7).

(2) Structure of BP artificial neural networks

Utilizing the BP-ANN, the MC parameter undergoes modelling. From the 1250 simulations, 937 data points (75%) are randomly selected for training the BP-ANN, while the remaining 313 data points (25%) are reserved for assessing its efficacy. Evaluation of the BP-ANN's performance can be conducted using metrics such as the mean absolute error (MAE), mean square error (MSE), and correlation coefficient (R), expressed as follows:

$$\mathrm{MSE} = \frac{1}{n}\sum_{i=1}^{n}(f_i - f_i')^2 \tag{5.9}$$

$$\mathrm{MAE} = \frac{1}{n}\sum_{i=1}^{n}|f_i - f_i'| \tag{5.10}$$

$$\mathrm{R} = \frac{1}{n-1}\sum_{i=1}^{n}\left(\frac{f_i-\overline{f_i}}{\sigma_i}\right)\left(\frac{f_i'-\overline{f_i'}}{\sigma_i'}\right) \tag{5.11}$$

where n is the number of simulated data. f_i' and f_i are the BP-ANN predicted value and the real one, $\overline{f_i'}$ and $\overline{f_i}$ are their mean values, σ_i' and σ_i are their standard deviations, respectively.

To determine the optimal structure for the BP-ANN, prediction errors are computed across varying numbers of hidden layer neurons. Table 5.2 illustrates these prediction errors. Notably, when the hidden layer neurons number 10 and 11, the MSE and MAE reach their minimum values, respectively, with corresponding maximum correlation coefficients (R). The updated gradient of MAE remains largely unchanged in most instances, and it may still exhibit considerable magnitude even when the loss value is minimal, offering limited benefit to model learning. Conversely, the updated gradient of MSE diminishes alongside decreasing loss values, facilitating swifter model convergence. Consequently, MSE is typically favoured as a performance metric for neural networks [112]. In this study, MSE is selected over MAE as the performance metric for the ANN. Accordingly, the number of hidden layer neurons is set to 10, based on the smallest MSE and largest R values. The final structure of the BP-ANN is thus determined, as depicted in Fig. 5.5.

Table 5.2 MSE, MAE and R using different numbers of hidden layer neurons.

Topology	MSE	MAE	R
4-8-1	1.6970E-05	0.0023109	0.99963
4-9-1	1.6963E-05	0.0024024	0.99963
4-10-1	**1.2683E-05**	**0.0016461**	**0.99972**
4-11-1	1.2875E-05	0.0016201	0.99972
4-12-1	14.57E-05	0.0089257	0.99684

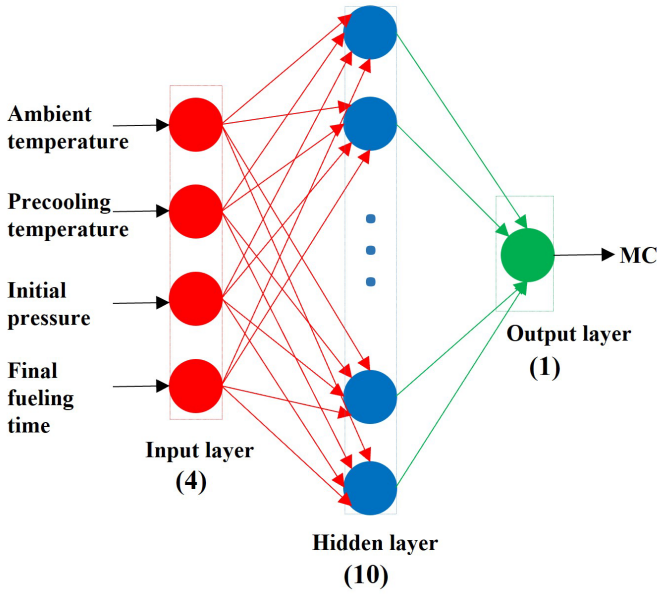

Fig. 5.5 Structure of the BP artificial neural networks used in our study.

(3) Optimizing artificial neural networks using genetic algorithm

During the model tuning phase of the BP-ANN, its initial weights and biases are randomized, potentially resulting in suboptimal global prediction outcomes. To address this issue, the genetic algorithm (GA) introduced in Section 4.2.2 is employed to optimize the initial weights and biases of the BP-ANN [113]. The optimization process is detailed in Fig. 5.6. Subsequently, the 313 simulated data points are utilized as real values for verifying prediction reliability. Fig. 5.7 juxtaposes the prediction errors of the BP-ANN before and after GA optimization. Evidently, the prediction error of the GA-BP-ANN is reduced compared to the BP-ANN. Moreover, Fig. 5.8 illustrates a comparison between the predicted values of the GA-BP-ANN and the actual values, demonstrating good agreement between the 313 predicted and actual values. In summary, the GA optimization enhances the BP-ANN, thereby improving its prediction accuracy.

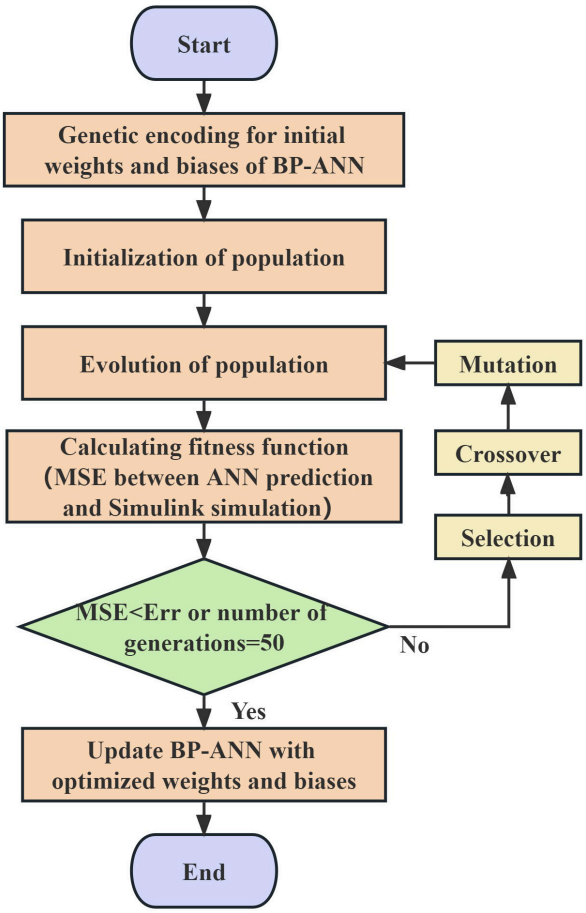

Fig. 5.6 Process of optimizing the initial weights and biases of the BP artificial neural networks using genetic algorithm.

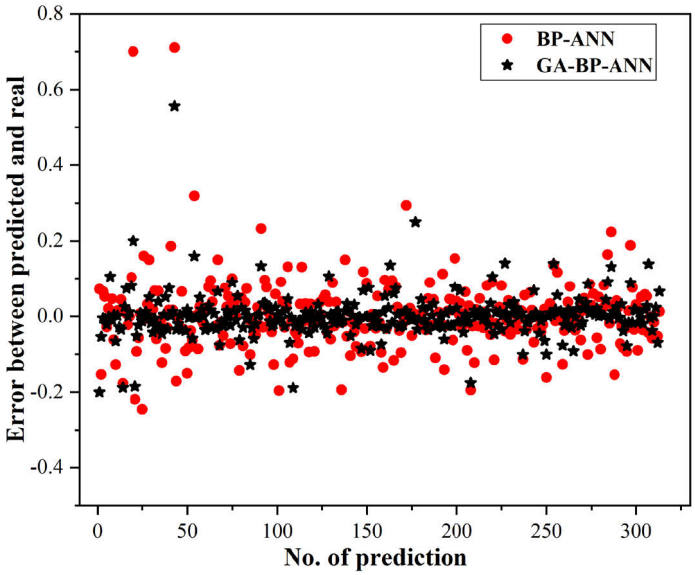

Fig. 5.7 Comparison of the BP artificial neural network's prediction error before and after using genetic algorithm for optimization.

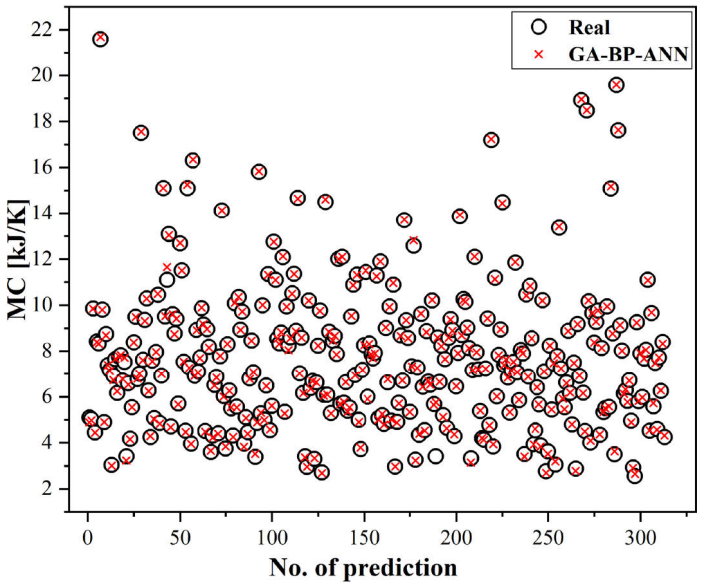

Fig. 5.8 Comparison of MC parameter values between GA-BP-ANN prediction and the real ones.

(4) Parametric study for the reliability of GA-BP-ANN

As illustrated in Fig. 5.5, the BP-ANN features four input variables: ambient temperature, precooling temperature, initial pressure, and final fueling time, alongside one output variable, the MC parameter. Fig. 5.9 depicts the variation trend of MC predicted by GA-BP-ANN when one independent variable fluctuates within the range outlined in Table 5.1 while the remaining three variables remain constant. Concurrently, the MC parameter is computed by incorporating the simulation outcomes of the 0D1D model into Eq. (5.5). This equation can be reformulated as $\mathrm{MC} = m_{\mathrm{final}} c_v (T_{\mathrm{adiabatic}} - T_{\mathrm{final}}) / (T_{\mathrm{final}} - T_{\mathrm{initial}})$, representing the defined formula for the MC parameter as per SAE standards. The MC parameter computed via this method is considered accurate and serves as a benchmark value. Fig. 5.9 demonstrates the close agreement between the MC values predicted by GA-BP-ANN and the simulated values obtained from the 0D1D model under various conditions, affirming the reliability of the GA-BP-ANN model for the MC parameter. Notably, Figs. 5.9(a) and (b) reveal an intriguing observation: the MC parameter remains nearly constant as ambient and precooling temperatures fluctuate. Thus, in the pursuit of establishing a new and more precise formula for the MC parameter, primary consideration should be given to initial pressure and final fueling time, akin to the consideration of $U_{\mathrm{adiabatic}}$, U_{initial} and Δt in Eqs. (5.6) and (5.7) by the original MC method.

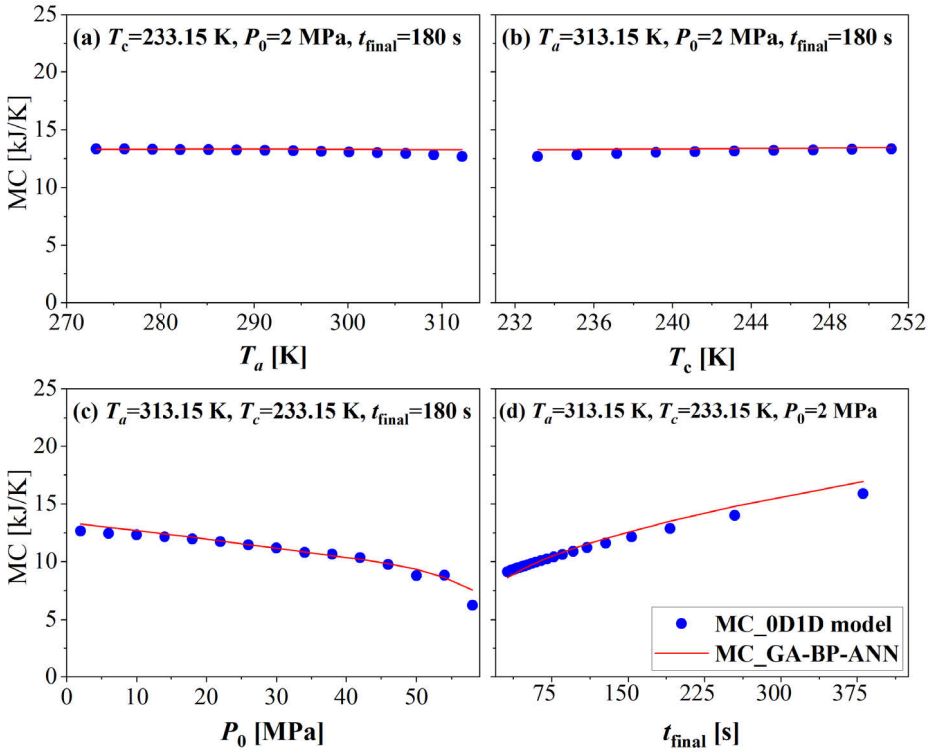

Fig. 5.9 Comparison between MC predicted by GA-BP-ANN and simulated by 0D1D model under various changing initial conditions. (a) ambient temperature, (b) precooling temperature, (c) initial pressure and (d) final fueling time.

(5) Sensitivity analysis for various initial conditions on MC parameter

To verify the conclusion above, we use the sensitivity analysis to calculate the influence of each model's input on the output [114]. The Sobol method based on variance is a type of global sensitivity analysis that can decompose the output variance into fractions attributable to input variables and variable combinations [115], including the main effect index and the total effect index.

The main effect index refers to the influence of a single independent variable on the dependent variable and can be written as [116]

$$S_i = \frac{\mathrm{Var}_{X_i}\left(E_{X_{\sim i}}(Y|X_i)\right)}{\mathrm{Var}\,(Y)} \tag{5.12}$$

where $\mathrm{Var}_{X_i}\left(E_{X_{\sim i}}(Y \mid X_i)\right) \approx \frac{1}{N}\sum_{j=1}^{N} f(B)_j * \left(f\left(\mathrm{AB}^i\right)_j - f(A)_j\right)$.

The total effect index refers to the influence on the dependent variable caused by the interaction between a single independent variable and other independent variables and can be expressed as [117]

$$S_{Ti} = \frac{E_{X_{\sim i}}\left(\mathrm{Var}_{X_i}(Y|X_{\sim i})\right)}{\mathrm{Var}(Y)} \tag{5.13}$$

where $E_{X_{\sim i}}\left(\mathrm{Var}_{X_i}(Y \mid X_{\sim i})\right) \approx \frac{1}{2N}\sum_{j=1}^{N}\left(f(\mathrm{A})_j - f\left(\mathrm{AB}^i\right)_j\right)^2$, $\mathrm{Var}\,(Y) = \mathrm{Var}\,(Y_A + Y_B)$.

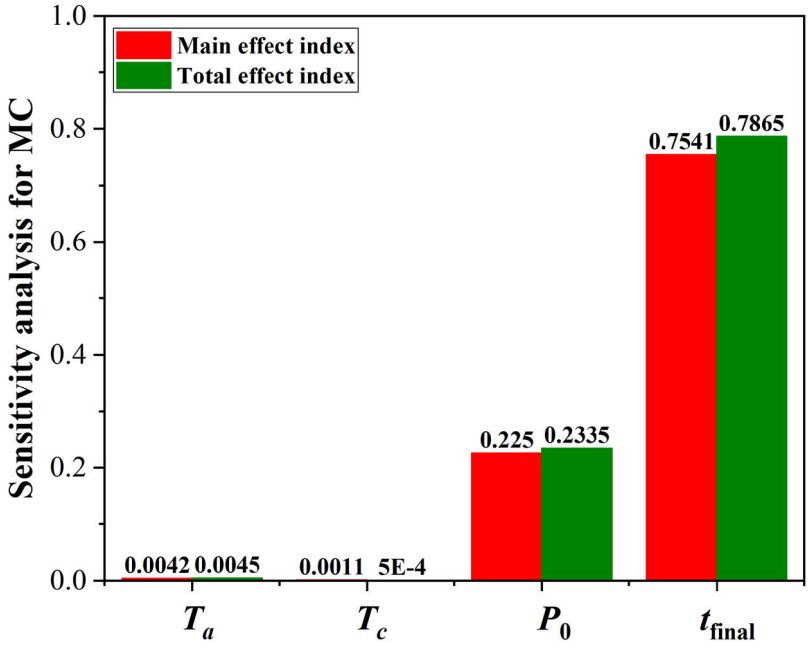

Fig. 5.10 Main effect index and total effect index of the final fueling time, initial pressure, and ambient and precooling temperatures on MC parameter.

The premise of Sobol sensitivity analysis, as depicted in Eqs. (5.12) and (5.13), aims to elucidate the functional relationship between independent and dependent variables. The explicit functional correlation between the MC parameter and various initial conditions is challenging to ascertain, a challenge overcome by the black box model of ANN. Utilizing the established GA-BP-ANN black box model, the main effect and total effect indices of different initial conditions on the MC parameter are computed. Fig. 5.10 illustrates that initial pressure and final fueling time exert significant influences on MC, whereas the impact of ambient and precooling temperatures is minimal. This observation aligns with the conclusions drawn in the preceding section. Despite the significant influence of precooling temperature on the final hydrogen temperature, its impact on the MC parameter is negligible. The MC parameter primarily reflects the system's inherent heat capacity characteristics. Moreover, it encapsulates certain process parameter characteristics, such as final fueling time and initial pressure, while exhibiting minimal correlation with precooling and ambient temperatures.

5.2.3 Comparison of various models for MC parameter

(1) Comparison between the modified formula and the original one for MC parameter

The simulated data of the MC parameter shown in Fig. 5 are fitted using Eqs. (13) and (14), respectively. We use the original formula (5-6) and the modified formula (5-8) of MC parameters to fit the simulation data of 1250 MC parameters obtained in Section 5.2.2, respectively. For formula (5-6), the fitting is divided into two steps: the first step uses the simulation data of MC30 to fit term of $AC+BC\ln\sqrt{U_{\text{adiabatic}}/U_{\text{initial}}}$ at that time of $t_{\text{final}}=30\text{s}$. Because at this time, $\Delta t=0$ and $GC\left(1-e^{-KC\Delta t}\right)^{JC}=0$. The second step fits the term of $GC\left(1-e^{-KC\Delta t}\right)^{JC}$ when $t_{\text{final}}>30\text{s}$, taking $\Delta t=t_{\text{final}}-30$ as the independent variable and taking $\Delta\text{MC}=\text{MC}-\text{MC30}$ as the dependent variable, where MC30 is the MC value when the final filling time is equal to 30s.

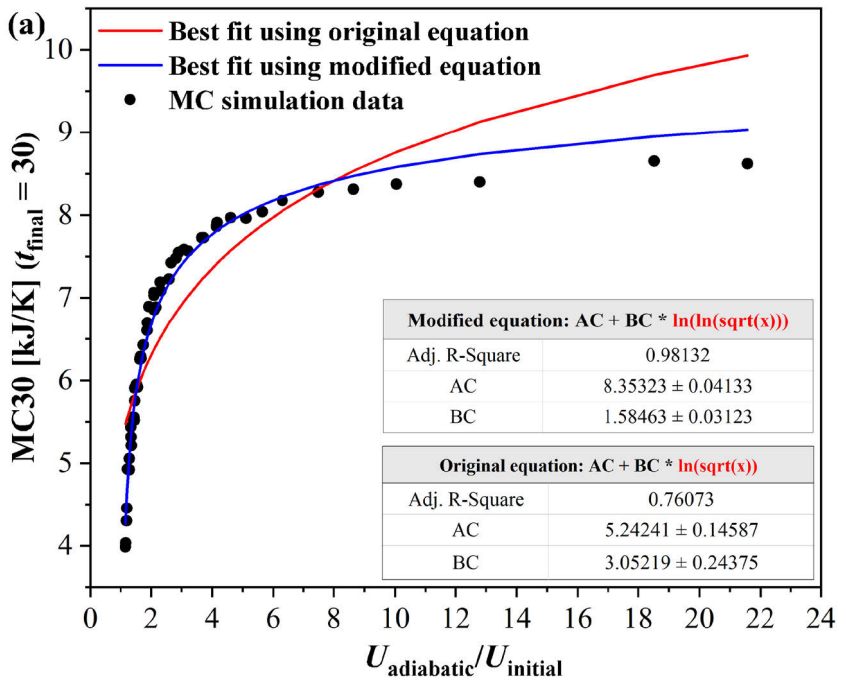

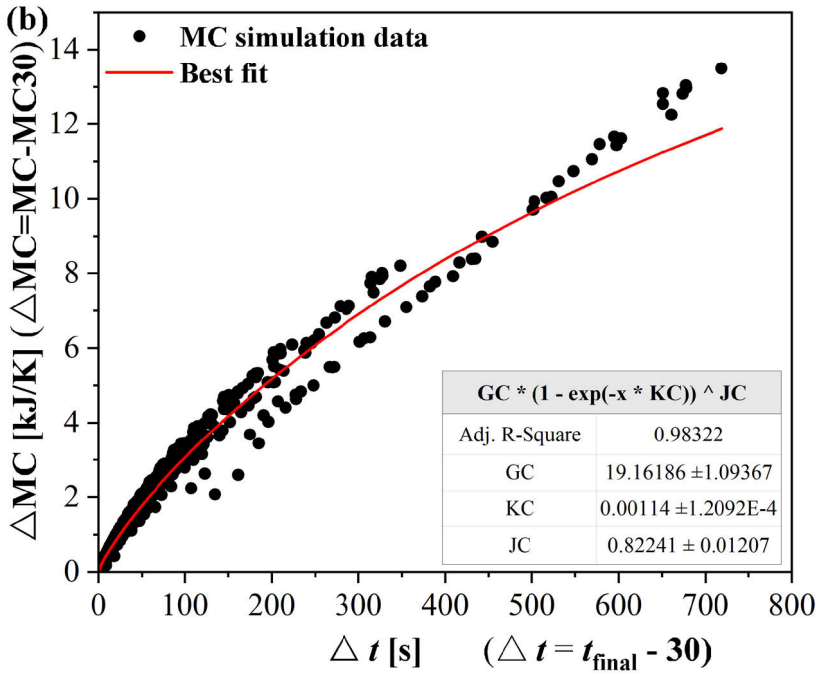

Fig. 5.11 Results of fitting the MC simulated data using the original Eq. (5.6) and the modified Eq. (5.8). (a) Fitting coefficients *AC* and *BC*, (b) Fitting coefficients *GC*, *KC* and *JC*.

Figs. 5.11(a) and (b) depict the fitting outcomes. When employing the original formula Eq. (5.6) for fitting, the coefficients $AC = 5.24241$, $BC = 3.05219$, $GC = 19.16186$, $KC = 0.00114$, and $JC = 0.82241$ closely resemble $AC = 1.10487$, $BC = 2.20466$, $GC = 22.2198$, $KC = 0.00163097$, and $JC = 0.823284$ specified in the SAE J2601 protocol, indicating the reliability of the fitting process for the MC parameter. Discrepancies may arise from variances between the 0D1D models we constructed and those established by SAE. With an R^2 value below 0.8 when employing simulated data from the SAE J2601 protocol to fit the first term of the original formula Eq. (5.6), so we opt to amend it to Eq. (5.8). Fig. 5.11(a) illustrates an increase in R^2 from the original 0.76073 to 0.98132 when utilizing the modified formula Eq. (5.8) to fit the simulated data for parameter MC, underscoring the enhanced accuracy achievable with the modified formula.

(2) Comparison between the ANN model and the original one for MC parameter

Per the range of initial conditions outlined in Table 5.1, we set T_a as 273.15, 293.15, and 313.15 K, T_c as 233.15 and 250.65 K, P_0 as 2, 30, and 60 MPa, and PRR ranges from 0.1 to 2.5 MPa/s with a step of 0.1. Utilizing the 0D1D model for simulation, the obtained simulated data are plugged into Eq. (5.5) to calculate MC, designated as

MC_0D1D and considered as standard values. The MC calculated by substituting simulated data into Eq. (5.6) and incorporating the fitted coefficients from Fig. 5.11 is termed MC_original. Similarly, the MC calculated using Eq. (5.8) and the fitted coefficients from Fig. 5.11 are termed MC_modified. Furthermore, the MC predicted by substituting simulated data into GA-BP-ANN is labelled MC_GA-BP-ANN.

A comprehensive comparison of MC calculated by different models is conducted under varying initial conditions. Fig. 5.12 depicts the relationship between MC and final fueling time when the precooling temperature T_c is 233.15 K, while ambient temperature T_a and initial pressure P_0 vary. Fig. 5.13 presents analogous cases with T_c set to 250.65 K. Specifically, simulations with PRR set at 0.1 MPa/s are scrutinized, representing instances with the longest final fueling time in each figure. Figs. 5.12(a), (b), and (c) reveal a decrease in final fueling time as initial pressure increases. This trend arises from a lesser amount of hydrogen being filled into the tank with higher initial pressure, resulting in shorter final fueling times. Additionally, Figs. 5.12(c), (f), and (i) demonstrate that final fueling time diminishes as ambient temperature decreases. This phenomenon is attributed to the ending target pressure during filling being lower with lower ambient temperatures, leading to shorter final fueling times due to fixed PRR conditions.

Notably, Figs. 5.12(c), (f), and (i) unveil an intriguing observation: as the final fueling time decreases, the error in the MC parameter value calculated by the original formula increases. For instance, the relative error between the original formula and the 0D1D model is approximately 26.6% in Fig. 5.12(c), 44.6% in Fig. 5.12(f), and 91.3% in Fig. 5.12(i). This discrepancy stems from the dominance of MC30 (the MC parameter value at the 30th s of fueling) when the final fueling time is short, leading to a larger error due to a relatively low R^2 value (0.76073) for MC30, as shown in Fig. 5.11(a). Conversely, when the final fueling time is lengthy, ΔMC (the difference between the MC parameter with fueling time exceeding 30 s and MC30) primarily dictates the MC value, resulting in smaller errors due to a higher R^2 value (0.98322) for ΔMC as shown in Fig. 5.11(b). Comparatively, the relative error between the modified formula and the 0D1D model is about 12.8% in Fig. 5.12(c), about 20.2% in Fig. 5.12(f), and about

32.5% in Fig. 5.12(i), indicating a reduction in error by approximately 13.8% to 58.8% compared to the original formula. This improvement can be attributed to the higher R^2 value (0.98132) fitted by the modified formula, as shown in Fig. 5.11(a), leading to a more accurate calculation of MC30. Moreover, the relative error between the GA-BP-ANN model and the 0D1D model ranges from approximately 10.0% in Fig. 5.12(c) to 9.0% in Fig. 5.12(i), indicating a reduction in error by approximately 16.6% to 82.3% compared to the original formula.

Considering the consistency between MC calculated by other models and the 0D1D model, the MC_GA-BP-ANN demonstrates superior performance, followed by the MC_modified, with MC_original exhibiting the least accuracy. Thus, the effectiveness of the proposed modified formula is evident. Furthermore, the comparison between Figs. 5.12 and 5.13 corroborate the aforementioned conclusion under varying precooling temperature conditions. In summary, the modified formula and GA-BP-ANN models enhance the calculation accuracy of the MC parameter. Additionally, the ANN model enables prediction of the MC parameter throughout the entire fueling process, while the MC formula relies on fixed values when the fueling time is less than 30 s.

For the non-communication MC method, the target pressure to control the end of filling is calculated based on the final hydrogen temperature formula, which contains a key parameter MC. This section proposes the modified formula and ANN model of the MC parameter. When fitting the simulation data of the MC parameter, the modified formula of the MC parameter increased R^2 from the original 0.76073 to 0.98132. When the filling time is short, compared with the original formula of the MC parameter, the modified formula and ANN model of the MC parameter reduce the relative error with the 0D1D model by about 13.8% to 58.8% and 16.6% to 82.3%, respectively. According to Eq. (5.5), improving the calculation accuracy of the MC parameter will help improve the calculation accuracy of the final hydrogen temperature. According to the $P_{\mathrm{target}} = f\left(T_{\mathrm{final}}, \mathrm{SOC}_{\mathrm{target}}\right)$, improving the calculation accuracy of the final hydrogen temperature will help improve the calculation accuracy of the pressure target, thereby improving the accuracy of the filling control and safety.

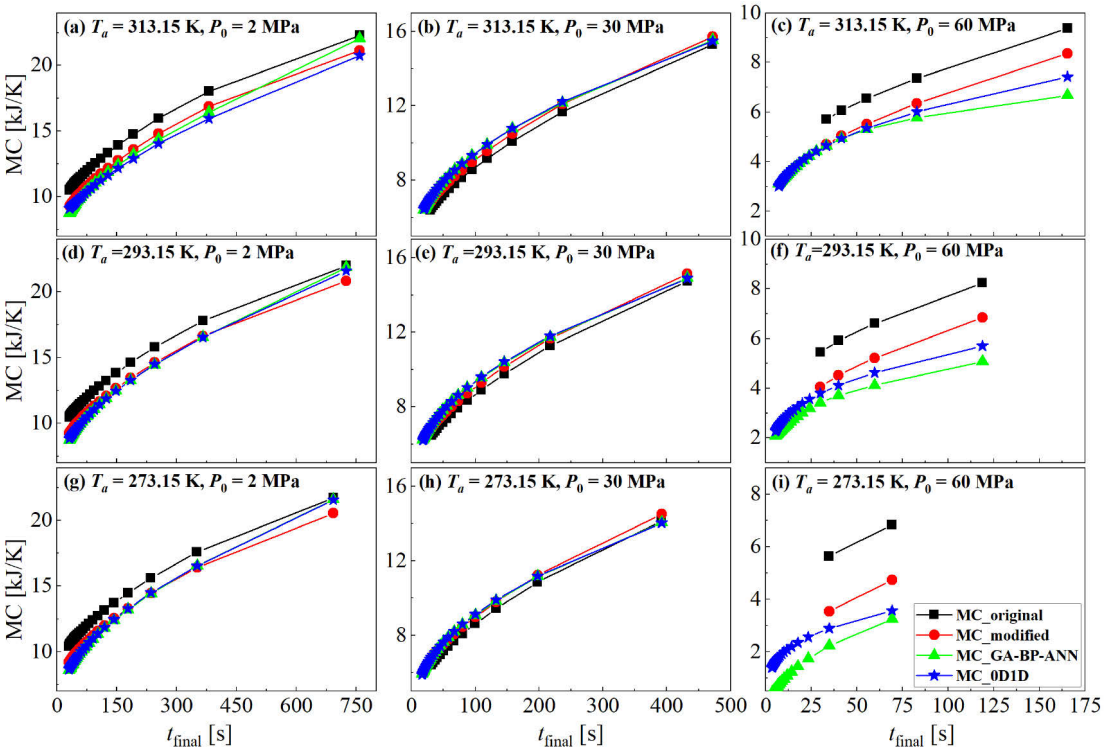

Fig. 5.12 Comparison of MC calculated by different models at the T_c of 233.15 K and different T_a, P_0.

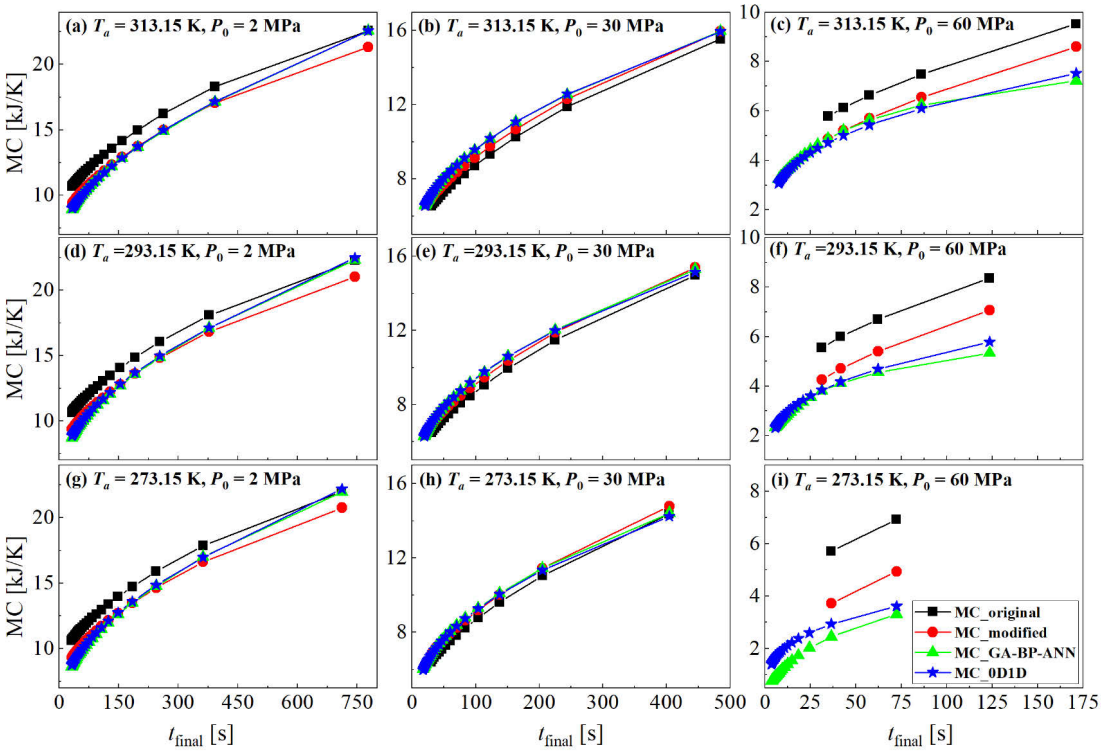

Fig. 5.13 Comparison of MC calculated by different models at the T_c of 250.65 K and different T_a, P_0.

This section only improves the formula of the MC parameter. The original MC method derived the formula for the final hydrogen temperature through a simplified dual-zone single-temperature tank model. There are differences between the dual-zone single-temperature model and the actual situation. The following section will use a dual-zone dual-temperature storage tank model that is more in line with the actual situation to improve the original MC method. Compared with the improvement of the MC parameter in this section, the next section is a deeper improvement of the original model of the MC method.

5.3 Improvement of MC method based on dual-zone dual-temperature model

5.3.1 Derivation of modified MC method

The refuelling method in SAE J2601 must ensure that the hydrogen temperature and SOC inside the storage tank do not exceed 85 °C and 100% under any refuelling conditions. So, the MC method adopts the conservative Cold Case Tank when determining the coefficients *AC*, *BC*, *GC*, *KC* and *JC* of Eqs. (5.6) and (5.7). Cold Case Tank is also adopted to develop the modified MC method, as shown in Table 5.1.

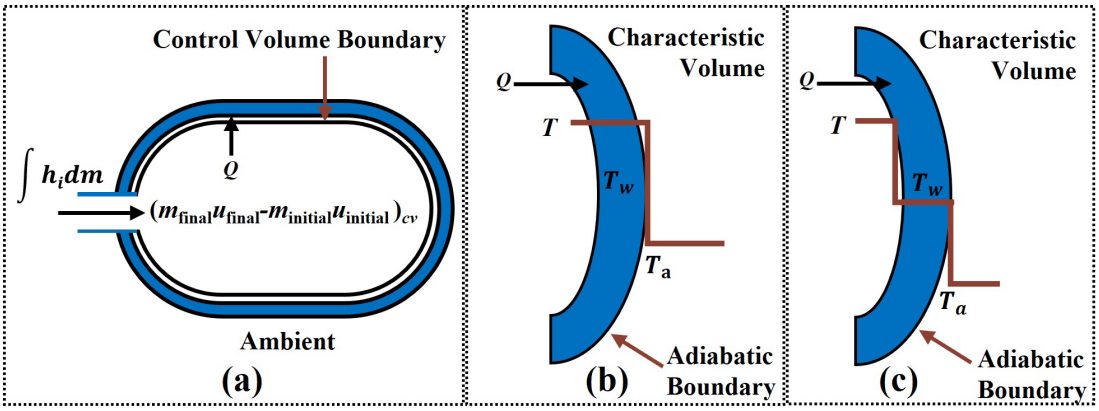

Fig. 5.14 Control volume (a), characteristic volume in original (b) and modified MC methods (c).

(1) Pressure target determined by dual-zone single-temperature model used in original MC method

For hydrogen inside the control volume shown in Fig. 14(a), during a filling time from t_{initial} to t_{final}, the hydrogen's energy conservation can be expressed as

$$m_{\text{final}}c_v T_{\text{final}} - m_{\text{initial}}c_v T_{\text{initial}} = \int_{t_{\text{initial}}}^{t_{\text{final}}} \dot{m}h_i dt - Q \tag{5.14}$$

where m_{initial} is the initial hydrogen mass. Q is the heat transferred by hydrogen to the tank wall. As shown in Fig. 5.14(b), the MC method assumes the characteristic volume of the tank wall to be a thermal mass with infinite thermal conductivity and heat transfer coefficient, and temperatures of the tank wall and hydrogen are equal. So, the model adopted by the original MC method can be defined as a dual-zone single-temperature model (hydrogen and tank wall zones). The MC method continues to assume that the outer boundary of the tank wall is adiabatic, and the heat transferred from the tank wall to the ambient can be ignored. So, the tank wall's energy conservation can be expressed as

$$\text{MC}(T_{\text{final}} - T_{\text{initial}}) = Q \tag{5.15}$$

Due to the assumptions of dual-zone single-temperature and adiabatic boundary, parameter MC is no longer just the tank wall's total heat capacity but includes the error caused by the assumptions. Eq. (5.6) shows that parameter MC changes with the filling time. Generally speaking, the heat capacity of the tank wall material does not change significantly with filling time. By solving Eqs. (5.14) and (5.15), we can get

$$\text{MC} = \frac{m_{\text{initial}} c_v T_{\text{initial}} + \int_{t_{\text{initial}}}^{t_{\text{final}}} \dot{m} h_i dt - m_{\text{final}} c_v T_{\text{final}}}{T_{\text{final}} - T_{\text{initial}}} \tag{5.16}$$

Assume that the control volume inside the tank is adiabatic with the outside. In this case, hydrogen's energy conservation can be expressed as

$$m_{\text{final}} c_v T_{\text{adiabatic}} = m_{\text{initial}} c_v T_{\text{initial}} + \int_{t_{\text{initial}}}^{t_{\text{final}}} \dot{m} h_i dt \tag{5.17}$$

By substituting Eq. (5.17) into Eq. (5.16), we can get

$$\text{MC} = \frac{m_{\text{final}} c_v (T_{\text{adiabatic}} - T_{\text{final}})}{T_{\text{final}} - T_{\text{initial}}} \tag{5.18}$$

Eq. (5.5) can be obtained from Eq. (5.18). It is assumed that the parameter MC during refuelling can be determined individually. At this time, the final hydrogen temperature can be calculated using Eq. (5.5), combining the dispenser's measurement. These measurements include hydrogen's initial pressure and temperature inside the storage tank, delivered gas temperature and pressure, and mass flow rate. Then, the pressure target will be calculated by combining the SOC target and the final hydrogen temperature inside the storage tank. Finally, the refuelling stops when the dispenser

output pressure reaches the pressure target.

To determine the correlations between the parameter MC and the initial/boundary conditions of refuelling, the MC method carries out specific refuelling simulations based on the 0D1D model. Then, they combine Eq. (5.18) to obtain many parameter MC simulation data. Finally, Eqs. (5.6) and (5.7) are determined by observing the simulation data, evaluating the correlation of parameters, and using multiple linear regression.

(2) Pressure target determined by dual-zone dual-temperature model used in modified MC method

As shown in Fig. 5.14(c), this thesis adopts a dual-zone dual-temperature adiabatic model, which distinguishes hydrogen and tank wall temperatures and regards the wall as a lumped parameter model with uniform temperature. The energy of hydrogen is transferred to the tank wall, and assuming that the outer wall of tank is adiabatic, so

$$m_{\text{final}} c_v (T_{\text{adiabatic}} - T_{\text{final}}) = m_w c_w (T_{w\text{final}} - T_{\text{initial}}) \tag{5.19}$$

where $T_{w\text{final}}$ is the final wall temperature. $m_w c_w$ is the total heat capacity of the Cold Case Tank wall and does not change with filling time, which can be calculated by using the mass average heat capacity, namely

$$m_w = m_{w\_\text{Liner}} + m_{w\_\text{Shell}} \tag{5.20}$$

$$c_w = \frac{m_{w\_\text{Liner}}}{m_w} c_{w\_\text{Liner}} + \frac{m_{w\_\text{Shell}}}{m_w} c_{w\_\text{Shell}} \tag{5.21}$$

where m_{w_Liner}, m_{w_Shell} and m_w are the mass of wall liner, wall shell and the whole tank wall. c_{w_Liner}, c_{w_Shell} and c_w are the specific heat capacity of wall liner, wall shell and the whole tank wall. The energy of hydrogen in the storage tank is transferred to the tank wall by thermal convection. According to Newton's law of cooling, we can get

$$m_{\text{final}} c_v (T_{\text{adiabatic}} - T_{\text{final}}) = \int_{t_{\text{initial}}}^{t_{\text{final}}} A_{\text{in}} a_{\text{in}} (T - T_w) dt \tag{5.22}$$

Assuming that the heat transfer coefficient a_{in} during filling is constant and defined as the average heat transfer coefficient a_{ave}, then

$$\int_{t_{\text{initial}}}^{t_{\text{final}}} A_{\text{in}} a_{\text{in}} (T - T_w) dt = k_1 A_{\text{in}} a_{\text{ave}} \int_{t_{\text{initial}}}^{t_{\text{final}}} (T - T_w) dt \tag{5.23}$$

where k_1 is the correction factor 1. According to the approximation of integration, Eq. (5.23) can be further transformed into

$$k_1 A_{\text{in}} a_{\text{ave}} \int_{t_{\text{initial}}}^{t_{\text{final}}} (T - T_w) dt = k_1 k_2 a_{\text{ave}} A_{\text{in}} t_{\text{final}} (T_{\text{final}} - T_{w\text{final}}) \tag{5.24}$$

where k_2 is the correction factor 2. $k_1$and k_2 should be the function of the initial temperature and pressure inside the storage tank, the ambient temperature, etc. By defining correction factor $K = k_1 k_2 a_{\text{ave}}$ and combining Eqs. (5.22) - (5.24), we can get

$$m_{\text{final}} c_v (T_{\text{adiabatic}} - T_{\text{final}}) = K A_{\text{in}} t_{\text{final}} (T_{\text{final}} - T_{w\text{final}}) \tag{5.25}$$

So, the total amount of heat transferred by convection between hydrogen and the inner tank wall during filling can be expressed as a formula of the tank's inner surface area, final filling time, final hydrogen temperature, final tank wall temperature and the correction factor. Solving Eqs. (5.19) and (5.25), the final hydrogen and tank wall temperatures can be written as

$$T_{\text{final}} = \frac{m_{\text{final}} c_v T_{\text{adiabatic}} + m_w c_w T_{\text{initial}}}{m_{\text{final}} c_v} - \frac{(m_w c_w)^2 T_{\text{initial}} (m_{\text{final}} c_v + K A_{\text{in}} t_{\text{final}}) + K m_{\text{final}} c_v T_{\text{adiabatic}} m_w c_w A_{\text{in}} t_{\text{final}}}{(m_{\text{final}} c_v)^2 m_w c_w + K (m_{\text{final}} c_v)^2 A_{\text{in}} t_{\text{final}} + K m_{\text{final}} c_v m_w c_w A_{\text{in}} t_{\text{final}}} \tag{5.26}$$

$$T_{w\text{final}} = \frac{K A_{\text{in}} T_{\text{final}} + m_w c_w T_{\text{initial}}}{m_w c_w + K A_{\text{in}} t_{\text{final}}} \tag{5.27}$$

Finally, the pressure target will be determined by combining the final hydrogen temperature and SOC target in the onboard tank, the same as the original MC method.

5.3.2 Correction factors for final hydrogen temperature

Similar to Eq. (5.5) in the original MC method, Eq. (5.26) shows that when we determine the value of correction factor *K* in advance and then combine the parameters m_w, c_w and A_{in} of the Cold Case Tank, we can calculate the final hydrogen temperature to determine the pressure target to control when to stop the refuelling.

By Eq. (5.25), we can get

$$K = \frac{m_{\text{final}} c_v (T_{\text{adiabatic}} - T_{\text{final}})}{A_{\text{in}} t_{\text{final}} (T_{\text{final}} - T_{w\text{final}})} \tag{5.28}$$

Eq. (5.26) shows that only the correction factor *K* is included. That is, only *K* is needed to calculate the final hydrogen temperature. However, as shown in Table 5.3, the formulas of *K* are relatively complex, so we conduct further exploration to obtain a more concise formula for correction factor *k*. On the one hand, we calculate the final hydrogen temperature directly using the relatively complex *K*. On the other hand, we bring concise *k* into Eq. (5.32) to calculate *K* first and then use *K* to calculate the final hydrogen temperature.

By rewriting Eq. (3.20), we can get

$$a_{\text{in}} = \frac{0.14\lambda \left(\frac{4\dot{m}}{\text{SOC}\pi\mu d_{\text{in}}}\right)^{0.67}}{D_{\text{in}}} = \frac{0.14\lambda \left(\frac{4}{\text{SOC}\pi\mu}\right)^{0.67} \left(\frac{\dot{m}}{d_{\text{in}}}\right)^{0.67}}{D_{\text{in}}} \tag{5.29}$$

We can have the average heat transfer coefficient:

$$a_{\text{ave}} = \frac{0.14\lambda \left(\frac{4}{\text{SOC}\pi\mu}\right)^{0.67} \left(\frac{\bar{\dot{m}}}{d_{\text{in}}}\right)^{0.67}}{D_{\text{in}}} =: k_3 \beta_{\text{ave}} \tag{5.30}$$

We define $k_3 = 0.14\lambda \left(\frac{4}{\text{SOC}\pi\mu}\right)^{0.67}$ and $\beta_{\text{ave}} = \frac{1}{D_{\text{in}}} \left(\frac{\bar{\dot{m}}}{d_{\text{in}}}\right)^{0.67}$, where average mass flow rate $\bar{\dot{m}}$ can be obtained by dispenser's measurement. By combining Eqs. (5.28), (5.30) and $K = k_1 k_2 a_{\text{ave}}$, we can get

$$k_1 k_2 k_3 \beta_{\text{ave}} = \frac{m_{\text{final}} c_v (T_{\text{adiabatic}} - T_{\text{final}})}{A_{\text{in}} t_{\text{final}} (T_{\text{final}} - T_{w\text{final}})} \tag{5.31}$$

By setting correction factor $k = k_1 k_2 k_3$, we can get

$$k = \frac{m_{\text{final}} c_v (T_{\text{adiabatic}} - T_{\text{final}})}{A_{\text{in}} t_{\text{final}} (T_{\text{final}} - T_{w\text{final}}) \frac{1}{D_{\text{in}}} \left(\frac{\bar{\dot{m}}}{d_{\text{in}}}\right)^{0.67}} = \frac{K}{\frac{1}{D_{\text{in}}} \left(\frac{\bar{\dot{m}}}{d_{\text{in}}}\right)^{0.67}} \tag{5.32}$$

That is, the correction factor *k* is obtained after introducing the average mass flow rate into the correction factor *K*. Referring to the modelling process of parameter MC in the original MC method, the 0D1D model established in Section 2.3.4 is used for simulation. The range of initial conditions is shown as Cold Case Tank in Table 5.1, consistent with the original MC method. PRR is set from 0.2 to 2.5 MPa/s and Δ=0.1.

The end-of-fill condition is 100% SOC. Then, we substitute the obtained simulation data into Eqs. (5.18), (5.28) and (5.32), respectively, and finally obtain a lot of parameter MC, *K* and *k* simulation data. Figs. 5.15(a) and (b) show the distribution of simulation data of MC and *K* versus final filling time, respectively. The data points of *K* show more obvious regularity than that of MC.

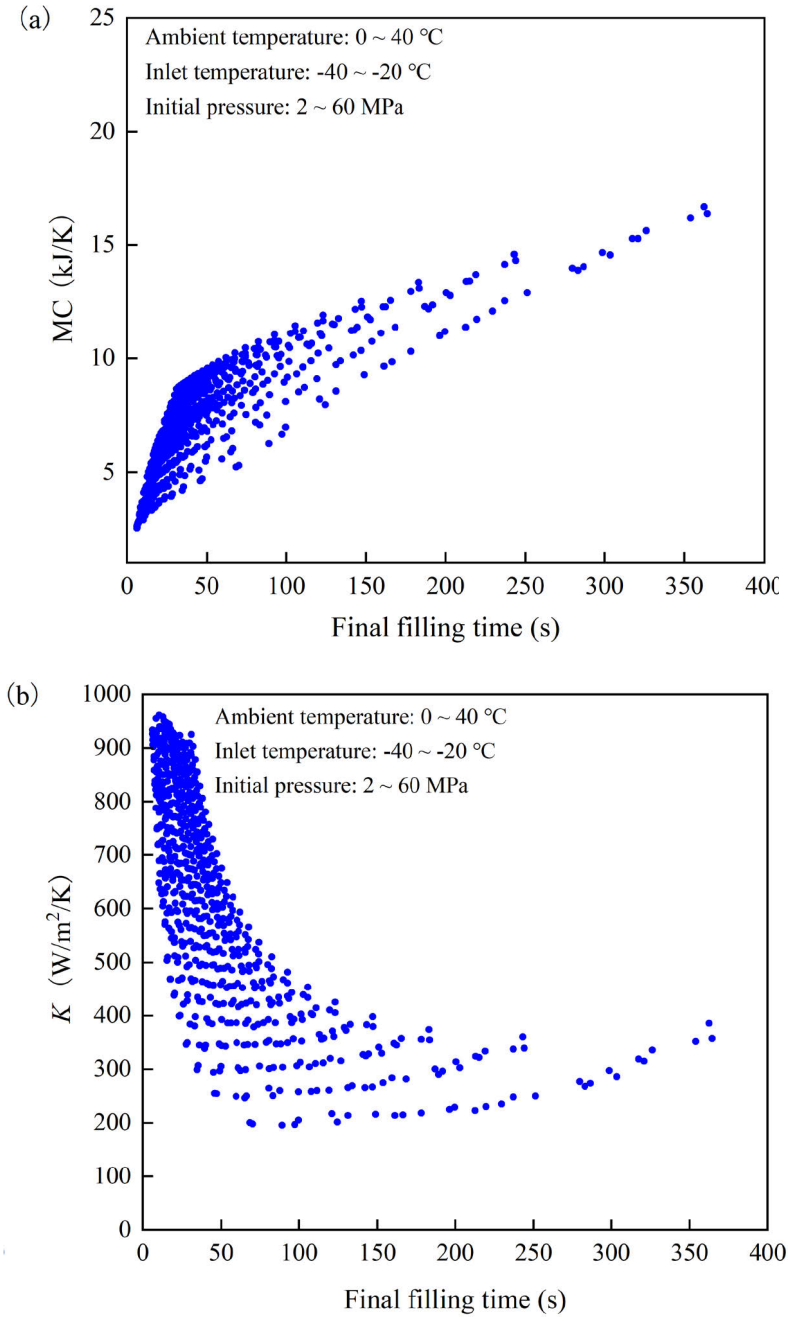

Fig. 5.15 Distribution of parameter MC (a) and *K* (b) versus final filling time under different ambient temperatures, precooling temperatures and initial pressures.

In order to establish the model of the data points K of Fig. 5.15(b), the simulation data of K and k under some initial conditions are plotted according to different initial pressures, ambient and precooling temperatures in Fig. 5.16. The data points K show an interesting phenomenon. Under the same initial pressure, the data points K basically overlap when the precooling and ambient temperatures change. The data points K show apparent differences when the initial pressure changes, indicating that the initial pressure and final filling time significantly impact the correction factor K, while the ambient and precooling temperatures have little impact. Therefore, this thesis ignores the influence of different ambient and precooling temperatures to simplify the process of fitting the correction factors K and k. So, only ambient temperature 0 °C, precooling temperature −22.5 °C and different initial pressures are used to determine the correction factors K and k. In Figs. 5.17 and 5.18, different ambient and precooling temperatures will be used to verify the modified MC method. Under various initial conditions, the data points k show a linear relationship with the final filling time.

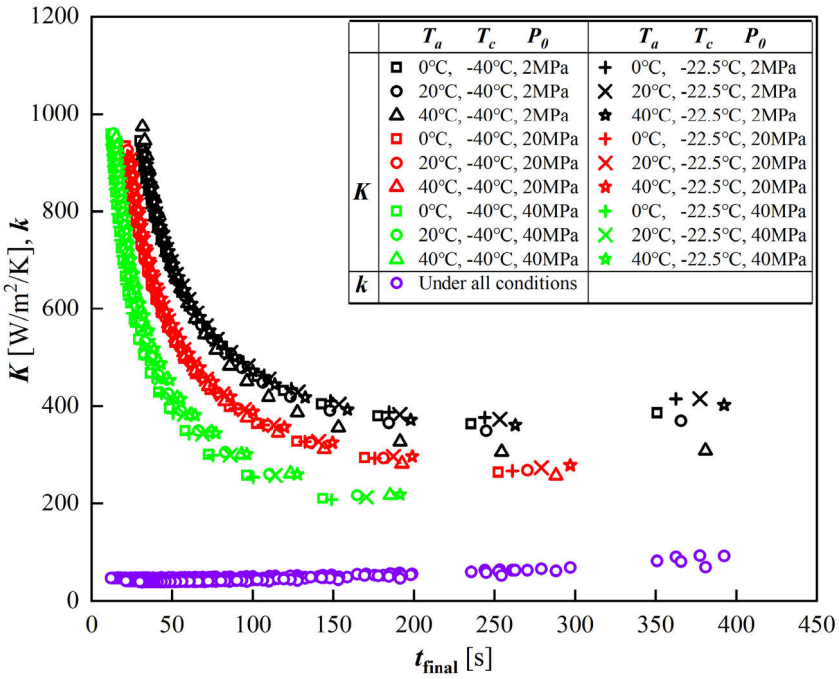

Fig. 5.16 Distribution of K and k versus final filling time under different ambient temperatures, precooling temperatures and initial pressures.

The ambient and precooling temperatures are set to 0 °C and −22.5 °C, and the initial pressures are set to 2, 5, 10, 15, 20, 25, 30, 35, 40, 45, 50, 55 and 60 MPa, respectively. The simulations are carried out using the 0D1D model, and many simulation data for

K and k are obtained. Finally, we fit K and k as the specific formulas related to the final filling time, as shown in Table 5.3.

Table 5.3 Fitting result of correction factors (K and k) versus final filling time under different initial pressures, ambient temperature 0 °C and precooling temperature −22.5 °C.

P_0	K							k		
	$K = A + Be^{-t/C}$ ($P_0 \leqslant 30$ MPa)				$K = Dt^E$ ($P_0 > 30$ MPa)			$k = F + Gt$		
	A	B	C	R^2	D	E	R^2	F	G	R^2
2	387.43	1187.1	37.47	0.997	-	-	-	31.19	0.1353	0.954
5	366.93	1133.3	38.03	0.997	-	-	-	32.23	0.1256	0.965
10	337.74	1103.81	38.17	0.996	-	-	-	34.43	0.1098	0.973
15	314.4	1107.57	36.83	0.995	-	-	-	36.472	0.0965	0.976
20	295.39	1118.87	34.71	0.994	-	-	-	38.39	0.085	0.975
25	279.86	1133.53	32.08	0.993	-	-	-	40.324	0.0738	0.974
30	265.77	1141	29.32	0.993	5407	−0.619	0.998	42.285	0.0617	0.975
35	-	-	-	-	5222	−0.635	0.998	44.074	0.0533	0.962
40	-	-	-	-	4872	−0.646	0.999	45.891	0.0436	0.950
45	-	-	-	-	4349	−0.652	0.999	47.585	0.0360	0.803
50	-	-	-	-	3652	−0.651	0.999	48.943	0.0324	0.530
55	-	-	-	-	2906	−0.650	0.995	51.258	0.0099	0.013
60	-	-	-	-	2061	−0.650	0.985	55.199	−0.075	0.0827

When $K = A + Be^{-t/C}$ is used alone to fit MC simulated data, the end of the fitting curves do not agree well when P_0 is greater than 30 MPa. When $K = Dt^E$ is used alone to fit MC simulated data, the end of the fitting curves do not agree well when P_0 is less than 30 MPa. So, K can be expressed as $K = A + Be^{-t/C}$($P_0 \leq 30$ MPa) and $K = Dt^E$($P_0 > 30$ MPa). k can be expressed as $k = F + Gt$. Simultaneously, the coefficients A, B, C, D, E, F and G are correlated with the initial pressure, respectively, and the results are shown in Table 5.4. Table 5.3 shows that for the correction factor k, R^2 is relatively small when P_0 is greater than 50 MPa. The reason is that the final filling time will be very short when the initial pressure is high. So, the data points of k versus the final filling time will be relatively clustered, leading to the small R^2 when linearly

fitting. We remove the three points in Table 5.3 with initial pressures of 50, 55 and 60 MPa and refit the coefficients F and G of correction factor k. The results are $F = 30.548 + 0.385P_0$ ($R^2 = 0.9991$), $G = 0.1344 - 0.0023P_0$ ($R^2 = 0.9893$). The comparison shows that the fitting results after deleting the three data with high initial pressure are not significantly different from the original ones in Table 5.4. Therefore, we still use the original fitting results of coefficients F and G because they can express a wider range of initial pressures. Moreover, the results in Figs. 5.17 and 5.18 show that the final hydrogen temperatures calculated using the correction factor k agree well with that of the 0D1D model at an initial pressure of 60 MPa. Therefore, the correction factor k is applicable when the initial pressure is high.

Table 5.4 Fitted correlations of the coefficients (A, B, C, D, E, F, G) in correction factors (K, k) versus initial pressure using data from Table 5.3.

Correction factor	Coefficient	Fitted Correlation	R^2
K	A	$A = 400.01 - 6.9341P_0 + 0.0831P_0^2$	0.9995
	B	$B = 1225.1 - 23.362P_0 + 1.3439P_0^2 - 0.022P_0^3$	0.9819
	C	$C = 37.383 + 0.1949P_0 - 0.0158P_0^2$	0.9929
	D	$D = 4015.5 + 127.7P_0 - 2.68P_0^2$	0.9993
	E	$E = -0.2575 - 0.0219P_0 + 0.00040P_0^2 - 0.0000024P_0^3$	0.9958
k	F	$F = 30.445 + 0.389P_0$	0.9947
	G	$G = 0.1329 - 0.0022P_0$	0.9891

5.3.3 Comparison between modified and original MC methods

In order to compare the final hydrogen temperature and SOC between the modified MC method and the original one, the initial conditions are set to T_a of 0, 20, 40 °C, T_c of −40, −22.5 °C, P_0 = 2, 30, 60 MPa. PRR is set from 0.2 to 2.5 MPa/s and Δ=0.1. Simulations are carried out based on the 0D1D model. The modified and original MC methods are based on the analytical solutions. The assumptions of the adiabatic boundary and the tank wall's uniform temperature are adopted in deriving the analytical solutions, leading to errors. The 0D1D model has been validated in Section 2.3.4 and is more accurate considering the complex one-dimensional tank wall and complex heat transfer outside and inside the tank, so the result of the 0D1D model can be considered

accurate and regarded as the reference.

(1) Comparison of final hydrogen temperature between modified MC method and original one

For the modified MC method, the values of the coefficients *A*, *B*, *C*, *D*, *E, F* and *G* are calculated according to the correlation with initial pressure in Table 5.4. Then, the correction factors *K* and *k* are calculated according to the correlation with the final filling time in Table 5.3. Finally, *K* and *k* are brought into Eq. (5.26) to calculate the final hydrogen temperature. For the original MC method, Eq. (5.6) is used to calculate the parameter MC according to the initial conditions. Then, parameter MC is brought into Eq. (5.5) to calculate the final hydrogen temperature.

The final hydrogen temperatures calculated by the modified MC method and the original one are thoroughly compared under various initial conditions. Figs. 5.17 and 5.18 show the comparison when the initial pressure and the ambient temperature take different values, and the precooling temperature are −40 and −22.5 °C, respectively. Under various initial conditions, the final hydrogen temperatures of the modified MC method are in better agreement with that of the 0D1D model. For example, in some situations, the errors of final hydrogen temperature between the 0D1D model are reduced by 2 to 7 °C for the modified MC method than the original one. In a word, the modified MC method has improved the calculation accuracy for the final hydrogen temperature. The comparison of Eqs. (5.26) and (5.5) show that a correction term is added to the modified formula of the final hydrogen temperature due to the distinction between hydrogen and tank wall temperatures. In Eq. (5.6), Δt is the filling time after 30 s, namely $\Delta t = t_{\text{final}} - 30$, so the original MC method is unsuitable when the final filling time is less than 30 s. However, the modified MC method overcomes this problem because the formulas of correction factors and Eq. (5.26) of modified final hydrogen temperature are suitable when the final filling time is less than 30 s. As shown in the situations on the right side of Figs. 5.17 and 5.18, when the final filling time is less than 30 s under the initial pressure of 60 MPa, the modified MC method can still calculate final hydrogen temperature while original one cannot.

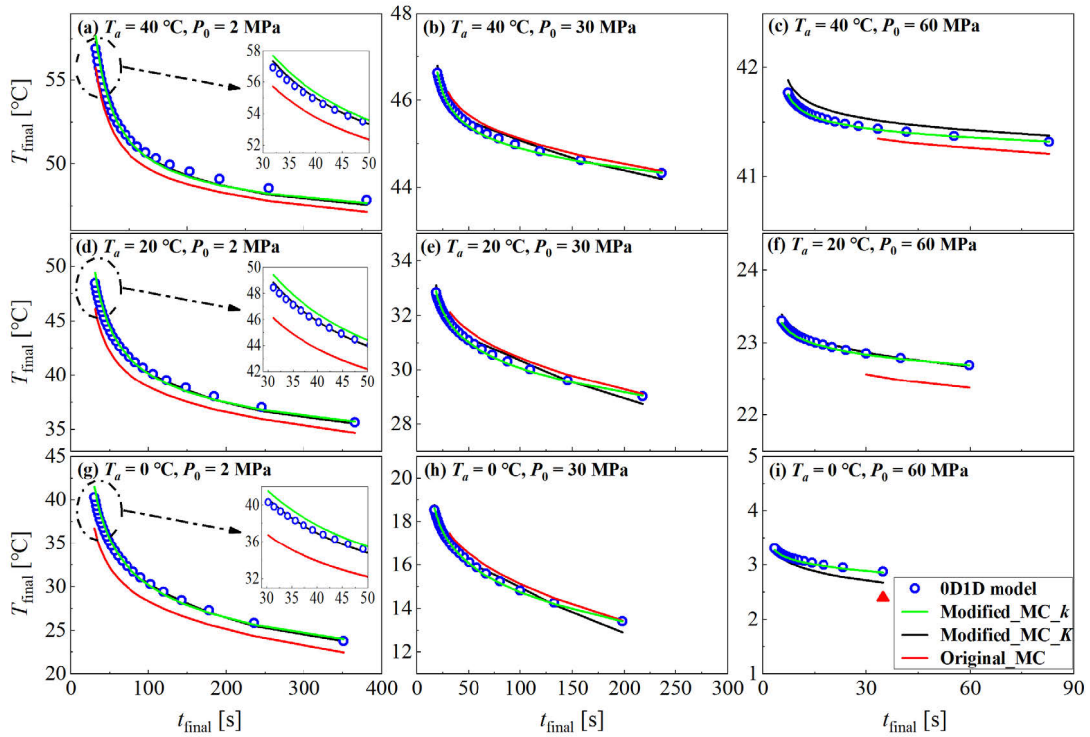

Fig. 5.17 Comparison of final hydrogen temperatures inside the onboard tank calculated by modified MC method and original one at the precooling temperature of −40 °C and different ambient temperatures and initial pressures.

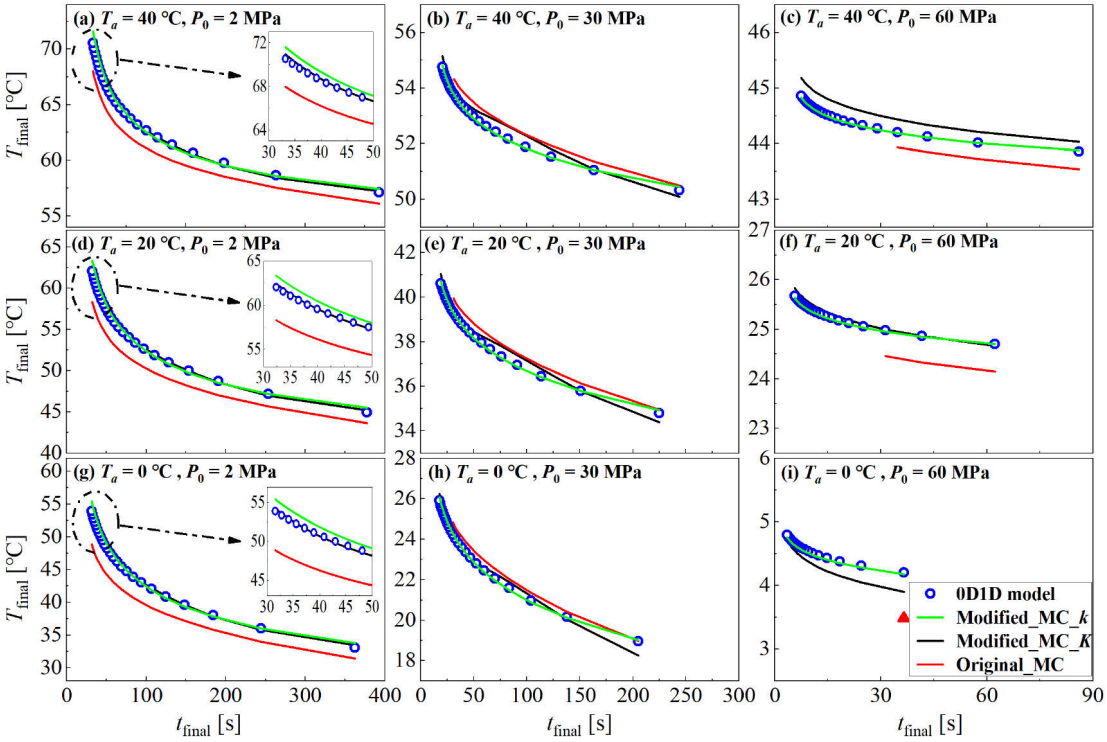

Fig. 5.18 Comparison of final hydrogen temperatures inside the onboard tank calculated by modified MC method and original one at precooling temperature of −22.5 °C and different ambient temperatures and initial pressures.

(2) Comparison of SOC between the modified MC method and the original one

The modified MC method, the original MC method and the 0D1D model are run simultaneously. When the SOC of the 0D1D model reaches 100%, all simulations stop immediately. The ideal situation is that the SOCs of the modified and original MC methods also reach 100% now. That is, the SOC of the onboard tank can accurately reach the value set by the operator.

Next, this section compares the SOC corresponding to the maximum error in the final hydrogen temperature calculated by the original MC method. Fig. 5.19 shows that the SOCs of the modified MC method are in better agreement with that of the 0D1D model. The comparison of SOCs and final hydrogen temperatures under the same initial condition shows that the SOC error is significant when the final hydrogen temperature error is large. That is, the modified MC method essentially improves the calculation accuracy of the final hydrogen temperature, thus improving the calculation accuracy of the pressure target and reaching a more accurate SOC. In a word, the modified MC method can control the dispenser to fill the onboard tank to achieve a more accurate expected SOC and has positive significance for the HRS' operational safety and the driver's refuelling experience.

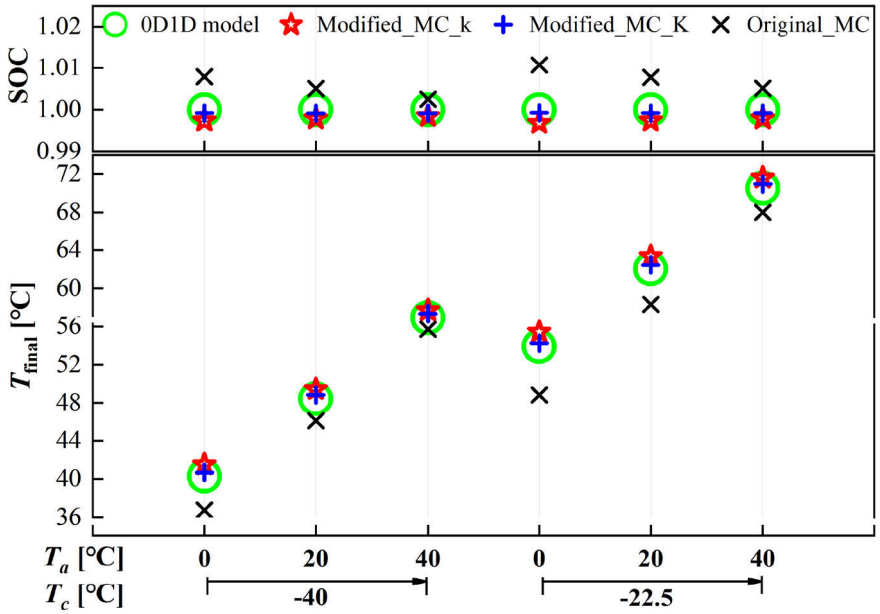

Fig. 5.19. Comparison of the SOCs and final hydrogen temperatures inside the onboard tank calculated by the modified MC method and the original one at different ambient and precooling temperatures.

Table 5.5 shows the comparison between the modified and the original MC methods. Comparing Eq. (5.5) of the original MC method with Eq. (5.26) of the modified one, the modified MC method does not need additional information required by the HRS. The coefficients A, B, C, D, E, F and G for K and k are derived from the conservative Cold Case Tank. The Cold Case Tank is a 25 L tank, smaller than the actual tank. Using a smaller tank than 25 L to develop the modified MC method can achieve a more conservative refuelling performance, but that is unnecessary. If we want to improve the refuelling performance of the modified MC method further, we can update the coefficients A, B, C, D, E, F and G using the parameters of the storage tank in the actual refuelling event. Likewise, if we want to improve the original MC method's refuelling performance, we can update the coefficients AC, BC, GC, KC and JC using the parameters of the actual storage tank. At this time, the hydrogen temperature, pressure, internal energy and other data obtained through 0D1D model simulation will change. The simulated value of MC obtained by bringing the obtained simulation data into Eq. (5.18) will change. The values of coefficients AC, BC, GC, KC, and JC will change when fitting the simulated data of MC using Eq. (5.6).

Table 5.5 Comparison between the modified MC method and the original one.

		Original MC method	Modified MC method
Filling speed		Eqs. (5.1) - (5.4)	Eqs. (5.1) - (5.4)
Pressure target	Model	Dual-zone single-temperature	Dual-zone dual-temperature
	Control equations	Eqs. (5.5) and (5.6)	Eq. (5.26) and K, k

This section uses a dual-zone dual-temperature model that distinguishes hydrogen temperature and tank wall temperature to improve the dual-zone single-temperature model of the original MC method and derives a modified formula for calculating the final hydrogen temperature, including a correction factor. The correction factor can be expressed as two formulas: one is $K = A + Be^{-t/C}$ ($p_0 \leq 30$ MPa) and $K = Dt^E$ ($p_0 > 30$ MPa). The other is after introducing the average mass flow rate $k = F + Gt$. The correlation between the coefficients in each correction factor formula and the initial pressure in the tank was determined. Under the conditions of ambient temperature of 0

to 40 °C, inlet temperature of −40 to −20 °C, and initial pressure of 2 to 60 MPa, the errors of final hydrogen temperature between the 0D1D model are reduced by 2 to 7 °C for the modified MC method than the original one. According to the $P_{\mathrm{target}} = f\left(T_{\mathrm{final}}, \mathrm{SOC}_{\mathrm{target}}\right)$, the modified MC method improves the calculation accuracy of the pressure target and achieves a more accurate SOC. In a word, the modified MC method improves the accuracy of refuelling control and has positive significance for the HRS' operational safety and the driver's refuelling experience.

5.4 Conclusion

This chapter proposes a two-level improvement plan for the MC method in the SAE J2601 hydrogen refuelling protocol to improve the safety of hydrogen filling system.

Plan I: The modified formula and ANN model of the MC parameter in the MC method are proposed. The results show that the ANN model of the MC parameter overcomes the problem that the original MC parameter formula is not suitable for the final filling time of less than 30s. Under the conditions of ambient temperature of 0 to 40 °C, inlet temperature of −40 to −20 °C, and initial pressure of 2 to 60 MPa, compared with the original formula of the MC parameter, the modified formula and ANN model of the MC parameter reduce the relative error with the 0D1D model by about 13.8% to 58.8% and 16.6% to 82.3%, respectively.

Plan II: We use a dual-zone dual-temperature model that distinguishes hydrogen temperature and tank wall temperature to improve the dual-zone single-temperature model of the original MC method and derive a modified formula for calculating the final hydrogen temperature. The results show that the modified formula for the final hydrogen temperature overcomes the problem that the original formula is not suitable for the final filling time of less than 30 seconds. Under the conditions of the ambient temperature of 0 to 40 °C, inlet temperature of −40 to −20 °C, and initial pressure of 2 to 60 MPa, the errors of final hydrogen temperature between the 0D1D model are reduced by 2 to 7 °C for the modified MC method than the original one.

Plan I only corrects the formula of the MC parameter in the MC method and is essentially just a further optimization of the MC method. Plan II replaces the

thermodynamic model of the hydrogen storage tank used in deriving the MC method and derives the modified formula and new correction factor for the final hydrogen temperature. At this time, the control equation of the pressure target is completely different from the original MC method (as shown in Table 5.5). The modified MC method can be considered a new filling method. In short, both levels of MC method improvement plans can improve the calculation accuracy of the pressure target, the control accuracy of the filling process and the safety of the hydrogen filling system.

Chapter 6 Hydrogen filling method based on analytical solution of dual-zone model

My specific contribution in this work was to propose a more concise new hydrogen filling method based on analytical solutions, which avoids some tables, formulas and coefficients in the development and use of the lookup table method and MC method.

As mentioned in the previous chapter, both the lookup table method and the MC method in the SAE J2601 hydrogen refuelling protocol require a large number of simulations under extreme working conditions to determine the relevant tables, formulas and coefficients in advance. For example, during the development process of the lookup table method, SAE used simulations under extreme working conditions to determine 54 special tables in advance. In the development process of the MC method, the final filling time Eq.(5.3) is a polynomial formula determined by fitting a large number of simulation data, and the coefficients *a*, *b*, *c* and *d* are also determined by a large number of simulation data under extreme working conditions. SAE has developed specific tables for these coefficients for query during actual use. The development process is cumbersome, as tables, formulas, and coefficients are developed through extensive simulations of extreme working conditions. When actually using the lookup table method and MC method, it is necessary to query the table according to the actual filling conditions to determine the correlation coefficient, and the use process is also cumbersome. Therefore, this chapter will propose a more concise new filling method using analytical solution control to improve the efficiency of the hydrogen filling process.

6.1 Control logic of new filling method

Fig. 6.1 shows the control logic of the non-communicating MC method, which essentially controls the filling speed and pressure target as introduced in Section 5.1. Fig. 6.2 shows the control logic of the new filling method based on analytical solutions proposed in this chapter. Comparing Fig. 6.1 and Fig. 6.2, the non-communication MC

method first calculates the final filling time through the measured mass average temperature, then calculates the filling speed of PRR and final hydrogen temperature based on the known final filling time, and finally uses the final hydrogen temperature to calculate pressure target. The new filling method is based on the dual-zone lumped parameter thermodynamic model established in Section 2.1.2. It first calculates the final hydrogen temperature, then calculates the final filling time and pressure target based on the known final hydrogen temperature, and finally calculates the filling speed of PRR based on the final filling time. The new filling method also determines the PRR to control the filling speed and the pressure target to control the filling stop. However, the new filling method can avoid the need to determine the coefficients *a*, *b*, *c* and *d* in Eq. (5.3) through a large number of simulations in the original MC method.

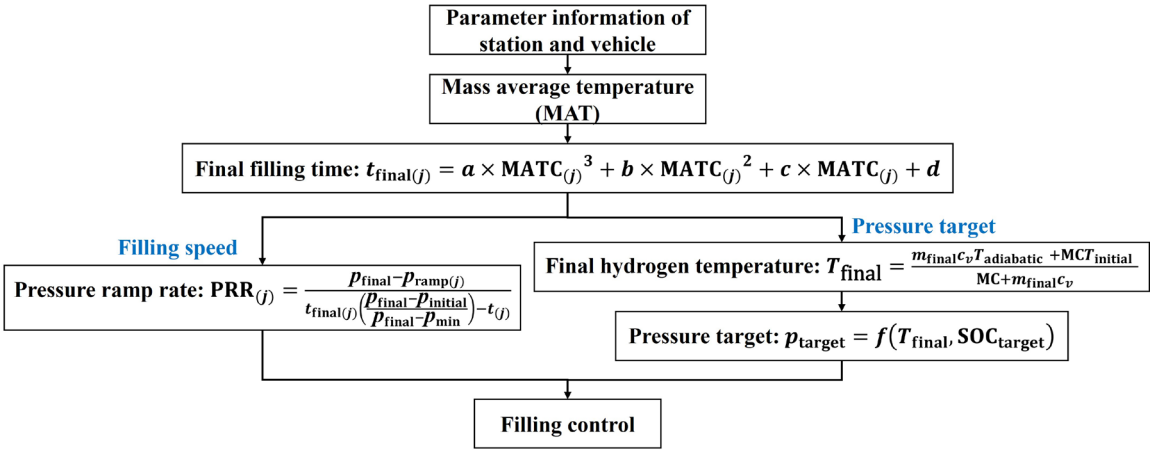

Fig. 6.1 Control logic of non-communication MC method.

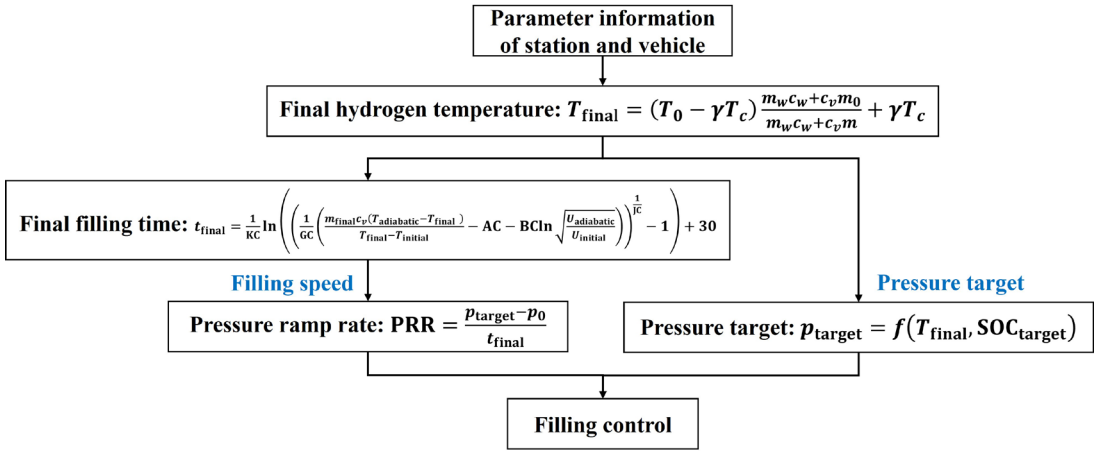

Fig. 6.2 Control logic of the new filling method.

6.2 Analytical solution of final hydrogen temperature

According to the dual-zone lumped parameter thermodynamic model of the hydrogen storage tank in Section 2.1.2, the energy conservation of hydrogen during the filling process can be expressed as

$$\frac{\mathrm{d}(mu)}{\mathrm{d}t} = \dot{m}h - \dot{Q} \tag{6.1}$$

where $\dot{m}$ is the mass flow rate of hydrogen. h is the specific enthalpy of hydrogen. $\dot{Q}$ is the heat transfer rate between hydrogen and the tank wall, $\dot{Q} = A_{\mathrm{in}}\alpha_{\mathrm{in}}\left(T - T_w\right)$. The energy conservation of the tank wall during the hydrogen filling process can be expressed as

$$\frac{\mathrm{d}\left(m_w c_w T_w\right)}{\mathrm{d}t} = \alpha_{\mathrm{in}} A_{\mathrm{in}}\left(T - T_w\right) - \alpha_{\mathrm{out}} A_{\mathrm{out}}\left(T_w - T_a\right) \tag{6.2}$$

We add the two sides of the equal sign of Eqs. (6.1) and (6.2), respectively. That is, considering the hydrogen and the tank wall as a whole, the energy conservation during the filling process can be expressed as

$$\frac{\mathrm{d}(mu)}{\mathrm{d}t} + \frac{\mathrm{d}\left(m_w c_w T_w\right)}{\mathrm{d}t} = \dot{m}h - \alpha_{\mathrm{out}} A_{\mathrm{out}}\left(T_w - T_a\right) \tag{6.3}$$

The MC method assumes that the hydrogen temperature and the tank wall temperature are equal, that is $T = T_w$, and assumes that the outer boundary of the tank is adiabatic. This chapter also adopts this assumption. At this time, Eq. (6.3) can be expressed as

$$\frac{\mathrm{d}(mu)}{\mathrm{d}t} + \frac{\mathrm{d}\left(m_w c_w T\right)}{\mathrm{d}t} = \dot{m}h \tag{6.4}$$

Eq. (6.4) can be further rewritten as

$$c_v m\frac{\mathrm{d}T}{\mathrm{d}t} + \dot{m}c_v T + m_w c_w \frac{\mathrm{d}T}{\mathrm{d}t} = \dot{m}c_p T_c \tag{6.5}$$

where $u = c_v T$, $h = c_p T_c$. T_c is the inlet temperature. c_v and c_p are the constant-volume and constant-pressure specific heat capacity of hydrogen, respectively.

We divide both sides of Eq. (6.5) by $\dot{m}c_v$ and define the ratio of specific heat capacity, $\gamma = c_p / c_v$. Then, Eq. (6.5) can be expressed as

$$\frac{\mathrm{d}T}{\mathrm{d}t} = \frac{\gamma T_c - T}{\frac{m_w c_w + c_v m_0}{\dot{m}c_v} + t} \tag{6.6}$$

Solving Eq. (6.6), the final hydrogen temperature can be expressed as

$$T_{\text{final}} = \left(T_0 - \gamma T_c\right)\frac{m_w c_w + c_v m_0}{m_w c_w + c_v m} + \gamma T_c \tag{6.7}$$

where m_0 is the initial mass of hydrogen. m is the final mass of hydrogen. m_w is the mass of the tank wall. c_v is the specific heat capacity of hydrogen at constant volume. c_w is the specific heat capacity of the tank wall material. T_0 is the initial temperature of hydrogen. T_c is the inlet temperature. γ is the ratio of specific heat capacity, $\gamma = c_p / c_v$.

6.3 Analytical solution of final filling time

As introduced in Chapter 5, the MC method obtains the formula of the final hydrogen temperature and the formula of the MC parameter through the simplified storage tank model:

$$T_{\text{final}} = \frac{m_{\text{final}} c_v T_{\text{adiabatic}} + \mathrm{MC} T_{\text{initial}}}{\mathrm{MC} + m_{\text{final}} c_v} \tag{6.8}$$

$$\mathrm{MC} = AC + BC\ln\sqrt{\frac{U_{\text{adiabatic}}}{U_{\text{initial}}}} + GC\left(1 - e^{-KC\Delta t}\right)^{JC} \tag{6.9}$$

where the MC parameter formula Eq. (6.9) contains the variable of final filling time Δt, $\Delta t = t_{\text{final}} - 30$. Solving Eqs. (6.8) and (6.9), and at this time, the final hydrogen temperature has been obtained in Eq. (6.7), which can be regarded as a known number so that the final filling time can be expressed as

$$t_{\text{final}} = \frac{1}{KC}\ln\left(\left(\frac{1}{GC}\left(\frac{m_{\text{final}}c_v\left(T_{\text{adiabatic}} - T_{\text{final}}\right)}{T_{\text{final}} - T_{\text{initial}}} - AC - BC\ln\sqrt{\frac{U_{\text{adiabatic}}}{U_{\text{initial}}}}\right)\right)^{\frac{1}{JC}} - 1\right) + 30 \tag{6.10}$$

6.4 Determination of filling speed and pressure target

6.4.1 Determination of filling speed

$U_{\text{adiabatic}}$ in Eq. (6.10) is unknown and needs to be calculated in advance. From the energy conservation of hydrogen, we know

$$U_{\text{adiabatic}} = U_{\text{initial}} + \Delta m\overline{h} \tag{6.11}$$

where $\overline{h}$ is the average enthalpy of hydrogen entering the storage tank during the filling process, which can be solved by the Runge-Kutta method:

$$\overline{h} = \frac{1}{4}\left[\begin{array}{l} \dfrac{h\left(T_{\text{c}}, p_{\text{S0}}\right) + h\left(T_{\text{c}}, \left(p_{\text{S0}} + \dfrac{p_{\text{S}} - p_{\text{S0}}}{4}\right)\right)}{2} + \\ \dfrac{h\left(T_{\text{c}}, \left(p_{\text{S0}} + \dfrac{p_{\text{S}} - p_{\text{S0}}}{4}\right)\right) + h\left(T_{\text{c}}, \left(p_{\text{S0}} + 2\dfrac{p_{\text{S}} - p_{\text{S0}}}{4}\right)\right)}{2} + \\ \dfrac{h\left(T_{\text{c}}, \left(p_{\text{S0}} + 2\dfrac{p_{\text{S}} - p_{\text{S0}}}{4}\right)\right) + h\left(T_{\text{c}}, \left(p_{\text{S0}} + 3\dfrac{p_{\text{S}} - p_{\text{S0}}}{4}\right)\right)}{2} + \\ \dfrac{h\left(T_{\text{c}}, \left(p_{\text{S0}} + 3\dfrac{p_{\text{S}} - p_{\text{S0}}}{4}\right)\right) + h\left(T_{\text{c}}, \left(p_{\text{S0}} + 4\dfrac{p_{\text{S}} - p_{\text{S0}}}{4}\right)\right)}{2} \end{array}\right] \tag{6.12}$$

where T_{c} is the inlet temperature of hydrogen. $p_{\text{S0}} = p_0 + \Delta p_{\text{S0}}$, $p_{\text{S}} = p_{\text{final}} + \Delta p_{\text{S}}$. p_0 and p_{final} are the initial hydrogen pressure and final hydrogen pressure in the storage tank. Δp_{S0} and Δp_{S} are the pressure drops between the onboard tank and the HRS at the initial and final moments. Tests by Powertech Company show that when the initial pressure of the storage tank is 2 MPa, $\Delta p_{\text{S0}} = 5\text{MPa}$. When the initial pressure is 17 MPa, $\Delta p_{\text{S0}} = 2\text{MPa}$. At higher initial pressure, $\Delta p_{\text{S0}} = 1\text{MPa}$. In all cases, Δp_{S} is

assumed to be 1 MPa [5].

If the new filling method is set to a constant filling speed, similar to the lookup table method in the SAE J2601 hydrogen refuelling protocol, the PRR controlling the filling speed can be expressed as

$$\mathrm{PRR} = \frac{p_{\mathrm{target}} - p_0}{t_{\mathrm{final}}} \tag{6.13}$$

where p_{target} and p_0 are the pressure target and initial pressure of hydrogen in the storage tank. p_{target} will be calculated below, and p_0 is known. t_{final} is the final filling time, which is calculated by formula Eq. (6.10).

6.4.2 Determination of pressure target

Since $\mathrm{SOC}_{\mathrm{target}} = \rho_{\mathrm{target}} \big/ \rho_{(70\mathrm{MPa},15^\circ\mathrm{C})}$ and $\rho_{(70\mathrm{MPa},15^\circ\mathrm{C})} = 40.2\mathrm{g/L}$. Therefore, the calculation formula of the pressure target in Fig. 6.2 can be rewritten as

$$p_{\mathrm{target}} = f\left(T_{\mathrm{final}}, \rho_{\mathrm{target}}\right) \tag{6.14}$$

The specific form of Eq. (6.14) can adopt the polynomial gas equation of state determined in Section 3.2.3:

$$p = \sum_{i=0}^{N} \sum_{j=0}^{N-i} a_{ij} T^i \rho^j \tag{6.15}$$

First, combine the initial and boundary conditions of filling and determine the final hydrogen temperature through formula Eq. (6.7). Then, the pressure target is determined by formula Eq. (6.15).

6.5 Performance verification of new filling method

In order to verify the effectiveness of the new filling method proposed in this chapter, the geometric parameters and physical properties of the 25 L type III storage tank in Table 5.1 in Section 5.1.3 are used for simulation. The reason for using the 25 L type III storage tank is that the new filling method has five parameters, namely *AC*, *BC*, *JC*, *GC* and *KC*, in formula Eq. (6.10). The original MC method also uses the parameters of the 25 L type III storage tank and determines these five parameters combined with

the simulation of the zero-dimensional gas one-dimensional tank wall (0D1D) model. Table 6.1 shows the initial and boundary conditions used in the verification process.

Table 6.1 Different initial and boundary conditions used when validating new filling methods

Parameter	Physical definition	Value
T_a	Ambient temperature (℃)	0, 20
T_c	Inlet temperature (℃)	−20, −10, 0
T_0	Initial temperature (℃)	Equal to ambient temperature
p_0	Initial pressure (MPa)	2, 6, 10

Fig. 6.3 shows the comparison of the simulation results of the new filling method and the 0D1D model when the ambient temperature is 0 and 20 °C, the inlet temperature is −20, −10 and 0 °C, and the initial pressure is 2, 6 and 10 MPa. The 0D1D model takes into account the complex tank wall structure and heat transfer conditions, and its calculation results can be considered accurate and can be used as a standard. Overall, the new filling method is in good agreement with the final hydrogen temperature, pressure and SOC of the 0D1D model.

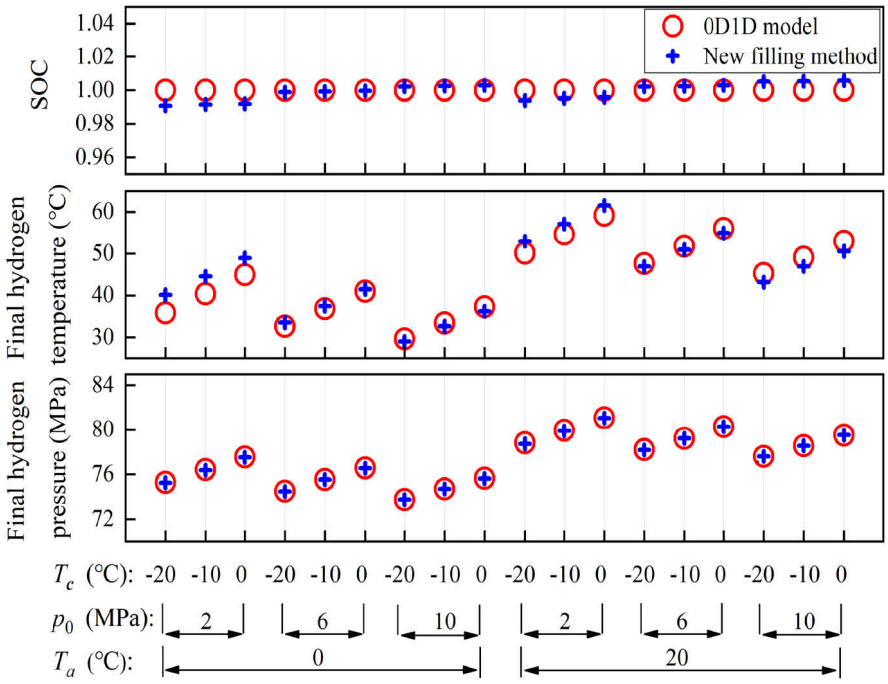

Fig. 6.3 Comparison of the final hydrogen temperature, final hydrogen pressure and SOC between the new filling method and the 0D1D model under different initial pressure, ambient temperature and inlet temperature.

Fig. 6.3 also shows an interesting phenomenon. That is, when the initial pressure is 2 MPa, there is a certain error between the new filling method and the 0D1D model results regardless of whether the ambient temperature and the inlet temperature change. Therefore, for our proposed new filling method, the lower the initial pressure of hydrogen in the tank, the greater the error. The reason is that the lower the initial pressure, the more hydrogen is filled, resulting in greater changes in hydrogen temperature and hydrogen pressure in the tank. In future work, a correction factor regarding the initial pressure can be introduced to further improve the accuracy of the new filling method.

6.6 Conclusion

Based on the dual-zone lumped parameter thermodynamic model of the hydrogen storage tank in Section 2.1.2, this chapter deduces the analytical solutions of the final filling time and the final hydrogen temperature and proposes a new filling method based on the analytical solutions.

The simulation results of the new filling method and the zero-dimensional gas one-dimensional tank wall (0D1D) model were compared. The results show that under the conditions of ambient temperatures of 0 and 20 °C, inlet temperatures of −20, −10 and 0 °C, and initial pressures of 2, 6 and 10 MPa, the final hydrogen temperature, pressure and SOC simulated by the new filling method agree well with the 0D1D model, proving the effectiveness of the new filling method. Initial pressure has a greater impact on the accuracy of the new filling method than ambient temperature and inlet temperature. In future work, a correction factor regarding the initial pressure can be introduced to further improve the accuracy of the new filling method.

The new filling method avoids some tables, formulas and coefficients in the development and use of the lookup table method and MC method, making the development and use process more concise and improving the efficiency of the hydrogen filling process.

Chapter 7 Conclusion, Contribution and Future Work

7.1 Conclusions

In order to improve the efficiency and safety of the hydrogen filling system, this thesis takes the filling system as the research object and carries out a modelling study, parametric study, optimization study and protocol study. The specific conclusions are as follows:

(1) Hydrogen storage tank model of hydrogen filling system: The lumped parameter thermodynamic model, analytical model and numerical model of the hydrogen storage tank were established and verified. The application scope of each model is determined. That is, the numerical model is used in the parametric study in Chapter 3, the optimization study in Chapter 4, and the protocol study in Chapters 5 and 6, and the analytical model is used in the protocol study in Chapters 5 and 6.

Based on the mass and energy conservation and gas equation of state (EOS), single-zone (ignoring the tank wall and only considering hydrogen), dual-zone (considering the tank wall as a whole with uniform temperature), triple-zone (considering the tank wall as a two-layer structure of liner and shell with uniform temperature in each layer) and one-dimensional tank wall with zero-dimensional gas (0D1D, considering that the tank wall has a multi-layer structure and the temperature of each layer is uniform) were built. Solving the mathematical and physical equations of the single-zone and dual-zone thermodynamic models, the corresponding analytical models of single-zone hydrogen temperature, dual-zone hydrogen temperature and tank wall temperature were obtained. Combining with the Redlich-Kwong gas EOS, the corresponding analytical model of hydrogen pressure was obtained. Based on the mathematical and physical equations of single-zone, dual-zone, triple-zone and 0D1D thermodynamic models of the hydrogen storage tank, the corresponding numerical models were established in Matlab/Simulink. The experimental data and CFD simulation results in

the references were used to verify the accuracy of single-zone and dual-zone analytical models, as well as the single-zone, dual-zone, triple-zone and 0D1D numerical models.

(2) Parametric study on the hydrogen filling system: The optimal gas EOS and heat transfer coefficient model were determined. That is, the numerical model of the hydrogen storage tank calculates the hydrogen temperature and pressure based on the NIST database, the analytical model of the hydrogen storage tank uses Redlich -Kwong modified gas EOS, the new filling method in Chapter 6 adopts polynomial gas EOS, and the heat transfer coefficient model adopts the empirical formula based on Reynolds number.

The hydrogen temperature and pressure calculated by different types of gas EOS and heat transfer coefficient models were compared. The results show that using the final hydrogen pressure calculated based on the NIST database as the standard, the relative error of the polynomial gas EOS is 0.30%, the Redlich-Kwong gas EOS is 1.83%, and the van der Waals gas EOS is 17.90%. That is, the polynomial gas EOS has the highest accuracy, followed by the Redlich-Kwong gas EOS, and the van der Waals gas EOS has the lowest accuracy. Compared with the heat transfer coefficients of the empirical formula based on real-time pressure and the filling time, the empirical formula heat transfer coefficient based on the Reynolds number has the smallest error between the standard heat transfer coefficient based on energy conservation.

(3) Optimization study on single-stage and cascade hydrogen filling systems: The cascade storage tank configuration and filling strategy of the hydrogen filling system are optimized, which reduces cooling energy consumption and maximum cooling demand, thereby reducing the operating cost and investment cost of the refrigeration system, improving the efficiency of the hydrogen filling system.

We extend the hydrogen storage tank model to the entire single-stage hydrogen filling system, including the station tank, onboard tank, reduction valve, heat exchanger, pressure drops, etc. The filling strategies of two-stage filling speed (average pressure ramp rate) and two-stage inlet temperature applied to a single-stage hydrogen filling system were proposed. The results show that when the inlet temperature is −20 °C, the two-stage filling speed strategy can reduce the maximum cooling power by

approximately 23.8%. When the filling speed is 0.428 MPa/s, the two-stage inlet temperature strategy can reduce the maximum cooling power by about 16.3%.

We expand the single-stage hydrogen filling system to a three-stage cascade hydrogen filling system. A multi-objective optimization method based on genetic algorithm and Pareto optimization was proposed to optimize the initial pressure and volume configuration of low-pressure, medium-pressure and high-pressure cascade storage tanks. The results show that when the ambient temperature is 20 °C, and the SOC is 0.98 to 0.99, the optimized cascade storage tank configuration can reduce cooling energy consumption by about 11.43%. A three-stage inlet temperature filling strategy applied to the three-stage cascade hydrogen filling system is proposed. The results show that when the ambient temperature is 5 to 45 °C, the three-stage inlet temperature filling strategy can reduce the maximum cooling power by approximately 16.69% to 17.38%.

(4) Research on hydrogen refuelling protocol: Two improvement plans for the MC method in the SAE J2601 refuelling protocol are proposed, which can improve the calculation accuracy of the pressure target and the control accuracy of the filling process, improving the safety of the hydrogen filling system.

Plan I: The modified formula and ANN model of the MC parameter in the MC method are proposed. The results show that the ANN model of the MC parameter overcomes the problem that the original MC parameter formula is not suitable for the final filling time of less than 30 s. Under the conditions of the ambient temperature of 0 to 40 °C, inlet temperature of −40 to −20 °C, and initial pressure of 2 to 60 MPa, compared with the original formula of the MC parameter, the modified formula and ANN model of the MC parameter reduce the relative error with the 0D1D model by about 13.8% to 58.8% and 16.6% to 82.3%, respectively.

Plan II: We use a dual-zone dual-temperature model that distinguishes hydrogen temperature and tank wall temperature to improve the dual-zone single-temperature model of the original MC method and derive a modified formula for calculating the final hydrogen temperature. The results show that the modified formula for the final hydrogen temperature overcomes the problem that the original formula is not suitable for the final filling time of less than 30 s. Under the conditions of ambient temperature

of 0 to 40 °C, inlet temperature of −40 to −20 °C, and initial pressure of 2 to 60 MPa, the errors of final hydrogen temperature between the 0D1D model are reduced by 2 to 7 °C for the modified MC method than the original one.

Plan I only corrects the formula of MC parameter in the MC method and is essentially just a further optimization of the MC method. Plan II replaces the thermodynamic model of the hydrogen storage tank used in deriving the MC method and derives the modified formula and correction factor for the final hydrogen temperature. At this time, the control equation of the pressure target is completely different from the original MC method, and Plan II can be considered as a new filling method.

(5) Hydrogen refuelling protocol research: A more concise new hydrogen filling method based on analytical solutions was explored, avoiding some tables, formulas and coefficients in the development and use of the lookup table method and MC method, making the development and use process more concise and improving the efficiency of the hydrogen filling process.

The simulation results of the new filling method and the 0D1D model were compared. The results show that under the conditions of ambient temperatures of 0 and 20 °C, inlet temperatures of −20, −10 and 0 °C, and initial pressures of 2, 6 and 10 MPa, the final hydrogen temperature, the pressure and SOC simulated by the new filling method and the 0D1D model are relatively consistent, proving the effectiveness of the new filling method.

7.2 Contributions

During the course of this Ph.D. work, I have successfully published five papers as the first author and submitted one manuscript for the second review:

[1] Luo H, Xiao J S, Bénard P, Yang T Q, Tong L, Chahine R, Yuan Y P, Yuan C Q, Yao C L. Improvement of MC method in SAE J2601 hydrogen refuelling protocol using dual-zone dual-temperature model. Journal of Energy Storage, 2024, 81: 110416. (Chapter 5)

[2] Luo H, Xiao J S, Bénard P, Zong Y, Chahine R, Tong L, Yuan C Q, Yang T Q, Yuan Y P. Optimal estimation of MC parameter in SAE J2601 hydrogen refuelling

protocol based on modified formula and artificial neural networks. Fuel, 2024, 365: 131315. (Chapter 5)

[3] Luo H, Xiao J S, Bénard P, Chahine R, Yang T Q. Multi-objective optimization of cascade storage system in hydrogen refuelling station for minimum cooling energy and maximum state of charge. International Journal of Hydrogen Energy, 2022, 47: 10963-10975. (Chapter 4)

[4] Luo H, Xiao J S, Bénard P, Chahine R, Yang T Q. Effects of filling strategies on hydrogen refueling performance. International Journal of Hydrogen Energy, 2024, 51: 664-675. (Chapter 4)

[5] Luo H, Xiao J S, Bénard P, Yuan C Q, Tong L, Chahine R, Yuan Y P, Yang T Q, Yao C L. Thermodynamic modeling and analysis of cascade hydrogen refuelling with three-stage pressure and temperature for heavy-duty fuel cell vehicles. International Journal of Hydrogen Energy, 2024, 63: 103-113. (Chapter 4)

[6] Luo H, Yuan C Q, Wang L, Yang T Q, Tong L, Ye F, Yuan Y P, Bénard P, Chahine R, Xiao J S. Heat transfer analysis methodology for compression hydrogen storage tank during charge-discharge cycle. International Journal of Energy Research, 2024, Second review. (Chapter 3)

The main innovations of this thesis are:

(1) The two-stage filling speed and two-stage inlet temperature filling strategies applied to a single-stage hydrogen filling system were proposed and further extended to a three-stage inlet temperature filling strategy applied to a three-stage cascade filling system, reducing the maximum cooling power demand and cooling energy consumption of the refrigeration system, and improving the efficiency of the hydrogen filling system.

(2) The formula of the MC parameter in the MC method has been revised to improve the calculation accuracy of the MC parameter. The dual-zone single-temperature model of the original MC method was further improved into a dual-zone and dual-temperature model, and a modified formula for the final hydrogen temperature was derived, which improved the calculation accuracy of the pressure target and the control accuracy of the filling process and improved the efficiency and safety of the hydrogen filling system.

(3) A new filling method based on the analytical solutions of the final filling time and final hydrogen temperature was explored, avoiding some tables, formulas and

coefficients of the lookup table method and MC method and improving the efficiency of the development and use process of the filling method.

7.3 Future works

This thesis has made certain progress in the modelling study, parametric study, optimization study, and protocol study of the hydrogen filling system, which has improved its efficiency and safety. However, there are still some issues worthy of further discussion:

(1) For the two-stage filling speed (average pressure ramp rate) and two-stage inlet temperature filling strategies proposed in this thesis, we first keep the inlet temperature constant and then propose the two-stage filling speed strategy. Then, we keep the filling speed constant and then propose a two-stage inlet temperature strategy. A filling strategy in which the filling speed and inlet temperature change simultaneously remains to be studied. Meanwhile, the effect of changes in inlet temperature due to equipment failure and other reasons on the results of the two-stage filling strategies also needs further study.

(2) Both the improvements of the MC parameter formula and the final hydrogen temperature formula proposed in this thesis improve the control accuracy of the pressure target of the MC method. The filling control process of the MC method also includes the control of the filling speed, so the improvement of the filling speed remains to be studied. Meanwhile, this thesis proves the effectiveness of the improved MC method through numerical simulation, and further field test verification is needed.

(3) For the new filling method proposed in this thesis based on the analytical solutions of the final filling time and hydrogen temperature, the initial pressure has an impact on the accuracy of the new filling method, and the lower the initial pressure, the greater the impact. In future work, a correction factor regarding the initial pressure can be introduced to further improve the accuracy of the new filling method.

(4) At present, this thesis only optimizes the hydrogen filling system from the perspectives of efficiency and safety. The optimization strategy can reduce the power demand of the refrigeration system. Economic analysis that links the reduction of power demand to the reduction of investment costs is our future work.

Reference

[1] 孟翔宇, 陈铭韵, 顾阿伦, 等. “双碳”目标下中国氢能发展战略[J]. 天然气工业, 2022, 42(04): 156-179.

[2] 倪耀琪, 朱恒恺. “双碳”目标下氢能发展机遇、难点与路径选择[J]. 现代化工, 2024, 44(02): 1-8.

[3] 毕希, 孙仁金, 张涵. 中国氢燃料电池汽车产业发展影响因素及对策分析[J]. 现代化工, 2023, 43(10): 1-6.

[4] 中国汽车工业协会. 2023 年 10 月汽车工业产销情况[EB/OL]. 2024 [2024-02-18]. http://www.caam.org.cn/chn/4/cate_38/con_5236270.html.

[5] SAE. SAE J2601. Fueling protocols for light duty gaseous hydrogen surface vehicles[S]. 2020.

[6] ISO. ISO/TS 15869. Gaseous hydrogen and hydrogen blends-Land vehicle fuel tanks[S]. 2009.

[7] Wu X, Liu J T, Shao J W, et al. Fast filling strategy of type III on-board hydrogen tank based on time-delayed method[J]. International Journal of Hydrogen Energy, 2021, 46(57): 29288-29296.

[8] Elgowainy A, Reddi K. Hydrogen fueling station precooling analysis[DB/OL]. 2014 [2024-02-18]. https://www.hydrogen.energy.gov/docs/hydrogenprogramlibraries/pdfs/progress15/iii_12_elgowainy_2015.pdf.

[9] Elgowainy A, Reddi K, Lee D-Y, et al. Techno-economic and thermodynamic analysis of pre-cooling systems at gaseous hydrogen refueling stations[J]. International Journal of Hydrogen Energy, 2017, 42(49): 29067-29079.

[10] CEN. CEN-EN 17127. Outdoor hydrogen refuelling points dispensing gaseous hydrogen and incorporating filling protocols[S]. 2020.

[11] JPEC. JPEC-S 0003. 圧縮水素充塡技術基準(案)[S]. 2016.

[12] 国家标准化管理委员. GB/T 42855-2023. 氢燃料电池车辆加注协议技术要求[S]. 2023.

[13] Kim S C, Lee S H, Yoon K B. Thermal characteristics during hydrogen fueling process of type IV cylinder[J]. International Journal of Hydrogen Energy, 2010, 35(13): 6830-6835.

[14] Zheng J Y, Guo J X, Yang J, et al. Experimental and numerical study on temperature rise within a 70 MPa type III cylinder during fast refueling[J]. International Journal of Hydrogen Energy, 2013, 38(25): 10956-10962.

[15] Ortiz Cebolla R, Acosta B, Moretto P, et al. Hydrogen tank first filling experiments at the JRC-IET GasTeF facility[J]. International Journal of Hydrogen Energy, 2014, 39(11): 6261-6267.

[16] de Miguel N, Ortiz Cebolla R, Acosta B, et al. Compressed hydrogen tanks for on-board application: Thermal behaviour during cycling[J]. International Journal of Hydrogen Energy, 2015, 40(19): 6449-6458.

[17] Bourgeois T, Ammouri F, Weber M, et al. Evaluating the temperature inside a tank during a filling with highly-pressurized gas[J]. International Journal of Hydrogen Energy, 2015, 40(35): 11748-11755.

[18] Hosseini M, Dincer I, Naterer G F, et al. Thermodynamic analysis of filling compressed gaseous hydrogen storage tanks[J]. International Journal of Hydrogen Energy, 2012, 37(6): 5063-5071.

[19] Xiao J S, Cheng J, Wang X, et al. Final hydrogen temperature and mass estimated from refueling parameters[J]. International Journal of Hydrogen Energy, 2018, 43(49): 22409-22418.

[20] Xiao J S, Bénard P, Chahine R. Estimation of final hydrogen temperature from refueling parameters[J]. International Journal of Hydrogen Energy, 2017, 42(11): 7521-7528.

[21] Rothuizen E, Mérida W, Rokni M, et al. Optimization of hydrogen vehicle refueling via dynamic simulation[J]. International Journal of Hydrogen Energy, 2013, 38(11): 4221-4231.

[22] Liu J, Zheng S Y, Zhang Z X, et al. Numerical study on the fast filling of on-bus gaseous hydrogen storage cylinder[J]. International Journal of Hydrogen Energy, 2020, 45(15): 9241-9251.

[23] Ramasamy V, Richardson E S. Thermal response of high-aspect-ratio hydrogen cylinders undergoing fast-filling[J]. International Journal of Heat and Mass Transfer, 2020, 160: 120179.

[24] Li H Y, Lyu Z W, Liu Y D, et al. The effects of infill on hydrogen tank temperature distribution during fast fill[J]. International Journal of Hydrogen Energy, 2021, 46(17): 10396-10410.

[25] de Miguel N, Acosta B, Baraldi D, et al. The role of initial tank temperature on refuelling of on-board hydrogen tanks[J]. International Journal of Hydrogen Energy, 2016, 41(20): 8606-8615.

[26] Melideo D, Baraldi D, Acosta-Iborra B, et al. CFD simulations of filling and emptying of hydrogen tanks[J]. International Journal of Hydrogen Energy, 2017, 42(11): 7304-7313.

[27] Melideo D, Baraldi D, De Miguel Echevarria N, et al. Effects of some key-parameters on the thermal stratification in hydrogen tanks during the filling process[J]. International Journal of Hydrogen Energy, 2019, 44(26): 13569-13582.

[28] Blanco-Aguilera R, Martinez-Agirre M, Berasategi J, et al. Effect of liner thermal properties and liner pre-cooling on the thermal management of fast-filling of hydrogen tanks[J]. International Journal of Hydrogen Energy, 2024, 52: 1159-1172.

[29] Gonin R, Horgue P, Guibert R, et al. Advanced turbulence modeling improves thermal gradient prediction during compressed hydrogen tank filling[J]. International Journal of Hydrogen Energy, 2023, 48(77): 30057-30068.

[30] Zhao L, Liu Y L, Yang J, et al. Numerical simulation of temperature rise within hydrogen vehicle cylinder during refueling[J]. International Journal of Hydrogen Energy, 2010, 35(15): 8092-8100.

[31] Suryan A, Kim H D, Setoguchi T. Three dimensional numerical computations on the fast filling of a hydrogen tank under different conditions[J]. International Journal of Hydrogen Energy, 2012, 37(9): 7600-7611.

[32] Melideo D, Baraldi D, Galassi M C, et al. CFD model performance benchmark of fast filling simulations of hydrogen tanks with pre-cooling[J]. International Journal of Hydrogen Energy, 2014, 39(9): 4389-4395.

[33] Ortiz Cebolla R, Acosta B, de Miguel N, et al. Effect of precooled inlet gas temperature and mass flow rate on final state of charge during hydrogen vehicle refueling[J]. International Journal of Hydrogen Energy, 2015, 40(13): 4698-4706.

[34] Liu Y L, Zhao Y Z, Zhao L, et al. Experimental studies on temperature rise within a hydrogen cylinder during refueling[J]. International Journal of Hydrogen Energy, 2010, 35(7): 2627-2632.

[35] Li Q F, Zhou J Q, Chang Q, et al. Effects of geometry and inconstant mass flow rate on temperatures within a pressurized hydrogen cylinder during refueling[J]. International Journal of Hydrogen Energy, 2012, 37(7): 6043-6052.

[36] Dicken C J B, Mérida W. Measured effects of filling time and initial mass on the temperature distribution within a hydrogen cylinder during refuelling[J]. Journal of Power Sources, 2007, 165(1): 324-336.

[37] Zheng J Y, Liu X X, Xu P, et al. Development of high pressure gaseous hydrogen storage technologies[J]. International Journal of Hydrogen Energy, 2012, 37(1): 1048-1057.

[38] Wang G X, Zhou J Q, Hu S J, et al. Investigations of filling mass with the dependence of heat transfer during fast filling of hydrogen cylinders[J]. International Journal of Hydrogen Energy, 2014, 39(9): 4380-4388.

[39] Sapre S, Vyas M, Pareek K. Impact of refueling parameters on storage density of compressed hydrogen storage Tank[J]. International Journal of Hydrogen Energy, 2021, 46(31): 16685-16692.

[40] Xiao L, Chen J Y, Wu Y M, et al. Effects of pressure levels in three-cascade storage system on the overall energy consumption in the hydrogen refueling station[J]. International Journal of Hydrogen Energy, 2021, 46(61): 31334-31345.

[41] Zheng J Y, Ye J J, Yang J, et al. An optimized control method for a high utilization ratio and fast filling speed in hydrogen refueling stations[J]. International Journal of Hydrogen Energy, 2010, 35(7): 3011-3017.

[42] Xu Z, Dong W P, Yang K, et al. Development of efficient hydrogen refueling station by process optimization and control[J]. International Journal of Hydrogen Energy, 2022, 47(56): 23721-23730.

[43] Wang X, Fu J Q, Liu Z, et al. Review of researches on important components of hydrogen supply systems and rapid hydrogen refueling processes[J]. International Journal of Hydrogen Energy, 2023, 48(5): 1904-1929.

[44] Zhao L, Li F G, Li Z Y, et al. Thermodynamic analysis of the emptying process of compressed hydrogen tanks[J]. International Journal of Hydrogen Energy, 2019, 44(7): 3993-4005.

[45] Melideo D, Baraldi D. CFD analysis of fast filling strategies for hydrogen tanks and their effects on key-parameters[J]. International Journal of Hydrogen Energy, 2015, 40(1): 735-745.

[46] Galassi M C, Baraldi D, Acosta Iborra B, et al. CFD analysis of fast filling scenarios for 70 MPa hydrogen type IV tanks[J]. International Journal of Hydrogen Energy, 2012, 37(8): 6886-6892.

[47] Guo J X, Xing L J, Hua Z L, et al. Optimization of compressed hydrogen gas cycling test system based on multi-stage storage and self-pressurized method[J]. International Journal of Hydrogen Energy, 2016, 41(36): 16306-16315.

[48] Kuroki T, Nagasawa K, Peters M, et al. Thermodynamic modeling of hydrogen fueling process from high-pressure storage tank to vehicle tank[J]. International Journal of Hydrogen Energy, 2021, 46(42): 22004-22017.

[49] Rothuizen E, Rokni M. Optimization of the overall energy consumption in cascade fueling stations for hydrogen vehicles[J]. International Journal of Hydrogen Energy, 2014, 39(1): 582-592.

[50] Sadi M, Deymi-Dashtebayaz M. Hydrogen refueling process from the buffer and the cascade storage banks to HV cylinder[J]. International Journal of Hydrogen Energy, 2019, 44(33): 18496-18504.

[51] Bauer A, Mayer T, Semmel M, et al. Energetic evaluation of hydrogen refueling stations with liquid or gaseous stored hydrogen[J]. International Journal of Hydrogen Energy, 2019, 44(13): 6795-6812.

[52] Reddi K, Elgowainy A, Sutherland E. Hydrogen refueling station compression and storage optimization with tube-trailer deliveries[J]. International Journal of Hydrogen Energy, 2014, 39(33): 19169-19181.

[53] Reddi K, Elgowainy A, Rustagi N, et al. Impact of hydrogen refueling configurations and market parameters on the refueling cost of hydrogen[J]. International Journal of Hydrogen Energy, 2017, 42(34): 21855-21865.

[54] Talpacci E, Reuβ M, Grube T, et al. Effect of cascade storage system topology on the cooling energy consumption in fueling stations for hydrogen vehicles[J]. International Journal of Hydrogen Energy, 2018, 43(12): 6256-6265.

[55] Rothuizen E, Elmegaard B, Rokni M. Dynamic simulation of the effect of vehicle-side pressure loss of hydrogen fueling process[J]. International Journal of Hydrogen Energy, 2020, 45(15): 9025-9038.

[56] Farzaneh-Gord M, Deymi-Dashtebayaz M, Rahbari H R, et al. Effects of storage types and conditions on compressed hydrogen fuelling stations performance[J]. International Journal of Hydrogen Energy, 2012, 37(4): 3500-3509.

[57] Bai Y F, Zhang C Z, Duan H, et al. Modeling and optimal control of fast filling process of hydrogen to fuel cell vehicle[J]. Journal of Energy Storage, 2021, 35: 102306.

[58] Xiao J S, Bi C, Bénard P, et al. Neural network based optimization for cascade filling process of on-board hydrogen tank[J]. International Journal of Hydrogen Energy, 2021, 46(3): 2936-2951.

[59] Farsi A, Dincer I, Naterer G F. Multi-objective optimization of an experimental integrated thermochemical cycle of hydrogen production with an artificial neural network[J]. International Journal of Hydrogen Energy, 2020, 45(46): 24355-24369.

[60] Ozcan H, Dincer I. Exergoeconomic optimization of a new four-step magnesium–chlorine cycle[J]. International Journal of Hydrogen Energy, 2017, 42(4): 2435-2445.

[61] Ozbilen A, Dincer I, Rosen M A. Development of a four-step Cu–Cl cycle for hydrogen production – Part II: Multi-objective optimization[J]. International Journal of Hydrogen Energy, 2016, 41(19): 7826-7834.

[62] Li B W, Lu L X. Genetic-algorithm-based fault detection of the heat transfer process in nuclear-based hydrogen production based on Cu–Cl cycle[J]. International Journal of Hydrogen Energy, 2017, 42(6): 3863-3875.

[63] SAE. SAE J2601. Fueling protocols for light duty gaseous hydrogen surface vehicles[S]. 2010.

[64] SAE. SAE J2601. Fueling protocols for light duty gaseous hydrogen surface vehicles[S]. 2014.

[65] SAE. SAE J2601. Fueling protocols for light duty gaseous hydrogen surface vehicles[S]. 2016.

[66] Mathison S, Harty R, Cohen J, et al. Application of MC method-based H_2 fueling[C]. SAE 2012 World Congress & Exhibition, Detroit Michigan, United States, 2012.

[67] Harty R, Mathison S. Improving hydrogen tank refueling performance through the use of an advanced fueling algorithm – The MC method[C]. NHA hydrogen conference & expo, Long Beach, 2010.

[68] Schneider J, Meadows G, Mathison S R, et al. Validation and sensitivity studies for SAE J2601, the light duty vehicle hydrogen fueling standard[J]. SAE International Journal of Alternative Powertrains, 2014, 3(2): 257-309.

[69] McGuire T, Brown T, Goldstein T, et al. Field validation of the MC default fill hydrogen fueling protocol[J]. SAE International Journal of Alternative Powertrains, 2015, 4(1): 130-144.

[70] Reddi K, Elgowainy A, Rustagi N, et al. Impact of hydrogen SAE J2601 fueling methods on fueling time of light-duty fuel cell electric vehicles[J]. International Journal of Hydrogen Energy, 2017, 42(26): 16675-16685.

[71] Chochlidakis C G, Rothuizen E D. Overall efficiency comparison between the fueling methods of SAE J2601 using dynamic simulations[J]. International Journal of Hydrogen Energy, 2020, 45(20): 11842-11854.

[72] Chae C K, Park B H, Huh Y S, et al. Development of a new real time responding hydrogen fueling protocol[J]. International Journal of Hydrogen Energy, 2020, 45(30): 15390-15401.

[73] Xiao J S, Bénard P, Chahine R. Charge-discharge cycle thermodynamics for compression hydrogen storage system[J]. International Journal of Hydrogen Energy, 2016, 41(12): 5531-5539.

[74] Xiao J S, Wang X, Zhou X, et al. A dual zone thermodynamic model for refueling hydrogen vehicles[J]. International Journal of Hydrogen Energy, 2019, 44(17): 8780-8790.

[75] Xiao J S, Xu N F, Cai W C, et al. Thermodynamic and heat transfer models for refueling hydrogen vehicles: Formulation, validation and application[J]. International Journal of Hydrogen Energy, 2024, 52: 172-190.

[76] Sears F W, Salinger G L. Thermodynamics, kinetic theory, and statistical thermodynamics[M]. Addison-Wesley Publishing Company, 1975.

[77] Bilgili M, Yumşakdemir R F. Effects of real gas equations on the fast-filling process of compressed hydrogen storage tank[J]. International Journal of Hydrogen Energy, 2024, 53: 816-828.

[78] Hendricks R C, Peller I C, Baron A K. Joule-Thomson inversion curves and related coefficients for several simple fluids [R]. NASA Technical Note D-6807, 1972.

[79] Bourgeois T, Ammouri F, Baraldi D, et al. The temperature evolution in compressed gas filling processes: A review[J]. International Journal of Hydrogen Energy, 2018, 43(4): 2268-2292.

[80] Bourgeois T, Brachmann T, Barth F, et al. Optimization of hydrogen vehicle refuelling requirements[J]. International Journal of Hydrogen Energy, 2017, 42(19): 13789-13809.

[81] Dicken C J B, Mérida W. Modeling the transient temperature distribution within a hydrogen cylinder during refueling[J]. Numerical Heat Transfer, Part A: Applications, 2007, 53(7): 685-708.

[82] Woodfield P L, Monde M, Mitsutake Y. Measurement of averaged heat transfer coefficients in high-pressure vessel during charging with hydrogen, nitrogen or argon gas[J]. Journal of Thermal Science and Technology, 2007, 2(2): 180-191.

[83] Clark G L. Zero-dimensional model of compressible gas flow in networks of pressure vessels: program TRIC [R]. United States, 1983.

[84] Wang L, Ye F, Xiao J S, et al. Heat transfer analysis for fast filling of on-board hydrogen tank[J]. Energy Procedia, 2019, 158: 1910-1916.

[85] Sakoda N, Onoue K, Kuroki T, et al. Transient temperature and pressure behavior of high-pressure 100 MPa hydrogen during discharge through orifices[J]. International Journal of Hydrogen Energy, 2016, 41(38): 17169-17174.

[86] Lemmon E W, Bell I H, Huber M L, et al. NIST Standard Reference Database 23: Reference Fluid Thermodynamic and Transport Properties-REFPROP[DB/OL]. 2018 [2024-02-18]. https://www.nist.gov/srd/refprop.

[87] Striednig M, Brandstätter S, Sartory M, et al. Thermodynamic real gas analysis of a tank filling process[J]. International Journal of Hydrogen Energy, 2014, 39(16): 8495-8509.

[88] Valenti G. 2 - Hydrogen liquefaction and liquid hydrogen storage[M]. Woodhead Publishing. 2016.

[89] Emerson. Handbook on pressure loss and valve sizing[DB/OL]. 2012 [2024-02-18]. https://studylib.net/doc/18723808/handbook-on-pressure-loss-and-valve-sizing.

[90] Çengel Y A, Cimbala J M. Fluid Mechanics: Fundamentals and Applications[M]. McGraw-Hill Education, 2006.

[91] Krex H. Maskin ståbi. 9 ed[M]. Copenhagen Nyt Teknisk Forlag, 2004.

[92] Yu Y H, Lu C, Ye S, et al. Optimization on volume ratio of three-stage cascade storage system in hydrogen refueling stations[J]. International Journal of Hydrogen Energy, 2022, 47(27): 13430-13441.

[93] Kuroki T, Sakoda N, Shinzato K, et al. Dynamic simulation for optimal hydrogen refueling method to Fuel Cell Vehicle tanks[J]. International Journal of Hydrogen Energy, 2018, 43(11): 5714-5721.

[94] Tian Z, Lv H, Zhou W, et al. Review on equipment configuration and operation process optimization of hydrogen refueling station[J]. International Journal of Hydrogen Energy, 2022, 47(5): 3033-3053.

[95] Schäfer S, Klein H. Thermodynamical analysis of a hydrogen fueling station via dynamic simulation[J]. International Journal of Hydrogen Energy, 2019, 44(33): 18240-18254.

[96] Caponi R, Monforti Ferrario A, Del Zotto L, et al. Hydrogen refueling stations and fuel cell buses four year operational analysis under real-world conditions[J]. International Journal of Hydrogen Energy, 2023, 48(54): 20957-20970.

[97] Caponi R, Monforti Ferrario A, Bocci E, et al. Thermodynamic modeling of hydrogen refueling for heavy-duty fuel cell buses and comparison with aggregated real data[J]. International Journal of Hydrogen Energy, 2021, 46(35): 18630-18643.

[98] Monde M, Woodfield P, Takano T, et al. Estimation of temperature change in practical hydrogen pressure tanks being filled at high pressures of 35 and 70 MPa[J]. International Journal of Hydrogen Energy, 2012, 37(7): 5723-5734.

[99] Yang B, Liang B X, Qian Y C, et al. Parameter identification of PEMFC via feedforward neural network-pelican optimization algorithm[J]. Applied Energy, 2024, 361: 122857.

[100] Graupe D. Principles of Artificial Neural Networks[M]. World Scientific Publishing Co., Inc., 2007.

[101] Borji M, Atashkari K, Ghorbani S, et al. Parametric analysis and Pareto optimization of an integrated autothermal biomass gasification, solid oxide fuel cell and micro gas turbine CHP system[J]. International Journal of Hydrogen Energy, 2015, 40(41): 14202-14223.

[102] Rabbani M, Dincer I, Naterer G F, et al. Determining parameters of heat exchangers for heat recovery in a Cu–Cl thermochemical hydrogen production cycle[J]. International Journal of Hydrogen Energy, 2012, 37(15): 11021-11034.

[103] Ouellet M, Goyette J, Xiao J S. A new approach to optimize the performance of a hydrogen reservoir using activated carbon as the storing material[J]. International Journal of Hydrogen Energy, 2017, 42(38): 24229-24236.

[104] Schneider J, Meadows G, Wistoft-Ibsen M, et al. Hydrogen fueling standardization: Enabling ZEVs with "Same as Today" fueling and FCEV range and safety[C]. International Conference on Hydrogen Safety, Yokohama, Japan, 2015.

[105] Hamut H S. Exergy and exergoeconomic analyses and optimization of thermal management systems in electric and hybrid electric vehicles[D]. Canada: University of Ontario Institute of Technology, 2012.

[106] Caponi R, Ferrario A M, Bocci E, et al. Single-tank storage versus multi-tank cascade system in hydrogen refueling stations for fuel cell buses[J]. International Journal of Hydrogen Energy, 2022, 47(64): 27633-27645.

[107] Xu W W, Yu Z H, Mu Q K, et al. Study of an integrated vortex tube used in hydrogen pre-cooling system[J]. International Journal of Hydrogen Energy, 2024, 54: 971-978.

[108] Wu Y M, Guo Y H, Yu H X, et al. Energetic assessment on a dual-temperature evaporation refrigeration system for hydrogen pre-cooling[J]. International Journal of Refrigeration, 2024, 159: 264-275.

[109] Aguila-Leon J, Vargas-Salgado C, Chiñas-Palacios C, et al. Energy management model for a standalone hybrid microgrid through a particle swarm optimization and artificial neural networks approach[J]. Energy Conversion and Management, 2022, 267: 115920.

[110] Navid A, Khalilarya S, Abbasi M. Diesel engine optimization with multi-objective performance characteristics by non-evolutionary Nelder-Mead algorithm: Sobol sequence and Latin hypercube sampling methods comparison in DoE process[J]. Fuel, 2018, 228: 349-367.

[111] Kosir S, Stachler R, Heyne J, et al. High-performance jet fuel optimization and uncertainty analysis[J]. Fuel, 2020, 281: 118718.

[112] Haykin S S. Neural networks and learning machines[M]. Third ed. Upper Saddle River, NJ: Pearson Education, 2009.

[113] Li C L, Ye F, Chahine R, et al. Genetic algorithm optimized artificial neural network models of single- and multi-component gas adsorption isotherms for hydrogen purification[J]. International Journal of Hydrogen Energy, 2024, 52: 1127-1142.

[114] Javadi M A, Khodabakhshi S, Ghasemiasl R, et al. Sensivity analysis of a multi-generation system based on a gas/hydrogen-fueled gas turbine for producing hydrogen, electricity and freshwater[J]. Energy Conversion and Management, 2022, 252: 115085.

[115] Saltelli A, Annoni P. How to avoid a perfunctory sensitivity analysis[J]. Environmental Modelling & Software, 2010, 25(12): 1508-1517.

[116] Saltelli A, Sobol' I M. Sensitivity analysis for nonlinear mathematical models: numerical experience[J]. Institute for Mathematical Modelling, 1995, 16-28.

[117] Homma T, Saltelli A. Importance measures in global sensitivity analysis of nonlinear models[J]. Reliability Engineering & System Safety, 1996, 52(1): 1-17.

Acknowledgement

Endless gratitude should be given to Prof. Jinsheng Xiao and Prof. Pierre Bénard for their helpful and patient directions throughout my Ph.D. project. I have benefited a lot from their profound insights and rigid attitudes toward researching and teaching. Thanks also should be given to the wife of Prof. Jinsheng Xiao, Ms. Lijun Zhu, for encouragement and support in life when I studied at Université du Québec à Trois-Rivières, Canada.

Gratefulness to all my teachers and colleagues at Wuhan University of Technology, Université du Québec à Trois-Rivières and Wuhan Business University, specifically:

Prof. Xianjun Hou, Prof. Shichun Mu, Prof. Pang-Chieh Sui, Prof. Yonghua Cai, Prof. Ben Chen, Dr. Tianqi Yang, Dr. Liang Tong, Dr. Shanshan Deng, Dr. Qianqian Xin, Mr. Longcheng Li, Mr. Cheng Bi, Mr. Ang Mei, Mr. Hao Hu, Mr. Pan He, Mr. Xu Zhang, Mr. Kang Sun, Mr. Wenchao Cai, Mr. Shenlin Su, Mr. Yaze Li, Mr. Guodong Li, Mr. Jin Li, Mr. Xianglin Yan, Mr. Zhili Xiao, Mr. Hanwei Xu, Mr. Zhiyu Yang.

Prof. Richard Chahine, Prof. Jacques Goyette, Ms. Patricia Tremblay, and Ms. Catarina Leote F. Pio.

I wish to thank the financial support from the National Natural Science Foundation of China (Project No. 52176191 and 51476120) and the International Cooperation Training Project of the China Scholarship Council (Project No. 202106950012).

Thanks to my family for their understanding and support over the past four years. Without them, I might not have been able to persevere. Their encouragement and support eliminated my worries and enhanced my confidence and motivation to complete my studies.

List of Publications

[1] **Luo H**, Xiao J S, Bénard P, Yang T Q, Tong L, Chahine R, Yuan Y P, Yuan C Q, Yao C L. Improvement of MC method in SAE J2601 hydrogen refuelling protocol using dual-zone dual-temperature model. *Journal of Energy Storage*, 2024, 81: 110416. (**JCR Q1, IF=9.4**)

[2] **Luo H**, Xiao J S, Bénard P, Zong Y, Chahine R, Tong L, Yuan C Q, Yang T Q, Yuan Y P. Optimal estimation of MC parameter in SAE J2601 hydrogen refuelling protocol based on modified formula and artificial neural networks. *Fuel,* 2024, 365: 131315. (**JCR Q1, IF=7.4**)

[3] **Luo H**, Xiao J S, Bénard P, Chahine R, Yang T Q. Multi-objective optimization of cascade storage system in hydrogen refuelling station for minimum cooling energy and maximum state of charge. *International Journal of Hydrogen Energy*, 2022, 47: 10963-10975. (**JCR Q1, IF=7.2**)

[4] **Luo H**, Xiao J S, Bénard P, Chahine R, Yang T Q. Effects of filling strategies on hydrogen refueling performance. *International Journal of Hydrogen Energy*, 2024, 51: 664-675. (**JCR Q1, IF=7.2**)

[5] **Luo H**, Xiao J S, Bénard P, Yuan C Q, Tong L, Chahine R, Yuan Y P, Yang T Q, Yao C L. Thermodynamic modeling and analysis of cascade hydrogen refuelling with three-stage pressure and temperature for heavy-duty fuel cell vehicles. *International Journal of Hydrogen Energy*, 2024, 63: 103-113. (**JCR Q1, IF=7.2**)

[6] **Luo H**, Yuan C Q, Wang L, Yang T Q, Tong L, Ye F, Yuan Y P, Bénard P, Chahine R, Xiao J S. Heat transfer analysis methodology for compression hydrogen storage tank during charge-discharge cycle. *International Journal of Energy Research*, 2024, Second review. (**JCR Q1, IF=4.6**)